Geomorphometrical Analysis of Glacial and Aeolian Lineaments on Satellite Images

George Che Fowajuh

**Thesis submitted to the Faculty of Pure Science,
University of Sheffield for the Degree of Doctor of Philosophy.**

August 1995

Department of Geography

University of Sheffield

England

Table of Contents

PAGE

NUMBERING

AS ORIGINAL

Abstract

Some glacial and aeolian geomorphological features express themselves as parallel lineaments on satellite images. These landforms represent readily available evidence for reconstructing Quaternary environments, and are believed to have preserved in their morphometry, evidence of their formation. Drumlins, megaflutes, flutes and mega-lineaments are typical examples of glacial lineaments, while linear sand dunes are examples of aeolian lineaments.

The main aim of this thesis was to develop an objective method of characterising the spacing between parallel glacial and aeolian lineaments and to attempt to answer some geomorphological questions about them.

The method of spectral analysis based on fourier transformation was used. Spectral analysis on radiometric transects taken perpendicular to the trend of parallel lineaments on satellite images permits the spacing between these lineaments to be assessed and thus the dominant spatial frequency to be determined. This provides a quick and efficient method of morphometric analysis. A methodology for doing this has been established and applied to examples of large scale ice moulded landforms in Canada and aeolian linear sand dunes from the Kalahari desert.

Analysis of the spacings obtained showed that for the case of aeolian lineaments in the study area, there was no significant trend in spacing up or downwind indicating equilibrium in spacing in the overall dunefield.

The analysis of the spatial frequency of glacial lineaments established that a significant relationship existed between lineament spatial frequencies and inferred velocities and that the behaviour of the spacing is systematic up/down ice. An important result obtained from analysing these lineaments was that the spatial distribution showed a concentration of spacing at a particular range of frequencies (150 to 750 metres) proving that the distribution of the landforms is not multimodal as has been previously hypothesised but is scale continuous.

Acknowledgement

This thesis was funded by the Cameroon Government. Images for the analysis were provided by a grant from the university research fund, University of Sheffield.

I would like to thank most importantly my supervisor Dr. Chris Clark for his invaluable assistance, for introducing me to the intricacies of lineaments and for devoting considerable time and energy in supervising this research.

Special thanks also go to Mr. Peter Bragg for Helping with some of the computer programs used in this thesis and to Dr. David Knighton for assisting with the mathematics of spectral analysis and also to Jane Knight for helping with digitisation of the lineaments.

The undertaking, continuation and completion of this research would not have been possible without the love and support I have received from my family. To whom I owe the greatest gratitude.

I would like to thank all my friends for their unstinting support throughout my years in the U.K. They are, Bekia, Chika, Chris, Eva, Hellen, Ian, Janet, Kaela, Lorraine, Marcus, Maurice, Patrick, Patsy and Williams.

Lastly but no the least, a big thank you to Comfort for having done a brilliant job in bringing up my son Ngang for the period that I have been an away father.

List of Figures

List of Tables

Chapter one

Introduction

1.0 Introduction

Many geomorphological features from glacial and aeolian environments express themselves as *lineaments*. Drumlins and linear sand dunes are typical examples. These features have been subjected to numerous methods of lineament analyses with the aim of seeking a better understanding of the nature of these landforms and how they were formed. Unfortunately such analyses have had their shortfalls, most importantly is the subjective nature of the results as the analyses often rely on field mapping or visual interpretation from satellite images, air photographs or topographic maps. The result has been a variation of results between scientists working in the same area or even when the same person has interpreted and analysed the same set of lineaments at different times. Another problem posed by the manual method of analysing lineaments has been the use of limited areas for study of these landforms. This has been due to the time consuming nature of data collection which has resulted in small sample sizes being analysed. With these limitations it is not surprising that there have been a myriad of conclusions about the morphometry of these features and theories about their formation.

There is therefore a need for a more objective means of quantifying these landforms and for one that can be applied with relative ease to large areas. These landforms represent readily available evidence for reconstructing Quaternary environments and are believed to have preserved in their morphometry, evidence of their formation. This belief has set many researchers seeking processes from pattern and thus the science of Geomorphometry was born.

The main aim of this thesis is to develop an objective method of characterising parallel glacial and aeolian lineaments and to attempt to answer some of the geomorphological questions about such lineaments. The novelty of this work is in its use of satellite imagery as the source of information and the use of a semi-automated technique for deriving some morphometric data.

1.1 Geomorphometry of Aeolian Linear Sand Dunes

There is still no clear understanding of the factors that are responsible for the formation of aeolian linear sand dunes apart from the knowledge that they are formed by aeolian sand accumulation.

In attempting to understand their formation, researchers have tried to seek relationships between morphometric parameters of these landforms and sand availability, grain size distribution, wind velocity distribution and variability, vegetation cover and growth characteristics, nature of underlying substrate, climatic and sea level changes and long-term patterns of tectonic drift and subsidence which are all thought to be determinants of the form and scale of aeolian sand accumulations.

Relationships between the spacings of linear sand dunes and grain size have been studied by Wilson (1972a; 1972b), Wasson *et al.* (1983) and Thomas (1988) with varying results, while the effect of wind and sand flow on linear sand dunes has been investigated by Tsoar (1979; 1983) and Livingston (1986) with no consensus view. The study of the spacing of linear sand dunes and their height proved that a strong relationship exists, but only when these lineaments are considered in blocks (Wilson, 1972; Breed and Grow, 1979; Lancaster, 1982; Wasson and Hyde, 1983; Lancaster et al. 1987; Thomas, 1988; Lancaster, 1989) with a block representing areas with uniform morphometric characteristics. Although this relationship exists,

they however showed that the correlation coefficient between height and spacing of linear sand dunes are not unique for different areas.

Disagreements in the results about linear sand dunes makes it difficult to formulate any concrete theories about the formation of these landforms based on their parameters. This could be due to the limited size of the study areas and the methods of collecting and analysing the data for this landform type. There is therefore a need for redefining or modifying methods of analysing data on linear sand dunes to seek an objective conclusion about their morphometry and morphogenesis.

1.2 Geomorphometry of Glacial Lineaments

Landforms represented by glacial lineaments are drumlins, megaflutes, flutes, mega-lineaments and fragmentary drift elements (Clark, 1990; 1993; 1994), all of which are ridges of sediment aligned in the direction of ice flow. The difficulty of understanding their formation is due to the fact that they were formed beneath the ice sheet which makes it difficult to observe the processes in operation. Only the geomorphological evidence exposed after ice retreat is available for studying these landforms.

The literature on these landforms suggests a great amount of uncertainty about them. For example there is still debate about the glaciodynamic setting where these lineaments are thought to form. Some authors have proposed ice margin location as the locus for drumlin formation (Alden, 1911; Smalley and Unwin, 1968) and another study by Rose (1987; 1989) found drumlins to be close to the ice centre. Clark (1994) however hypothesised that drumlins may simultaneously form along flow lines that extend for hundreds of kilometres. Recently proposed theories, such as those by Shaw (1983), have increased our uncertainty as he regards glacial lineaments to have been formed by water and not the direct action

of ice. There is now a large school of thought in Canada that invokes water as the main lineament forming agent (Shaw, 1994).

It is impossible to form a solid conclusion on the formation of these landforms in light of the conflicting arguments about them. There is therefore the need for redefining or modifying methods of analysing data on glacial lineament to seek an objective conclusion about their morphometry and morphogenesis.

1.3 Spectral Analysis

Transects taken perpendicularly across a satellite image depicting a lineament field representing parallel glacial landforms or linear sand dunes will produce the *radiometric transect*. This is a 2-d graphic representation with the X-axis representing the position of lineament with respect to one another as observed by the image and the Y- axis, the measured radiance *(DN values)* of points along the transect. The radiometric transect is therefore a *spatial series* defined as the set of DN values, which are the variables in this case, ordered with respect to spatial co-ordinates (distance along the transect).

Any phenomenon spread in space as described above will form a statistical surface which may reveal spatial form that may be of interest to geomorphologists. It is very often that the characteristic, i.e. DN value for a lineament, will be related to that of other points along the transect suggesting a spatial dependency between points along the transect. Because of this the characteristic value of points on the transect will be able to give statistical information about adjacent ones. This dictum of spatial ordering of geographical data has been a basic assumption of geographical analyses throughout history (Unwin and Hepple, 1974) and has been used here to devise a method of analysing parallel lineaments on satellite images.

It has been explained how lineaments represented on an image can be transformed into a spatial series. Since this series maintains the relative position of the

lineament and their character (DN values), it is possible to apply statistical techniques to determine the presence of regularity in the data and the wavelength at which this cylicicity occurs. This wavelength will give the measure of the spacing between the lineaments if the lineaments are regularly arranged on the transect. For transects with the same lengths, a shorter wavelength will imply more lineaments on the transect than for transect with longer wavelengths, hence density of lineaments can also be measured from the transect.

The spectral analysis method for time series, used in studying the variation in series in terms of relative importance of different frequencies or wave-bands (Rayner, 1971; Bloomfield, 1976; Chatfield, 1984) has been extended and applied to the radiometric transect containing information about the lineaments (Fowajuh and Clark, 1992; Clark and Fowajuh, 1993). The aim has been to decompose and isolate the different scale of variation representing the spacing between the lineaments by fourier analysis.

Fourier analysis can also be performed on the whole image as opposed to analysis on the transect to produce an amplitude spectrum of the image which contains information regarding the frequencies and phase angle of the waveforms into which the image has been decomposed. The ability of isolating different frequencies makes it possible to apply filtering in the frequency domain by either isolating unwanted spatial frequencies or highlighting them as part of image enhancement in image processing. Other applications of fourier analysis are in characterising images since the location of points on the amplitude spectrum (which is the result of fourier analysis on the image) has information about the spatial variability of the image.

1.4 Aims and Approach of the Thesis

In light of the preceding discussions, the main aim of this thesis is to develop a methodology of analysing the spacing between parallel glacial and aeolian

landforms. Radiometric transects taken across images depicting these types of landforms as lineaments provide a spatial series which can be analysed.

Given that lineaments possess orientation, length, width, height and spacing, some explanation is needed as to why the focus here is just on spacing. It is for the following reasons:

1. For bedforms which glacial and aeolian lineaments clearly are, the spatial frequency is of fundamental importance. It can be argued that lineament spacing is the best measure of spatial frequency.

2. Spacing is probably the only parameter that can be automatically extracted from satellite data, and as such it provides a lineament parameter for which we can collect sample sizes which are large enough to be meaningful. Great progress is being made in the field of pattern recognition, and one day it is hoped that lineaments may be automatically detected which will provide the full morphometric information. Currents efforts at automatic lineament detection however, are woefully inadequate for the geomorphological features of interest in this study, field boundaries and roads are the main goals at the present time.

3. Spacing has been a relatively neglected parameter in lineament studies and hence could be a profitable avenue of investigation.

The method of spectral analysis of time series was extended for radiometric transects and FORTRAN 77 programs were written and some adopted from the NAG subroutines and Ghost-88 graphical packages for carrying out the analysis.

The application of spectral analyses of the transects have been explored in two case studies:

1.4.1 Application to Aeolian Linear Sand Dunes

Spectral analysis of radiometric transects on aeolian landforms was to establish the presence or absence of regularity in the spacing between linear sand dunes and

quantify these regularities if present, and also to search for any variation of spacing along the wind direction.

An attempt has been made to apply the results of these findings to answering some of the geomorphological questions about these landforms.

1.4.2 Application to Glacial Landforms

Just as in the example above, the spectral analysis of the transects represented by these landforms was used to establish the presence or absence of regularity in the spacing of these landforms and quantify these regularities if present.

The morphometric spacings for these landforms were used to:

1. Seek if there were any relationships between lineament morphometry and inferred ice velocity and glaciodynamic setting.

2. Find out if glacial lineaments have a scale continuous distribution or if they are concentrated at specific frequencies

3. Provide a method of isolating discrete ice flow events from a complex ice flow pattern.

This has been achieved by answering questions posed by hypotheses relating to the above three points.

1.5 Structure of the Thesis

The development of a methodology for quantifying glacial and aeolian lineaments and applying the method to answering some of the key geomorphological questions about these lineaments are reported under 7 main chapters:

Chapter two reviews the literature on earth surface lineaments. A concise definition of the term lineament is given and the various types described: structural

and geomorphological lineaments are explained. The chapter also explains the various parameters of lineaments and concludes with the relevance of this kind of approach.

Chapter three explains how lineaments appear on images and why we see them, and discuses the property of images and imaging systems that makes this possible.

Chapter four gives a brief discussion of past methods of lineament analysis and the short falls which are the source of inspiration for the search for a new method for analysing lineaments (*spectral and fourier analysis).* The use of spectral and fourier analysis in Geography and remote sensing is outlined. The radiometric transect is described and illustrated. The chapter then outlines the method of spectral analysis and significance testing of the results, followed by explanation of the various computer programs for analysing the transects. The use of two dimensional analysis on the image is discussed in this chapter and other uses of fourier and spectral analysis are explained.

In chapter five a number of experiments are designed to test the validity of spectral analysis, the best waveband to use for spectral analysis, and the effect of spectral analysis on some of the more popular image processing routines are assessed.

Chapter six is a composite chapter featuring two sections relating to aeolian and glacial lineaments. The first section is a case study on linear sand dunes from the Kalahari desert using Landsat TM images. The second section studies glacial lineaments in Canada from Landsat TM and MSS images. A scanned hardcopy image was also used for this study.

Chapter seven provides a summary of the research and the main conclusions from the work. It also gives an assessment of the extent to which the original object of the research were met, and recommendations for further research.

Chapter Two

Earth Surface Lineaments.

2.0 Introduction

The science of remote sensing has existed since the 1940's and 1950's when aerial photographs were first acquired and since this time remote sensing has grown to become an important and powerful tool in earth sciences. One area in which remote sensing has found an application is in the study of earth surface lineaments.

The term "Lineament" is used in slightly different ways by different people, and the context in which it is used varies. The original definition was provided by Hobbs (1904) who coined the term lineament as earth's features manifest in the landscape by: "crest of ridges or boundaries of elevated areas; drainage lines; coast lines; or boundary lines of petrographic rock types or outcrops."

Tectonic geological meaning was later added to the term. This has led to a new definition of lineament by O'Leary *et al.* (1976) as mappable, simple or composite linear features of the Earth's surface, whose parts are aligned in a rectilinear or slightly curvilinear relationship and which differs distinctly from the patterns of adjacent features and presumably reflects a subsurface phenomenon.

Lineaments are said to be simple when they consist of a single continuous feature and composite if they are detached features in a linear alignment. The features are mappable if they can be discerned on the image and are clearly distinguishable from surrounding features such that they can be traced.

In this thesis the term lineament will be used in two contexts;

1. as part of the structure of an image; a mappable linear feature aligned in a rectilinear fashion is termed an image lineament. This definition makes no

assumptions regarding the geophysical nature of the feature. It is simply an image-based description of pattern.

2. Once a geophysical context or explanation has been made to describe an "image lineament" it can be regarded as an earth surface lineament, e.g. structural geological lineament, glacial geomorphological lineament, linear sand dunes.

The ability to recognise lineaments depends on the scale of the images used. This will therefore have an effect on mapping lineament parameters as they will be observed differently at different scales and will not be recognised at all scales. It is possible for example to map lineaments on an image of a particular area where they are not detectable on a different scale image of the same area. Clark (1990) for example examined differences in detection of glacial lineaments for six different image types and scales; from aerial photographs through Landsat to AVHRR images. In his study of structural lineaments in Connecticut, Shuman (1989) showed that the distribution of lineament parameters of orientation, frequency and length are non uniform i.e. they vary with the scale of the image. The scale of the image is therefore important in recognising and mapping lineaments.

2.1 Types of Earth Surface Lineaments

The reasons as to why and how earth surface lineaments are expressed in raster-based remotely sensed imagery is discussed in a later section (3.2 and 3.3). It is first necessary to consider the geophysical features themselves. Lineaments on satellite images can be studied under the broad headings of: structural geological lineaments, parallel glacial lineaments, linear sand dunes and miscellaneous, including anthropogenic lineaments such as roads. The first three types of lineaments will now be described.

2.1.1 Structural Geological Lineaments

These comprise of lineaments depicting geological features. They give clues to the internal structure of the lithosphere and represent the surface expression of faults, folds, joints, lithologic contacts, or other geological discontinuities. The study of such features is called structural geology. The next section describes the different type of geological lineaments according to their sizes.

1. **Local Structures Indicated by Lineaments**

   Lineaments of this type are poorly seen on satellite images but are easily discernible on aerial photographs. They are usually not more than 10 km in length (Rowan and Lathram, 1980). At this level the lineaments represent the form and location of individual faults, joints, folds, lithological contacts and other detailed geological features. Their geological significance is readily determined from surface and near-surface geological and geophysical data. In structural geology, these features are best studied with aerial photographs. Using satellite images is likely to be a waste of resources.

2. **Regional Structural Regimes Indicated by Lineaments**

   These are features with lengths ranging from 10 to 200 km. They can be longer in some areas and some may be part of a longer significant lineament. Features of this type indicate the general geometry of folds, faults, and other structures that characterise a foldbelt. They can be related to 'ground truth' i.e. surface geological data or to near surface magnetic data (Rowan and Lathram, 1980). They are discernible on satellite images but occur less abundantly on the ground than lineaments indicating local structures. A regional pattern can be observed with these types of lineaments indicating regional structural regimes.

3. Crustal Tectonic Elements Indicated by Lineaments

They are less abundant than lineaments indicating structural regimes and are usually greater than 200 km in length and are generally 1000 km or more in length (Rowan and Lathram, 1980). They demarcate the boundaries of regional structural elements or zones separating areas within these elements. They may traverse the entire extent of regional structural elements or transgress the boundaries of elements having structural regimes of differing types with little significant change in the surface geology.

Lineaments of these types are broad and diffuse and are poorly resolvable for short sections along their length. They occur as alignments that are combinations of surface geologic structures, linear valleys or ridges, and changes in tonal contrast marking differences in soil types, moisture, and vegetation.

Their extensive lengths mean that they can only be studied on mosaics of satellite imagery such as Landsat and SPOT or on smaller scale images from satellites such as NOAA. AVHRR. Although these lineaments can be discernible on Landsat and SPOT images, they tend to be more diffuse and the accuracy of locating them is very marginal.

Sometimes the shorter lineaments from large scale satellite images are in reality probably portions of much larger ones which are intermittently perceptible. The sharpness of larger scale satellite images may lead to wrong conclusions where unrelated shorter lineaments may be chosen to represent the trace of crustal features and thus cause misinterpretation.

It is ironic that some of these lineaments although visible on low resolution images i.e. NOAA AVHRR will not be easily recognisable on Landsat and Spot images which have higher resolution.

2.1.2 Geomorphological Lineaments

Lineaments reflecting geomorphological landforms have been studied to a lesser extent than structural lineaments. Glacial and aeolian activity commonly gives rise to a multitude of landforms that are expressed as lineaments.

2.1.2.1 Glacial Geomorphological Lineaments

The last ice age occurred in the Pleistocene Epoch which began 2 million years ago and ended about 10 thousands years ago. During this epoch, great ice sheets periodically spread over much of northern Europe, North American and Asia. They left behind them, as they melted, a variety of landforms, some of which are thought to be ice eroded and others are thought to be made of glacial deposits. Almost the entirety of Canada, for example, is covered by such landforms. The importance of these landforms is that they provide evidence for reconstructing the dynamic behaviour of former ice sheets.

Some of these landforms exist in parallel sets whose orientation is a record of the former direction of ice flow. They exist at a variety of scales, from flutes which are typically of the order of tens of metres in length through to mega flutes and drumlins which are typically of the order of kilometres in length. They appear as lineaments on satellite images. Analysis of Landsat imagery has recently revealed that a larger linear component of ice moulding exists (Clark, 1993). Glacial lineaments of the order of tens of kilometres and up to 80 km in length have been reported and are regarded as part of the assemblage of ice moulding (Clark, 1990)

Clark (1993) Classified glacial lineaments into 2 categories:

- **Drumlins and megaflutes:** These can often be seen on aerial photographs as individual forms and due to their size, which is slightly larger than the size of the resolution of Landsat MSS images, they appear as a grain. They are the product of subglacial moulding by the ice sheet producing swarms of whale-shaped mounds which present a topography that has been aptly described as a

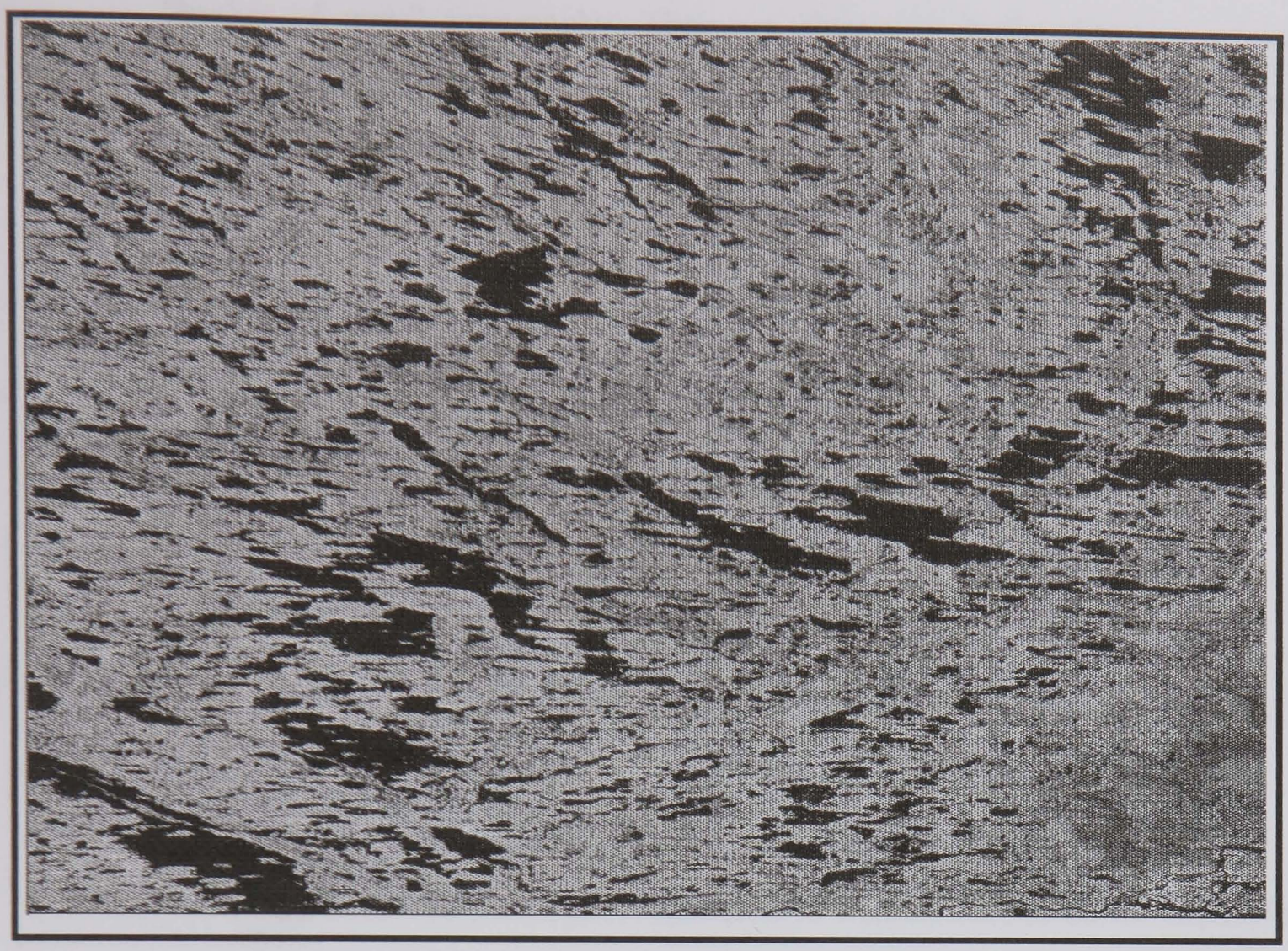

Figure 2.1 Landsat MSS image (band 1) of section Canada depicting Mega-scale glacial lineament.

"basket of eggs" topography. They are elongated in the direction of ice movement with the upstream end appearing broader and more blunt compared with the tapering dowm stream end.

- **Mega-Scale Glacial Lineaments:** These are glacial lineaments of large dimensions (figure 2.1) that Clark (1990) was able to observe on Landsat images. They represent a hitherto undocumented scale of glacial lineaments that have been analysed by Clark (1993; 1994).

Table 2.1 Parameters of mega-scale glacial lineaments (Clark, 1993)

Feature	Lengths	Widths	Spacing
Megascale glacial lineaments	**8-70 km**	**0.2-1.3 km**	**0.3-5 km**

These values are only estimates. Quantitative studies need to be conducted to ascertain these estimates. If these measurements are true, it implies that their distinctive difference from drumlins and mega-flutes suggests a distinct landform and therefore a different process of formation.

2.1.2.2 Aeolian Lineaments

About a fifth of the land surface is desert and on an average 20 percent of the desert is mantled with sand. In these deserts, a high percent of the desert floor is an erosion surface of bedrock, locally strewn with coarse rock-waste. In regions of shale and limestone, little or no sand is present but where sandstone is being eroded or mixed alluvium is being deflated, the wind picks up the loose grains and concentrates them into vast sand wastes (sand seas) which are often organised into dunefields displaying distinctive landform patterns. Many of these patterns can be readily observed on satellite images.

Mckee (1979) classified three major dunes types as: crescentric, star, and linear dunes. This research will focus on the linear dune type as they are expressed as

lineaments on satellite images and aerial photographs. The next section describes the different types of aeolian lineaments.

- **Linear Sand Dunes:** These are straight or slightly sinuosymmetrical or asymmetrical sand ridges which are much longer than they are wide (Embabi, 1993) and illustrated in figure 2.2. Their lengths range from 1 metre to tens of kilometres and their heights from tens of centimetres to more than 150 metres (Pye and Tsoar, 1990). They may be either vegetated or unvegetated (Tsoar, 1989). The unvegetated type have a sharp crests thus rendering the name seif. The vegetated types have a more rounded crests. The seif dunes are found extensively in the African sand seas (Thomas, 1988). Vegetated linear dunes occur widely in central Australia (Bukley, 1981), and the Kalahari, (Thomas, 1988). They exhibit parallelism and cyclicity in their spacing. Some of them have 'Y' connections as can be seen in figure 2.2. Linear sand dunes cover more area in a desert sand sea than any other dune type.

  Linear sand dunes are termed **simple** if the dunes have single sharp narrow crest ridges and termed **compound dunes** if the ridges are broader with relatively smaller subsidiary linear dunes which intersect or spread obliquely from the main ridges, the dunes are termed complex if they have other dunes types i.e. barchanoid or star dunes superimposed or integrated with them.

- **Yardangs:** These are desert features which appear as lineaments on satellite images. They are formed by wind erosion in contrast to wind deposition for sand dunes. Highly directional winds abrade and lift particles from exposed surface in areas of homogeneous lithology causing wind erosion of these surfaces to produced streamlined, lemmiscate Yardangs that are repeated in a parallel array. They are found in many deserts on earth and suspected to be present on mars, they measure tens of metres high and kilometres long (McCauley *et. al.*. 1977)

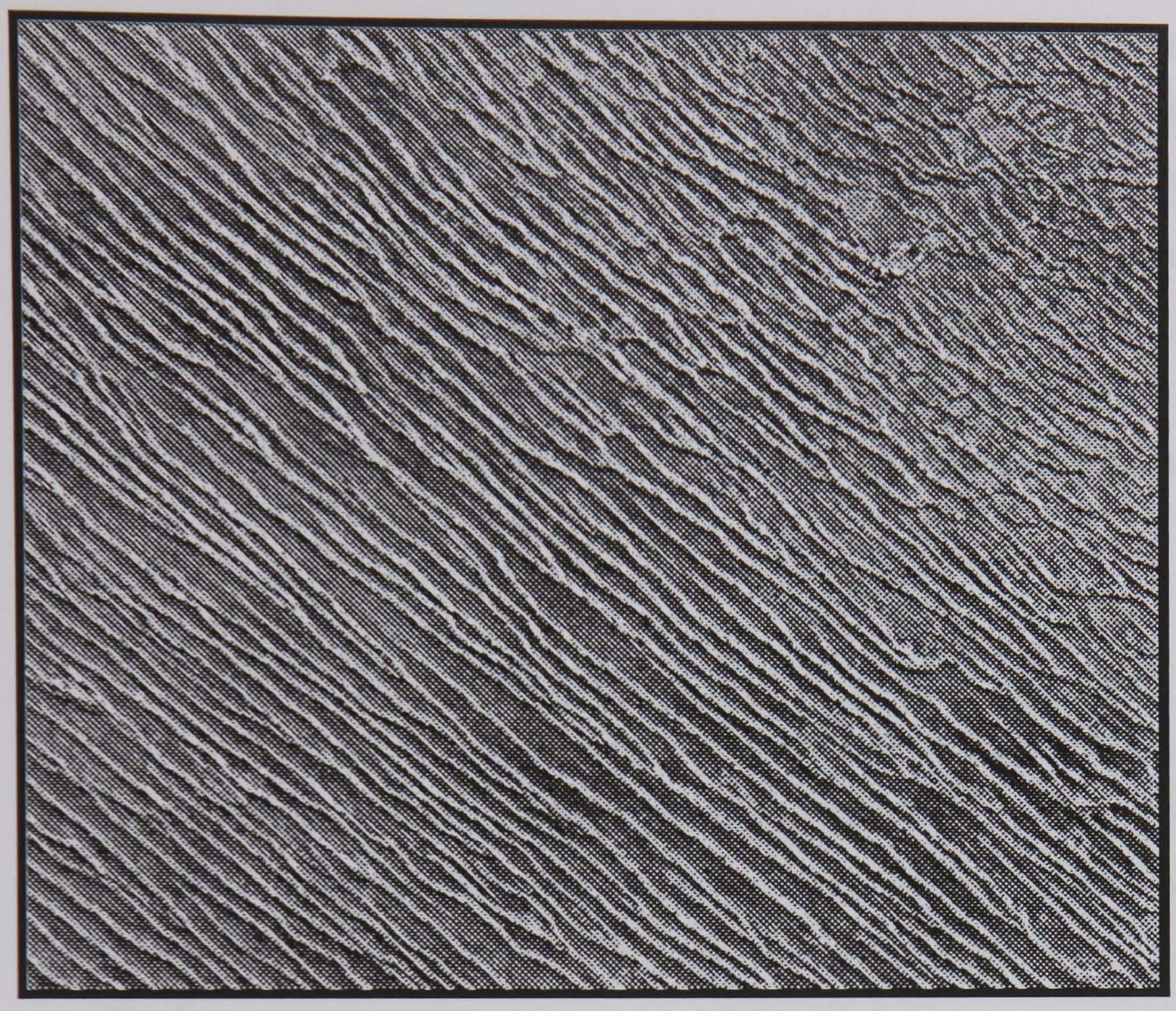

Figure 2.2 Landsat TM image (band 4) of section of the Kalahari desert depicting linear sand dunes.

2.2 Parameters of Lineaments

The mappable aspect of lineaments means that there are some parameters defining them. The aim of mapping is therefore to isolate one or all the parameters pertaining to lineaments from which interpretation and explanation can be sought depending on the researchers interest. The following lineament parameters on satellite images and air photographs can be defined with reference to figure 2.3. Since this thesis is based on parallel lineaments representing glacial and aeolian landforms, the parameters will be described in relation to this type of lineaments.

1. **Length**

   The length of lineaments (l) is the distance of the long axis figure 2.3b On satellite images, lineaments are usually discernible as a single line with limited width. Mapping this parameter by photointerpretation of satellite images poses no problem. In conjunction with orientation, most lineament studies have been based on this parameter. This is especially true where satellite imagery has been utilised.

2. **Width**

   This is simply defined as the short axis of lineament(w) measured from the centre and perpendicular to its length. It is a parameter which is seldom studied with reference to lineaments and when such studies have been attempted, aerial photography as opposed to satellite images have been utilised.

   On satellite images, the width of a pencil mark on the images can represent distances that are even greater than the width of lineaments due to the scale of satellite images. Aerial photography and large scaled remote sensing using aircraft are therefore necessary for studying this parameter

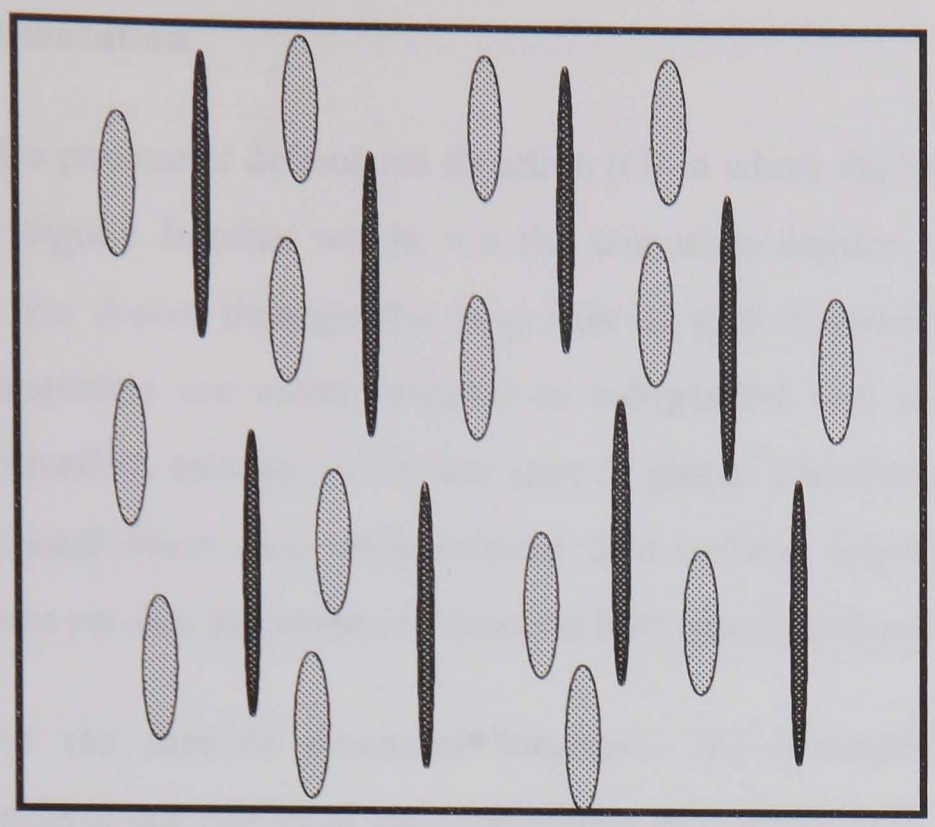

Figure 2.3a Sketch showing lineament field with two different sets of lineaments

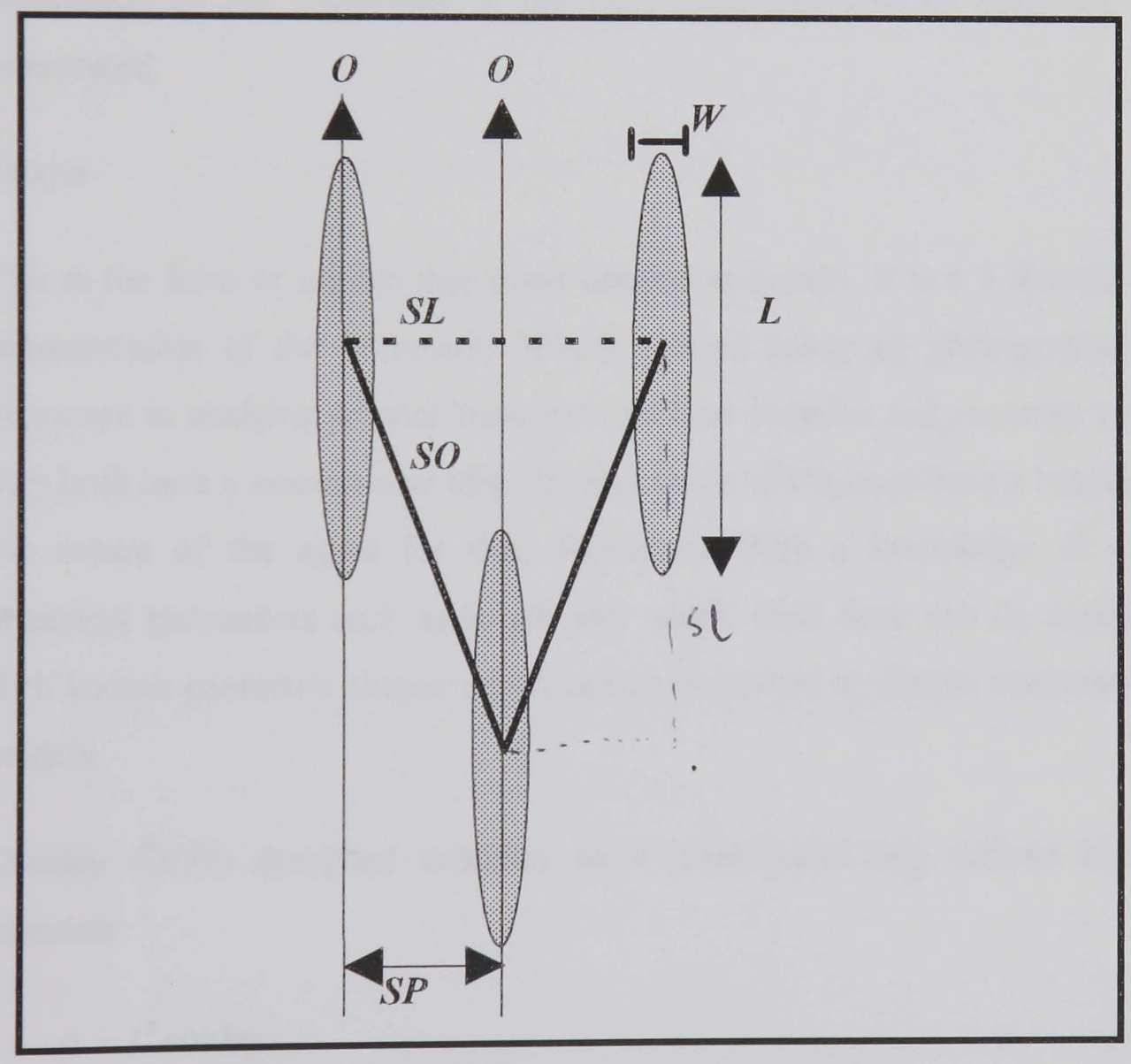

Figure 2.3b Parameters of lineament, O = orientation, *L* = length, *W* = width, *SL* = parallel spacing, *SO* = oblique spacing, *SP* = perpendicular spacing

3. Orientation

This parameter defines the direction (*O)* in which the long axis of the lineament is aligned. In other words, it is the azimuth in degrees east or west of north, of a line drawn through the long axis of each lineaments. Glacial and aeolian lineaments are mostly aligned as sub-parallel sets since the agents of their formation, moving ice for the case of glacial lineaments and wind for the case of sand dunes were unidirectional. This uniform direction has given rise to the term parallel lineaments to describe both glacial and aeolian lineaments.

For the case of structural lineaments the orientations are not necessarily uniform but can have multi-directions in a single field. In studies of this type, the orientation of the single lineaments together with their lengths and width can be measured and plotted on a rose diagram from which the dominant orientation of the lineaments in the field concerned can be observed and interpreted.

4. Shape

This is the form or outline that some lineaments posses. It is a 3 dimensional representation of the lineament. Mostly studied using air photographs and important in studying parallel lineaments such as drumlins and yardangs where they both have a smooth near ellipsoid like shape which must have a bearing to the nature of the agent for their formation. With a knowledge of other lineament parameters such as length and width, their form can be described with known geometric shapes which can be described by simple mathematical models.

Chorley (1959) described drumlins as a lemmiscate loop defined by the equation:

$$\rho = l^2 \cos kq \qquad \textbf{2.1}$$

Where *l* is the length of the long axis and k is determined by the shape of the loop such that unity represents a circle, and as k increases the elongation of the lemminiscate loop increases as well.

Reed et. al (1962) use the equation of the ellipsoid of the form:

$$\mathbf{x^2bc + y^2ac + z^2ab = abc} \qquad \mathbf{2.2}$$

to describe the shape of drumlins, where the centre of the ellipsoid is at the origin and the its semi-axes, a, b, c coincides with the rectangular co-ordinates direction x, y, and z.

This parameter has been used in drumlin research but is not relevant to most lineaments types.

5. Height

This is the measure of the distance of lineaments above the surrounding terrain (*h*). It is difficult to map this parameter on satellite images and is only possible on air photographs when a stereo model is used. With the ability of off-nadir viewing in SPOT imaging, stereo pair images can be utilised. Images from this satellite could therefore be useful for mapping this parameter if the spatial resolution is sufficient. Interferometry is also a possible means of deriving height information from spaceborne SAR images.

6. Density

This parameter measures the number of lineaments per unit area(*d*). The drawback to this definition which was applied to study drumlins is that it measures lineaments as a set of points (Doornkamp and King, 1971) without taking into consideration the aerial extent and volume of the lineaments. The simplistic view of this parameter is not enough. Factors such as topography, aerial extent, and other influencing landforms or features and the changing

dimensions of the individual lineaments need to be taken into account in order to give an accurate definition to this parameter (Menzies, 1979)

7. **Spacing**

Spacing is the measure of the distance between lineaments. Three types of spacing can be defined thus:

***Parallel Spacing(sl)*:** Which is the distance between the centres of any two adjacent lineaments measured in the direction of the mean local orientation (figure 2.3b)

***Oblique Spacing(so)*:**The distance between the centre of the two lineaments (figure 2.3b)

***Perpendicular Spacing(sp)*:** This is a measure of the distance between lineament centres measured at right angles to the mean orientation (figure 2.3b)

Spacing and density are off course fundamentally related in an inverse manner in that the greater the lineament spacing, the lower the density.

8. **Distributions**

This is not a parameter of individual lineaments but is a description of the location of lineaments in relation to one another. Key questions to answer are whether there is an ordered pattern in the distribution of lineaments or whether they are randomly located. A non random distribution will suggest the presence of a pattern, which may be important for developing process hypotheses or testing them. To test for randomness of a group of lineaments in an area, the method of nearest neighbourhood analysis has been commonly used (Smalley and Unwin., 1968; Trenhaile, 1971; Pinder and Witherick, 1972; Menzies, 1979). This statistic tests how the distribution of a set of lineaments departs from a random one. The statistic is defined as:

$$\mathbf{r} = \frac{\mathbf{2d}}{\sqrt{\frac{\mathbf{A}}{\mathbf{N}}}} \qquad \mathbf{2.3}$$

where d is the mean linear distance between the centre of lineaments of a specific area and the nearest neighbouring lineament, A is the area in metres square of study section, and N is the total number of lineaments in the whole

area. The value $2\sqrt{\frac{N}{A}}$ is used to predict the average distance between randomly distributed nearest neighbours and the nearest neighbourhood analysis involves computing this predicted value with the observed value d.

The nearest neighbourhood statistic, r given by the predicted and observed value can be interpreted thus: If r is less than 1, it implies that the expected average distance between lineaments must be greater than the calculated mean distance d. For this to happen, the lineaments be closer together i.e. clustered, with perfect clustering attained when r = 0. If on the other hand r = 1, it implies that the expected and the calculated distances for the lineaments are the same and thus random in their distribution.

Alternatively, if r is greater than 1, it means that the expected average distance between lineaments is less than the calculated mean distance. This occurs when the points are more regularly spaced than in a random situation. Maximum regularity is achieved when r is 2.15 (Pinder and Whitherick, 1972)

Results of neighbourhood analysis lie along a continuous scale from 0 which is a random arrangement of lineaments to 2.15 which is a perfectly regular arrangement of lineaments.

The expected average distance is based on randomly distributed points. This means that the results will be random with slight variation. The precision of this expected average distance is given by the range;

$$r - \left(\frac{0.26136}{\sqrt{\frac{n^2}{a}}} \right) \leq r \leq r + \left(\frac{0.26136}{\sqrt{\frac{n^2}{a}}} \right) \qquad 2.4$$

Which is the 95 percent confidence limit (Clark and Evans, 1954)

2.3 The Relevance of Lineament Parameters

In recent years, geomorphologists and geologists have approached studies on land-forms by making use of numerical information. To distinguish measurement of landforms from other application of geomorphology, the term 'Geomorphometry' has been used to describe the numerical analysis and portrayal of the earth's surface. It has been explained in the previous section that some of these features on the earth's surface manifest themselves as lineaments on satellite images and air photographs and that they exhibit parameters which can be quantified.

The term geomorphometry is not only limited to lineament studies on satellite images and air photos alone. It embraces the use of both map and field derived data

The next section discusses the relevance of the study of lineament parameters in relation to structural, glacial and aeolian lineaments.

2.3.1 Structural geological lineaments

The availability of Landsat imagery in the 1970's heralded a new era in structural geological analysis. It permitted the detection of lineaments representing important structural features that had gone undetected even in areas that had been extensively mapped by traditional fieldwork (Goetz and Rowan, 1981). Satellite images are now being used on a routine basis to map exposed and buried folds, faults and fractures.

Satellite images provide an orthographic view of the Earth's surface which can help to develop global tectonic models. Changes in vegetation and surface texture which are related to faults are difficult to see at close range in the field. The synoptic view of photographs and satellite images enable widely separated pieces of lineament to be linked as sharp and semi-continuous lineaments. In the case of

air photo imaging, the vertical exaggeration that is brought about by stereoscopic viewing will emphasise even the most subtle topographic features and reveal clearly any vertical displacement associated with faulting.

Satellite remote sensing of lineaments has the added advantage that lineaments buried beneath deep, unconsolidated sediments may have geomorphological expression visible at the ground surface. Berger (1982) for example located buried faults and topographic highs in the East Texas basins through their effects on drainage, vegetation and soil characteristics. Thumult (1984) also observed basement expressions of brittle fracturing on Landsat imagery of the Athabasca basin, despite cover of several hundred metres of sedimentary rocks and unconsolidated materials. In another case study, bedrock lineaments were revealed to be visible beneath 200m of glacial drift from Landsat images of the Michigan Basin (Vincent and Coupland, 1979). Satellite images are therefore useful for detecting and mapping buried structure (lineaments) where seismic information is not adequate.

Knowledge of the extent of known faults can be extended by analysing lineaments which have not been mapped previously from satellite images and their existence corroborated by gravity magnetic, and surface data.

Since structural lineaments are expressions of basement tectonic activity that have propagated upwards into the younger rocks, they can be used to infer stress and strain conditions at depth and thus aid as warnings for location of large scale engineering and architectural construction, nuclear power stations in particular.

There has been considerable interest in lineament mapping in recent years in the search for fractured reservoirs because many petroleum fields have reservoirs with fracture controlled porosity. In many instances, significant correlation of zones of concentration of lineaments derived from satellite images and petroleum reservoirs have been realised. Saunders and Thomas (1973) were among the first to make

this observation and determined that some spatial correlation existed between surface lineaments and subsurface oil and gas fields.

Other examples of studies using lineament mapping by remote sensing for petroleum exploration can be found in Henninger (1984); Wielchowsky and Davidson (1984); Stakowski (1984); Mathews et. al. (1984); Macdonald (1980).

Lineament mapping of fracture traces for locating weathered zones with relatively high porosity and permeability within the bedrock for the purpose of locating potential water wells have been studied by Lattman et. al. (1964) and Parizek (1967). As in the petroleum studies, they too show high correlation of lineament location parameter with well yield. The British Geological Survey have been involved in using lineament mapping from Landsat TM data to aid in well location in arid parts of Africa.

Although some productive wells can be located on non lineament areas, the consistency in well yield is less variable when located on fracture traces in favourable topographic and fracture setting.

With the increasing demand for mineral resources, remote sensing applications in the field of structural and lithological mapping is playing an important role in mineral exploration through the regional study of lineaments. Park and MacDiarmid, (1970) noted that structural studies have "unquestionably led to the discovery of more ore than has any other directed effort."

The use of satellite images to interpret lineaments by geoscientists who are well versed in aspects of tectonics and mineralisation can produce a powerful alternative tool for mineral exploration.

2.3.2 Glacial Lineaments

Glacial lineaments i.e. drumlins, drumlinnoids, flutes, crag and tails are one of the most prominent glacial features that are visible on air photos and satellite images. They are important for two reasons:

1. They record former direction of ice flow which thus enables the dynamics of palaeo ice sheets to be reconstructed. This contributes to the major scientific aim that seeks to understand the operation of the global climate system, and changes therein.

2. The inaccessible nature of the subglacial environment has resulted in us still not knowing the process activities that operate at the base of ice sheets. The nature of these processes and the controls on them are crucial for an understanding of ice sheet dynamics and stability. The morphometry of the landforms produced in this environment provide valuable tests for process hypotheses.

Studies on glacial lineaments have been focused mostly on drumlins, which are just one of the many types. They have been recognised as the most suitable landforms for geomorphometrical analysis (Trenhaile, 1971) because of their ease of identification. Their morphometry has been extensively studied with the aim of seeking solutions to their mode of formation and understanding Quaternary environments.

Their form has been studied by attempting to fit mathematical curves to their outlines by (Chorley, 1959; Reed et al., 1962; Doornkam and King, 1971) and their densities have been studied by (Reed *et al.*, 1962; Vernon, 1966; Hill, 1968; Smalley and Unwin, 1968; Doornkam and King, 1971; Miller, 1972; Gravenor, 1974). Explanations for the variations of densities have been suggested. Smalley and Unwin (1968) for example suggested that drumlin density might be expected to decrease up-ice in contrast to Hill (1968) who suggested the opposite.

Random distribution has been attributed to drumlin fields examined by Smalley and Unwin (1968) who analysed them using both the random placement model and the nearest neighbour analysis. This result has been contradicted by authors working in other areas. One study by Trenhaile (1971) showed a distribution between random and uniform spacing. The spacing of drumlins have been studied by Vernon (1966) who found non uniformity in spacing. Contrary to this, Reed *et. al.*, (1962) found spacings in drumlin fields to be normally distributed with a cyclicity in spacing. Trenhaile (1971) also found a similar results in the distribution of the spacings of these lineaments.

Drumlin fields have also been analysed in terms of their group orientation by Smalley and Unwin (1968); Reed *et al.*, (1962); Trenhaile (1971; 1975) to indicate directions of ice flow. The distribution of orientation has also been studied by Reed *et al.* (1962) and as expected shows a normal distribution. This is expected as the orientation of the lineaments are parallel. In areas where there are cross cuttings patterns (Clark, 1993) representing more than one flow pattern, orientation will be multimodal depending on the number of flow sets that can be observed.

The parameters of width, length and height have been used to describe drumlins by Hollingsworth, 1931; Charlesworth, 1939. Alden (1905) and Muller (1963) combined width and length ratio in order to classify streamlined features.

The width and length ratio have also been used to compare the morphometry of streamlined features between areas by Hollingworth (1931); Trenhaile (1971); Vernon (1966); Heidenrich (1964); Karczewski (1976).

As illustrated above morphometrical parameters such as length, width, height, spacing, density and shape of ice moulded landforms have long been thought to be crucial if theories of the genesis and glaciological significance of such landforms are to be constructed and tested. In the past these glacial linear features have been

studied mostly from information on air photographs, topographic and geological maps and from field mapping.

The representation of these features on topographic maps has been shown to be extremely inconsistent and unreliable (Rose and Letzer, 1975) and aerial photographs cannot be relied upon as they depict drumlins under specific lighting conditions. Field mapping has been championed as the best and most reliable means of deriving glacial lineament information. Unfortunately however, this is an extremely slow method of collecting data (e.g. 1 km square per day) and if morphometric analysis is performed, it is inevitable that the sample sizes will be rather small and often of the order of 50-200. It may be hypothesised that the lack of consensus that has arisen from the many morphometric studies performed in the 1970's and 80's relates to the small sample sizes.

The use of remote sensing provides an alternative source of data at varying scales which can be used to compliment past studies of these features and to extend sample sizes into the realm where consistent spatial patterns may be detected.

The use of satellite images with particular reference to glacial lineaments and ice sheet dynamics has led to some important advances. They permit glacial lineaments to be mapped over extremely large areas with a minimum of effort. Landsat imagery has been utilised to this effect and has provided valuable insight into former ice dynamics and the spatial pattern of glacial lineaments. For example, Punkari (1982) mapped the whole of Finland and Clark (1990) mapped most of previously glaciated Canada, with both studies providing completely new reconstructions of ice dynamics.

Remotely sensed data in the form of satellite images (Landsat, SPOT, etc.) and digitally scanned air photographs thus provide the capability for collecting extremely large data/sets pertaining to the morphometry of parallel lineaments. Once a methodology has been established it can be applied with the minimum of effort, relative to manual methods. Such analysis performed over large areas will

permit valuable inferences to be made regarding the genesis and significance of ice moulded landforms. A technique for quantitatively assessing the spacing and dominant frequency of parallel lineaments from remotely sensed data has been developed in chapter four.

It is clear from past studies that there are still many questions in glacial lineament analysis that have not been resolved. The inconsistencies are likely to be as a result of the limited area of study due to the limitations of the methodologies. Studying these lineaments from satellite images where wide area coverage can be obtained and defining a new methodology of collecting and analysing the data will contribute in arbitrating these contradictions and help in solving the long standing enigma of the formation of subglacial lineaments.

2.3.3 Aeolian Lineaments

Despite the harsh environmental conditions of arid areas where aeolian lineaments are located, these portions of the earth support a large proportion of the Earth's population and accounts for about 30 percent of the world's land surface.

There have been many attempts to explain the processes that occur in this type of environment and also the mode of formation of the many landform types. The search for the causes of the variation of aeolian sedimentary features which appear as lineaments on satellite images and air photos is one of the greatest challenges in aeolian sedimentology (Pye and Lancaster, 1993). A full understanding of this problem requires knowledge of the nature of the operative processes that have brought about these forms. It is believed that there must be a relationship between these processes and the morphometry of the features.

Studying active and late Quaternary aeolian systems provide vital information and aids in our knowledge of past aeolian deposits and climate and hopefully helps us to understand what the future response of deserts systems might be to climate change.

There have been numerous studies of aeolian lineaments and yet there is still no clear understanding of the factors that are responsible for their formation, and desert dynamics are still not properly understood. It has been accepted that these desert lineaments are formed by aeolian sand accumulation and the following factors are thought to be determinants of the form and scale of aeolian sand accumulations (Pye 1993):

- Sand availability
- Grain size distribution
- Wind velocity distribution and directional variability
- Vegetation cover and growth characteristics
- Nature of the underlying substrate
- Climatic and sea level changes
- Long term patterns of tectonic uplift and subsidence.

Researchers in this field have tried to seek relationships with parameters of these lineaments and one or more of the factor responsible for aeolian accumulation. Of all these factors, wind regime and sediment characteristics are thought of as the most influencing factor on the morphometry of individual lineaments and the relationship between adjacent ones (Thomas, 1988; Lancaster; 1981; 1986) shows that the granulometric characteristics of sand affects dune formation both across dune profile and within dune fields.

The relationship of the spacing between linear sand dunes and grain size has been studied by Wilson (1972a; 1972b) who concluded that widely spaced dunes were associated with coarser grain sizes. Contrary to Wilson's conclusion, Wasson *et al.* (1983) in their study of the Australian linear dunes did not find this spacing/coarse grain size relationship. Thomas (1988) also studied this relationship with linear dunes in the Kalahari desert and found that grain size was not a controlling factor for influencing dunes spacing.

Literature of the morphometry of linear sand dunes agree that there is a relationship between the spacing of linear dunes and their heights. Although there

is no strong relationship for individual linear dunes, a strong relationship exists when these lineaments are considered in blocks with a block representing a spatial unit of uniform morphometric characteristics (Wilson, 1972; Breed and Grow, 1979; Lancaster, 1982; 1983; Lancaster et al. 1987; Wasson and Hyde, 1983; Thomas, 1988; Lancaster, 1989). Their results showed that the correlation coefficient between mean height and spacing is different for differing areas. Wasson and Hyde (1983) explained that the these differences could be due to grain size and volume of sand available for their formation.

On the effect of wind and sand flow on aeolian lineaments, the case for linear sand dunes has been investigated by Tsoar (1979; 1983), and Livingstone (1986). Their results however are not in agreement.

With all these disagreements in the results of studies of aeolian lineament morphometry, the origin and development of these features have remained a controversial issue. There is therefore the need to redefine or modify strategies (methodologies) for collecting, analysing and testing new and or old hypotheses to come to objective conclusions.

Study areas have been limited in the past probably due to the harsh nature of the environment and the difficulty in collecting and analysing the data. Data were either collected from field studies or from large scale air photographs and maps. Satellite images can provide area wide coverage, providing large quantities of data which can be used to test old hypotheses or develop new ones. New methodologies too can be developed to analyse these data. This should contribute to the recognising and explanation of the different units of aeolian forms. The study could be extended to aeolian forms in different planetary systems of the universe.

2.4 Conclusion

Summarily, the importance of remote sensing to lineament study can not be underestimated. Remote sensing is changing the methods of data analysis. Its use may strengthen, discard or maintain our results from past studies and provides us with new models of our understanding of lineaments.

Despite the scepticism about "linear geo-art" from some authors (Wise, 1982) image interpretation is here to stay. It is a powerful tool for detecting and analysing geologic, geomorphic and cultural lineaments and their economic and environmental significance. It is more efficient, reliable, time saving, cost effective than conventional methods.

Advances in satellite imaging are growing rapidly. More satellites are being launched with varying spatial resolution from fine to coarse and with high spectral resolution across the electromagnetic spectrum. This is good news for lineament studies. Spatial resolution will discriminate the different features in terms of their sizes and the spectral resolution will distinguish lineaments according to their different composition.

The aim of this research is to use remote sensing techniques to characterise the spacing between parallel lineaments representing glacial features and linear sand dunes. A new methodology for analysing these spacings will be developed.

Chapter Three

Lineament Expression on Remotely Sensed Imagery

3.0 Introduction

An image is simply a picture of the distribution of radiance of a scene. We see lineaments on satellite images because the radiance, which has been converted to digital numbers(DN) and assigned different tones on an image varies across the scene, thus discriminating the different features. Lineaments are seen on the image when they contrast with the background and this is brought about by the variation of DN values.

The variation of DN across the scene depends on a number of factors such as the instrumental, operational and the radiometric quality of the imaging system and the physiography of the natural target. The lineaments considered in this thesis are mostly larger than the resolution of the images, but for sub-pixel sized lineaments there is the possibility that whilst they exist they do not influence the DN of that pixel to a great enough degree to be detected. In a situation where lineament size is smaller than the pixel size, the DN value will represent a mixed signature, thus a pixel may include a variety of covers and the brightness value may therefore not be indicative of the lineaments unless they dominates the pixel.

One of the characteristics of an imaging system that is important in capturing lineaments is the resolution of the system. Because of its importance in recognising lineaments, the next section will explain the various resolutions available and how they affect the imaging of lineaments.

3.1 Resolution of Satellite Images

The resolution discussion here pertains only to satellite images that use the visible and infrared portion of the electromagnetic spectrum.

Resolution is defined as the measure of the ability of imaging systems to distinguish signals that are nearly similar in a spectral sense and or close together in a spatial sense. Three types of resolutions namely spatial, spectral and radiometric resolutions can be defined for satellite imaging system. Successful identification of individual classes of lineaments within the image depends on both the spectral and spatial characteristics of the ground features making up the image and to a lesser extent on the radiometric resolution. Resolution is therefore an important factor which influences the ability to recognise and map lineaments. It is therefore necessary to establish understanding of the different meaning of the various resolution .

3.1.1 Spectral Resolution

This refers to the size of the specific wavelength intervals in the electromagnetic spectrum to which a sensor is sensitive (Jensen, 1986). The Landsat Thematic Mapper has a spectral resolution of seven bands with band 2 for example, measuring the range $0.52-0.62\mu m$ (visible green radiance influx). The other 6 bands are also sensitive to radiation from different parts of the electromagnetic spectrum. Having this number of wavebands is a plus in imaging lineaments as it increases the likelihood of distinguishing the different spectral response of a lineament from the background features.

Studying lineaments with multi-spectral resolution is useful as some of the features on the image may be hidden if the different spectral bands are considered one at a time. Band combination can display images in composites when the bands are well chosen to successfully identify features of interest on the image. Careful choice of

spectral bands to display an image could improve the detectability and mapping of lineaments.

In black and white aerial photography with a spectral resolution ranging from $0.4-0.7\mu m$ (i.e. visible light), the spectral resolution is said to be coarse and will be limited in discriminating lineaments in situations where there is a narrow range of spectral difference between lineaments and their surroundings.

3.1.2 Radiometric Resolution

The radiometric resolution measures the sensitivity of a detector on a satellite sensor to differentiate the strength of the radiant flux reflected or emitted by the lineaments. It defines the number of just-discriminable signal levels (Jensen, 1986). For Landsat 4 and 5 the radiometric resolution is 8 bits with values of signal strength ranging from 0 to 255. Previous Landsat sensors had 7 bit radiometric resolution.

This resolution is an important characteristic in studying lineaments in monochrome because in situations where lineaments and surrounding background have almost similar spectral characteristics, their radiometric character will be different if the radiometric resolution is large enough to differentiate slightly differing signal strength of lineaments and surrounding features.

In general, the greater the number of signal levels, the greater the detail of information the satellite can acquire, although Tucker (1979) found only less than 3 percent difference between radiometric resolution of 256 and 64 levels in distinguishing between vegetation types.

3.1.3 Spatial Resolution

This is the most widely mentioned resolution of satellite imaging systems. Short (1982) defined the spatial resolution as the fineness of detail depicted in an image which refers to the measure of the smallness of objects on the ground that can be

distinguished as separate entities. This definition is not rigorous because of the lack of quantitative meaning to it. To attach some quantity to it, Townshend (1981) used four criteria based on:

1. The geometric properties of the imaging system

In this case the spatial resolution is determined by sensor geometry in one of two ways either as the equivalent distance XY on the ground which is the diameter of a circle or as the solid angle *a* measured by the lines touching the scene edges (Figure 3.1). This represents the portion on the ground scene that is effectively measured by a sensor mounted on a platform orbiting the earth called the Instantaneous Field Of View (IFOV). The equations for IFOV are:

$$IFOV = \frac{Hd}{f}(metres) \qquad 3.1$$

$$IFOV = \frac{a}{f}(radians) \qquad 3.2$$

Where H is the height above the surface, d is the size of the satellite's detector, and f is the focal length of the satellite's optics and a is the angular instantaneous field of view projecting the IFOV (figure 3.1). In effect, IFOV represent the small section of the surface area that is reflecting or emitting radiation during the instant of sampling. The spatial resolution for satellite images is therefore controlled by the focal length of the optical telescope and the height of the space craft above the earth.

The IFOV of the TM sensor for example is given as 30 metres or 0.43 miliradians. This simply means the detector measures radiance from a ground area of 30 m and records it as a discrete signal which is represented by a vector defining its location and the strength of the signal (DN) associated with a picture elements (Pixel). Spatial resolution defined in this way affects the imaging of lineaments. It was discussed in the previous chapter how measured lineament parameters may vary with image scale. Because scale is dependent on the resolution of the image, the

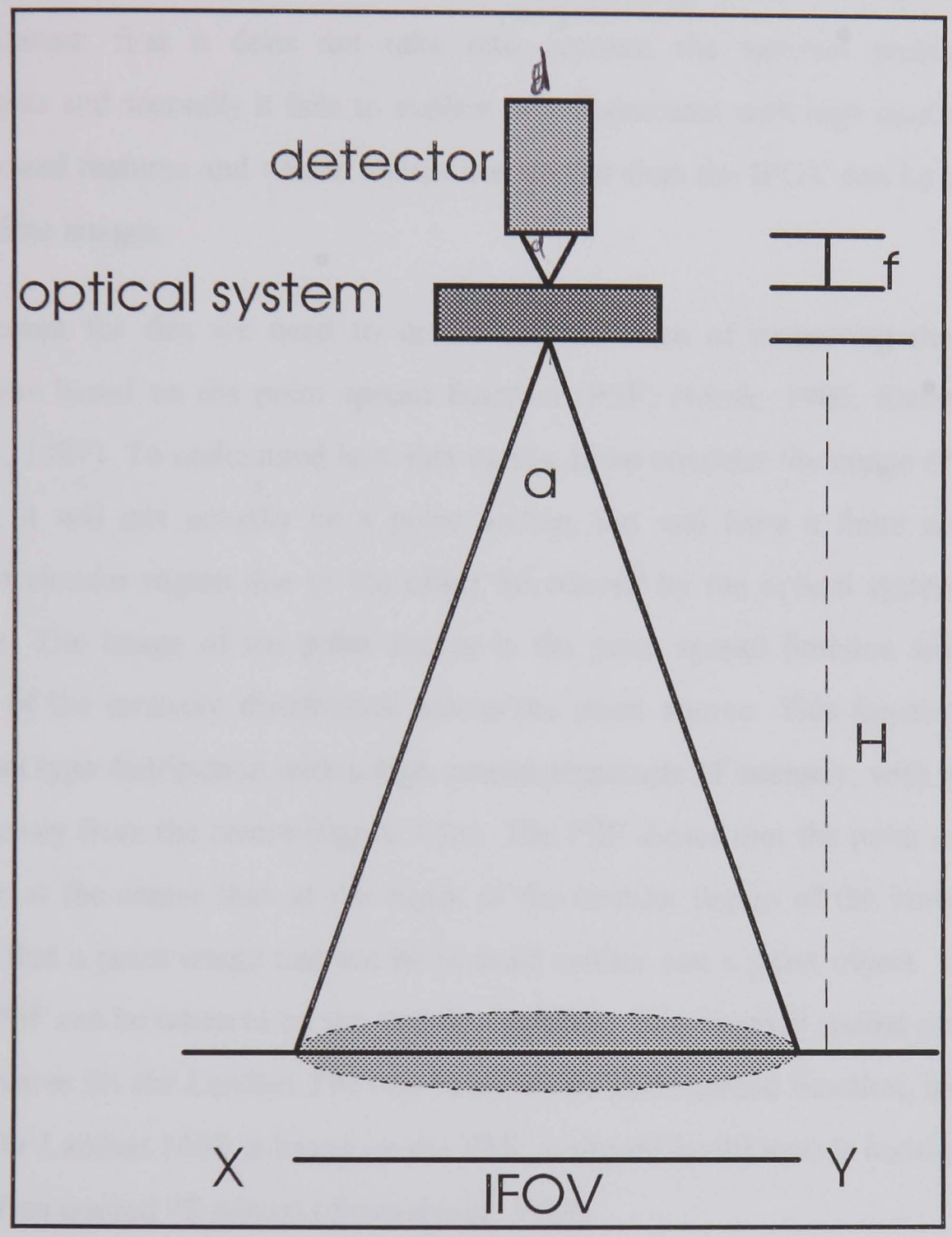

Figure 3.1. Instantaneous field of view based on the geometry of the imaging system. i.e. the angular instantaneous field of view(a), the detector size(d), the focal length(f) and the altitude of the satellite(H)

spatial resolution is a prime factor in detecting lineaments. By this definition one can conclude that lineaments with spatial wavelengths (i. e. spacing) larger than the spatial resolution of the satellite will be discernible and those with wavelengths smaller than the resolution of the satellite will not.

This definition however is not adequate for describing the spatial resolution for two reasons; first it does not take into account the spectral properties of lineaments and secondly it fails to explain why lineaments with high contrast with background features and whose widths are smaller than the IFOV can be detected on satellite images.

To account for this we need to define another form of measuring the spatial resolution based on the point spread function (PSF) (Moik, 1980; Slater, 1980; Mather, 1987). To understand how this works, if we consider the image of a point source, it will not actually be a point source, but will have a finite area with diffused circular region due to the effect introduced by the optical system of the satellite. The image of the point source is the point spread function and is the record of the intensity distribution across the point source. This function has a Guassian type distribution with a high central amplitude of intensity, with intensity tailing away from the centre (figure 3.2a). The PSF shows that the point source is brighter at the centre than at the edges of the circular region of the image. This proves that a point image can not be realised neither can a point object. The size of the PSF can be taken to be the spatial resolution. The nominal spatial resolution of 30 metres for the Landsat TM was based on its point spread function, and if the IFOV for Landsat MSS is based on the PSF, it should be 90 metres instead of the more often quoted 79 metres (Townshend, 1981).

An image can thus be regarded as the summation of point spread functions of points in the scene with each having an amplitude corresponding to its scene radiance. For darker points, the PSFs are inverted. Where there are spectral variation within the IFOV of the sensor, the PSF will vary in amplitude depending on this spectral variation.

The ratio between the brightness of a point source and its background is the contrast and the higher the contrast, the more detectable the point is. The more rapid the change away from the point to the level of the background is, the better the resolution as shown by the PSF represented by the solid line in figure 3.2a. The broken line represents low contrast and a smaller brightness gradient resulting in poorer resolution. Whether two points can be discriminated depends on their separation and their contrast as figure 3.2b shows. The solid lines show two points that can be distinguished since the gradient of PSF is high implying high contrast, but are barely distinguishable at low contrast.

Definition of IFOV in terms of PSF explains why lineaments which are smaller than the IFOV, 79 metres for the case of Landsat MSS can still be observed on these images. Slater showed that the object should be at most 25 percent of the resolution for it to be indistinguishable in size from a point source. This means that for a Landsat TM, of 30 m resolution, any object less than 7.5 m in size on the ground would be imaged with the same image size as that of the point spread function of the system.

2. The Ability to Measure Repetitive Targets

This is another measure of spatial resolution, but which uses targets to define the measure. When based on the ability to measure periodicity of repetitive targets, the targets are assumed to be linear and parallel with a known separation which is related to their spatial frequency. The spatial resolution is the measure, when the objects contrast strongly with their background, of the separation at which the contrast between the parallel linear objects becomes too small to permit visual distinction as an individual line. The unit of measurement is line pairs per millimetre or cycles per millimetre

By this method, the spatial resolution is measured by utilising the contrast of the targets and their background. This is measured by the Modulation(M) defined by the equation:

$$M = \frac{I_{max} - I_{min}}{I_{max} + I_{min}} \qquad 3.3$$

Where I_{max} and I_{min} are the maximum and minimum radiance intensity parameters respectively (Mather, 1987).

The ratio of the image to object modulation produces a value between 0.0 and 1.0 called the modulation transfer function(MTF) This ratio varies with spatial frequency i.e. the spacing between the periodic linear targets .

The spatial resolution can be defined using MTF as the effective instantaneous field of view EIFOV which is defined as the ground distance corresponding to the number of pairs of the linear objects per millimetre at the 50 percent modulation transfer function point. Mather reported a value for EIFOV for Landsat MSS and TM to be 66m and 30m respectively with that for Landsat TM compiled at the 35 percent of the maximum value for MTF. This is different from the IFOV based on the geometry of the sensor which are 79 metres and 45 metres for Landsat MSS and TM respectively.

The problem with this method of defining spatial resolution is that it is based on theoretical targets and is likely to be different when the instrument is based on actual field targets like lineaments. The method is mostly used for defining spatial resolution for photographic sensors.

3. The Ability to Measure Spectral Properties of Small Finite Targets

This definition takes into account the spectral properties of the targets and can be viewed as a better way of defining it as remote sensing is basically the measurement of the spectral properties of scenes.

Resolution in this case is defined by the effective resolution element (ERM). This element is considered to be a single homogeneous circular object, surrounded by a larger homogenous object field whose radiance is 30 percent of the full scale capability of the measuring sensor (Short, 1982). Short defined ERM as the

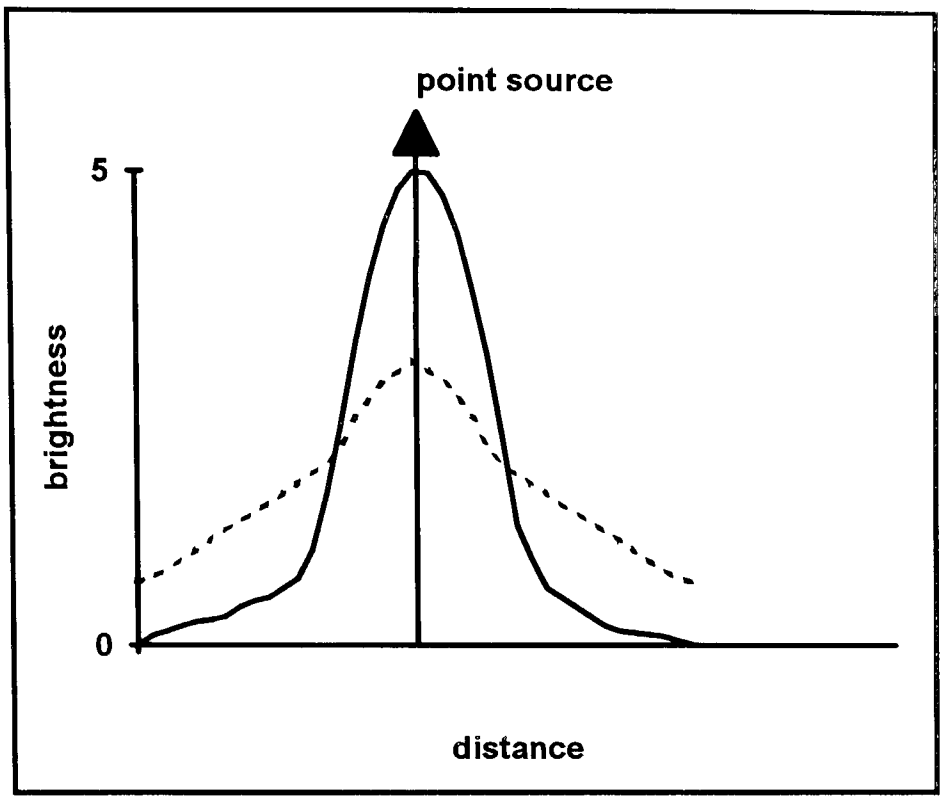

Figure 3.2a. Point spread function of point source. Centre of point source is brighter shown by the arrow and the edges of the point source exhibiting tailing of the PSF are less bright. Resolution and contrast is better for point source of solid line and poorer for that of the broken line.

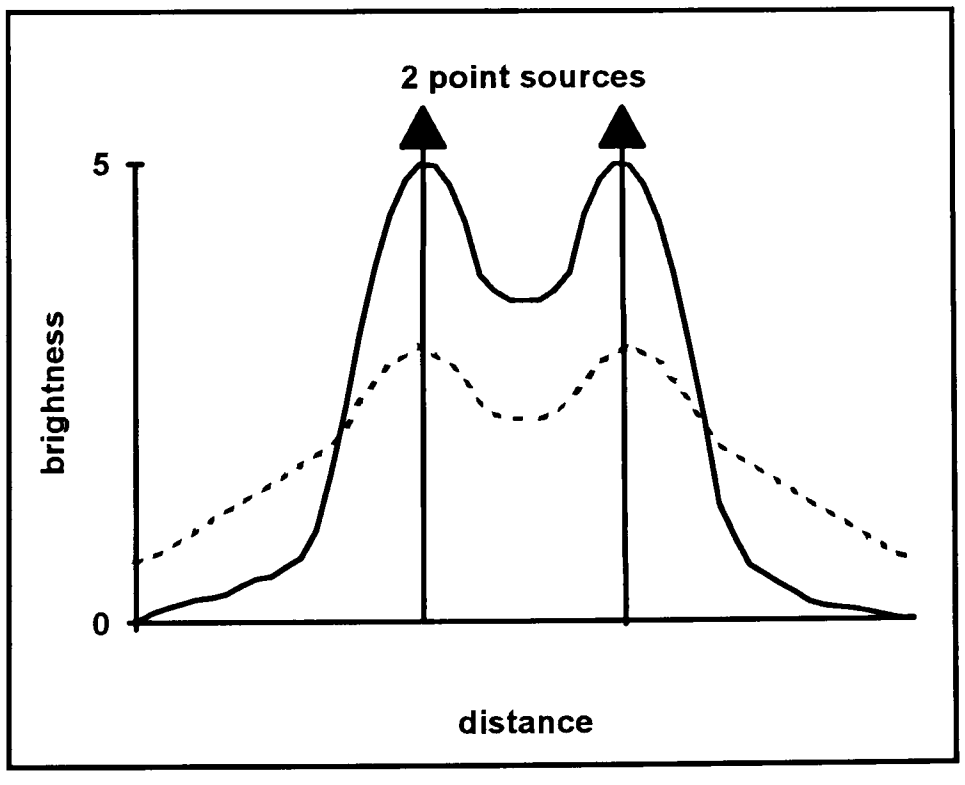

Figure 3.2b. Two point sources close to one another. The points will be resolved when contrast is high as in the case of the solid line and are barely distinguishable with low contrast as in the case of the broken lines

minimum area of the central object whose spectral properties may be distinguished from the surrounding field with a 95 percent confidence that the recorded value differs from the actual values by no greater than 5 percent of the sensor full scale value. Simonett (1983) gave the ERE for Landsat MSS to be 86 metres and 35 metres for Landsat TM.

Although this method based on radiometric as well as spatial characteristics of the signal source is a more realistic indicator of spatial resolution, it is difficult to conduct measurements on the earth's surface and thus the method is impracticable. Mather (1987) noted that spatial resolution based on this method is more relevant in classification of multispectral images.

4. **The Ability to Distinguish between Point Targets**

This is concerned with the ability of the imaging lens to recreate the image of a single point on a target as a diffraction pattern in the image plane. The pattern is considered to be a bright central disc surrounded by light and dark rings. Two points target become resolved when the bright central spot of the first disc falls on the outer most dark ring of the second. The minimum separation between the two points sources to achieve this is the measure of the spatial resolution of the imaging system. This method is mostly used for defining resolution for photographic systems.

3.2 Representation of the Image

Remote sensing images can be represented in two ways either in the frequency domain or in the spatial domain:

1. **Frequency Domain:** Conceptually this system of representing an image can be likened to fitting a continuous function through the discrete DN values plotted along each row or column. If we consider this graph of brightness

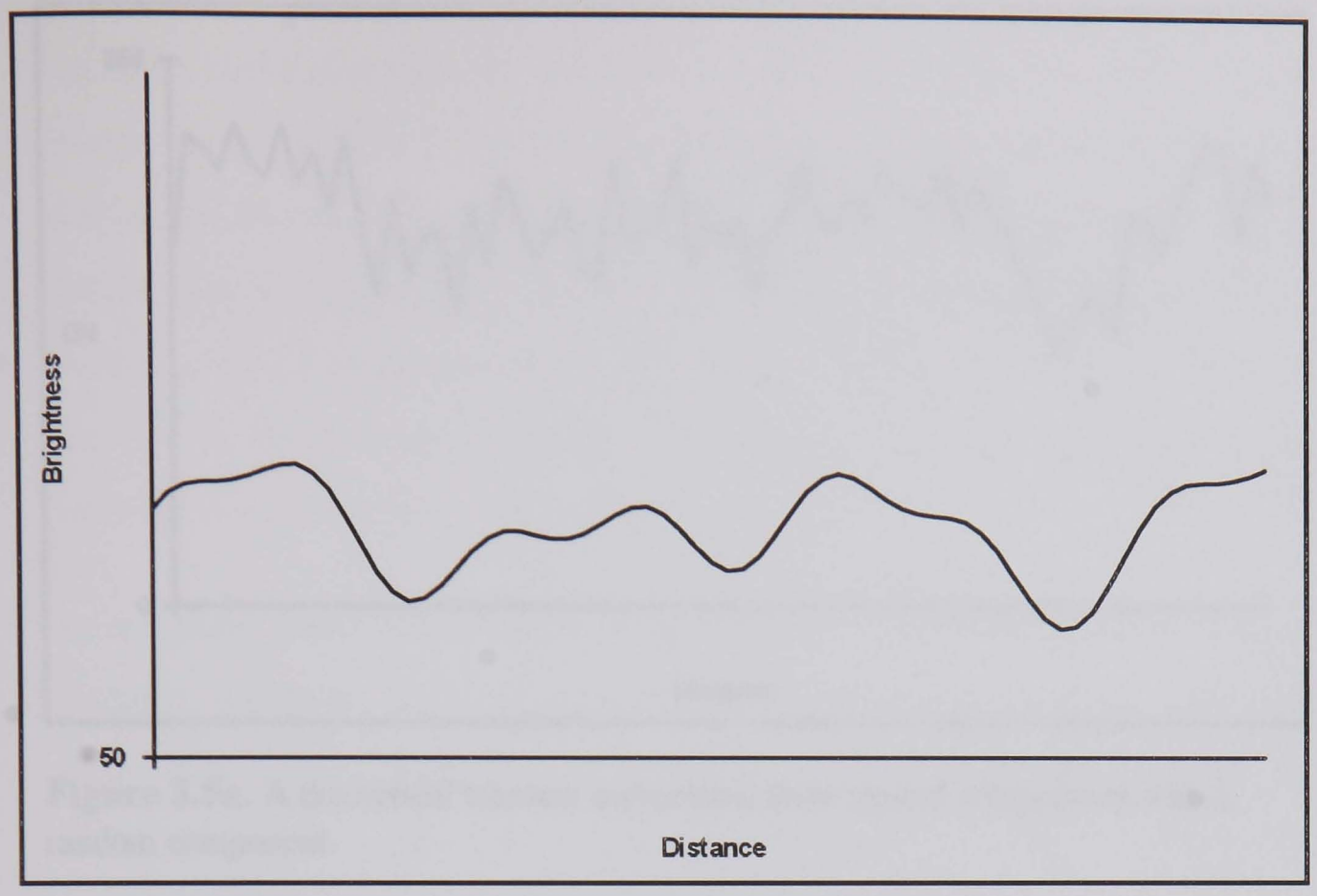

Figure 3.3. Radiometric transect representing the image in the frequency domain

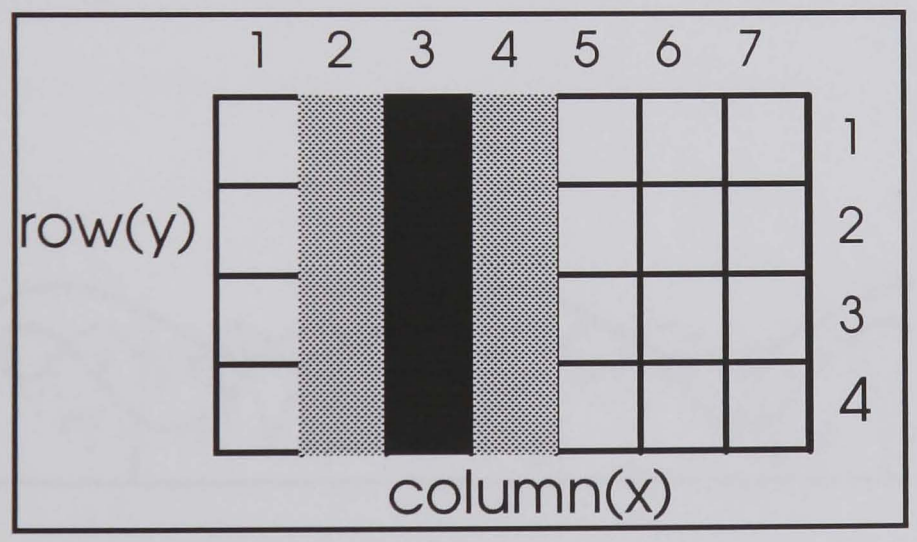

Figure 3.4. Raster format representing the image in the spatial domain

Figure 3.5a. A theoretical transect comprising three spatial components with a random component.

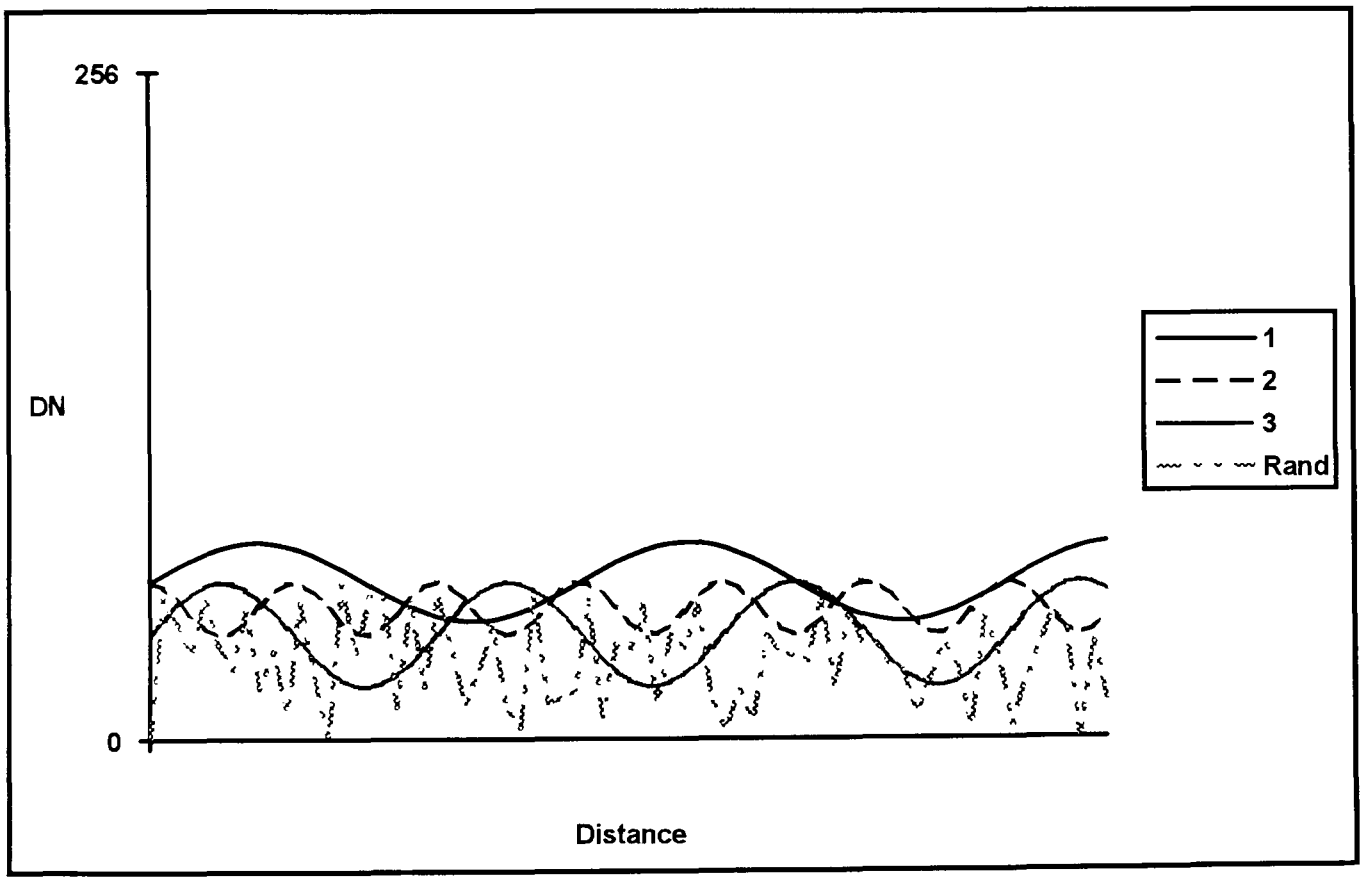

Figure 3.5b. Decomposition of transect of figure 3.5a into its constituent spatial frequencies and random component.

(DN) against distance between two points on the image, we will have a complex curve (figure 3.3). This curve gives the value of the PSF at specific points along the line. The curve has been plotted with the DN values. These values are related to the PSF as they relate to the scene brightness value. For bright points along these lines, the curve is a maximum and minimum for darker points. This curve can be seen as the representation of the image along the line in the frequency domain. Throughout this thesis, the curve will be referred to as the radiometric transect.

In an image, there is a complete range from high frequency to low frequency features. All these features are interwoven in the image structure. A graph of DN value against distance is a complex curve representing the different features on the image with edges representing lineaments having a steep gradient of DN. Peaks and valleys along a transect taken from an image containing parallel lineaments are very prominent.

The image in the frequency domain can therefore be broken down to its constituent spatial frequency components by a mathematical technique as illustrated by figure 3.5. It is the aim of this research to develop mathematical method for isolating this spatial frequency from images with parallel lineaments and extract meaningful information about the parameters of the lineaments.

2. **Spatial Domain** This is the row and column co-ordinate system in which images are normally expressed. The image is formed from a regular two dimensional arrangements of the picture elements(pixel) in X-Y space or column/ row space, with each pixel representing finite area in the scene. The size of the ground area represented by the pixel is also related to the effective spatial resolution of sensor imaging system. The final dimension of the pixel may be affected by the electronic sampling rate of the detector. This is why although the IFOV for Landsat MSS is 79 metres, the pixel size is 79 by 56 metres instead of 79 by 79 metres.

Within the image X-Y array, another varying parameter introduces a third dimension in the Z -direction to represent the value of the radiance which is recorded as the digital number(DN) within each picture element.

A two dimensional array can be built from all the pixels from an imaging system with each pixel 's DN value represented as different grey levels. These pixels are usually arranged in their proper relative position with respect to their corresponding position on the surface's of the earth. This gives an accurate geographically portrayal of that portion of the earth.

A representation of the DN values of the different pixels generates a rectangular array of different DN values thus producing an image in the raster format Figure 3.4. This is the image in the spatial domain.

Considering the different resolutions and the representation of images, the next sections explain why and how we see lineaments.

3.3 How Lineaments appear on Imagery

The detection of lineaments on satellite imagery depends on the single requirement that lineaments differ from their background features spatially and spectrally. These requirements can be accounted for by the resolution of the imaging system as explained earlier. The DN values representing the lineament should be different from that of the DN values of the background. Lineaments are therefore expressed on imagery as straight tonal boundaries.

There are a number of considerations regarding how lineaments are expressed in remotely sensed imagery: generic explanation describing how the arrangement of

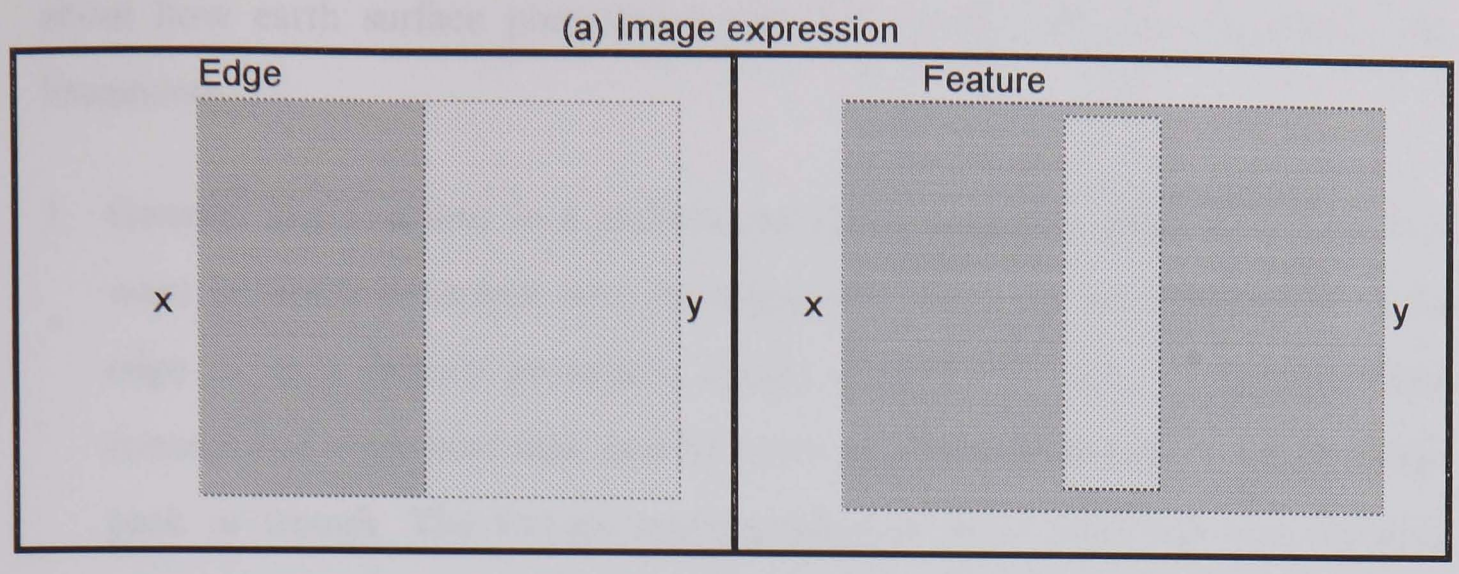

Figure 3.6 Raster array representation of an image expressing lineaments as (i) edge or as (ii) a feature

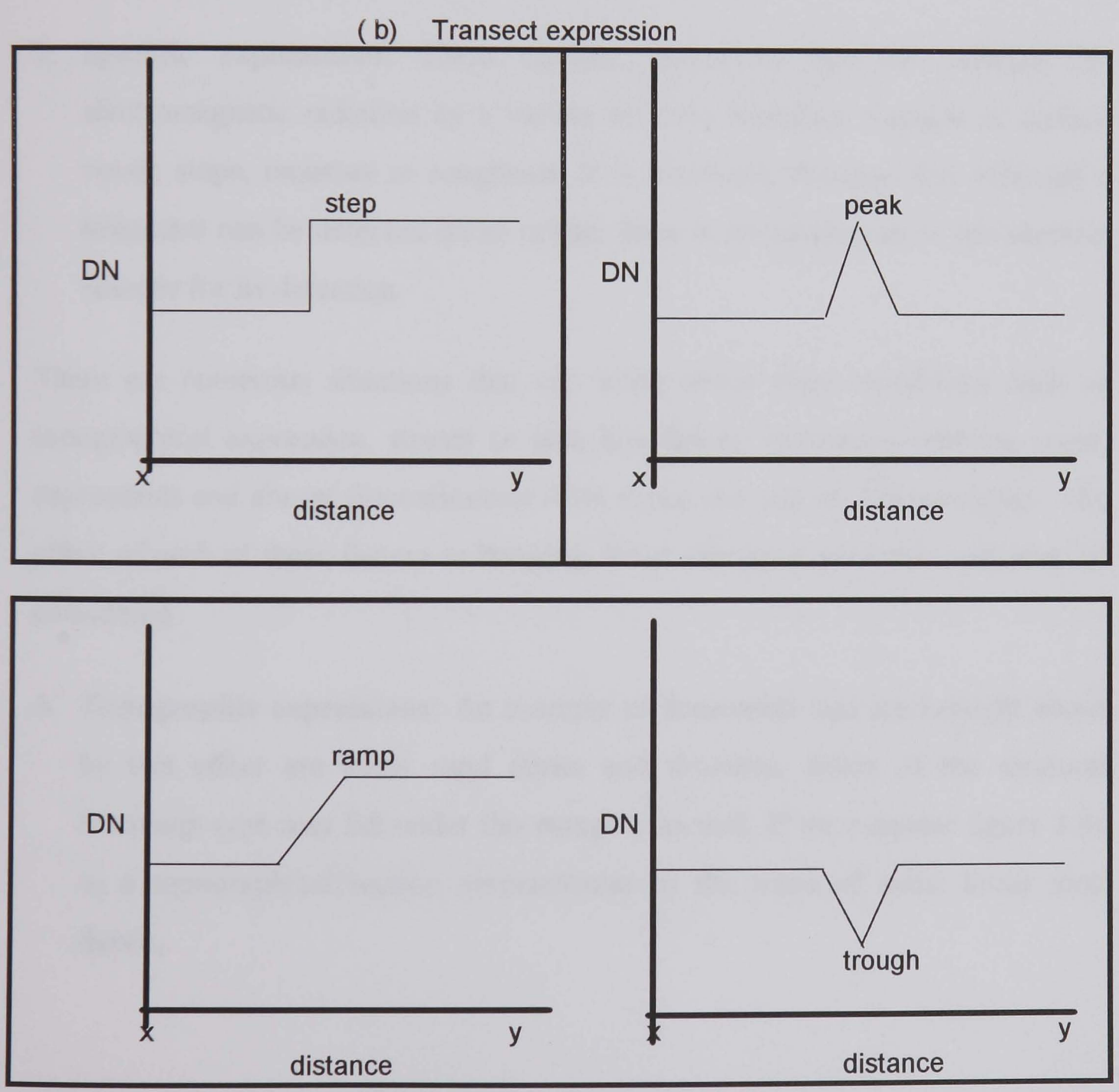

Figure 3.7 Illustration of the image on a transect as a step and a peak for the edge, and feature representation respectively. The ramp and trough representation does not apply in this case.

individual measurements (DN) produce lineaments; and specific explanations about how earth surface phenomena give rise to the DN that demarcate the lineaments.

1. **Generic explanation:** In a raster array representing an image, there are two ways in which lineament may be expressed. They can be represented as an edge or as a feature possessing width. Figures 3.6 and 3.7 illustrate this concept and show how they may be represented on a transect, as a step, ramp, peak or trough. The feature representation is more than just two adjacent edges in that there is a spectral difference between the area bounded by the edges and the background . These features may be between one and many hundreds of pixels wide, whereas an edge has no width.

2. **Specific explanation:** Earth surface lineaments can be detected by electromagnetic radiation by a variety of ways including changes in surface cover, slope, moisture or roughness. It is commonly the case that although a lineament can be detected on an image, there is uncertainty as to the physical reasons for its detection.

There are numerous situations that can bring about these conditions such as topographical expression, stream or lake boundaries, vegetation patterns, gaps, depressions and abrupt discontinuities from rocks and soil of different types. The effect of each of these factors in bringing about this tonal gradation will now be considered.

A. **Topographic expressions:** An example of lineaments that are brought about by this effect are linear sand dunes and drumlins. Folds of the strutural lineament type may fall under this category as well. If we consider figure 3.8a as a topographical section perpendicular to the trend of some linear sand dunes,

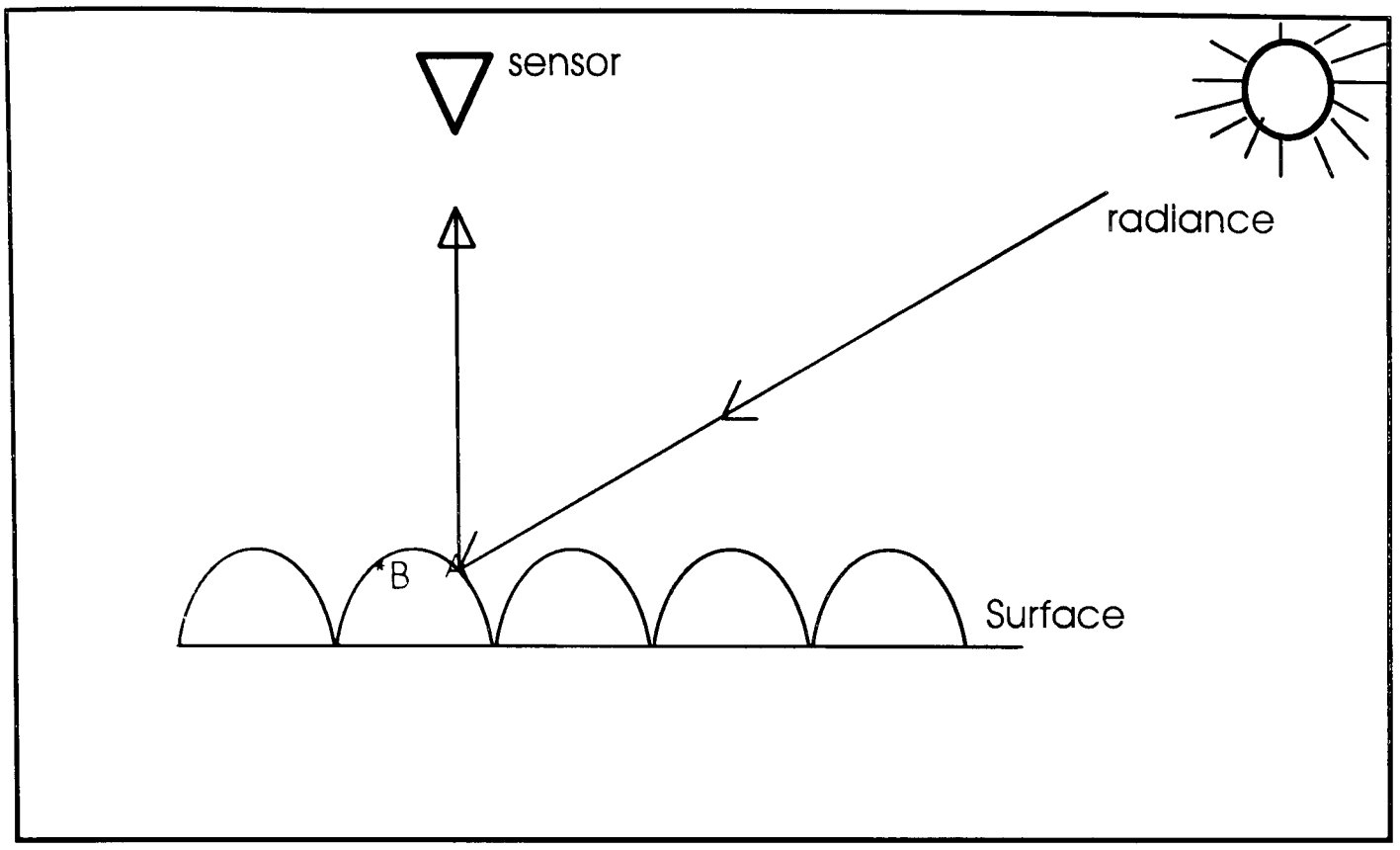

Figure 3.8a Representation of lineaments due to topographic characteristics as in linear sand dunes where the peak of the figure is the crest of the dune and the trough is the bed of the dunes.

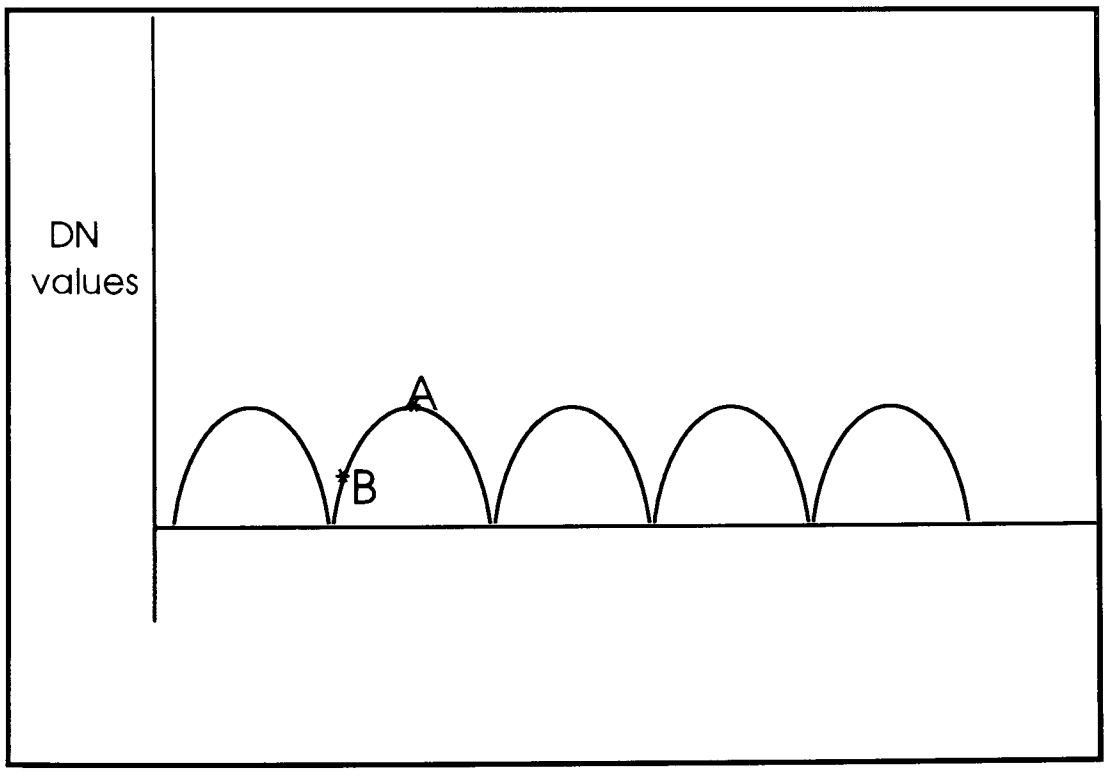

Figure 3.8b The plot of DN values along the transect of figure 3.8a. with a shift in phase. The relative spatial position of points along the transect of figure 3.8a remains the same as does the wavelegth.

then electromagnetic radiation falling on the point A on the figure will be most highly reflected to the imaging sensor due to the angle at which it meets the bed of the linear sand dune. Meanwhile point B on the dunes will receive little radiation and limited illumination will be received by the satellite.

The imaging system will measure a high DN value for point A and a lower one for point B, thus displaying the linear dunes as lineaments with tonal variation. Point A reflecting more radiation will appear brighter than point B which reflected less radiation. The same applies to glacial lineaments and other lineaments with topographic character. A plot of the DN values along the transect will plot as a sinuous curve (figure 3.8b) with a phase shift but maintaining the wavelength of figure 3.8a. Since points A and B have different DN values due to difference in the effect of illumination, they will be detectable in the transect.

B. **Vegetation** In some situations vegetation can be found on the linear sand dunes with bare sand in between. This is often also true for the case of glacial lineaments. This effect may overshadow the effect of topography as vegetation is highly reflected by the electromagnetic radiation in certain wavelengths. It has been shown that the spectral reflectance of vigorous vegetation shows a low reflectance at the red and blue region of the visible spectrum with a higher reflectance in the green region. Pigments in the vegetation absorb energy for photosynthesis and reflect the green light to give vegetation their green colour. The infra red region shows a very high reflectance of radiation by vegetation (Curran, 1980, Curran and Milton, 1983, Mather, 1987, Elvidge, 1990, Murphy and Wadge, 1994).

Figure 3.9a represents linear sand dunes with vegetation on the crest of the dunes. Since the vegetation effect overshadows the topographic one, the

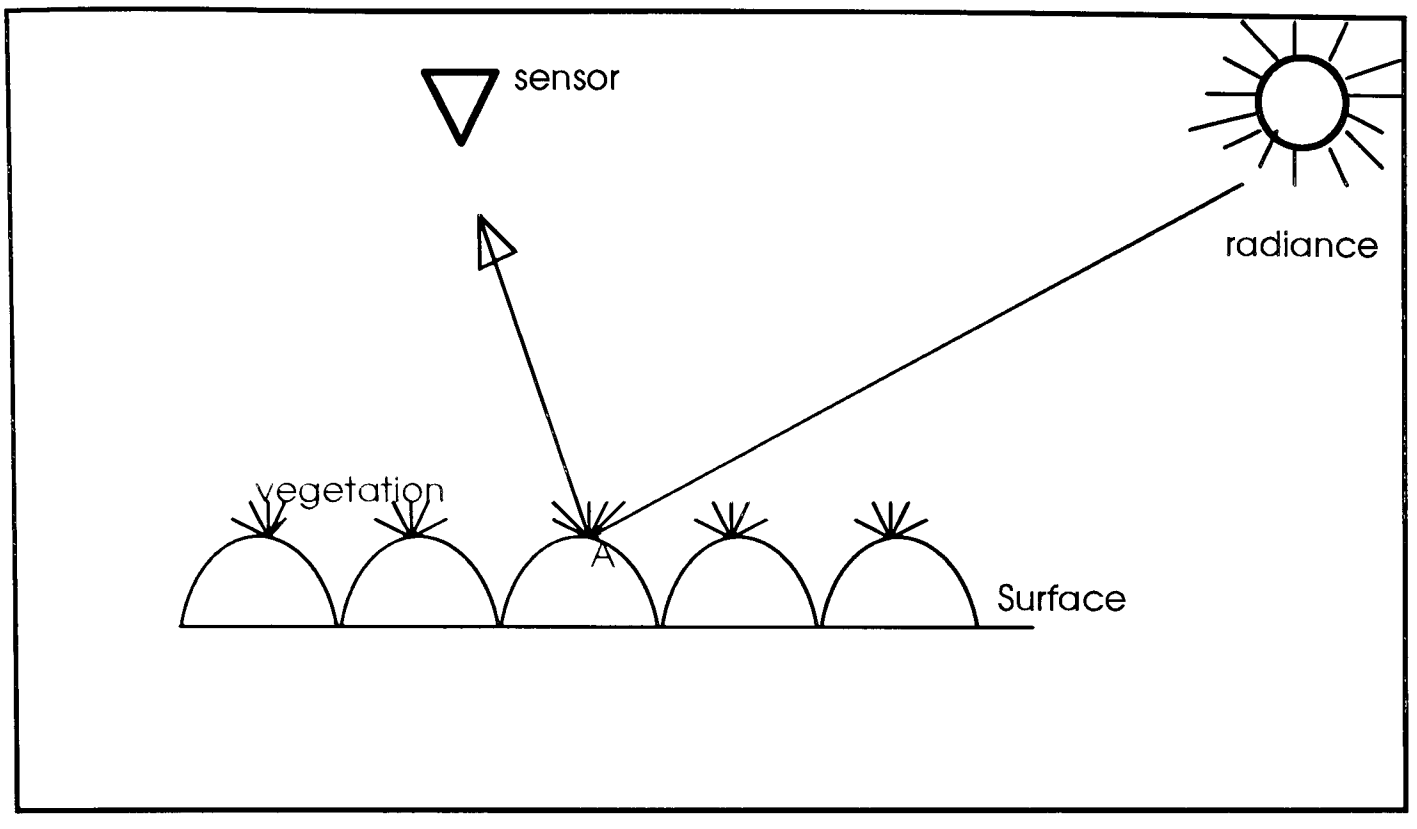

Figure 3.9a: Lineaments influenced by both physiographic and vegetation effect.

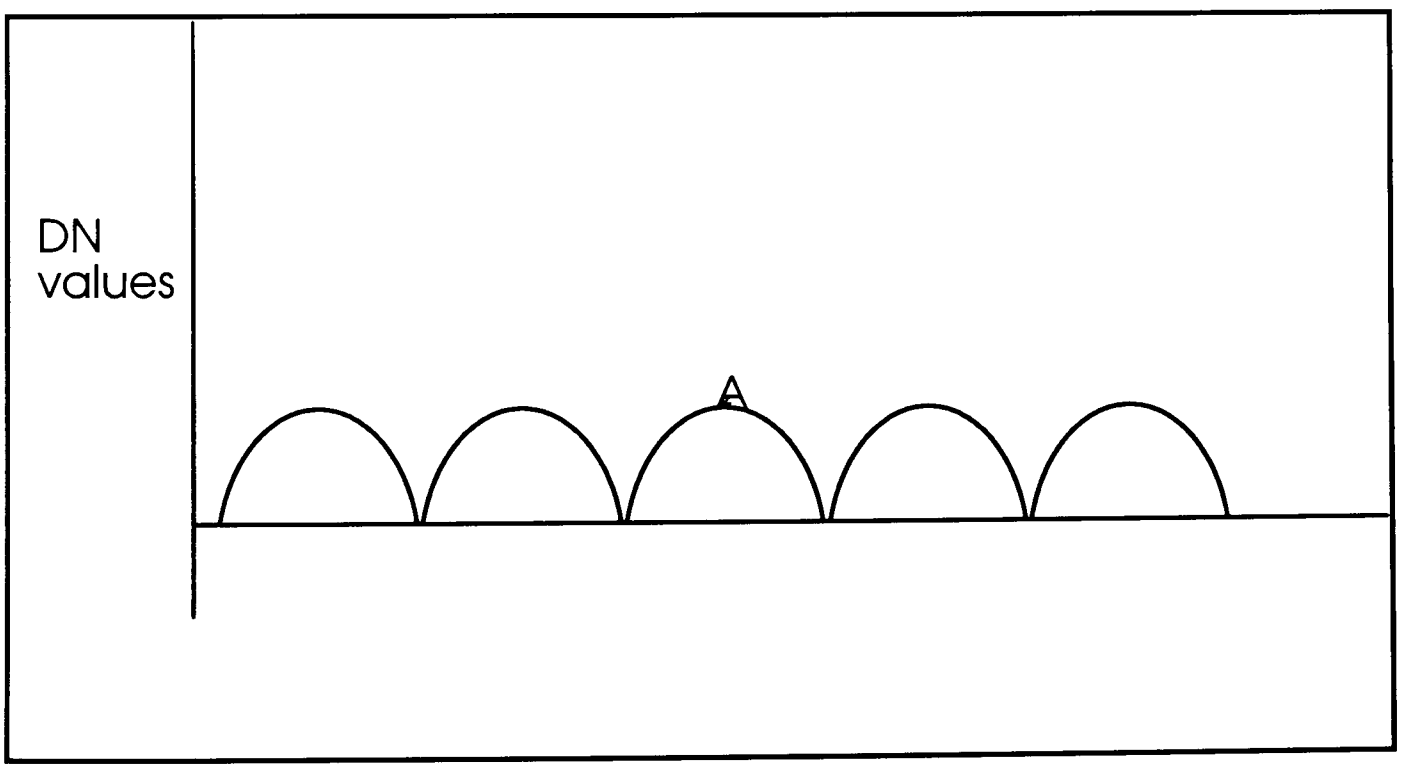

Figure 3.9b: Radiometric transect of figure 3.9a. Effect of vegetation is dominant in contributing to radiance sensed. Hence the high reflectance of the portion of vegetation on the lineament.

radiometric transect represented by the figure 3.9b will be in phase to figure 3.9a representing the lineaments. The crest with vegetation will have high DN value and will appear brighter when represented in the spatial domain while the troughs with poor vegetation will be represented by low DN values and will appear darker.

C. **Streams and Lakes**: Lineaments in this situation are demarcated by lakes and other types of water bodies, which in low lying terrain serve to highlight topographic variation. Electromagnetic radiation falling on this type of lineament field will be reflected by the lineament much more than the water bodies. Water bodies are known to be good absorbers and transmitters of radiation. Water has a high transmittance for all visible wavelengths but the transmittance decreases as wavelength increases(Mather, 1987, Curran, 1985). On meeting a water body, a small proportion of the incident radiation is absorbed and a small percentage is reflected while the majority is transmitted by the visible part of the spectrum whereas water absorbs the infra red radiation strongly and reflects and transmits only a tiny portion. This property of water will result in a sharp contrast between any water body and land boundaries, especially at infra red wavelengths, which in this case often highlights the lineaments. The situation is different in cases where there could be found suspended sediments and aquatic flora in the water body or when the water is so shallow that materials at the bottom will reflect radiation to the sensor. Even in such occasions the power of the reflected signal recorded on the detector will be different hence the DN value of the lineament and water body will be different and will be distinguishable on the satellite images.

D. **Gaps, Depression and Abrupt Discontinuities:** Where fractures occur along fault lines, there may be variation in vegetation or moisture content in the fault zone especially in gaps or depressions brought about by fault activity. The DN of the gap or depression may be different from that of the surrounding area and will contrast markedly from surrounding features giving rise to the

representation of a lineament. In some extreme cases a situation is seen where a boundary represents abrupt change from an area of uniform DN to another area with a uniform DN. This may occur where vegetation change is observed or where there is a change in the boundary between rock or soil or different reflective properties. These give rise to edge lineaments representated on a radiometric transect as a step.

3.4 Radar Imagery and Lineaments

Radar images are considered separately because the imaging system, operation, and mode of formation are different from the other systems. Description so far has been based on lineaments imaged from sensors that utilise electromagnetic radiation from the visible part of the spectrum and the infra red portion.

Radar images however use longer wavelengths measured in millimetres or centimetres. They employ active illumination i.e. the satellite sends its own radiation and records the return signal. The longer wavelengths of the radar signal means that they are less affected by the atmosphere and can penetrate the atmosphere in adverse condition. Its active illumination means that imaging can be obtained at all time, day or night and independent of solar illumination.

3.4.1 How Radar Images are Formed.

Being an active system, the radar imaging system transmits short pulses of microwave energy and records the signal backscattered from the Earth's surface received in order of arrival. Since electromagnetic waves travel at the speed of light, transmission and receiving time of the signal is short and many pulses can be transmitted per second. Radar images therefore measure distances to the reflecting object. The return signals are collected by an antenna very like a radio telescope which is different from a solid state detector. The signals are then processed, amplified and recorded onto photographic films or digital tapes (Loor, 1983,

Koopmans, 1983, Gibert and Paul, 1976, Crandall, 1969, Krul, 1983, Curran, 1985,)

For two objects on the ground to be distinguishable, the return signal from each object for the whole pulse must reach the antenna at different times. If there is an overlap between the two sets of signals, the object will merge into one an be indistinguishable.

3.4.2 Parameters Influencing Radar Backscatter

The factors that influence the radar returned signal (backscatter) are partially instrumental and partially dependent on properties of the ground targets. Many of these factors are interrelated and cannot be considered independently. Each of these factors will be considered in turn.

1. **Imaging system:** There are two types of radar imaging system, The Real Aperture Radar(RAR) and Synthetic Aperture Radar (SAR). The main difference between the two systems is that the spatial resolution of the imaging product for RAR is dependent on the distance between the radar and targets and but this is not the case for SAR where spatial resolution remains apparently constant throughout the image (Koopmans, 1983).

2. **Frequency Band:** Radar imaging systems make use of the atmospheric transmission windows from the 8 mm band upwards. Usually the 8-11 mm, 24-38 mm, 38-75 mm and 150-300 mm bands called the Ka band, X band , C band and L band respectively (Koopmans, 1983). These longer wavelengths are less affected by atmospheric attenuation.

3. **Polarisation:** The radar signals are polarised when the electrical field vector of the signal is oriented in a single plane (Drury, 1986) perpendicular to the direction of propagation, as like-polarisation HH or VV which are horizontally transmitted and horizontally received signal and vertically transmitted and received signal respectively. The HH polarisation gives higher return signals

than the VV. There could also be cross-polarisation such as HV or VH where in the later case the transmitted polarisation is vertical and the return signal is horizontally polarised and vice versa for the former case. Multiple polarisation is likely to give additional information of the terrain as the return signal will vary with surface texture and composition for different polarisation.

4. **Look Direction and Depression Angle:** The formation of radar imagery is highly direction dependent. A flight direction parallel to the orientation of the features on the ground will enhance these features on the image as the look direction will be perpendicular to the orientation of the features. The features will be suppressed if the look direction is parallel to the orientation of the features to be imaged, and in some cases the lineaments will be invisible.

   Depression angle for a radar system is important in determining the detectability of lineaments. Blom (1988) for example illustrated how linear sand dunes become invisible at certain depression angle.

5. **Surface Roughness:** The surface roughness refers to the effect of micro relief of surface materials or vegetation cover and has no relationship to topographic terrain of a mountainous nature. It must be thought of in terms of the order of the radar wavelengths. A rough surface will scatter the incident radar energy to all directions and there is a high chance of a proportionate amount of this backscatter reaching the antenna. Such surfaces will appear in relatively bright tones on the image. Meanwhile smooth surfaces have a specular reflection and will hardly scatter any incident radiation back to the antenna unless the signal meets the surface at 0 degrees from the normal. So a smooth surface will result in a dark image tone, or an extremely bright one in the case of slopes perpendicular to the incident beam.

6. **Dielectric Properties:** This measures the electrical properties of the surface material. Surface materials with high metal content or water will have a high electrical constant and thus make very good reflectors of radar energy. The

lower the dielectric constant of a surface, the more energy is absorbed. Wet soil or rock will therefore reflect more radar energy than dry ones which will absorb most of the energy. Wet soil will thus appear brighter in tone than dry soils.

7 **Terrain Orientation:** This is directly related to look direction and depression angle and is the most important factor influencing radar backscatter. Orientation of slopes in areas of pronounced topographic relief with respect to impinging radar signal affects the strength and direction of the returned signal more than any other property (Curran, 1985). The effect is a mixed blessing . Some authors are happy with this effect where an impression of relief and enhancement of topography is realised especially in lineament studies while some authors lament about the loss of information.

3.4.3 Lineaments from Radar Imagery

Authors who use radar imagery for lineaments analysis are very happy with the additional linear features that can be obtained by it for undetected lineaments or already known lineaments (Gillerman, 1970; Kirk, 1970; Clark and Knight, 1994). The drawback is that radar imaging is highly directionally dependent and lineaments will be missed out if oriented in the same direction as the look direction. By the same reasoning they will be enhanced if oriented perpendicular to the look direction.

The compositional differences in lineaments and their surroundings such as faults, linear sand dunes and drumlins may cause local changes in the dielectric constant of the surface material giving a tonal variation between the lineament and its surroundings . Vegetation in a fault zone or on sand dunes or drumlins will also affect the return signal and hence tonal variation and contrast of the image. This will help, in the identification of lineaments on the basis of the signature difference between lineaments and their surroundings due to radar backscatter.

The use of radar in lineaments studies have yielded very positive results. Studies by Koopmans (1983; 1988) compare lineaments from air photos and from radar imagery and found lineaments from radar approximately two times longer than those on air photos when the look direction of the radar was perpendicular to the orientation of the lineaments. When the direction was parallel to the lineaments, more lineaments were found on the air photos. Comparative studies have also been made between radar imagery and low sun angle aerial photography by Lyon and Lee (1970); Clark (1971). Sabins (1978) found that lineaments representing fault traces were more visible than on the low sun angle aerial photography. In another comparative study with Landsat imagery, Sabins et al. (1980) it was possible to detect traces of the San Andreas fault zone on a radar imagery that were not detected on Landsat. Also, Borengasser and Taranik (1988) showed a correlation of lineaments with known faults using Shuttle Imaging Radar-B (SIR-B). Clark and Knight (1994) have also demonstrated the better lineament detection abilities of ERS-1 radar images over Landsat images.

Summarily, the advantages of radar images in lineament studies is immense. Its independence from weather conditions and its enhancement of lineaments with topographic characteristics is highly beneficial for lineament studies.

Chapter Four

Spectral Analysis of the Radiometric Transect

4.0 Introduction

Methods of analysing lineament parameters have been subjected to much criticism because of the subjective nature of the results e.g Wise, 1982. There is therefore a need for devising a new and more objective method of analysing lineaments.

Results of lineament mapping, analysis and interpretation have been dependent on the interpreter's ability to recognise lineaments. It is thus not surprising that it has been possible for two researchers interpreting and analysing lineaments from the same area to produce different results (Podwysock , et al. 1975).

The methods available for lineament mapping and analysis from satellite images and aerial photographs are usually by on-screen-digitisation of the lineaments or ink-on-hard-copy marking of these lineaments (Vernon, 1966; Lake et al, 1984; Stefouli and Osmaston, 1984; Gravelle and Akhavi, 1989; Kleeman and Woodreff, 1989; Raj, 1989; Shuman, 1989; Clark, 1990; 1993; 1994; Deroin and Tammain 1990; Tsombos and Kalogeropoulos, 1990; Yésou and Rolet, 1990; Clark and Knight, 1994).

With the digitisation approach, since the co-ordinates of the digitised lineaments are known, there is the added advantage that algorithms can be incorporated into the digitisation software for calculating lineament parameters. Clark and Wilson (1994), for example, use specially written software to derive lineament lengths,

spacings, orientations, and nearest neighbour indices from a digitised data set of lineaments.

On the other hand, lineament marking on hard copy needs the parameter to be laboriously measured on the hard copy. Both methods are subjective and time consuming and it is likely that some of the features will be missed out or other linear features which have no relationship to the type of lineament being studied may be mistakenly considered in the study. For example, roads may be mistaken for structural lineaments or soil boundaries may be considered as glacial lineaments. Even when the image is subjected to rigorous enhancement techniques such as high pass filtering and edge detection, mapping of lineaments in whatever manner will still introduce a subjective element to the results.

In order to eliminate the problem of operator bias and speed up lineament analysis, automatic methods of lineament analysis have been developed (Daoust *et al.* 1989). These methods involve enhancing and delineating lineaments using the digital image processing technique called pattern recognition. This method has been used by Joshi (1989) to successfully map lineaments on Landsat MSS. In another application, Wand and Howarth (1989) extracted structural lineaments from Landsat TM image of the Canadian Shield near Sudbury Antario and showed that automated interpretation identified more structural lineaments than visual interpretation. An added advantage of the automatic method of lineament mapping is that lineament maps obtained by this technique are in digital form and can be combined with other types of data e.g. geological and geomorphological data for decision making. Unfortunately most automatic lineament detection algorithms are only capable of mapping strong lineaments and usually fail to detect the more subtle ones.

Of all the methods available for lineament mapping and analysis, some lineaments can still be missed out or even be wrongly associated with other lineaments which have no relationship to each other. This situation can be observed in the following example. If the method of analysing digitised lineaments was to be used on figure

4.1 to map and analyse the lineament given by the transect from point A to B, the operator will map lineaments k1, k2, k3, k4, k5, k6 and L1, L2, L3, L4, L5, L6 as similar sets of lineaments. If the spacing between these lineaments were to be measured, the operator will make the fatal mistake of measuring the spacing between lineament type k and L. The results will be misleading as the two different sets of lineament will be considered as one set. This limitation will also be present in the automatic method since, the method identifies lineaments from their orientation and magnitude of the features on the image. The method recognises lineaments by determining the locations, scale and direction where maximum changes occur in the signature values (Digital Number) of the image. Here also different lineament types may be associated with one another.

The subjectivity of the results in lineament analysis therefore inspires the search for a new method of analysis. In this thesis, a new method based on fourier and spectral analysis has been developed. This method uses the radiometric transect between two points in the image as the data (Figures 4.2 and 4.3.)

Fourier and spectral analysis are robust and powerful tools for establishing the presence or absence of cyclicity in any data by decomposing the data into their constituent frequencies in the case of time series and wavelengths in the case of spatial series.

This technique has been applied extensively in many fields of studies. In Geography, Rayner (1971) gives a general introduction of the subject, and in Hydrology, Speight (1965) applied the technique to search for meander periodicities in the Angabunga river, while Ferguson (1975) using spectral analysis, established that meander patterns in some British rivers are typically irregular. Using this technique, Balek and Andel (1971) analysed mean annual discharge of 15 rivers from various climatic region to establish hydrological periodicities while Hardisty (1993) used spectral technique to analyse wave-current data from Slapton Sands in Devon. Meteorological periodicities have been studied by Ward and Shapiro (1961) using fourier analysis and Carson (1963)

applied the method to study heat-transfer processes operating in the soil by measuring the annual and diurnal soil temperatures cycles. Periodicities in surface pressure have been studied by Rayner (1967). In another application, Anderson and Koopman (1963), applied spectral analysis to study periodicities in varve sequences represented as meteorological time series while Chatfield and Pepper, 1971 explained some of the practical problems in analysing time series using geophysical time series derived from atmospheric conditions. The technique has also been applied by Lee and Kaulu (1967) for spherical harmonic analysis of the earth's topography, and by Stone and Dugundi (1965) for studying micro relief, while Webster (1977) studied spatial variation of soil boundaries using the technique.

In remote sensing, fourier analysis has been modified for use in enhancing digital images. It has been used for selectively enhancing (filtering in the frequency domain) certain frequencies in the image (Gillespie, 1980; Jensen, 1986; Drury, 1987; Mather, 1987) and has been used by Leachtenauer, (1977) to characterise terrain types. Fowajuh and Clark (1992) and Clark and Fowajuh (1993) use the method to identify specific spatial frequencies of lineaments on simulated radiometric transects while Bauer et al, (1967) studied Greenland glaciers from aerial photographs using the methods. The method has also been used by Grover *et. al.* (1993) on radar imagery to assess the radiometric quality of the SAREX-92 airborne SAR.

Spectral and fourier analysis has also made its impact in engineering and economics and it is in the former area where development have been most prominent.

In this thesis spectral analysis is used on the radiometric transect which is the image in the frequency domain to identify and quantify the spatial frequency (wavelength or spacing) between parallel lineaments depicting glacial and aeolian features.

4.1 The Radiometric Transect.

The terms radiometric transect and spatial series are used interchangeably to refer to the image in the frequency domain which is a plot of the DN values between two points on an image that defines the transect (Figures 4.2 and 4.3). The transect can be obtained from satellite or airborne images, digitised aerial photographs or ground data depicting elevation. It is important to note here that this thesis does not consider the elevation of lineaments in defining the transect. The nature and location of points on the transect are solely determined by the spectral response of the terrain elements.

Figure 4.2 is an extract of the transect and lineaments of figure 4.1, taken between the points A and B. Lineaments on the image of figure 4.1 are brighter than the background features and their DN values will therefore be higher than the background features. Also, the DN values of lineaments L are higher than those of k as they are brighter. The transect (Figure 4.2) captures these differences graphically showing the relative spectral signatures of the different lineaments L and k and the background along the length AB. The transect thus represents DN values between two points on the image and is formed by extracting DN(x) at different points x along the transect where x =1, 2, 3, ..., n pixels. This means that the regular interval of extraction is 1 pixel and the transect length is n pixels.

Most often, the lineaments are brighter than their background feature and will therefore appear as peaks on the radiometric transect. In a situation where x(i) and x(r) marks the positions of two adjacent lineaments, the parameter of spacing can be obtained from equation 4.1

$$spacing = |x(r) - x(i)| \qquad \textbf{4.1}$$

It has been discussed that the objective of this thesis is to develop a method for analysing the spacing between lineaments from the transect. The method of

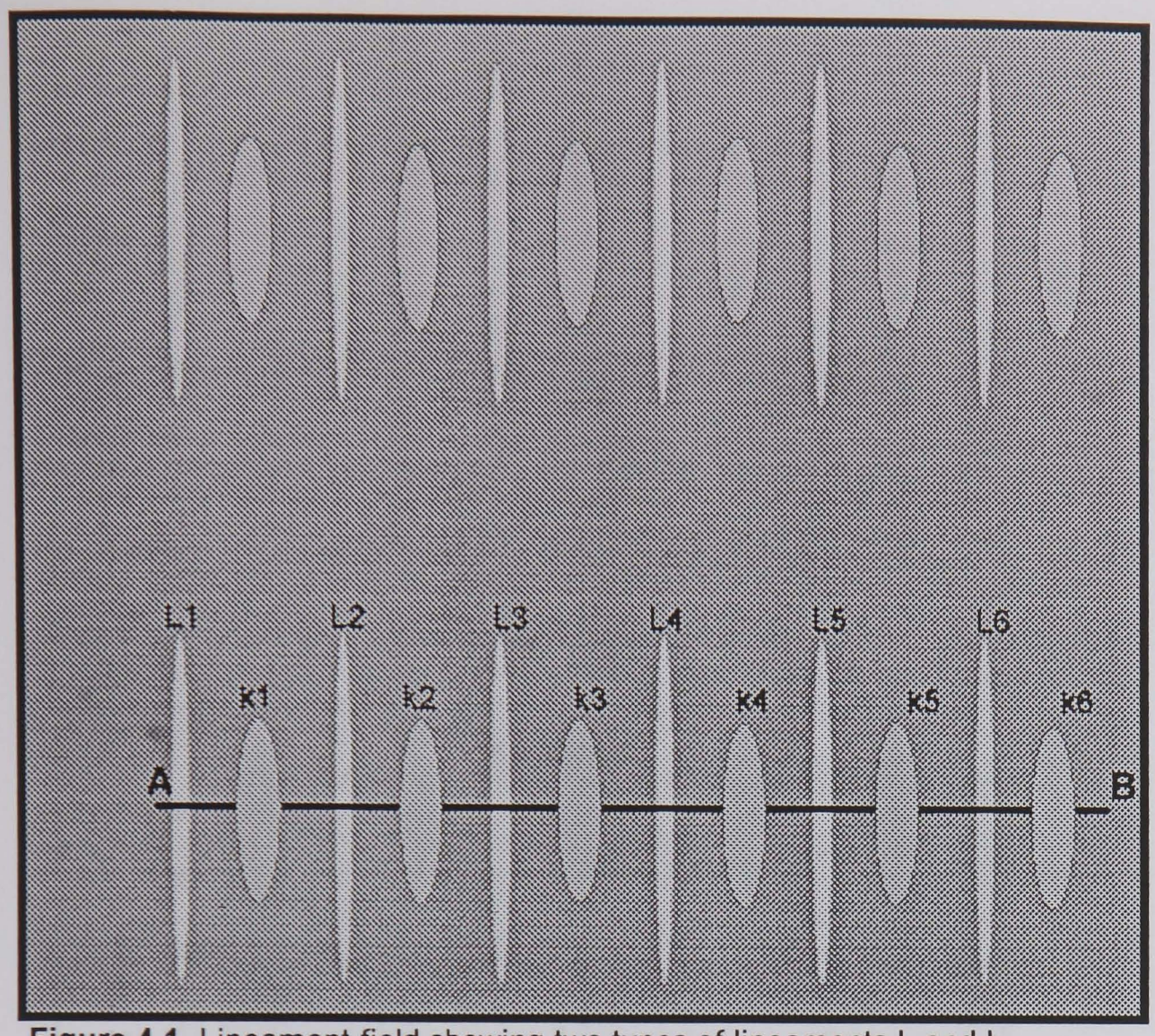

Figure 4.1 Lineament field showing two types of lineaments L and k with position and direction of transect **AB**

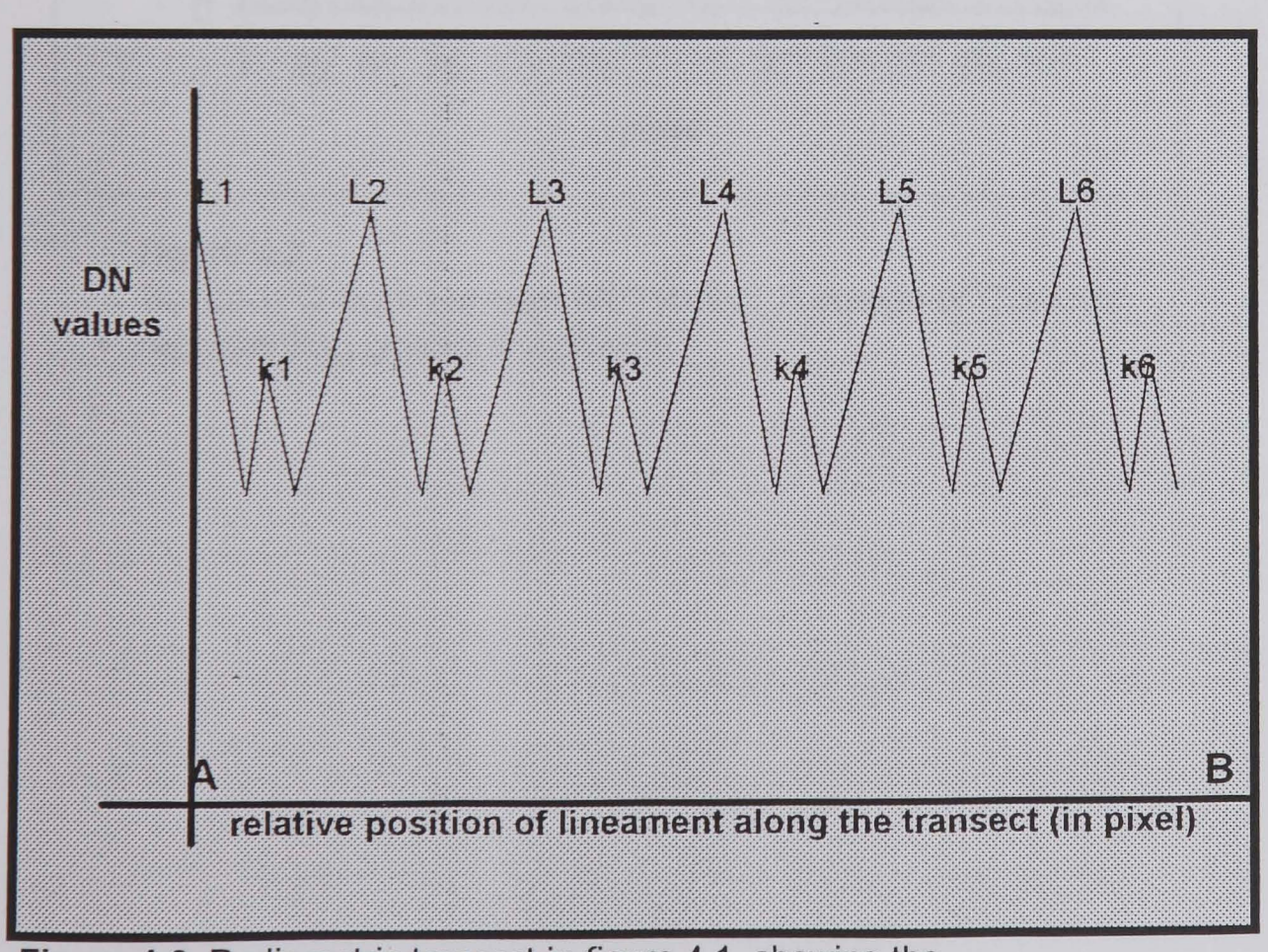

Figure 4.2 Radiometric transect in figure 4.1, showing the relative position of lineaments in relation to their brightness value

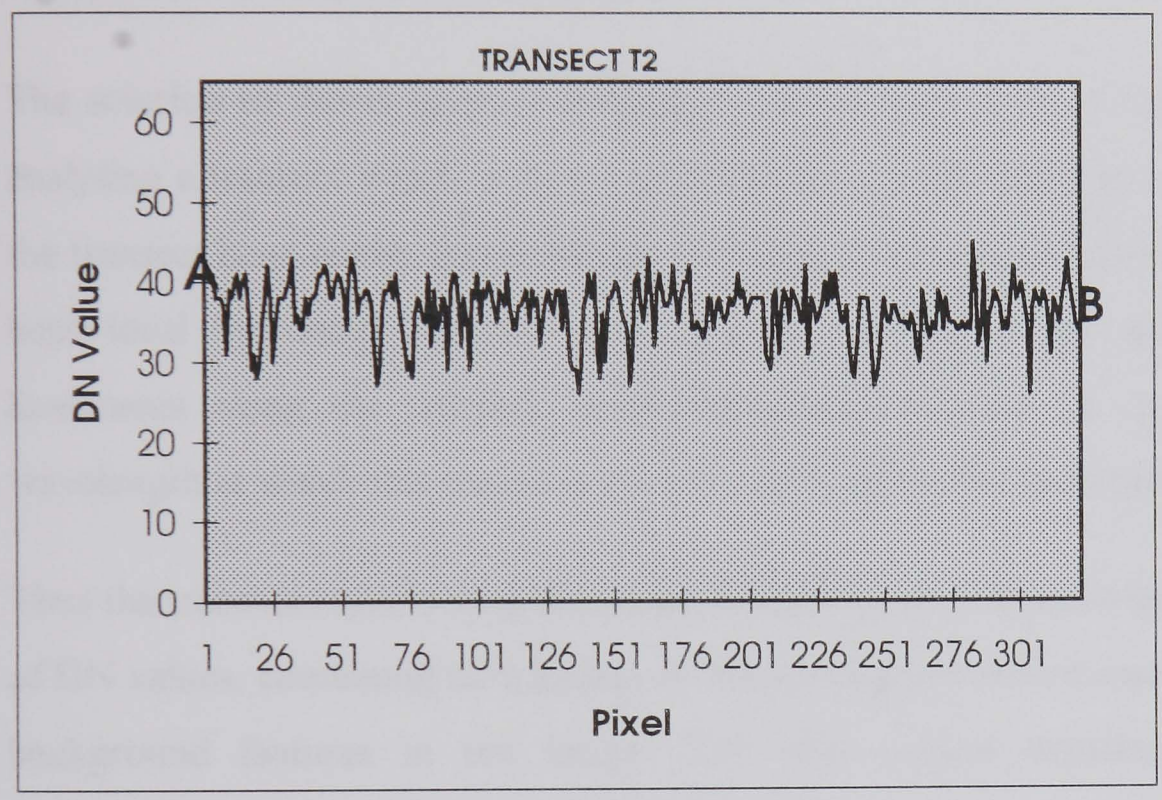

Figure 4.3
Transect T2 from Landsat MSS (band 1) image of Canada representing galcial lineament

measuring the spacing between lineaments from the transect or an image using equation 4.1 above requires explicit identification of lineaments and measurement between them, and is extremely time consuming. In addition, there is usually lots of background information and noise incorporated into the transect which hinders identification of lineaments and thus obscures accurate measurement. Lineament identification may not be as easy as figure 4.2 suggests.

For a real transect (Figure 4.3), taken from an MSS image showing glacial lineaments, background features tend to make visual identification of the lineaments from the transect difficult. To characterise the lineaments will therefore require a completely different method.

The solution to this is spectral analysis of the transect. It is an ideal method for analysing a transect which contains dominant cyclicities together with noise. Had the transect been purely deterministic as in figure 4.2, fourier analysis would have been ideal for doing the job. With spectral analysis, if the spacing between lineaments along the transect occurs at regular interval i.e. is periodic, the wavelength at which this occurs is the spacing between the lineaments.

Thus the transect representing the image in the frequency domain is a spatial series of DN values, containing information on the spacing between lineaments and other background features in the image. The next section explains the different variations that can occur within the transect.

4.1.1 Variation within the Transect

The transect most often contains other variations that are different from the ones we are seeking to analyse. Some of these variations are:

- **Cyclic Variations:** Spectral analysis is used in this thesis to estimate wavelengths within the transect data, which represent the spacing between

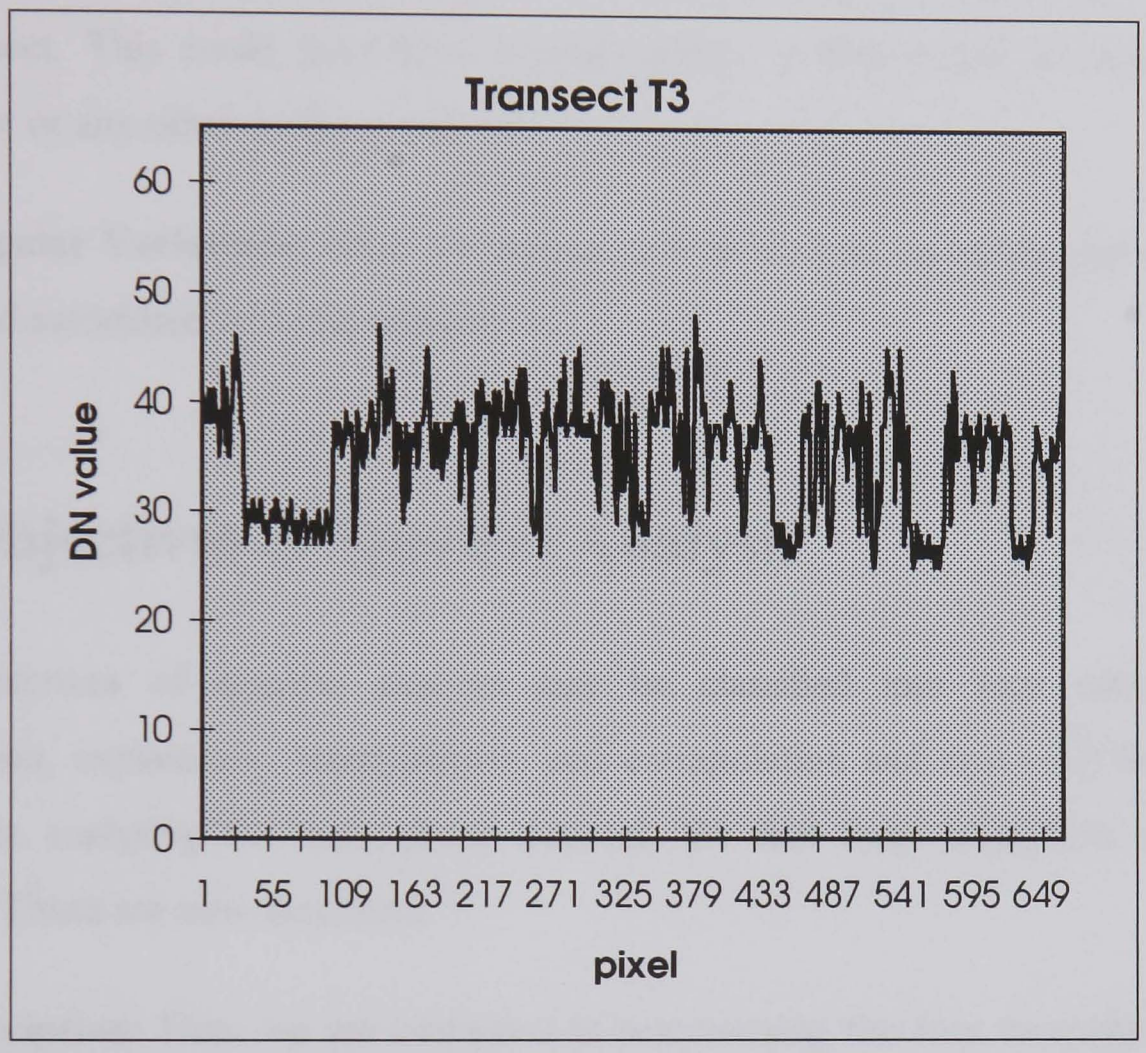

Figure 4.4
Transect showing non stationarity, the means along sections of the transect are not constant along the entire length of the transect

lineaments. Cyclic variation within the transect is a variation of paramount importance in this work. Such variations repeat themselves at regular intervals.

- **Trend:** The transect is said to exhibit trend if there is a significant change in the mean along different portions of the transect. Usually, the wavelength of the trend component exceeds the length of the entire transect (Granger 1966). The transect represented by figure 4.4 exhibits some form of trend. Observation shows that the mean is not constant along the entire length of the transect. This could have been brought about by differences in vegetation cover or any other surface material.

- **Irregular Variations:** Other variations such as random variations can also be found associated with the transect.

4.2 Objectives of Spectral Analysis

The objectives of spectral analysis may be classified into four categories: description, explanation, interpolation, and extrapolation and control (Chatfield, 1984). In analysing the radiometric transect, the first three objectives will be applied. These are now described.

1. **Description:** Here we are interested in summarising the data to enable us to spot simple variations in the transect. This involves plotting the data on a graph as in figure 4.4. This will help in spotting and checking important properties of the transect such as cyclicities, trend or outliers which appear to be inconsistent with the rest of the data.

2. **Extrapolation and Interpolation:** A knowledge about a series can be used to forecast future events by extrapolating information into the future using spectral analysis. This is most applicable with time series, especially economic time series.

With spatial series, we are interested in finding hidden properties within the data series and hence interpolation is what is required here.

3 **Explanation:** This is where explanations are sought as to the mechanism which generates the series. For lineament spacing we are interested in explaining the variations of these spacings in terms of geomorphology.

In developing the methodology for spectral analysis, the transect will be extracted from the image. This will constitute the descriptive stage of the analysis. The transect will then be analysed (interpolated) and the results explained.

4.3 Conditions for Spectral Analysis

Spectral analysis establishes the presence or absence of cyclicities in data and the wavelengths (spacing in pixels) at which they occur. But before spectral analysis is carried out, the transect has to meet the following conditions:

1. The data on the transect i.e. DN values for the case of radiometric transect must be measured at regular intervals. There is no problem in analysing transects since the pixels provide a regular sampling framework .

2. The transect must be stationary. This condition is fundamental to statistical analysis of spatial series. The transect is said to be strictly stationary if there is no systematic change in the mean or variance.

   Mathematically, if the spatial series with a joint distribution of $DN(x_1),\ldots,DN(x_n)$ is the same as the joint distribution of $DN(x_1+L),\ldots,DN(x_n+L)$ for all $x_1,\ldots,x_n$ and L, the series is said to be strictly stationary (Jenkins and Watts 1968; Bloomfield, 1976; Chatfield, 1984; Kendall and Ord, 1990).

In practice, stationarity is usually defined in a less restricted way as weak stationarity if the mean and variance is constant at all point along the transect. This definition will be used to establish stationarity of the transects in this research.

4.4 Detrending the Transect.

The mean function of a spatial series must be constant at all point along the transect before spectral analysis can be carried out. Unfortunately most series that are analysed exhibit behaviour contrary to that which is desired due to the presence of trend in the series. The presence of trend in a transect will mask any regularity in the data which might be missed by spectral analysis. It will also render the transect unstationary.

If the trend is deterministic, mathematical functions such as polynomials can be used to represent the trend. The residuals, given by the differences between the fitted trend function and the series would provide an estimate of a stationary local fluctuations which can then be analysed. However, most trends that occur in practice are non-deterministic (or stochastic) and can be isolated using one of the following methods:

A **Smoothing:** Smoothing converts the spatial series with trend to a new series without trend by a linear operation. Example of a smoothing function is Sheppard's five-term equation (Davis, 1973) represented as

$$DN_x^{'} = \frac{1}{35}\left\{17.DN_x + 12.\left(DN_{x+1} + DN_{x-1}\right) - 3.\left(DN_{x+2} + DN_{x-2}\right)\right\} \qquad 4.2$$

This is essentially a moving average.

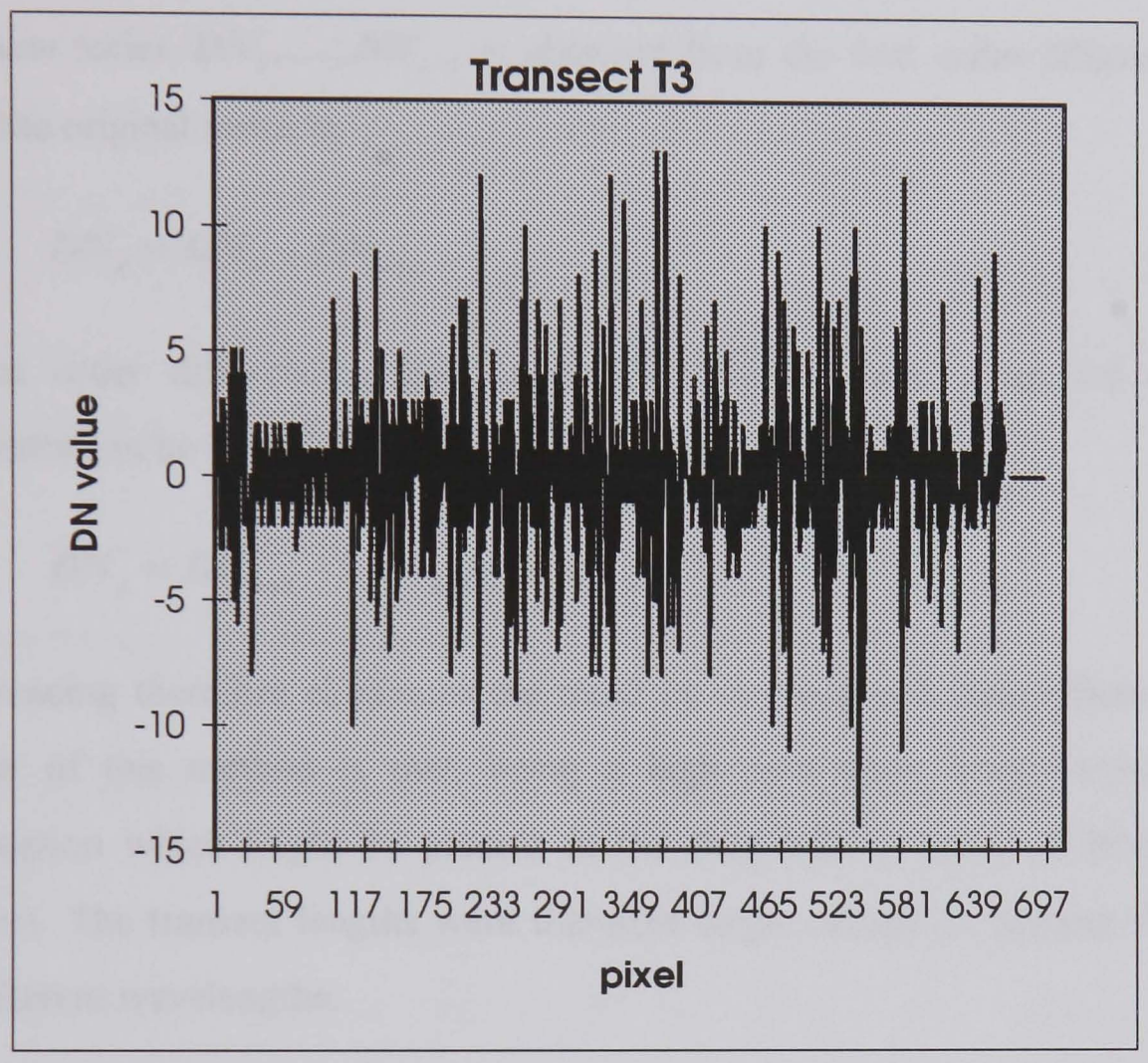

Figure 4.5
Transect of figure 4.4 detrended using first difference method to establish stationarity

B Differencing: A more popular method of detrending is differencing. Trends that turn to be embedded in the transect are stochastic and are typified by random changes in level and slope of the transect. Differencing is particularly suitable for detrending series with stochastic trend (Chatfield,1984) and it is used in this thesis to establish stationarity. In this method, the difference is computed between successive points and spectral analysis is performed on the differenced data rather than on the raw data.

The new series $DN_1^{'},\ldots,DN_{n-1}^{'}$ is obtained from the first order differencing from the original series by

$$DN_x^{'} = DN_x - DN_{x-1} \qquad \textbf{4.3}$$

If first order differencing fails to stabilise the transect, a second order difference can be used which is given by the equation

$$DN_x^{''} = DN_{x+2} - 2DN_{x+1} + DN_x \qquad \textbf{4.4}$$

Differencing therefore eliminates the trend by converting it into offsets. The danger of this method is that, being a high pass filter, long wavelength information which might be present in the data will be removed from the transect. The transect lengths were therefore large enough to account for all the inherent wavelengths.

Using the first order difference method, the non stationary transect of figure 4.4 was stabilised as shown in figure 4.5.

4.5 Number of Data Points

One of the fundamental choices for any analysis is the number of data points. The number of data points and the separation of the data points influences amongst

If the fast fourier transform is used, then it is necessary that the number of data points be equal to a whole power of two. If the number of data points departs from being a power of two, zeros can be added at both ends of the series and the data can then be tapered to give a smooth transition between the ends of the data and the strings of zeros.

The question of how large a series must be to get a reasonable estimate of the spectrum is not easy to answer. A consideration of the wavelengths expected should definitely influence the choice of the size of transect. Chatfield (1984) recommended series of size containing between 100 and 200 observations as a minimum. Experiment with smaller transect lengths have been done by Granger and Hughes (1968). They found that only very gross features of the spectral shape such as large peaks were observed but subtle features particularly those with bigger wavelengths did not show up in the spectral estimates.

4.6 Mathematical Analysis of the Transect

Jean-Baptiste Joseph Fourier, a French mathematician, showed that a single-valued function defined for a finite range can be represented by the sum of sine and cosine functions. The method of doing this is called fourier analysis. Unfortunately fourier analysis only works for deterministic functions. The radiometric transect can be regarded as a single-valued function and contains information about lineaments and background information and it is therefore far from being deterministic. In order to determine the wavelengths (spacing between lineaments) of the sine and cosine waves that constitute the radiometric transect, spectral analysis is used. The next section describes the mathematics of spectral analysis.

4.6.1 Theory of Spectral Analysis

The power spectral density function (psdf) is the tool in spectral analysis used for considering the wavelengths and frequencies of series. In estimating the psdf we need the following parameters: the mean, variance, covariance and autocovariance function.

For a transect measured over the range $DN_1, DN_2, DN_3, \ldots, DN_n$ where n is the size of the transect, we define the mean (μ) as the measure of the central tendency of the transect and is given by the equation

$$\mu = \frac{1}{n}\sum_{x=1}^{n} DN_x \qquad 4.5$$

The Variance (δ^2), on the other hand, measures the spread of the observations about the mean and is given by the equation

$$\delta^2 = \frac{1}{n}\sum_{x=1}^{n}(DN_x - \mu)^2 \qquad 4.6$$

The positive square root of equation 4.6 is the called the standard deviation of the observation.

For an independent stationary transect, the mean, variance and standard deviation are enough to describe the transect completely. However, transects do exhibit non-independence between observations and a third parameter, the autocovariance function needs to be included to describe the psdf completely.

The autocovariance function measures the relationship between points (observations) on the transect separated by some distance k called the lag number. The autocovariance function can be calculated from the formula

$$C_k = \frac{1}{n-1}\sum_{x=1}^{n-k}(DN_x - \mu)(DN_{x+k} - \mu) \qquad 4.7$$

where μ is the mean of the transect and k=1,2,3,...,M and M<n

For a stationary transect where the mean along the entire transect is fairly constant, the series can be corrected by subtracting the mean from every observation on the transect so that the transect has zero mean. Although this does not affect the result, it makes the calculation easier. For a mean-corrected transect the autocovariance is give by

$$C_k = \frac{1}{n-1}\sum_{x=1}^{n-k}(DN_x)(DN_{x+k}) \qquad \textbf{4.8}$$

Another ensemble parameter for characterising the psdf is the autocorrelation coefficient r_k. Using equation 4.8, the autocorrelation coefficient is obtained from the equation

$$r_k = \frac{C_k}{C_0} \qquad \textbf{4.9}$$

This is the normalised autocovariance and $C_0 = \delta^2$ is the variance of the transect.

The autocorrelation coefficient on its own can also give useful information about the transect but is difficult to interpret. A plot of the ordered set of coefficients, $r_1, r_2, \ldots, r_M$ as ordinate against k as abscissa gives the correlogram of the transect. The plot oscillates between the values of ± 1

For a random transect, $r_k \cong 0$ for all k with a distribution of $N\left(0, \frac{1}{n}\right)$ (Chatfield 1984). If there is any trend in the transect, $r_k > 0$ except for very large values of the lag and, if the transect has cyclic fluctuation at a particular wavelength, the correlogram will also exhibit cyclic fluctuation with the same wavelength.

The autocovariance function and its normalised form, the autocorrelation coefficients are inter-dependent and are not enough by themselves to describe the spacing between lineaments from a transect.

To carry out a spectral analysis, the autocovariance coefficients are transformed using the fourier method to give the power spectral density function $S(\omega)$, given by the equation

$$S(\omega) = \frac{1}{2\pi}\left[C_0 + 2\sum_{k=1}^{n-1} C_k \cos(\omega k)\right] \qquad \textbf{4.10}$$

where n is the length of the transect, and ω is defined by

$$w = \frac{\pi j}{L} \qquad \textbf{4.11}$$

for j=0,1,2,...,L and L is the spectral computation number and is often chosen to be equal to M defined earlier as the lag number or the truncation point. ω is the angular frequency but for interpretation purposes the frequency f is given by $f = \frac{j}{2L}$. Frequency is only useful when dealing with time series, where periods and frequency are useful results. With spatial series as in the radiometric transects, it is the wavelengths that are important. The wavelength Θ gives a measure of the spacing in terms of pixels. The wavelength and frequency are however reciprocal of one another.

$$wavelength = \frac{1}{f} = \frac{2L}{j}(pixel) \qquad \textbf{4.12}$$

The power spectral density function therefore shows how the variance is distributed for any particular frequency or wavelength.

If the lineaments represented in the transect occur at regular intervals this will be revealed by a sharp peak when the psdf is plotted against the wavelength. With a knowledge of the position of the peak and the computation number L, the spacing in pixels between lineaments can be obtained using equation 4.12

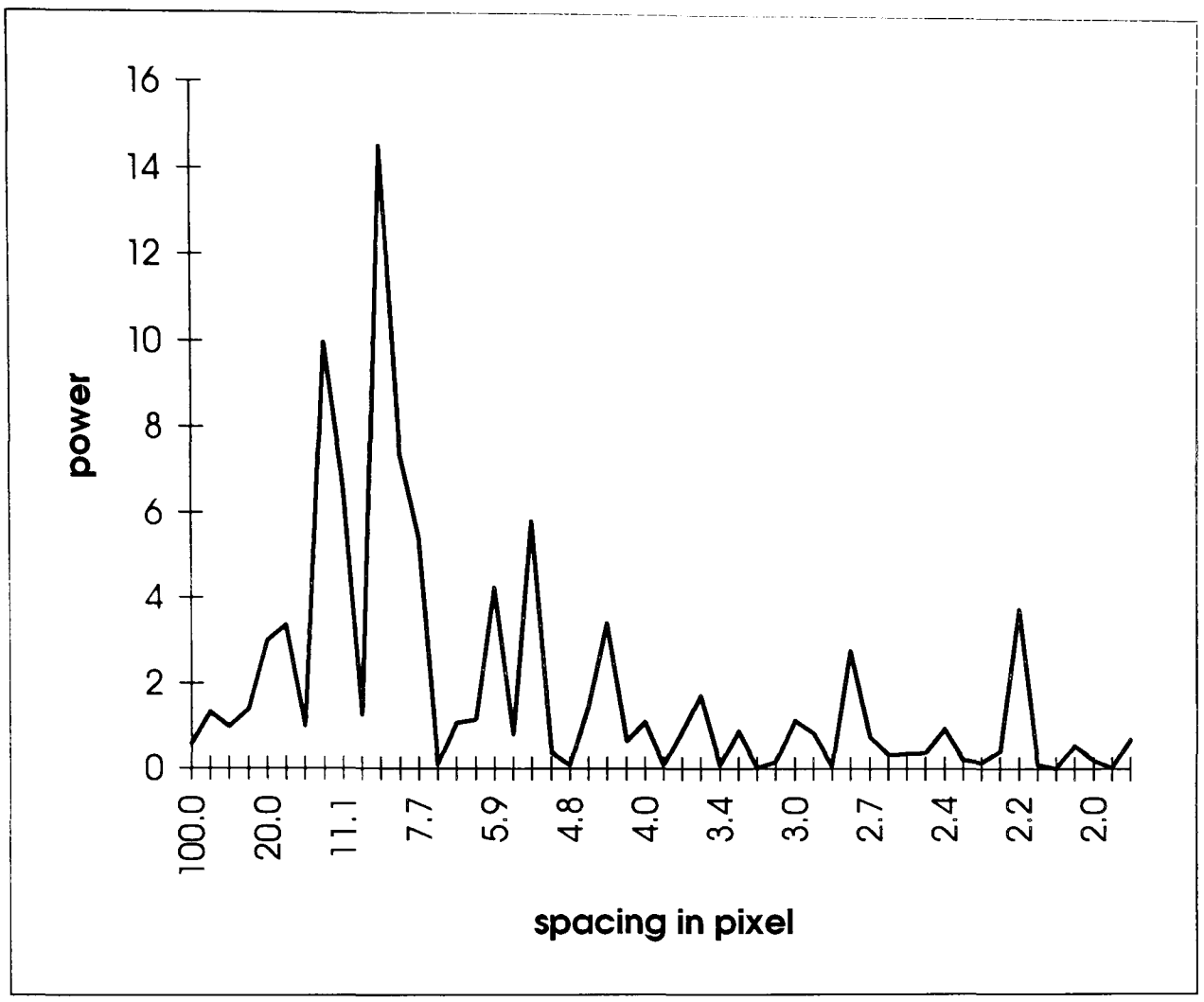

Figure 4.6
Power Spectral density function
of transect T2 figure 4.3

The strength of spectral analysis is derived from the fact that deterministic components embedded within purely stochastic components can still be isolated even though the latter may completely mask the former in the original transect.

To demonstrate the application of spectral analysis to the radiometric transect, the transect of figure 4.3 was analysed using equation 4.10. The results of the analysis are plotted for the different wavelengths (in pixels) as shown by figure 4.6. From the figure, it can be observed that the estimated psdf fluctuates widely showing erratic behaviour. Some of the peaks are spurious and may lead to wrong conclusions if all the peaks are considered as significant. The way to tackle this problem is to carry out a fourier transform on the smoothed autocovariance function.

4.6.2 Spectral Smoothing by Lag Windows

The fourier transform of the smoothed autocovariance function will give a more stable estimate of the power spectral density function. Chatfield, (1984) pointed out that the precision of the auto covariance decreases with an increase in k since points which are further apart on a series may not be related. It is therefore reasonable that any smoothing function should give smaller weights to values of C_k as k increases. This can be achieved by using the lag window λ_k and the ones in common use are :

1. **Parzen window** (Parzen, 1961)

   It is given by the equation

$$\lambda_k = 1 - 6\left(\frac{k}{M}\right)^2 + 6\left(\frac{k}{M}\right)^3 \qquad 0 \le k \le \frac{M}{2}$$

$$\lambda_k = 2\left(1 - \frac{k}{M}\right)^3 \qquad \frac{M}{2} \le k \le M \qquad \textbf{4.13}$$

where k and M are the lag number and the truncation point respectively. The advantage with the Parzen window is that only positive estimates will be given.

2. **Tukey Window** (Blackman and Tukey, 1958)

   It is given by the equation

$$\lambda_k = \frac{1}{2}\left(1 + \cos\frac{\pi k}{M}\right) \qquad \textbf{4.14}$$

Also called Hanning or Blackman-Tukey window, the Tukey window will give almost the same estimate as the Parzen window.

Many other windows have been defined such as the Daniel window (Daniel, 1946) and the rectangular window. The smoothing windows should be able to account for all the structure in the transect. The literature on spectral analysis recommends the use of either the Tukey or the Parzen windows.

The choice of the truncation point M is not clearly defined and needs to be chosen with care. Chatfield (1984) suggest a choice to balance resolution against variance. If M is too small, important features of $S(\omega)$ may be smoothed out and if it is too large, $S(\omega)$ will maintain its erratic nature. Chatfield gives a rough guide for choosing M to be about $2\sqrt{n}$.

Whichever window is chosen, it is advisable to use more than one truncation point to begin with. Comparing the results for the different truncation points will ascertain whether a peak at a particular wavelength appears to represent real spacing between lineaments or not. The Tukey window will be used in this thesis for carrying out spectral analysis on the radiometric transects. This window is favoured because it has a smaller variance and can thus reduce the large variance of the estimated sample spectrum to make interpretation of the result easier (Jenkins and Watts, 1968). It is also easier to implement in both the frequency and time domain analysis of series.

$$S(\omega) = \frac{1}{2\pi}\left\{C_0 + 2\sum_{k=1}^{M-1}\lambda_k C_k \cos k\omega\right\} \qquad 4.15$$

where k=0,1,...,M-1, $\omega = \frac{\pi j}{L}$ for j=0,1,...,L and L is the spectral computational number.

To avoid losing information, the value of L should be at least as big as M. Chatfield and Pepper (1971) suggest L=2M, where M is the truncation point and M<n. From equation 4.15 it can be seen that the values of C_k for $M < k < n$ are no longer used while values for $k \leq M$ have been scaled by a factor λ_k.

This method is one of the many computational methods of calculating the power spectral density function. Another method is to calculate the fourier transform of the auto covariance function first and then smooth the result afterwards using the Hanning or Hamming filter. These techniques are called the Hanning and Hamming techniques respectively.

Using equation 4.15 and setting M equal to 10, 30, 40, 60 and 661, the transect of figure 4.3 was analysed. The result is presented in figure 4.7. From the figure it can be observed that when M=10, the power spectral density function (psdf) is over smoothed on the other hand, it is very erratic when M=60, the psdf behaves as if no smoothing had taken place. The psdf when M=60 is similar to the psdf when M=n. The psdf for M=40 and M=30 look reasonable, indicating clear peaks at 2, 10 and 23 cycles per 100 pixels representing wavelengths or spacing of 50, 10 pixels and 4 pixels respectively in the transect of figure 4.3.

The psdf for the non stationary transect in figure 4.4 (Figure 4.8a) shows the absence of a peak due to the presence of trend in the transect while the differenced transect (Figure 4.5) shows the presence of two major peaks representing spacings of 6 and 3.4 pixels in the transect of figure 4.4.

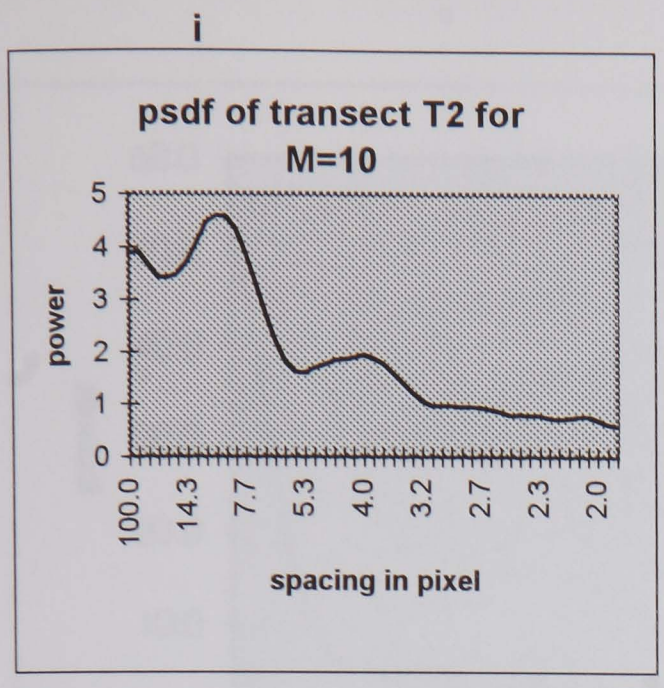

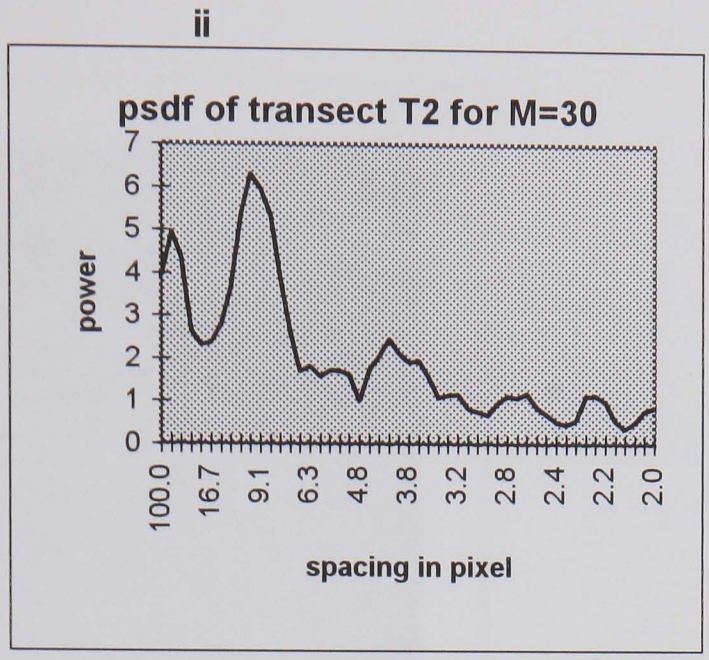

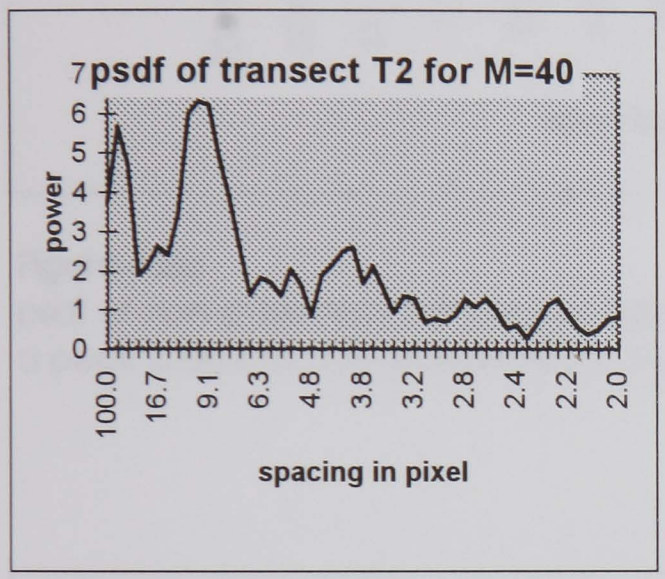

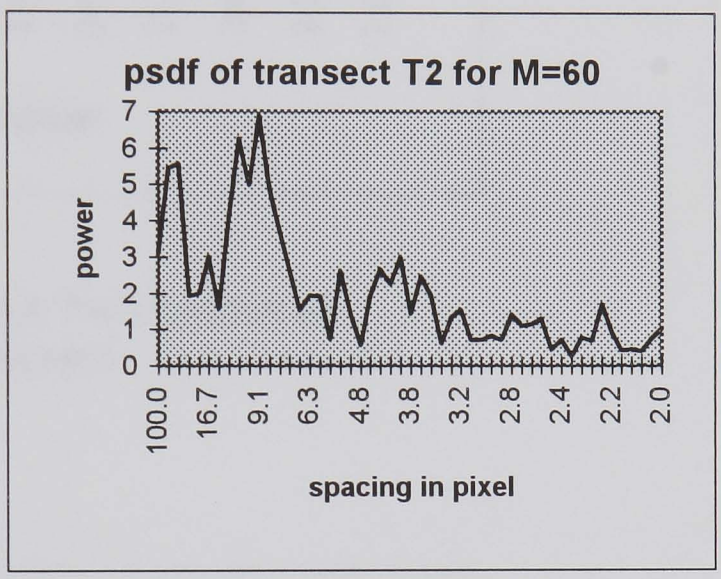

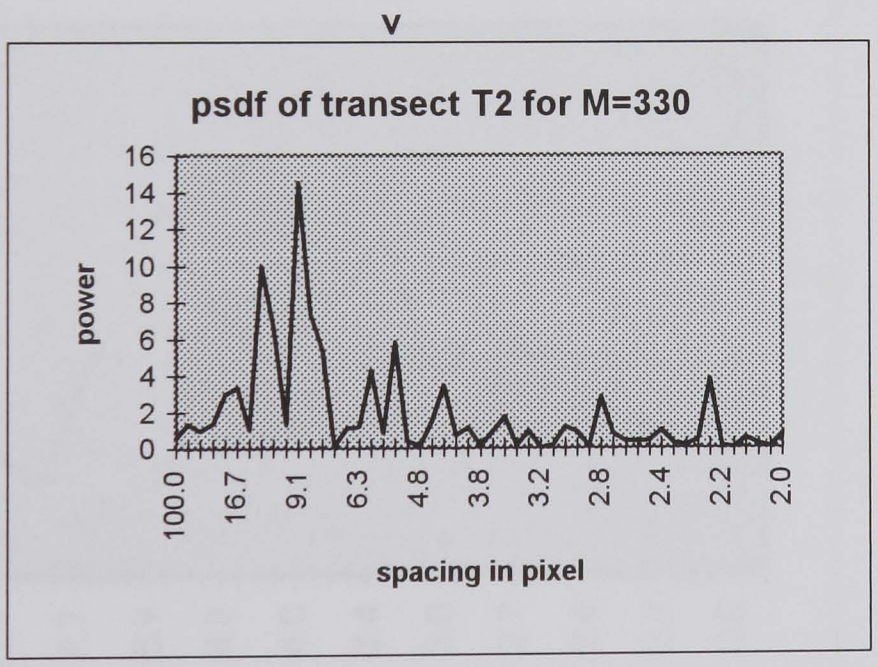

Figure 4.7
power spectral density function
of transect T2 in figure 4.3 when M=10, 30, 40, n and n=330

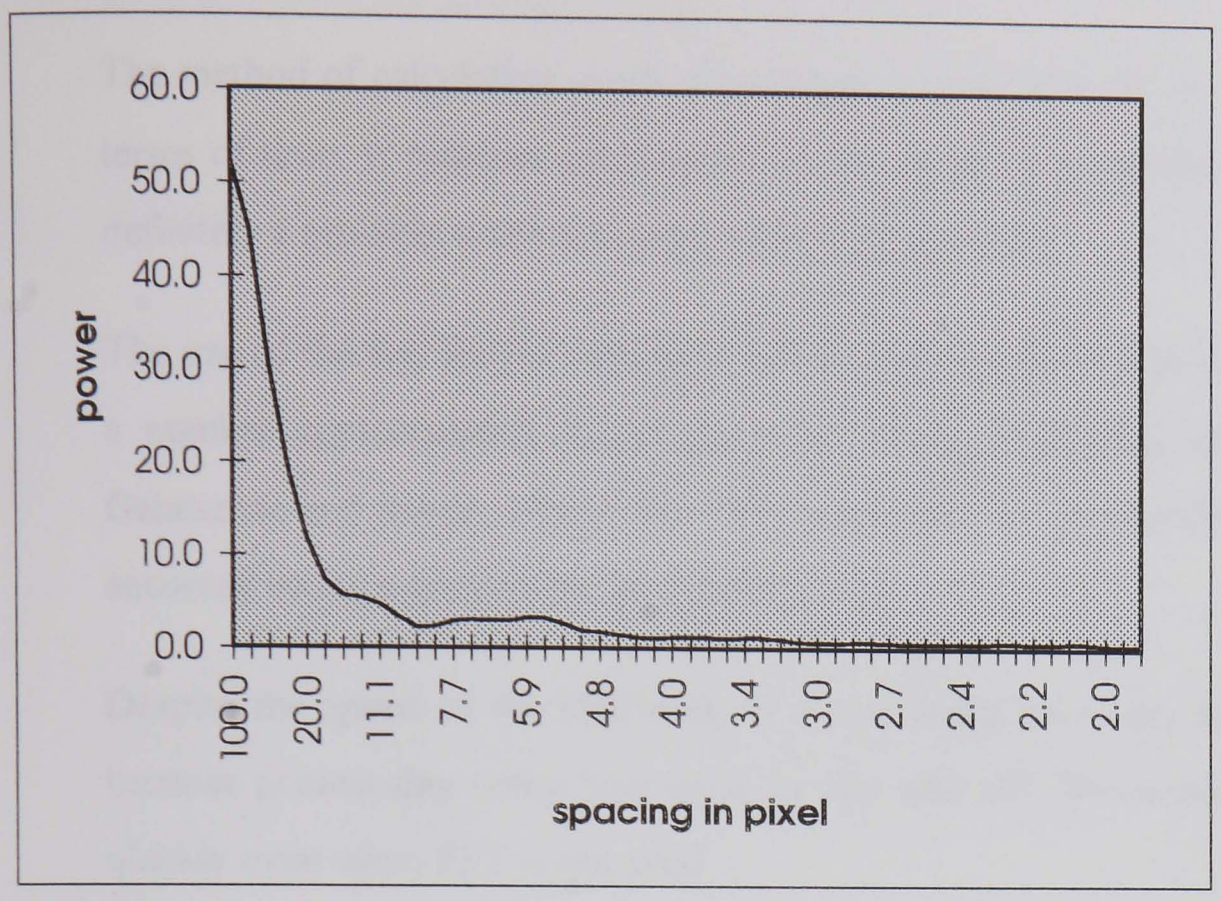

Figure 4.8a
psdf of non stationary transect of figure 4.4. The absence of a peak is due to non-stationarity in the transect.

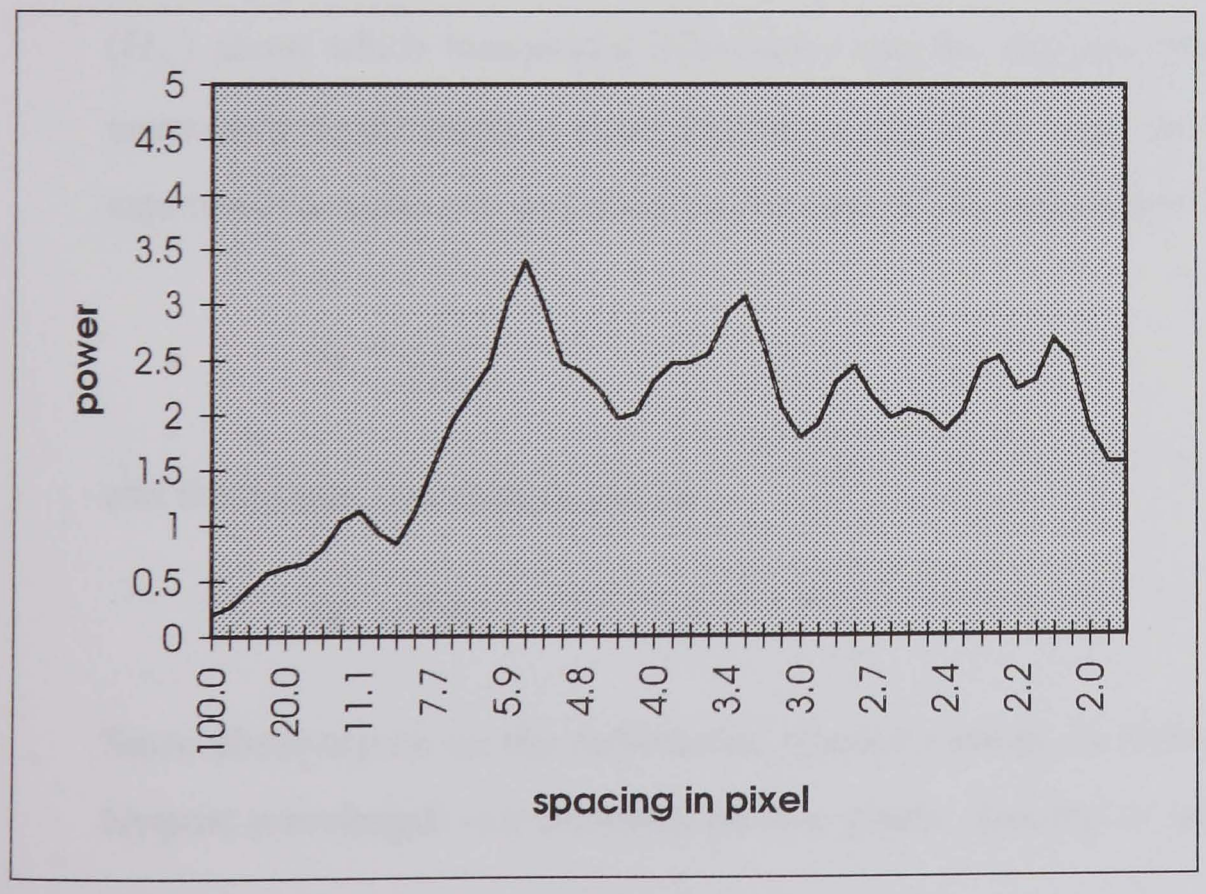

Figure 4.8b
psdf of detrended transect of figure 4.5 showing peaks which were not revealed in figure 4.8a

4.7 Fast Fourier Transform (FFT)

The method of calculating spectral estimates described so far is very expensive in terms of time. It requires calculations of the order of n^2 (Rayner, 1971). This is definitely a problem when analysing very large transects.

The use of the fast fourier transform (FFT) reduces the number of calculations to a number approximately proportional to $2n\log_2 n$ (Cooley and Tukey; 1965, Gentleman and Sande, 1966). The FFT is therefore an algorithm which retains the accuracy of the estimates but at a faster speed.

Despite the speed of the algorithm, it is not really necessary today to use FFT because present-day computers are very fast and will give results of large series quickly even when FFT is not used.

4.8 Nyquist Frequency and Wavelength

The Nyquist frequency is the highest frequency (f_N) or the minimum wavelength (Θ_N) about which meaningful information can be obtained from the transect. If measurements are made at equal interval of length Δx, then the Nyquist frequency expressed in cycles per unit pixel for the case of the radiometric transect will be

$$f_N = \frac{1}{2\Delta x} \qquad \textbf{4.16}$$

and the nyquist wavelength will be

$$\Theta_N = 2\Delta x \qquad \textbf{4.17}$$

Since observations on the radiometric transects are at an interval of 1 pixel, the Nyquist wavelength will therefore be two pixels. Spacing or wavelengths smaller

than this wavelength will not be given by spectral analysis. Only lineament spacings which are greater than 2 pixels apart will be resolved by spectral analysis.

4.9 Aliasing

Aliasing results in short wavelength components appearing to have longer wavelengths than is actually the case (Stout et al, 1993). This is brought about by poor sampling strategies where the sampling interval has been chosen too large such that important data points between the sampling intervals have been missed out. In this thesis there is no control over this effect as the observations on the transect have been obtained to the optimum of the technique of obtaining the transect (1 pixel apart) which may not correspond with the optimum of the ground features.

4.10 Echo Effects or Harmonics

These are multiples of the fundamental frequency. When the power spectral density produces a large peaks at some frequency f, related peak may occur at 2f, 3f and so on. These are called harmonics and should not pose a problem in spectral analysis of the radiometric transects.

4.11 Significance of Spectral Estimates.

The purpose of analysing radiometric transects by spectral method is to determine whether a significant cyclicity in the landscape is embedded in the transect. This is determined by the presence or absence of peaks in the psdf. Unfortunately, a random transect can also produce a peak by chance when subjected to spectral analysis.

Naturally the question of the significance of the estimates arises. There are two ways to test for this using the Fisher's test which test for the significance of suspected peaks on the spectral density function and the confidence limit test.

4.11.1 Fisher's Test

Fisher (1929) developed a test of significance for spectral estimates. The test was expanded by Grenander and Rosenblatt (1957), Nowroozi (1967) and later by Shimshoni (1971) to test for multiple cyclicities in the estimates as previous tests only accounted for single ones.

With the Fisher's test, the null hypothesis is that the transect has no cyclicity and represents a random noise which is normally distributed

Grenander and Rosenblatt showed that if the values of the power spectral density function were to be computed at the different wavelengths r such that $s(\omega) = s_1, s_2, \ldots, s_r, \ldots s_Q$, where Q is the number of spectral estimates, then the ratio g_r can be defined as

$$g_r = \frac{s_r}{\frac{2}{N}\sum_{i=1}^{n}(DN_i - \mu)^2} \qquad \textbf{4.18}$$

If g_r is arranged in decreasing order and if $\overline{g}_r$ is the r-th largest term of the rearranged sequence such that $\overline{g}_1$ is the largest of the g_r ratios, then the probability P_r that $\overline{g}_1$ exceeds a parameter g is given by

$$P_r = \frac{Q!}{(r-1)!}\sum_{j=r}^{T}\frac{(-1)^{j-r}(1-jg)^{Q-1}}{j(Q-j)!(j-r)!} \qquad \textbf{4.19}$$

where $T = \frac{1}{g}$ is the largest integer less than $\frac{1}{g}$ and r=1,2,3,...,Q represents the number of peaks

This relationship gives g as a function of P_r and Q and is the basis for the test statistic. Shimshoni calculated different values of g for probabilities of P equal to .01 and .05 representing the 99 and 95 percentage confidence intervals respectively for different values of Q and for r =1, 2, 3, ...,10. Values for P=.05, $5 \leq Q \leq 50$ and r=1, 2, 4, and 7 have been reproduced in table 4.1. From the table, it can be seen that g varies linearly and so intermediate values of Q and r can be interpolated

For practical purposes, the decision as to the confidence level of the test should be made prior to the application of the test. If r spectral estimates (peaks) are suspected to be significant, then the ratio g_1 for the first suspected value is calculated from equation 4.18. If $g_1 < g$ where g is some appropriate percentage of the distribution given by equation 4.19 or obtained from the Shimshoni table, then the hypothesis that there is no dominant wavelength present in the data is accepted at the 95 percent confidence level. On the other hand, the hypothesis is rejected. The exercise is repeated for the other estimates.

Table 4.2 is a worked example showing the use of Fisher's test. The transect of figure 4.3 was subjected to spectral analysis using equation 4.15 with a truncation point for the smoothing window M=40 and the number of spectral estimates Q=50. The smoothed power spectral estimates(SE) are presented in table 4.2a and the graph of the results is shown in figure 4.9. From the graph and the table it can be seen that there are three peaks in the results, at spacings of 50, 10 and 4 pixels.

The g_r ratios from the Fisher test for the spectral estimates representing estimated wavelengths of 50, 10 and 4 pixels are shown in table 4.2b as 0.1606, 0.2493 and 0.0958 respectively while the g values for the suspected estimates of 50, 10 and 4 pixels from the shimshoni tables for Q=50 are 0.09244, 0.13135 and 0.07548 respectively. Since the calculated ratios are greater than those derived from the Shimshoni tables, it can be established that the three peaks are significant at the 95 percent confidence level.

TABLE 4.1 Significance parameters for periodic components. P=0.05

M\r	1	2	4	7
5	0.68377			
10	0.44495	0.26511		
15	0.33461	0.21016	0.10738	
20	0.27040	0.17457	0.09559	0.07324
25	0.22805	0.15139	0.08612	0.06768
30	0.19784	0.13360	0.07846	0.06275
35	0.17513	0.11986	0.07215	0.05847
40	0.15738	0.10890	0.06687	0.05475
45	0.14310	0.09993	0.06238	0.05150
50	0.13135	0.09244	0.05851	0.04865

source: Shimshoni, 1971

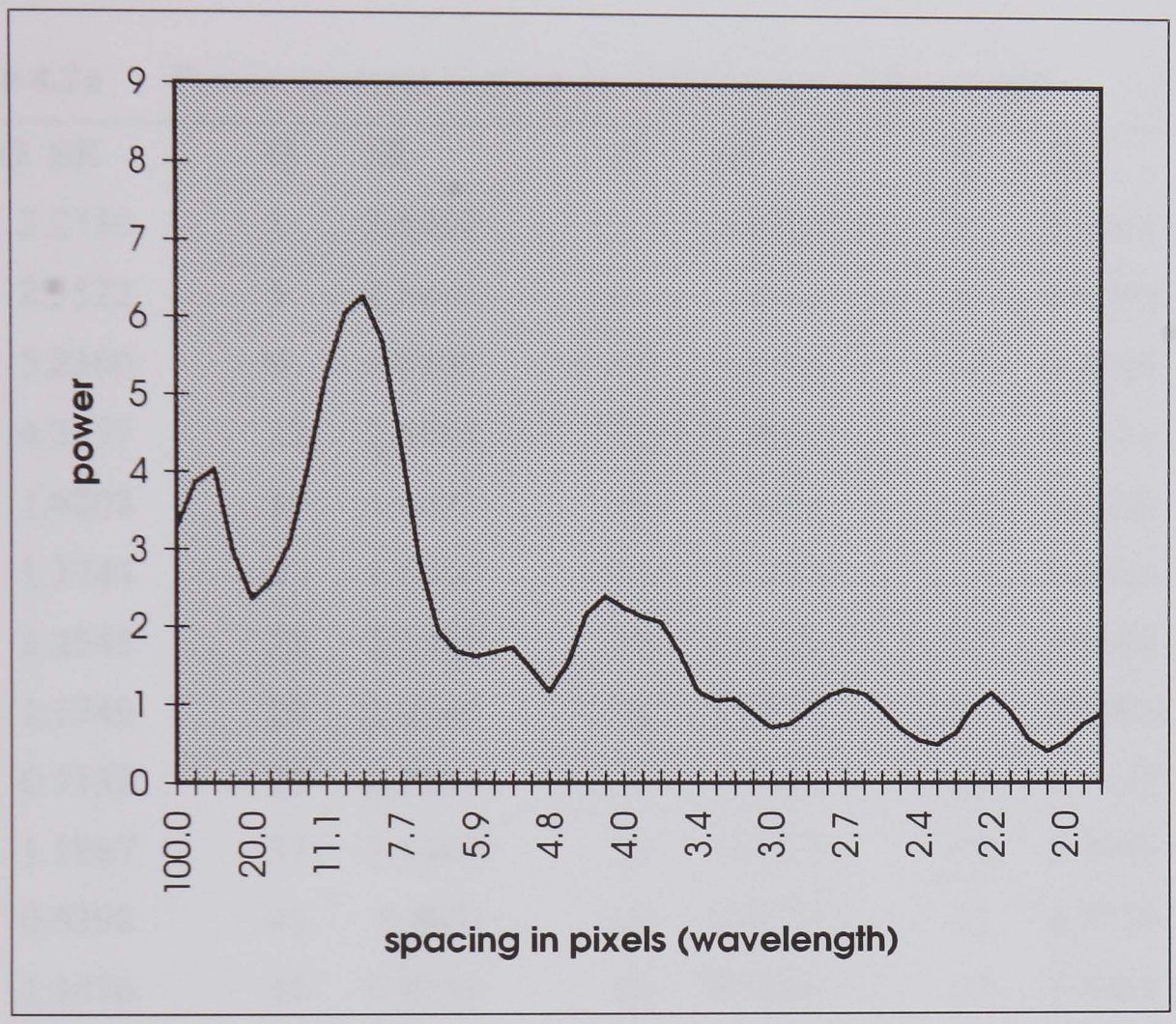

Figure 4.9
Smoothed power spectral density function of transect T2 , figure 4.3

Table 4.2a Power spectral Estimates of Transect of figure 4.3

(SP)Q	SE	Q	SE	Q	SE	Q	SE
0	3.2730	1	3.8480	2	4.0311	3	2.9733
4	2.3522	5	2.5817	6	3.0762	7	4.0406
8	5.2360	9	6.0400	10	6.2580	11	5.6940
12	4.3557	13	2.8573	14	1.9409	15	1.6823
16	1.6208	17	1.6697	18	1.7429	19	1.4489
20	1.1744	2	1.5500	22	2.1765	23	2.4038
24	2.2545	25	2.1310	26	2.0706	27	1.6883
28	1.1749	29	1.0543	30	1.0740	31	0.8804
32	0.7132	33	0.7583	34	0.9327	35	1.1133
36	1.1967	37	1.1447	38	0.9527	39	0.7079
40	0.5398	41	0.4871	42	0.6378	43	0.9786
44	1.1476	45	0.9193	46	0.5640	47	0.4094
48	0.5173	49	0.7591				

Q = Spectral computational number, **SE** = Spectral Estimates

Wavelength (spacing in pixels) = $\frac{2.L}{Q} = \frac{2(50)}{Q}$

Table 4.2b g_r **Ratios for Spectral Estimates of Transect of figure 4.3**

Q	g_r	Q	g_r	Q	g_r	Q	g_r
0	0.1304	1	0.1533	2	0.1606	3	0.1184
4	0.0937	5	0.1028	6	0.1225	7	0.1610
8	0.2086	9	0.2406	10	0.2493	11	0.2268
12	0.1735	13	0.1138	14	0.0773	15	0.0670
16	0.0646	17	0.0665	18	0.0694	19	0.0577
20	0.0468	21	0.0617	22	0.0867	23	0.0958
24	0.0898	25	0.0849	26	0.0825	27	0.0673
28	0.0468	29	0.0420	30	0.0428	31	0.0351
32	0.0284	33	0.0302	34	0.0372	35	0.0443
36	0.0477	37	0.0456	38	0.0379	39	0.0282
40	0.0215	41	0.0194	42	0.0254	43	0.0390
44	0.0457	45	0.0366	46	0.0225	47	0.0163
48	0.0206	49	0.0302				

4.11.2 Confidence Limits

Another method of testing the statistical significance of the spectral estimates is to find the confidence limits of the spectrum based on the method described by Jenkins and Watts (1968). For the estimated spectrum $S(\omega)$, Jenkins and Watts show that the ratio

$$\frac{\gamma . \textit{Spectral Estimates}}{\textit{Theoretical Estimates}} \qquad \textbf{4.20}$$

is approximately distributed as chi-squared (χ^2) where

$$\gamma = \frac{2n}{\sum_{k=-M}^{M} \lambda_k^2} \qquad \textbf{4.21}$$

γ is the number of the degrees of freedom of the lag window and M, k and λ are as defined by equations 4.13 and 4.15

For any of the spectral estimates, Jenkins and Watts (1968), and Chatfield (1987) showed that the confidence limit will be given by

$$\frac{\gamma . \textit{Spectral Estimates}}{\chi^2_{\gamma,\frac{\alpha}{2}}} \quad \textit{To} \quad \frac{\gamma . \textit{Spectral Estimates}}{\chi^2_{\gamma,1-\frac{\alpha}{2}}} \qquad \textbf{4.22}$$

where α is the confidence level.

The spectral estimate is considered as independent, non significant if it falls within the range of the confidence limit and significant if it falls outside this range.

This research makes use of the fisher's test to establish the significance of the spectral estimates because it is mathematically more rigourous than the confidence limit test.

Table 4.3: Example of a transect output file

Transect output: 4-Jan-1994

Image name: TBOT.lan

Image size: 1446 rows, from 1 to 1234

1446 columns, from 1 to 1235

Number of bands:7

Transect from row 386, column 225

to row 390, column 225

Number of points in transect: 5

Band selected: 4

Row	**Col**	**Value**
386	225	91
387	225	90
388	225	73
.....		
.....		

4.12 Programme for Spectral Analysis

The analysis of spatial series of lineaments is achieved in two stages. First of all the transect is extracted from the image with the program TRANSECT and then it is analysed using the program SPECTAN.

4.12.1 Extraction of the Transect.

ERDAS image processing software was used for processing the images in this thesis. Unfortunately there is no routine in ERDAS for extracting the transect. The Program *TRANSECT* written by Peter Bragg of the Geography department, University of Sheffield has been incorporated into ERDAS and was used for obtaining the transect.

In the program operation, the name of the image file (fname.lan) and the start and end co-ordinates of the transect are input. The program also asks for the band to be utilised since *TRANSECT* can only work on one band at a time. On exit, the transect, table 4.3 is produced with header information that contains the date when the transect was produced, the name of the image from which the transect was extracted, the size of the image, number of bands in the image, the start and end co-ordinates of the transect, number of points on the transect and lastly the band selected.

The data information follows immediately after the header, showing the co-ordinates of the transect and their respective DN values

4.12.2 Analysis of the Transect

For the analysis of the transect, the author has written FORTRAN 77 programs (see appendix 1) and some adapted from the *NAG* and *GHOST-88* routines at the Sheffield University Computer services to create the program *SPECTAN.*

SPECTAN is portable to any computer with a FORTRAN compiler containing the *NAG* and *GHOST-88* routines.

Before the program is executed, the values for the cut off point of the Tukey window M, the frequency division L and the number of autocovariances to be calculated are set. A decision as to whether the mean should be corrected is made and the data tapered.

If the plot of the transect provides evidence of non-stationarity of the transect or if analysis shows tailing of the power spectral density function with no apparent peak in the result, then the transect can be detrended. A routine for doing this has also been incorporated into the program *SPECTAN*.

At this stage, *SPECTAN*, calculates the autocovariance coefficients which are in turn used to calculate the smooth power spectral estimate using the fast fourier transform technique. Using the spectral estimates and the transect data, the test statistics are calculated by the Fisher (1929) method.

The output of the analysis consists of a printout of the smoothed spectral estimates for each frequency division (Table 4.2a)and a plot of these values against the frequencies or wavelengths (Figure 4.9), and the Fisher test statistics (table 4.2b).

The presence of any significant peak in the results will reveal the presence of cyclicity in the transect and the wavelength in pixel at which this occurs.

4.13 Methodology for Analysing the Transect

The flow chart represented in figure 4.10 describes the method employed in the analysis of a transect.

4.13.1 Practical Steps in Analysing the Transect

The major steps in the analysis as shown on the flow chart are as follows

1. Correct trend and mean of the transect if plotting shows non stationarity of the mean. The transect is made stationary by the difference method. The mean from the detrended transect is also corrected by subtracting it from the transect values.

2. Calculate the sample autocovariance function

3. Smooth the sample autocovariance function using the Tukey window and then transform the smoothed sample autocovariance function to get the smooth spectral estimates by the fast fourier transformed.

4. Test for the significance of the smoothed spectral estimate using Fisher's test.

5. Interpret results.

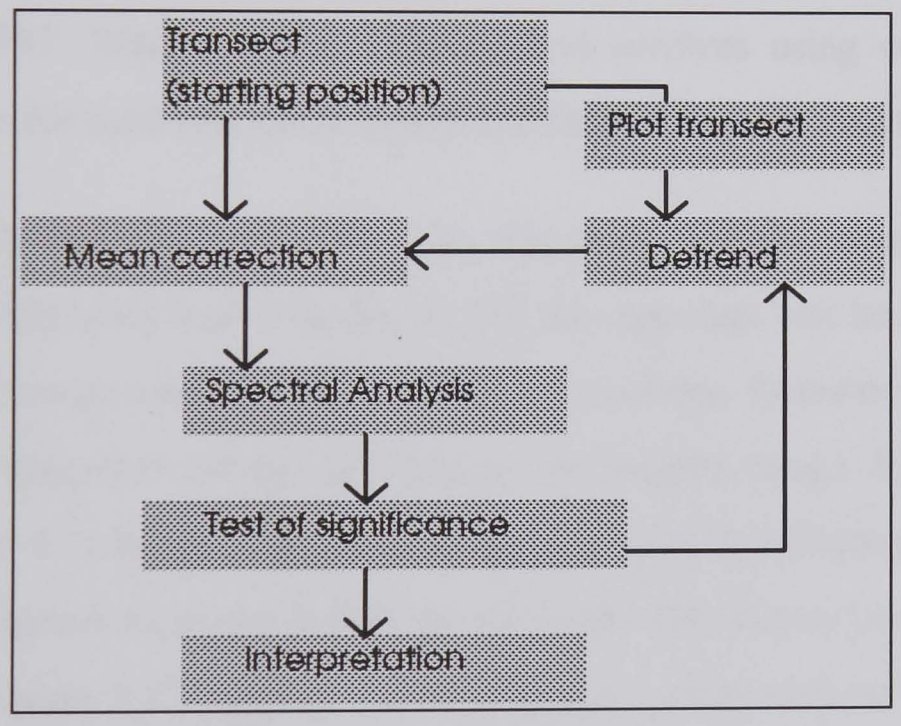

Figure 4.10

Flow diagram of the method for analysing transects

4.14 Fourier Analysis on the Image

So far, the use of spectral analysis has concentrated on the radiometric transect extracted from the image. Spectral analysis can also be performed on the satellite image. Conceptually, the grey scale value of a single band image can be viewed as a 3 dimensional surface which is defined by the row and column as the X and Y axis respectively with the grey scale value (DN) defining a third axis (Z). A series of waveforms can thus be fitted to the grey level surface to define the image in the frequency domain.

Defining the image in this fashion can therefore help in providing information about the different frequency scale components present in the image and the proportion of information associated with each frequency by using fourier analysis.

The result of fourier analysis on the image is the amplitude spectrum and its calculation is similar to that of a radiometric transect or a time series (Gonzalez and Wintz, 1987, Marion, 1991). The method involves using one-dimensional fourier analysis for each row of the image and then adding the results.

Having transformed the image into the frequency domain, operations can be performed on the individual frequencies and the spectrum can be re-transformed to the original image using the inverse fourier transform. Features represented on the amplitude spectrum can be identified on the original image. For example the image of figure 4.11 has been analysed using the fourier technique and the result is presented in figure 4.12 as the amplitude spectrum. The cluster forming a uniform orientation in figure 4.12 suggests the presence of a major feature (lineaments) in the image arranged orthogonally to the orientation of the cluster.

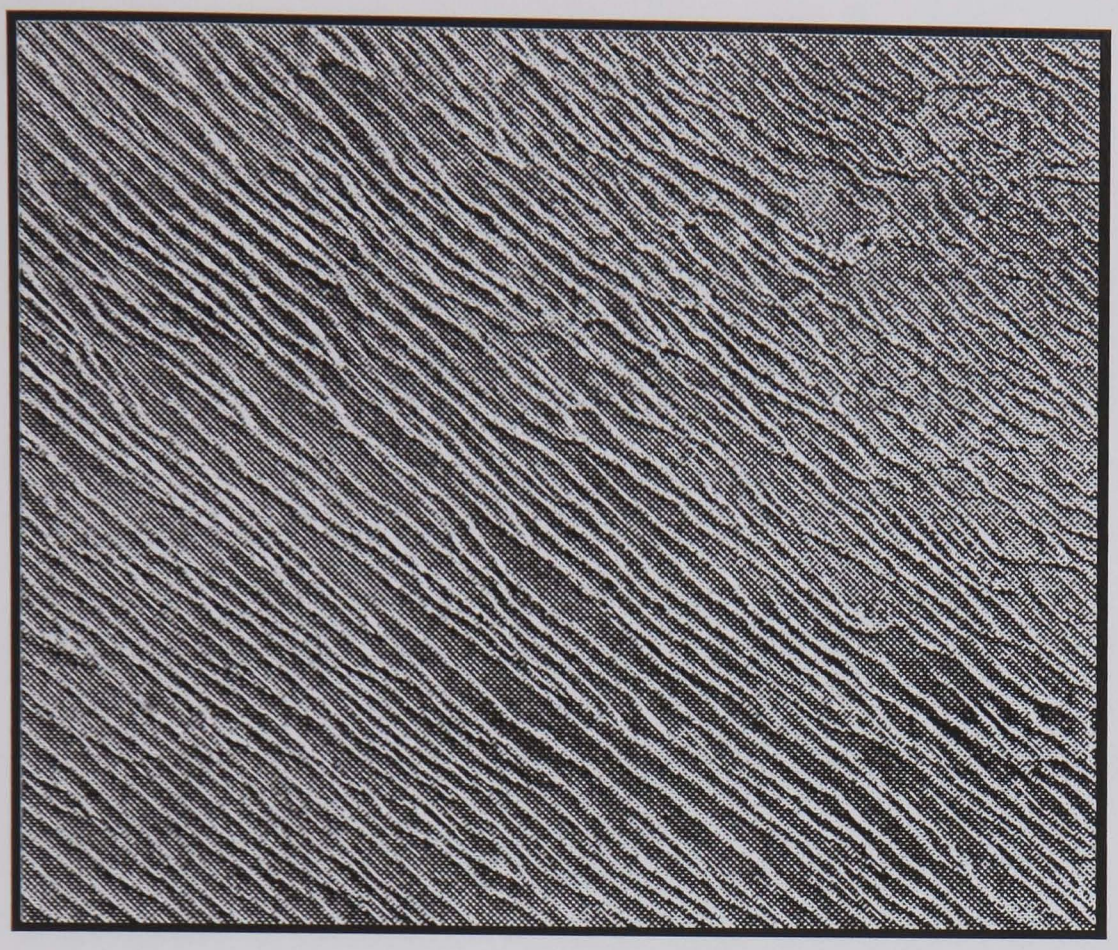

Figure 4.11 Satellite image(Landsat TM) showing linear sand dune lineaments

Figure 4.12 Fourier analysis(amplitude spectrum) on image of figure 4.11.

4.15 Other Applications of Spectral (Fourier) Analysis

The amplitude spectrum obtained from fourier analysis of the image contains information regarding the frequency and phase angles of the waveforms into which the image has been decomposed. The major use of fourier analysis in remote sensing is in:

- **Frequency domain filtering:**

Filtering using this method consists of the following operations:

1. The forward fourier transform is performed to compute the amplitude spectrum.
2. Frequencies that are of interest are highlighted by multiplying by a factor or by stretching and those that are not wanted are suppressed.
3. Performing an inverse fourier transform will give the enhanced image.

This method of filtering is useful for removing noise such as striping and spots in imagery. By identifying their periodicities, they can then be removed from the imagery.

- **Characterisation of terrain types;**

The amplitude spectrum obtained from the fourier transform of the image is arranged in such a way that points closest to its origin will represent low frequency features or smoothly varying features while those furthest away from the origin will represent high frequency or rapidly changing features. Blom and Daily, 1982; Stromberg and Farr, 1986 have used this characteristic of amplitude spectrum to measure texture or the spatial variability in images. From the amplitude spectrum of two images or two different bands of the same image, the location of points on it will determine the relative spatial variability of the images

or bands and hence made it possible to characterise the terrain types depicted on the image.

The method has also been applied by Townshend and Justice, 1990 to test for spatial variation of vegetation changes at different scales which showed that variations from a wide variety of scales contributed substantially to the overall variance of a particular image. This explains the difficulty of obtaining a particular spatial resolution for studying lineaments.

4.16 Spectral Analysis on Simulated Transects

In order to test the validity of spectral analysis, the method was applied to the designed transects represented by figure 4.13. The transects were generated such that figure 4.13a has a wavelength of 12 pixels and figure 4.13b a wavelength of 6 pixels while figure 4.13c was randomly generated with no apparent periodicity. Figure 4.13d was formed by combining transects of figures 4.13a, b, and c.

Spectral analysis on these transects gave the results shown on the spectral density functions represented by figure 4.14. The spectral density functions established the presence of periodicities and the wavelengths at which they occurred. Figures 4.14a, b, c, and d corresponds to spectral density function of transects of figures 4.13a, b, c, and d.

Spectral analysis has thus been able to isolate the wavelength from the transects except for the random transect which has no cyclicity. Most importantly, spectral analysis has been able to isolate multiple wavelengths from the transect even though the transect was masked by the random transect. The strength of this analysis is derived from the fact that the method can isolate periodicities from transects even when noise components are embedded in the transect, which is likely to be the case for many remotely sensed images.

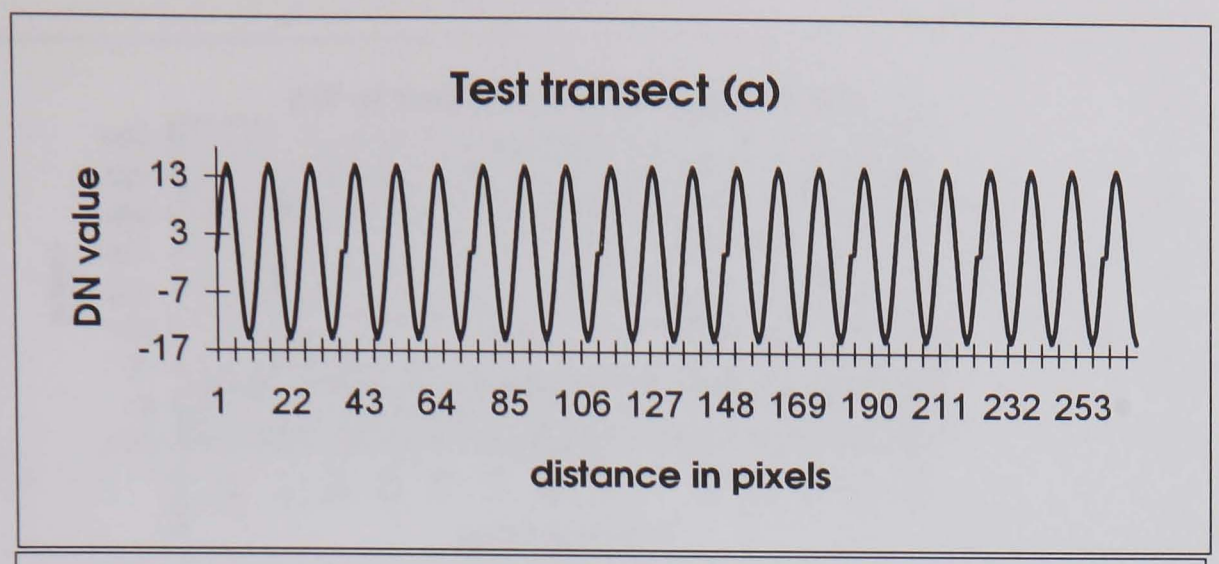

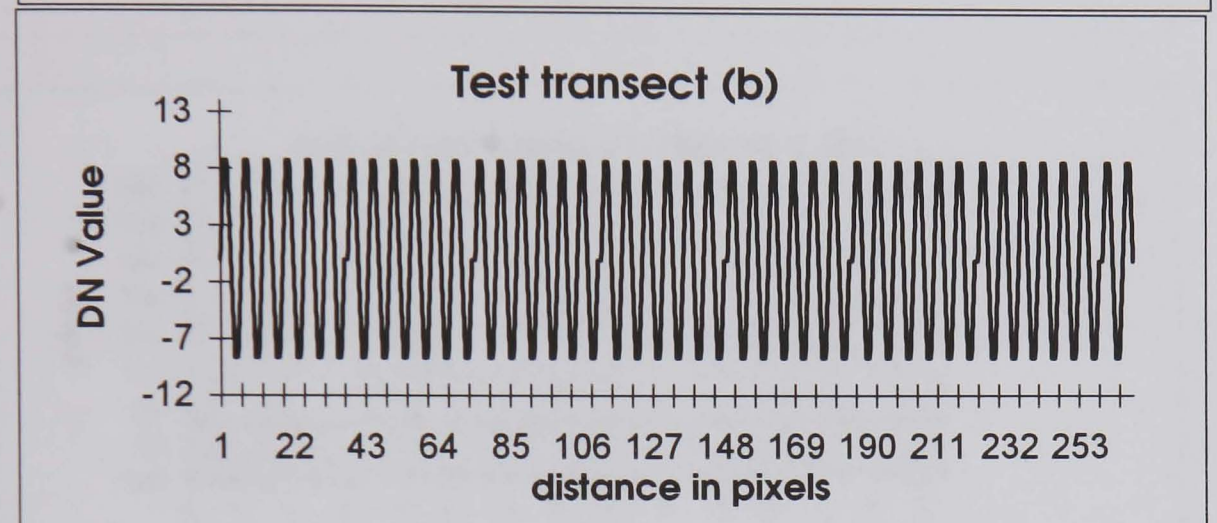

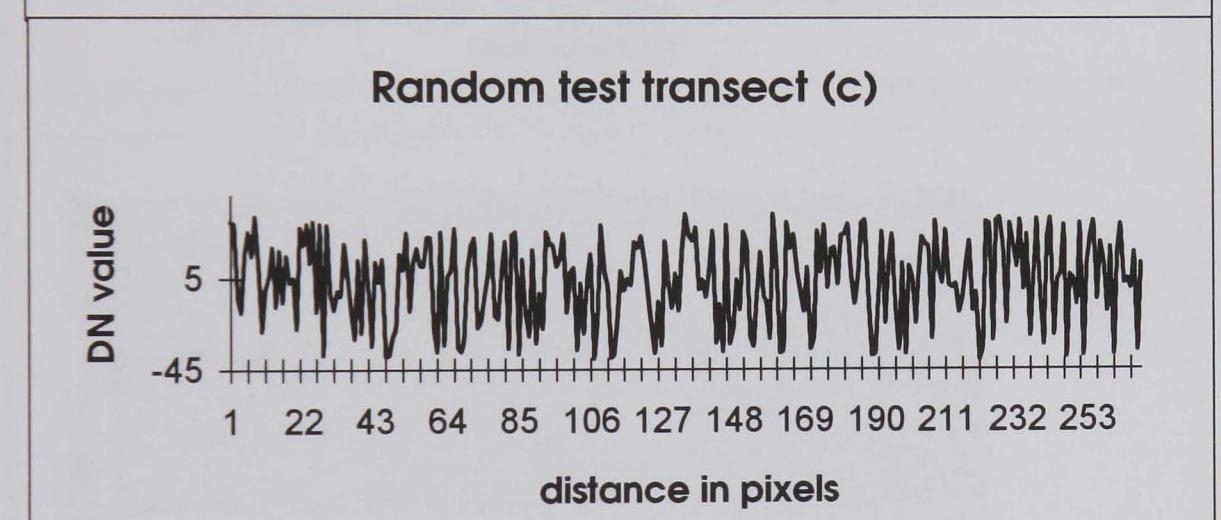

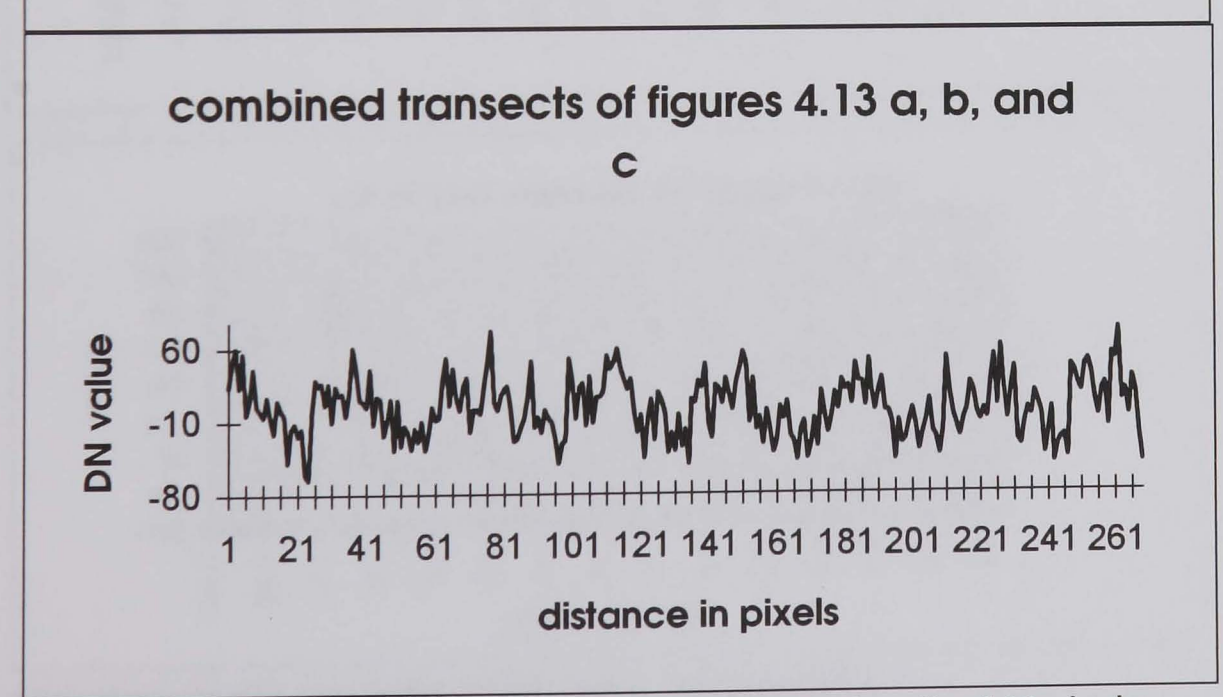

Figure 4.13 Generated test transects (a) with wavelength of 12 pixels (b) with wavelength of 6 pixels (c) random transect with no periodicity (d) combination of transect a, b, and c

a

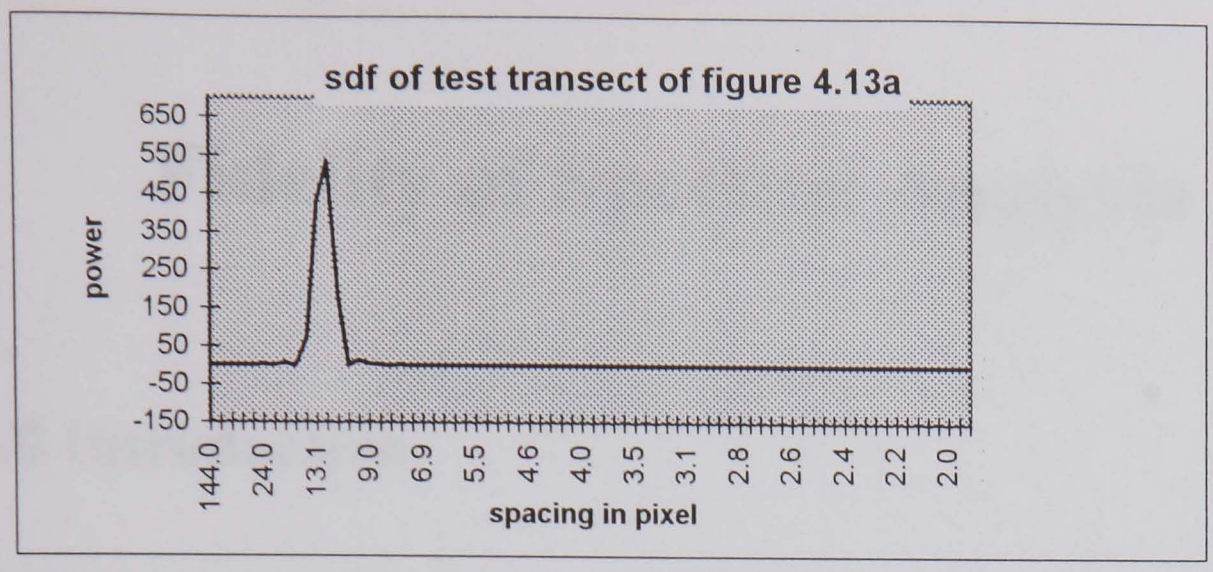

b

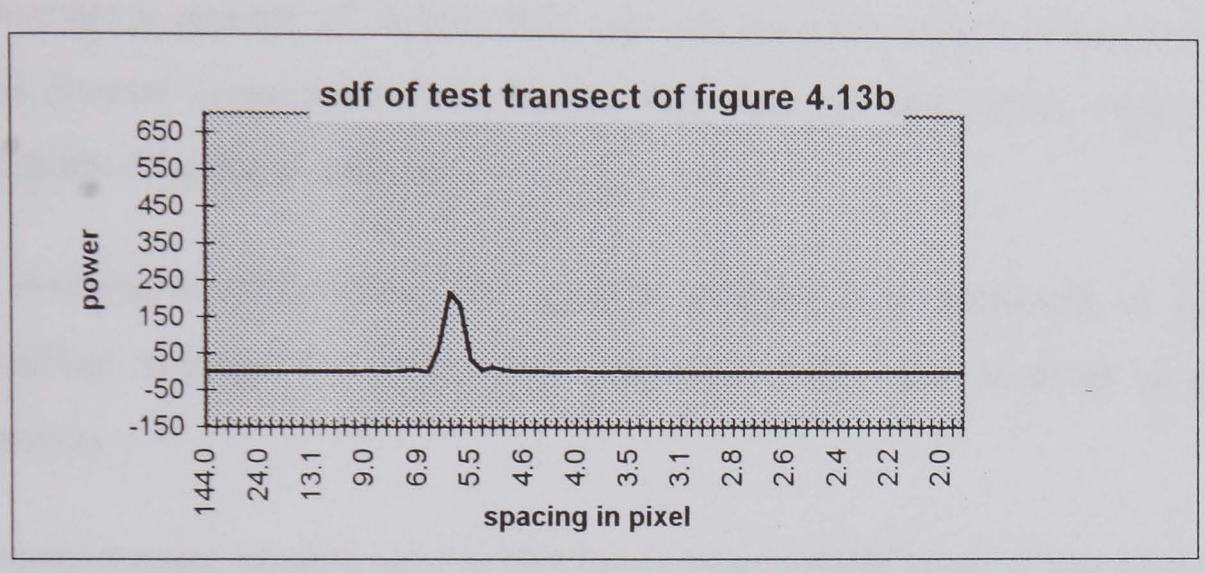

c

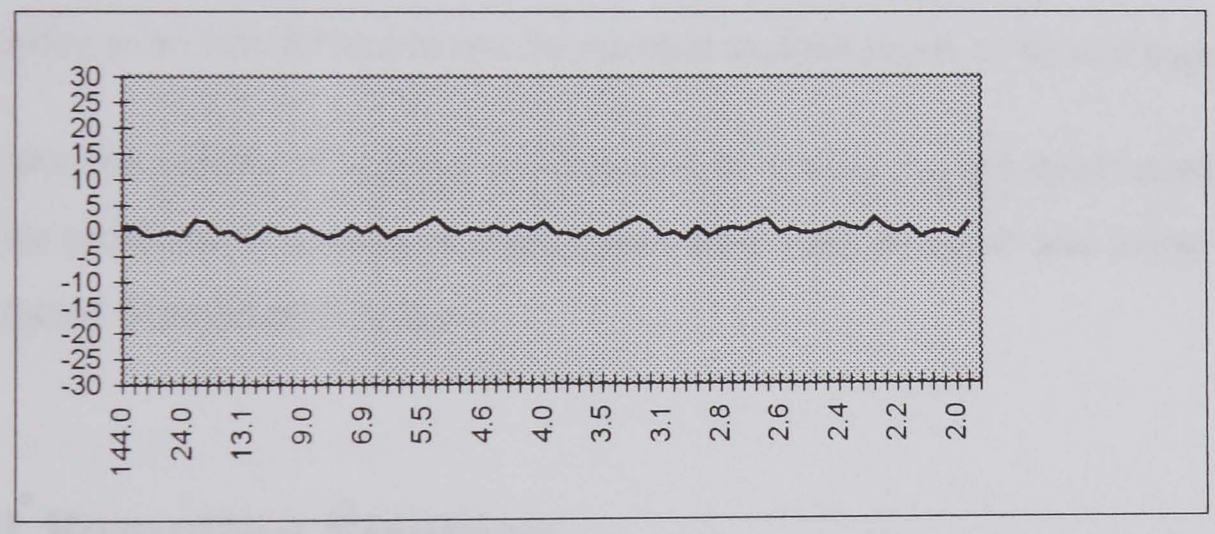

d

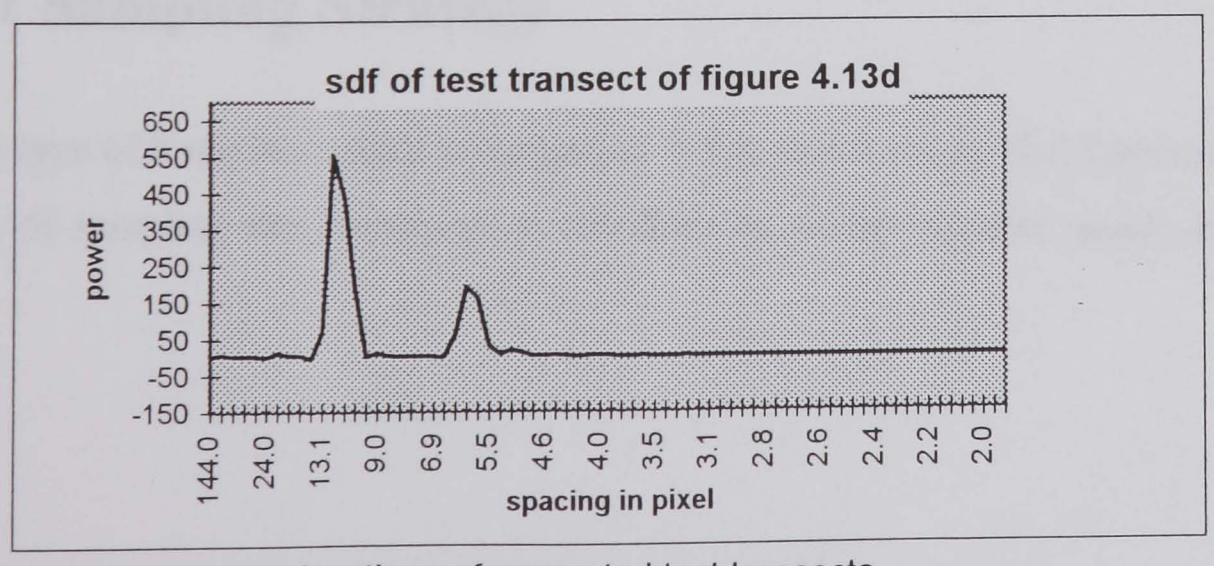

Figure 4.14 spectral density functions of generated test transects
(a) with wavelength of 12 pixels (b) with wavelength of 6 pixels
(c) random transect with no periodicity (d) combination of transect a, b, and c

Chapter 5

Fidelity of Spectral Analysis

5.0 Introduction

There are a number of factors that can influence the results of spectral analysis. This chapter investigates these factors and also provides further support for the reliability of spectral analysis.

In devising a methodology for spectral analysis it is necessary to establish a sampling strategy for identifying lineament fields and locating positions of transects.

Remote sensing images used in this thesis have a multi spectral resolution and the question as to which band to use for spectral analysis needs to be investigated.

To test the validity of spectral analysis and to answer the questions posed by the above problems, a number of experiments have been designed and tested on data extracted from satellite images.

5.1 Sampling Strategy

The type of lineament under investigation in this thesis are parallel lineaments. The aim of sampling the lineaments is therefore to locate sections (lineament field)

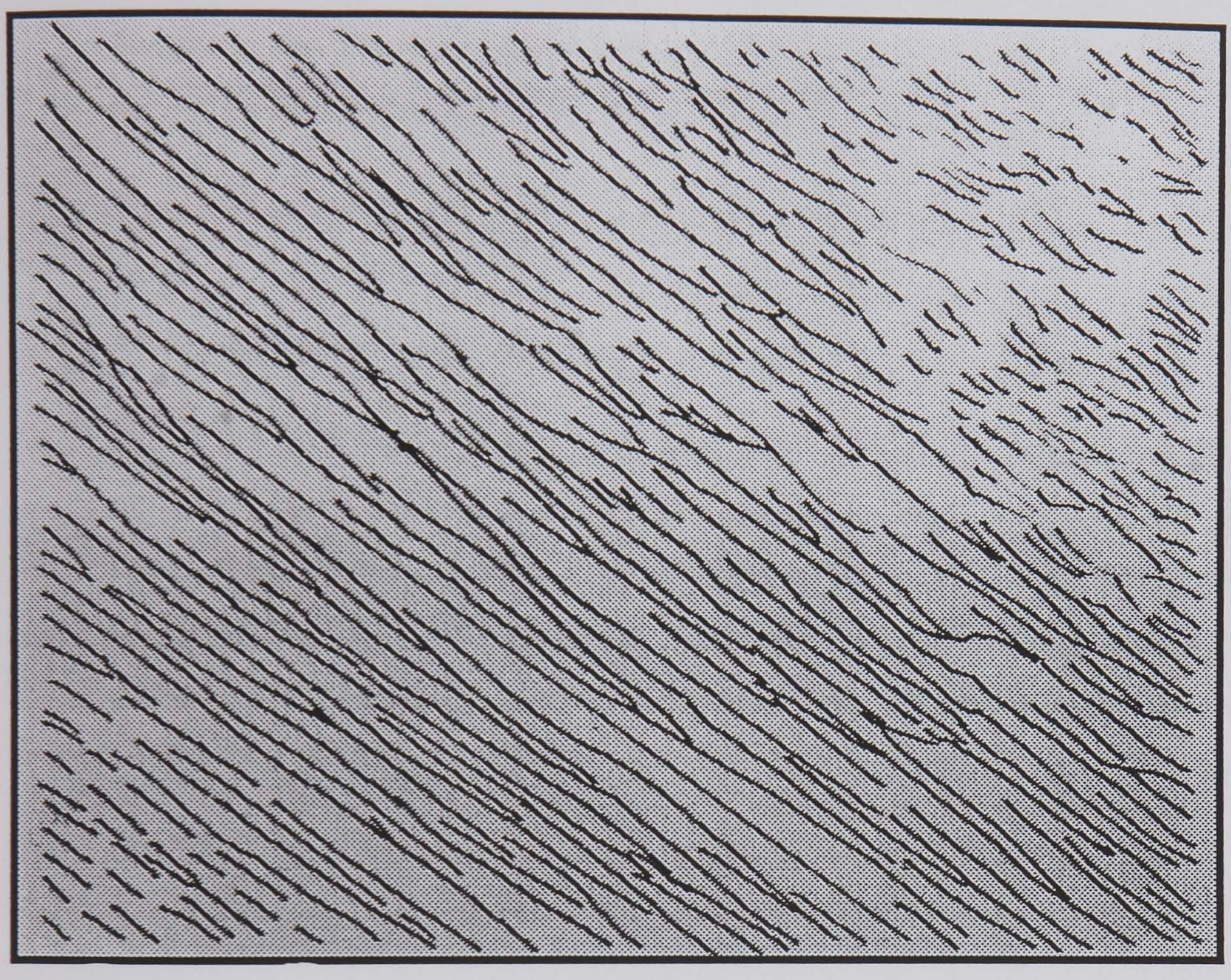

Figure 5.1

Pattern of a lineament field

within the image having lineaments of uniform orientation (lineament set). This helps in positioning the transects and defining the topological pattern (chapter 6) of the lineaments.

The term *lineament field* here refers to an area on an image covered by parallel lineaments and *lineament set* to a group of lineaments with the same orientation but not necessarily uniform in the distribution of the other parameters

The strategy for sampling used in this thesis was to make a hard copy of the images and then on tracing paper to mark some of the lineaments. This establishes a flow pattern such as in figure 5.1

Figure 5.1 is a trace of lineaments made from one of the images used in this research. The trace shows a parallel flow oriented in the NW-SE direction. Two flow sets have been located in the figure differentiated only by the dimensions of the lineament. In other situations, flow sets may be differentiated by the orientation of lineaments. This approach was used for all the other images to establish the different flow sets present.

5.2 **Band Selection for Spectral Analysis**

Since satellite images have a multispectral resolution, the question of which band to use for spectral analysis is of prime consideration in order to establish an optimal methodology. To answer this question, two study areas were chosen; from a Landsat MSS image depicting glacial lineaments and a Landsat TM image depicting aeolian lineaments (Figure 5.2.) These images have spatial and spectral resolutions of 79m and 4 wave bands for the Landsat MSS image and 30m and 7 wave bands for the Landsat TM image.

a

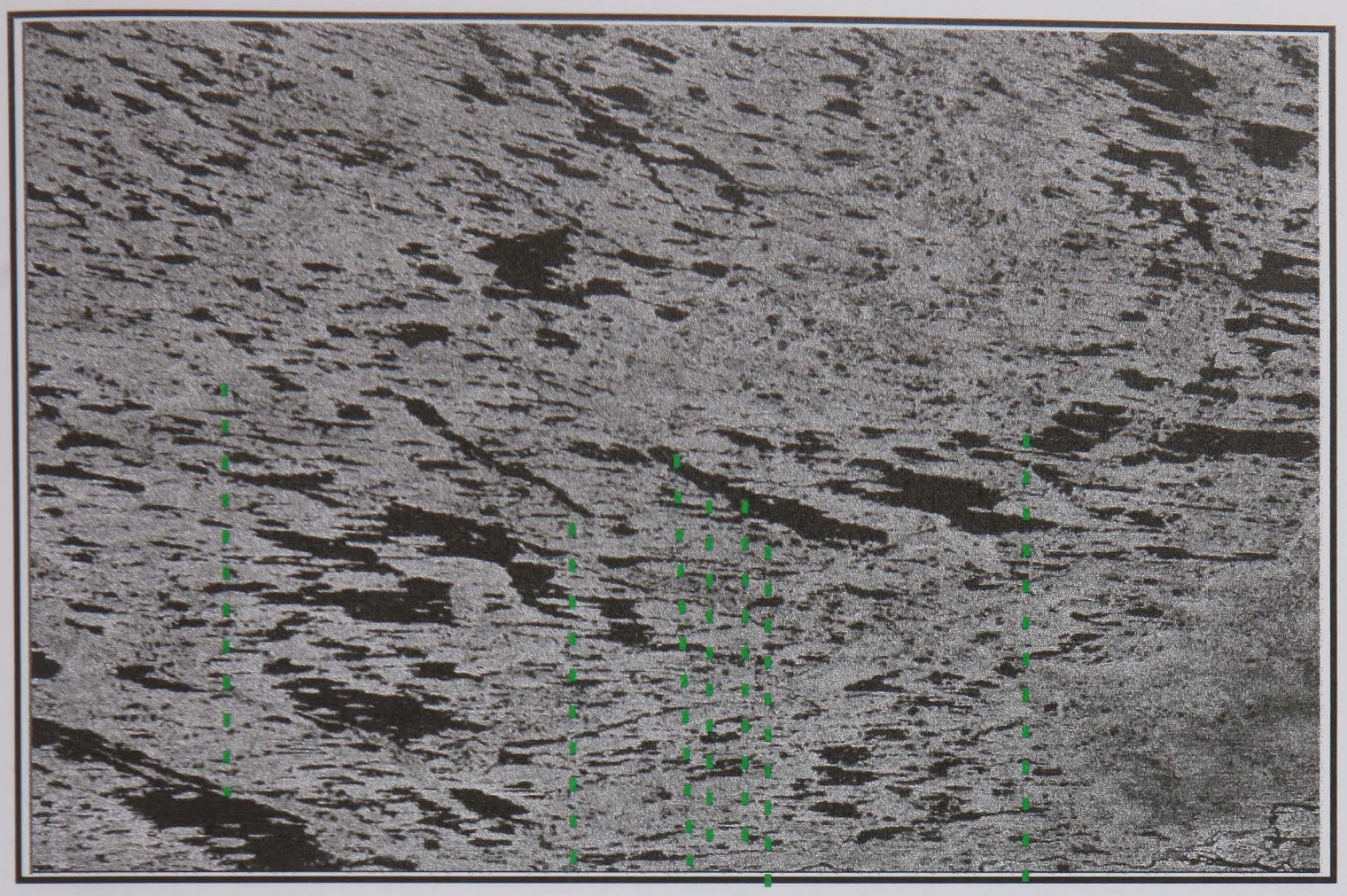

b

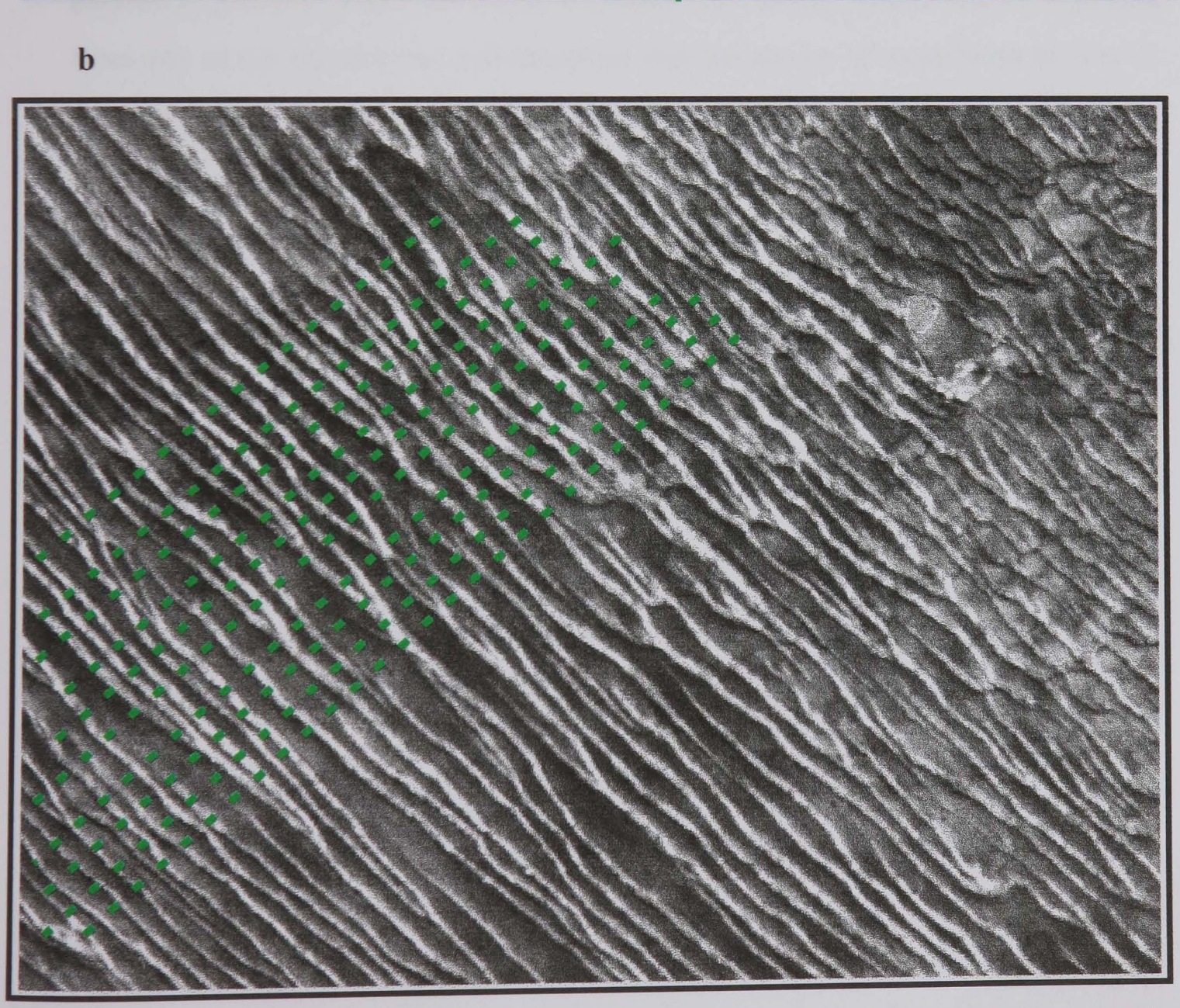

Figure 5.2 (a) Landsat MSS image (band 1) and TM image (band 4) showing transects positions used for band selection.

Transects were defined for each of the study areas for the two images such that they were perpendicular to the orientation of the lineaments. Using the program *TRANSECT*, the transects were obtained for each of the bands.

5.2.1 Band selection for the Landsat MSS image

For the Landsat MSS image, 7 transect locations were defined (Figure 5.2a) and for each location, four transects were obtained i.e. of each band 1, 2, 3, and 4. The transects were analysed using the program *SPECTAN*, and the result are presented in table 5.1.

From table 5.1b, it can be observed that the results from spectral analysis for any particular transect is similar for all the bands used. The spacings are depicted in pixels and it can be observed that most of the transects have multiple spacings. There are instances of differences of only a pixel between different bands for a particular transect. This experiment indicates that similar results will be obtained from any of the wavebands, and therefore that the choice of wave band for use in spectral analysis is not critical. The high degree of similarity of the results between bands for a particular transect is not surprising considering the high positive correlation coefficients between the bands, as shown in table 5.1a.

For subsequent analysis using Landsat MSS images, band 1 was chosen with the knowledge that use of any other band would give the same results.

5.2.2 Band selection for the Landsat TM image

For this image, 10 transect positions were defined (figure 5.2b) and for each position, 7 transect were extracted for each of bands 1, 2, 3, 4, 5, 6 and 7. The result of spectral analysis performed on these transect is presented in table 5.2.

For most band combinations with the exception of band 1 against 3, 4, and 7 and for any other combination involving band 6, wavebands are often fairly highly

Table 5.1a Correlation coefficient between bands for Landsat MSS Image.

	Band 1	Band 2	Band 3	Band 4
Band 1				
Band 2	**0.89**			
Band 3	**0.65**	**0.79**		
Band 4	**0.60**	**0.75**	**0.99**	

Table 5.1b Results of spectral analysis (depicting spacing in pixels) using all bands for the raw Landsat MSS image.

Transects	Band 1	Band 2	Band 3	Band 4
T1	4, 5, 10	4, 5, 10	4, 5, 9	4, 5, 9
T2	7, 10, 20	8, 10, 20	7, 9, 20	7, 10, 20
T3	4, 5, 8	4, 5, 9	4, 5, 9	5, 8
T4	5, 8, 13	4, 8, 13	5, 9, 13	5, 9, 13
T5	5, 6, 8, 25	4, 5, 8, 25	4, 5, 8, 25	5, 6, 8, 25
T6	5, 6, 8, 20	5, 6, 8, 20	5, 6, 9, 20	5, 6, 9, 17
T7	5, 9, 17	5, 9, 17	6, 9, 17	6, 9, 17

Table 5.2a Correlation coefficients between bands of the Landsat TM image

	Band 1	Band 2	Band 3	Band 4	Band 5	Band 6	Band 7
Band 1							
Band 2	**0.78**						
Band 3	**0.48**	**0.87**					
Band 4	**0.41**	**0.83**	**0.98**				
Band 5	**0.78**	**0.76**	**0.81**	**0.80**			
Band 6	**0.12**	**0.0039**	**-0.09**	**-0.13**	**0.12**		
Band 7	**0.47**	**0.74**	**0.81**	**0.80**	**0.97**	**0.15**	

Table 5.2b Results of spectral analysis (depicting spacing in pixels) using all bands for the Landsat TM image.

Transect	Band 1	Band 2	Band 3	Band 4	Band 5	Band 7
T1	**5, 13**	**6, 13**	**6, 13**	**6, 13**	**6, 13**	**6, 13**
T2	**9, 13**	**9, 13**	**9, 13**	**9, 13**	**9, 13**	**9, 13**
T3	**4, 10**	**5, 11, 15**	**4, 11, 15**	**4, 11, 15**	**5, 11, 15**	**4, 11, 15**
T4	**6, 11**	**7, 11**	**11**	**11**	**11**	**11**
T5	**12**	**13**	**13**	**13**	**13**	**9, 14**
T6	**7, 11, 16**	**8, 12, 16**	**8, 12, 16**	**8, 12, 16**	**8, 12, 16**	**8, 12, 16**
T7	**10, 14, 18**	**9, 13, 17**	**9, 13, 17**	**9, 13, 17**	**9, 13**	**9, 13**
T8	**7, 15**	**8, 12**	**5, 9, 12**	**8, 12**	**8, 12**	**8, 12**
T9	**9, 16**	**8, 16**	**7, 16**	**8, 10, 16**	**10, 16**	**7, 16**
T10	**8, 13, 18**	**10, 18**	**10, 18**	**10, 18**	**10, 18**	**10, 18**

correlated. The reasons for these lower values are because band 1 suffers from atmospheric attenuation and band 6 is a thermal channel, sensing in a very different part of the electromagnetic spectrum. The high positive correlation between bands must indicate a linear relationship of information between bands thus implying that the spacings obtained from each of the band would be related.

The results tabulated in table 5.2b show that the spacings derived for each band for the same transect position are extremely similar except for band six which is a thermal and much longer wavelength band with a coarser spatial resolution of 120 metres and so should not be used for comparison purposes. Although there is a difference of 1 pixel between bands, this is due to the method of analysis rather than the bands and the result is within the accuracy of spectral analysis. It can therefore be concluded that the results of spectral analysis are independent of the band used. For subsequent analysis using Landsat TM images, band 4 was utilised with the knowledge that any other band would give the same results.

5.3 Relationship between the Transect and the Image.

Throughout this thesis, the transect has been thought of as the image in the frequency domain (section 3.2). The purpose of this section is to demonstrate how the image matches with the transect and to make a direct comparison between spacings manually measured along the transect and spectral analysis. The main objective of the section is to show that the transect is indeed the image in the frequency domain and does record lineament character along the line where the transect was made. To carry out this test three test sites were located on 3 of the images used in this thesis called Testdunes, Testboyd and Testesk.

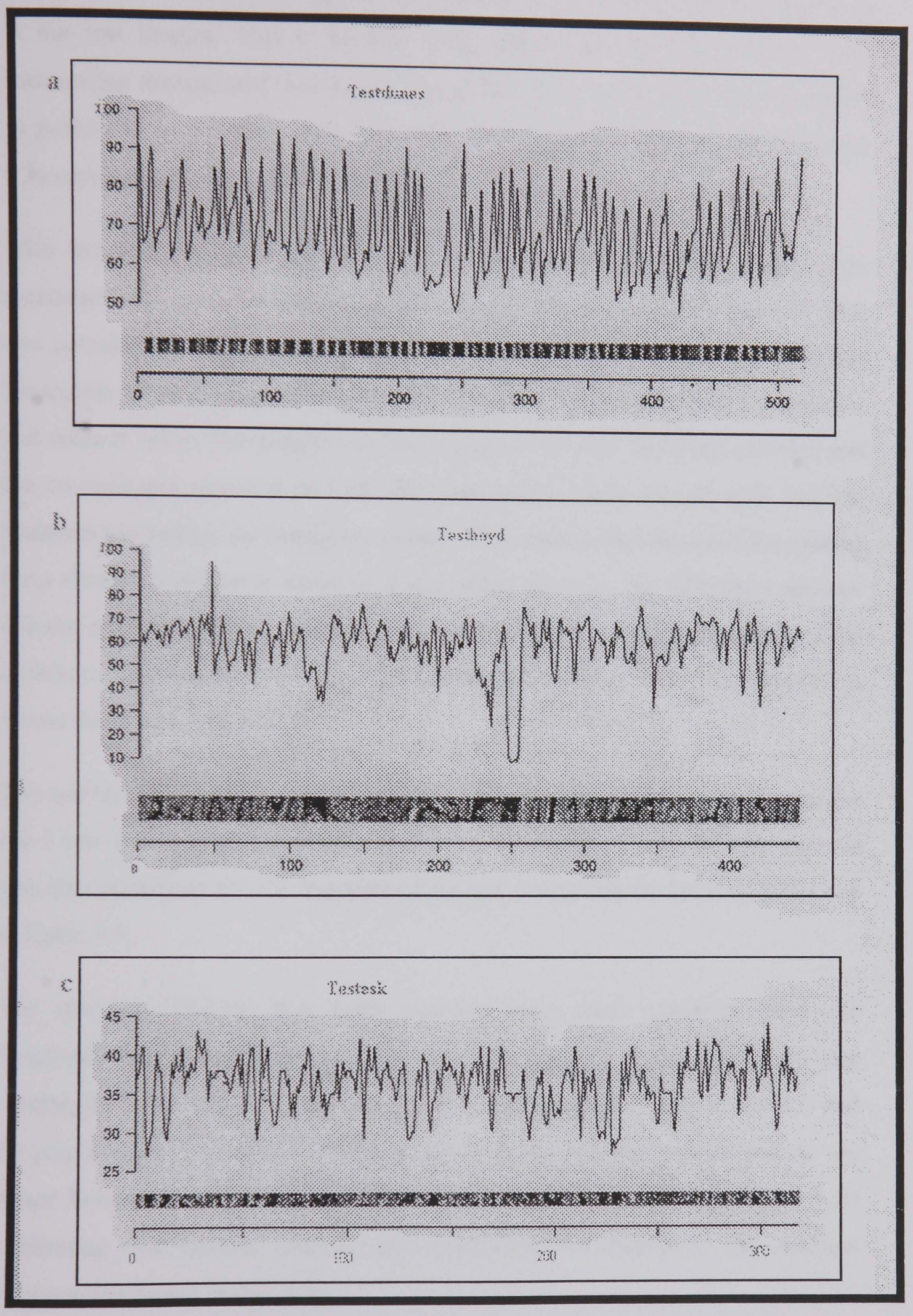

Figure 5.3
Test images with their corresponding radiometric transect, (a) Testdunes, (b) Testboyd, (c) Testesk

Figure 5.3 shows the test images and their corresponding transects. From the figures, it can be observed that the peaks in the transects represent the lineaments in the test images. This is because these lineaments are brighter than their surrounding features and thus have a higher DN value which have been registered as peaks on the transects. This is particularly evident with the transect of figure 5.3a representing the aeolian lineaments .

With the test images of figure 5.3 the spacing between the lineaments were measured using a cursor routine in the image processing software ERDAS. This was actually a semi-manual method. The cursor was placed at the centre of the lineaments at the position of the transect and the co-ordinates recorded as the row and column value. The cursor was then placed at the next lineament position and the co-ordinates recorded as well. The test images were rotated such that the transects were either horizontal or vertical. This made computation of the spacing from cursor co-ordinates easier as it was either given by the difference between column co-ordinates for a transect that cuts across the image horizontally and the difference between the rows gave the spacing for the case when the transect cut across the image vertically.

This method of test measuring the spacings between lineaments was performed for the 3 test transects and the result is summarised in figure 5.4. Spectral analysis was also performed for the transects of the test image and the result is presented in figure 5.5.

The spacings obtained from both methods show some similarity. With the Testdunes image, cursor measurement on the image and transect gave spacings ranging from 5 pixels to 21 pixels with dominant spacings falling between 7 and 10 pixels(figure 5.4i) while spectral analysis of the transect represented by the image Testdunes, established spacings (cyclicities) of 7 and 10 pixels(figure 5.5i) confirming that spectral analysis has established and quantified the spacings between lineaments in this image.

(i)

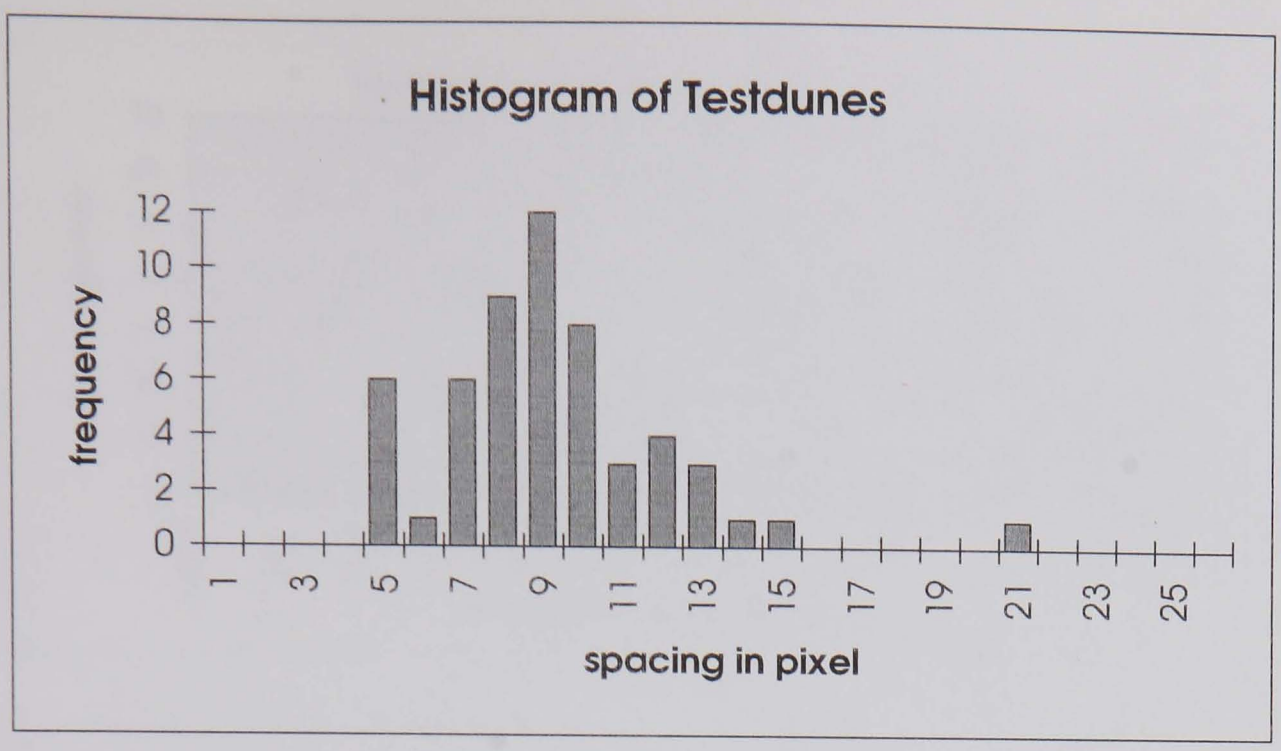

(ii)

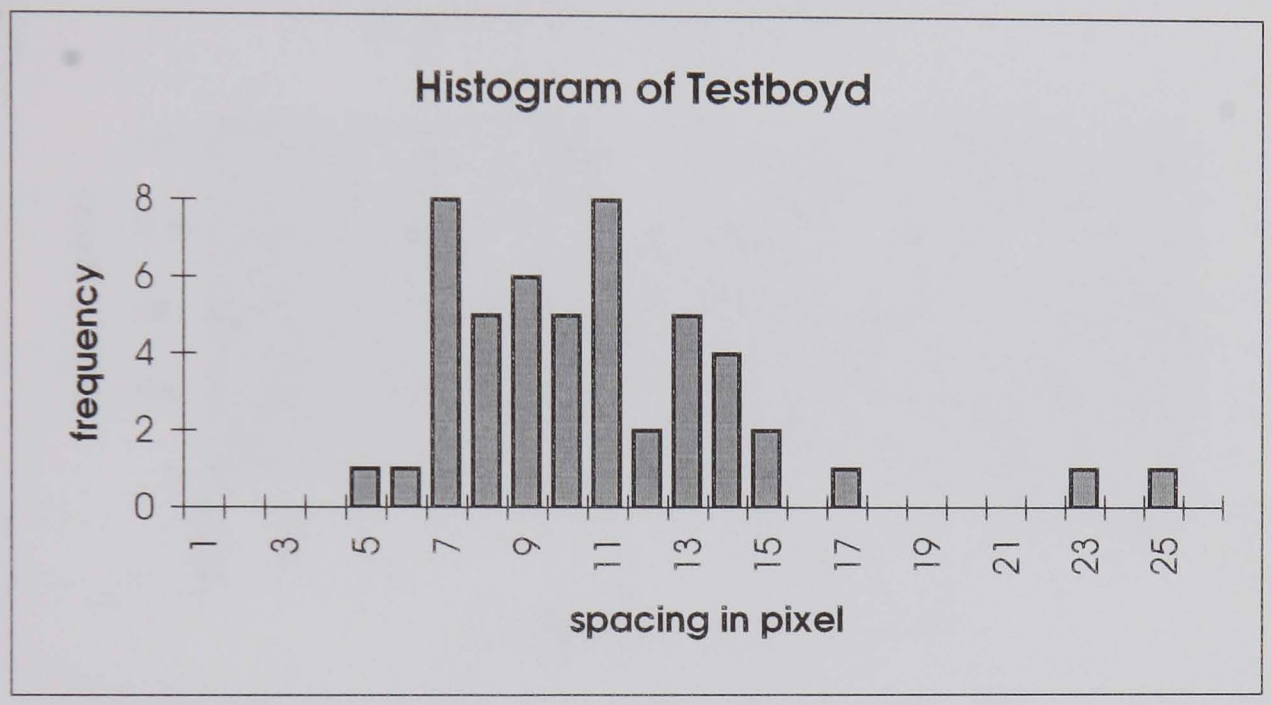

(iii)

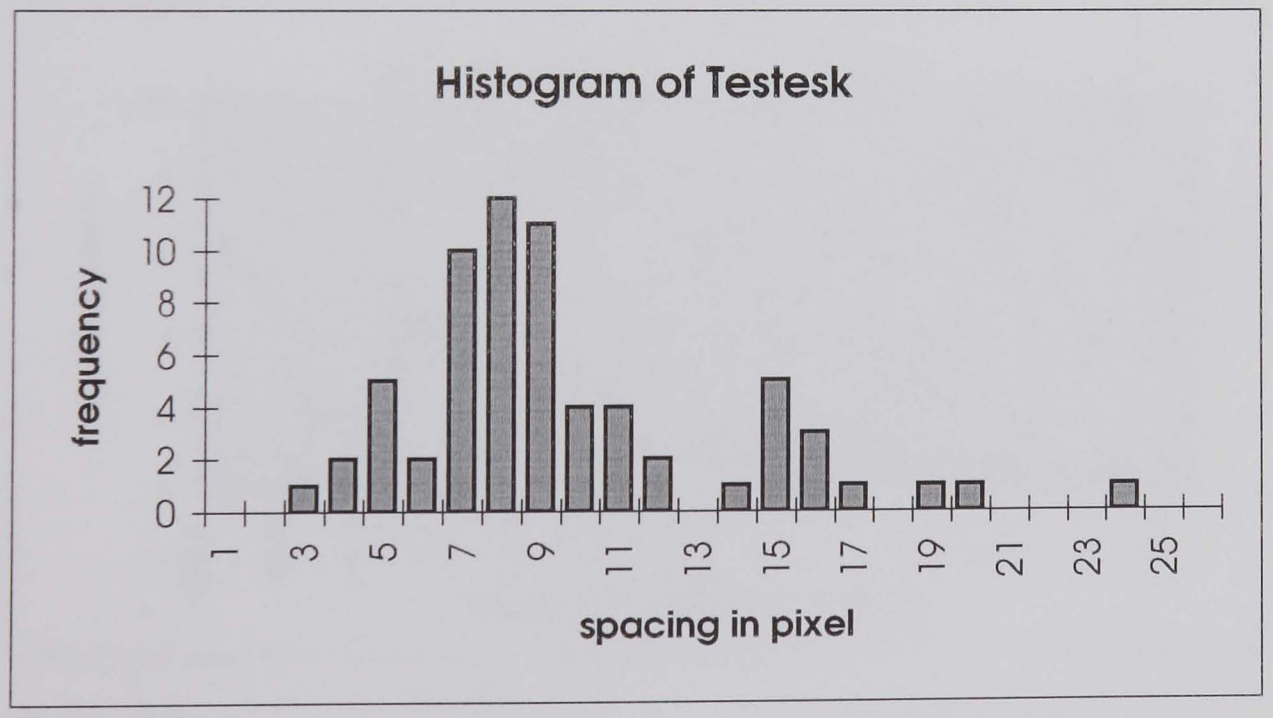

Figure 5.4 Histogram of spacing for the test areas obtained by cursor measurement on the images (i) Testdunes (ii) Testboyd (iii) Testesk

(i)

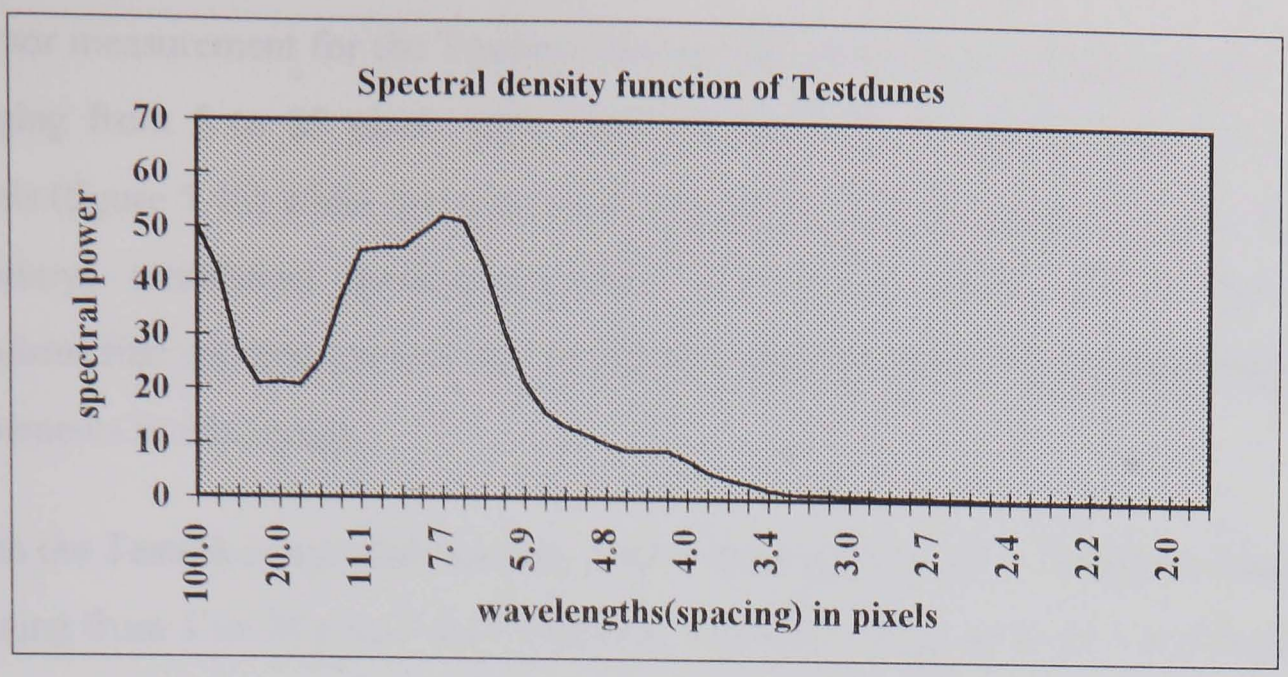

(ii)

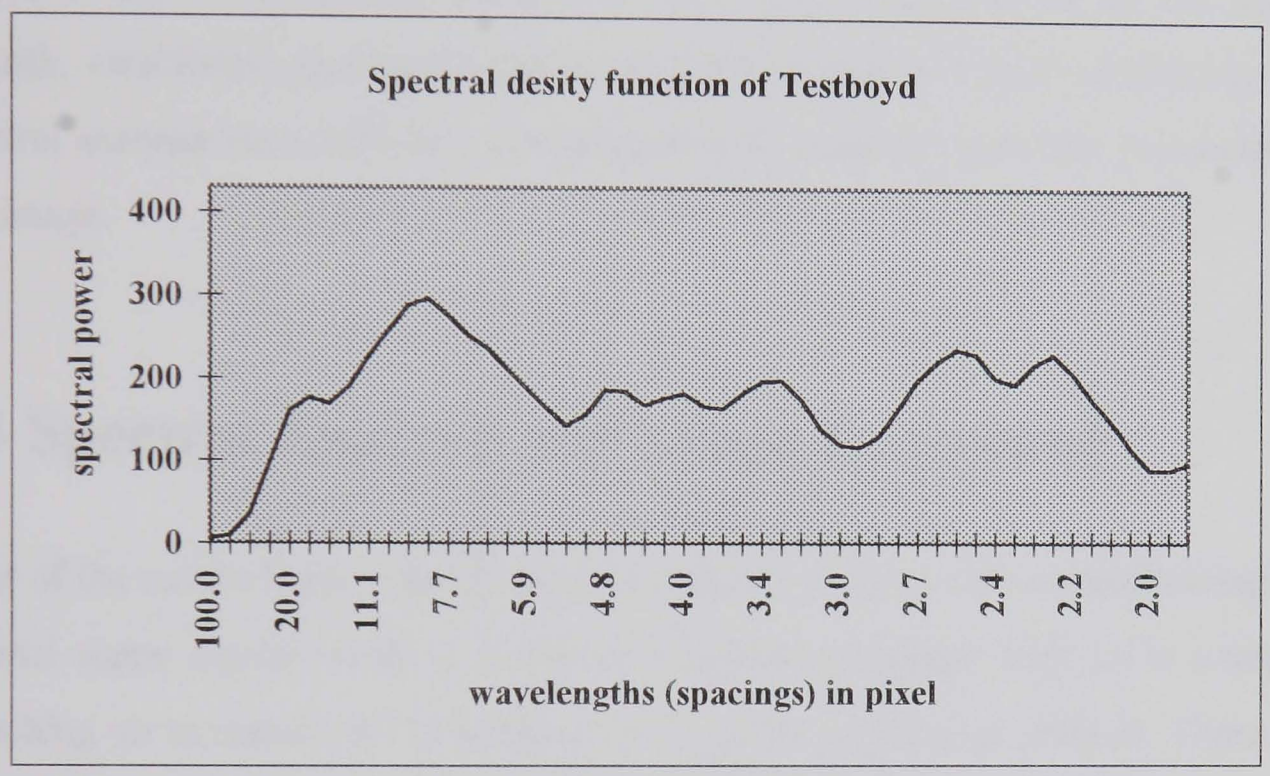

(iii)

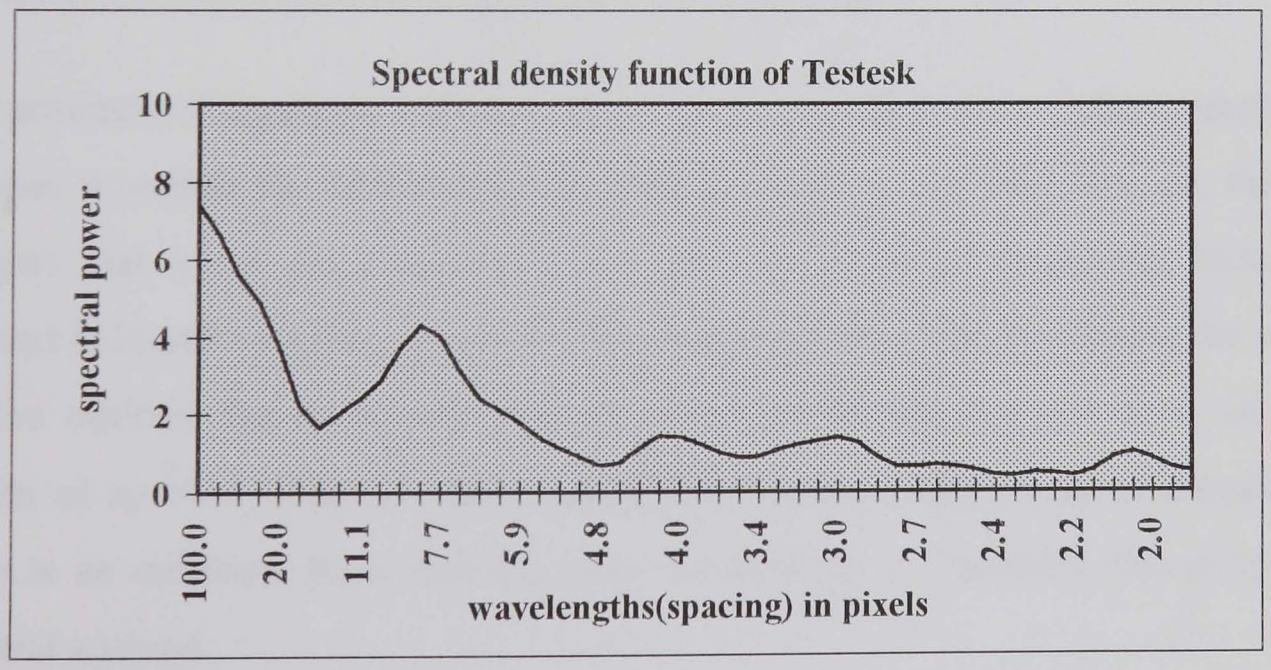

Figure 5.5
Spectral density functions of transects of test image (i) Testdunes (ii) Testboyd (iii) Testesk

Cursor measurement for the Testboyd image and transect gave lineament spacings ranging from 5 to 25 pixels with dominant spacings falling between 7 and 11 pixels (figure 5.4ii) while spectral analysis of the transect represented by the image Testboyd established spacing (cyclicity) of 9 pixels (figure 5.5ii). This too confirms that spectral analysis has established and quantified the spacings between lineaments in this image.

With the Testesk image and transect, cursor measurement gave lineament spacings ranging from 3 to 24 pixels with dominant spacings falling between 7 and 9 pixels (figure 5.4iii) while spectral analysis of the transect represented by the image Testesk, established spacing (cyclicity) of 8 pixels (figure 5.5iii). confirming that spectral analysis has established and quantified the spacings between lineaments in this image.

5.4 Spectral Analysis and Image Processing

Most of the results from image analysis and interpretation involve transforming the original scene digital numbers either to enhance the image such as in contrast stretching or to transform the image as in principal component analysis. These are all part of the many types of image processing available to a user.

The presence of regularity between lineaments can be isolated by spectral analysis because it utilises the relationship between lineaments, and therefore any image analysis that alters the relationship between the pixels of lineaments along a transect is bound to affect the results of spectral analysis. For this reason the next section outlines the effect that popular image processing routines have on the results of spectral analysis. These experiments were conducted to investigate if there is an optimum form that the data should have to maximise the utility of spectral analysis.

5.3a Results of spectral analysis using all 4 bands for the linear contrast stretched Landsat MSS image.

Transects	Band 1	Band 2	Band 3	Band 4
T1	4, 5, 10	4, 5, 10	4, 5, 9	4, 5, 9
T2	7, 10, 20	8, 10, 20	7, 9, 20	7, 10, 20
T3	4, 5, 8	4, 5, 9	4, 5, 9	5, 8
T4	5, 8, 13	4, 8, 13	5, 9, 13	5, 9, 13
T5	5, 6, 8, 25	4, 5, 8, 25	4, 5, 8, 25	5, 6, 8, 25
T6	5, 6, 8, 20	5, 6, 8, 20	5, 6, 9, 20	5, 6, 9, 17
T7	5, 9, 17	5, 9, 17	6, 9, 17	6, 9, 17

Table 5.3b Results of spectral analysis using all bands for the linear contrast stretched Landsat TM image.

Transect	Band 1	Band 2	Band 3	Band 4	Band 5	Band 7
T1	5, 13	6, 13	6, 13	6, 13	6, 13	6, 13
T2	9, 13	9, 13	9, 13	9, 13	9, 13	9, 13
T3	4, 10	5, 11, 15	4, 11, 15	4, 11, 15	5, 11, 15	4, 11, 15
T4	6, 11	7, 11	11	11	11	11
T5	12	13	13	13	13	9, 14
T6	7, 11, 16	8, 12, 16	8, 12, 16	8, 12, 16	8, 12, 16	8, 12, 16
T7	10, 14, 18	9, 13, 17	9, 13, 17	9, 13, 17	9, 13	9, 13
T8	7, 15	8, 12	5, 9, 12	8, 12	8, 12	8, 12
T9	9, 16	8, 16	7, 16	8, 10, 16	10, 16	7, 16
T10	8, 13, 18	10, 18	10, 18	10, 18	10, 18	10, 18

5.4.1 Contrast Stretch

The raw data of an image usually fall within a narrow range of values which is narrower than the capabilities of the display device. The purpose of contrast stretching is therefore to expand the range so as to utilise the dynamic range of the display device (usually 0 to 255 for 8 bit data). The result is a brighter image with a sharp contrast.

Utilising the previous images with transects positions identical to those used for the previous experiments, and using band 1 for the Landsat MSS image and band 4 for the TM image, the effect of linear contrast stretching on the results of spectral analysis were tested.

The results are presented in table 5.3. They are identical to those from the raw image (Table 5.1b, 5.2b) showing that linear contrast stretching does not affect the results of spectral analysis. This may be expected since contrast stretching increases transect amplitude whilst maintaining the spatial relationship between pixels. There is therefore no advantage in using contrast stretched data over raw values.

5.4.2 Principal Component Analysis (PCA)

The purpose of principal component analysis (PCA) in remote sensing is to reduce the dimensionality of the data. In short it is a method of data compression where redundant data is compacted into fewer bands with minimal correlation between the PCA bands. The PCA bands are usually independent in contrast to the bands from the raw image which are often highly correlated. The same image used in band selection with same transect locations were used to test for the effect of PCA on spectral analysis, and to see if there is any advantage in using PCA1.

Principal component analysis for the Landsat MSS image yielded four components named PCA 1, 2, 3 and 4, with PCA1 accounting to 97.14% of the total variation of information in the image and PCA 4 accounting for 0.020% of the variation.

5.4a Results of spectral analysis on PCA image of Landsat MSS image

Transects	PCA1	PCA2	PCA3	PCA4
T1	4, 5, 10	4, 5, 6, 10	4, 6, 8, 14	3, 5, 25
T2	7, 10, 20	4, 7, 11	3, 5, 8	3, 7, 20
T3	4, 5, 8	4, 5, 7	5, 8, 14	2, 5, 8
T4	5, 8, 13	5, 6, 8, 14	2, 6, 10	5, 7, 13, 20
T5	5, 6, 8, 25	4, 6, 13	2, 4, 6, 17	2, 4, 7, 13
T6	5, 6, 8, 20	8, 20	3, 6, 8, 17	6, 8, 17
T7	5, 9, 17	3, 6, 9, 20	4, 8, 14	3, 5, 10, 25

Table 5.4b Results of spectral analysis on PCA image of Landsat TM image

Transect	PCA1	PCA2	PCA3	PCA4	PCA5	PCA6	PCA7
T1	6, 13	14	None	None	None	None	None
T2	9, 13	9, 14, 20	"	"	"	"	"
T3	4, 11, 15,	11, 20	"	"	"	"	"
T4	11	11, 20	"	"	"	"	"
T5	13	5	"	"	"	"	"
T6	8, 12, 16	13, 17	"	"	"	"	"
T7	9, 13, 17	10, 13, 17	"	"	"	"	"
T8	8, 12	13, 20	"	"	"	"	"
T9	8, 10, 16	10, 17	"	"	"	"	"
T10	10, 18	10, 14	"	"	"	"	"

For the Landsat TM image depicting aeolian lineaments, 7 bands were utilised to realise 7 PCA components named PCA 1, 2, 3, 4, 5, 6 and 7 with the first component accounting for 87.35% of the total variation of information in the image, and the last component PCA7, accounted for 0.08 of the total variation.

The results of spectral analysis on the PCA bands is presented in table 5.4a and table 5.4b. Comparison of these results with those derived from wavebands (Table 5.1b and 5.2b) reveals that for the Landsat MSS image, the results are identical and for TM they are very similar. There were however some spacings revealed in the other PCA components that were not revealed by PCA1 or the raw image. Since the first PCA components accounted for more than 80% of the variation of the information in the image (transect) and since this information is predominantly lineament in nature, it can be concluded that PCA1 contains most of the information about the lineaments. From these results, it is clear that using PCA1 does not provide any extra information on spacing although lower order PCs reveal extra information but exactly what this information represents is hard to ascertain.

5.4.3 Laplacian Filtering

This is an edge enhancement filter that operates without regard to edge direction and is useful for edge and boundary detection. Hence it is a useful filter for lineament detection. It works by emphasising maximum values within the image.

This filtering technique was applied to the Landsat images and same transect locations as used for previous experiments. Unfortunately no significant spacing was detected. This is not unexpected since Laplacian filtering acts upon the boundaries and therefore highlights all high frequency features such as lineaments as well as other features, thus mixing with lineaments and therefore interfering with the regular spatial arrangement of the lineaments.

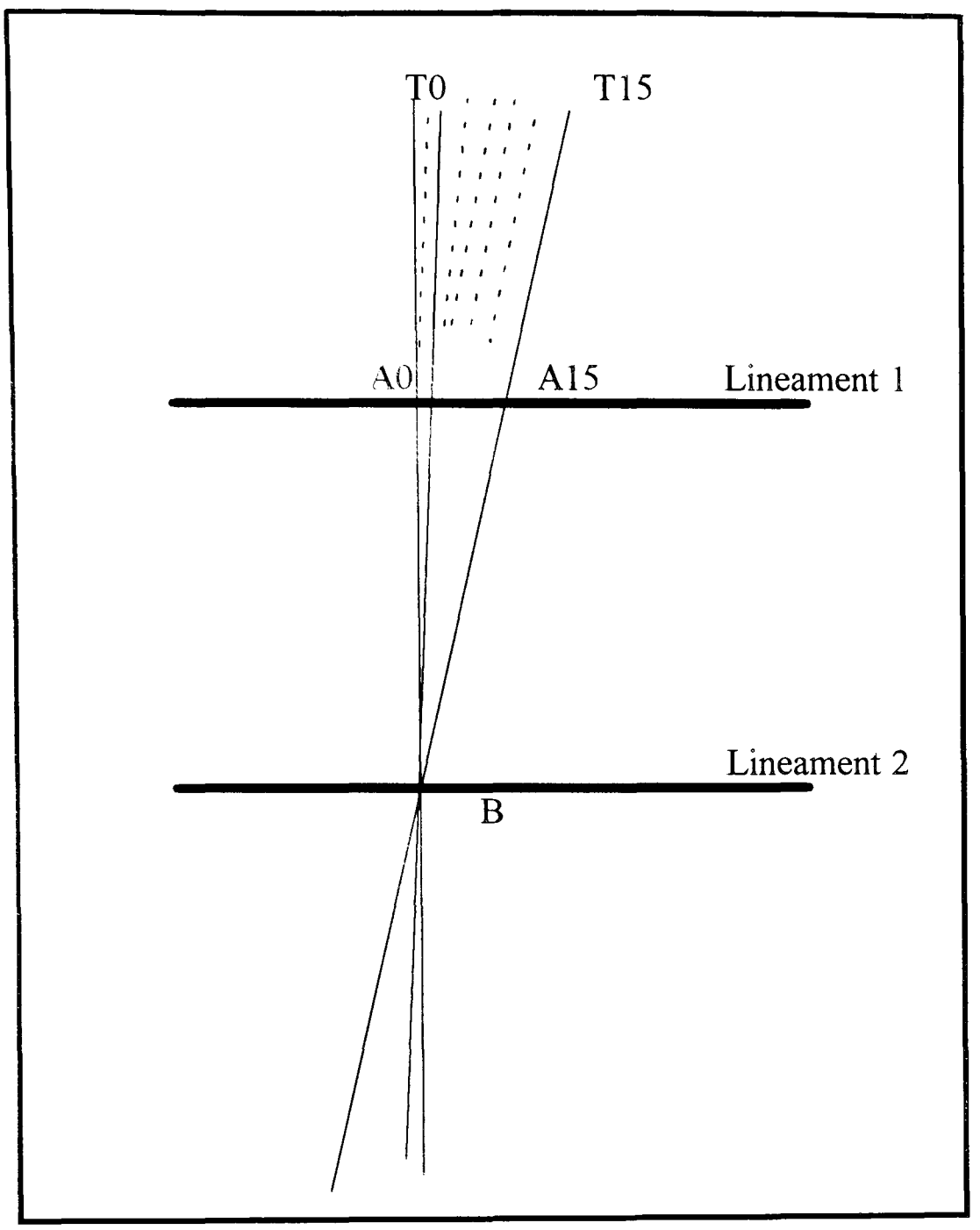

Figure 5.6
Sensitivity testing of transect misalignment from transect T0

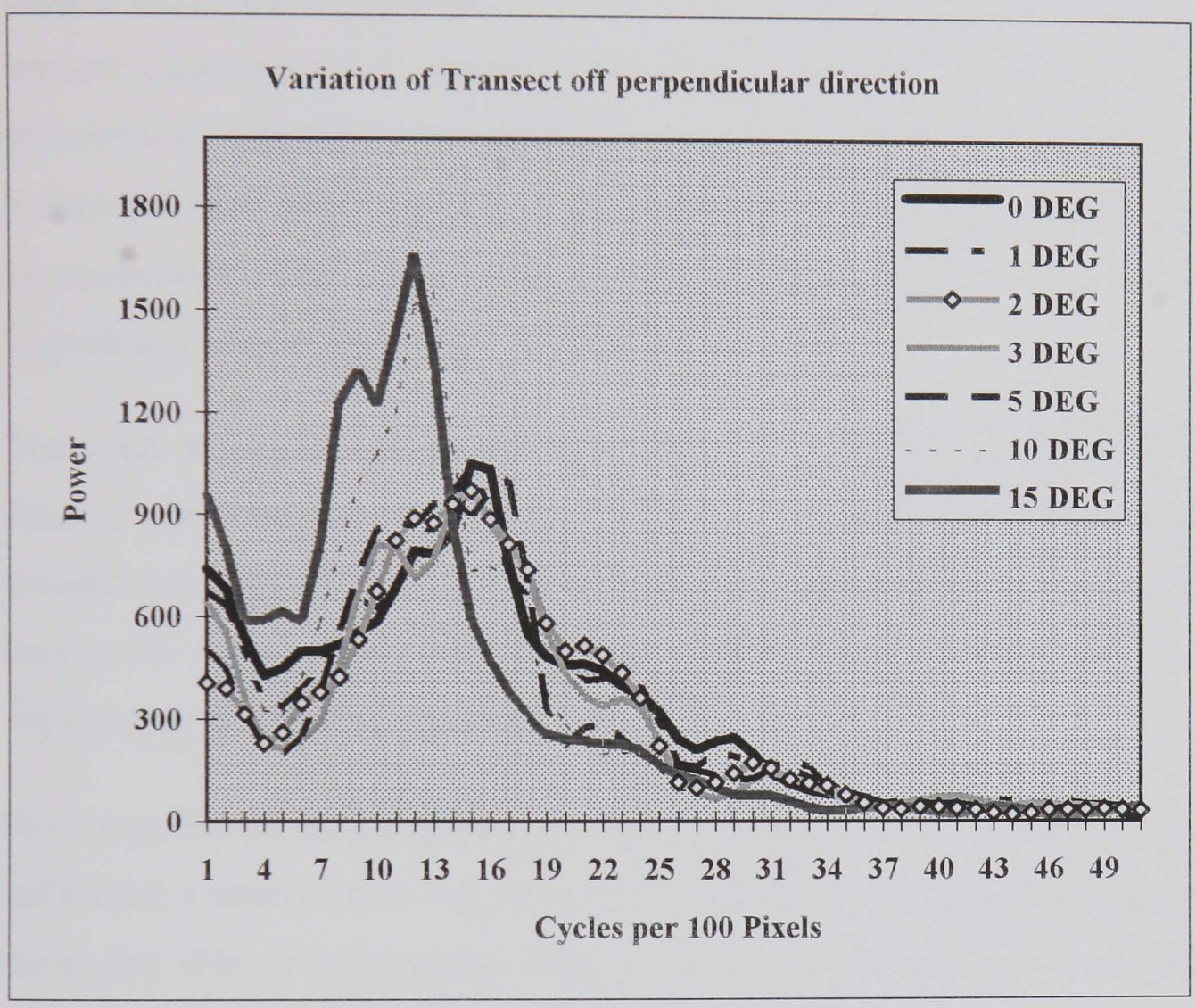

Figure 5.7 Result of transect misalignment from perpendicularity

5.5 Perpendicularity of the Transect.

The spacing between lineaments was defined in chapter two as the perpendicular distance between lineaments. To derive this spacing from the transect the transect needs to be taken perpendicularly to the orientation of the lineaments.

This section analyses the effect on the results of spectral analysis when the transect departs from perpendicularity i.e. a test of the sensitivity of the results due to transect misalignment. To test for this, the Landsat TM image was utilised. A transect was positioned such that it was perpendicular to the orientation of the lineaments. Six other transects were defined such that they departed from perpendicularity with respect to the positioned transect by 1, 2, 3, 5, 10, and 15, degrees as shown in figure 5.6.

The result of spectral analysis for these transects is presented in figure 5.7. From these graphs, it can be observed that the spacing obtained from the perpendicular transect and those which were 1, 2, 3, 4 degrees away from perpendicularity were very similar whereas the 10 and 15 degree deviation show low frequency (longer wavelength) spacings as illustrated in figure 5.7.

From experiments on positioning transects, it was discovered that the chances of estimating a transect that was more than 5 degrees away from perpendicularity were very slim. It is therefore unlikely that any of the transects would depart significantly from perpendicularity so as to effect the results.

5.6 Spectral Analysis Versus Digitisation

As explained previously, spectral analysis is an automated method of analysing lineaments which does not require the time consuming task of actually identifying individual lineaments. As a simple test it was thought appropriate to compare the automated and the manual methods. If lineaments are manually mapped and

digitised it is possible to obtain the spacing of lineaments from the co-ordinates of the digitised lineaments. Utilising this method of measuring the spacings between lineaments, the results were compared with results from spectral analysis.

To perform this experiment, the Landsat MSS image was utilised. The area selected was the area covered by the 7 transects used for previous experiments. The lineaments in this area were interpreted and digitised using the GIS software, Arc Info. From the co-ordinates of the digitised lineaments it was possible to make calculations with regard to the characteristics of the lineaments based on well known geometrical theories. A computer program for doing this has been incorporated into Arc Info by Clark and Wilson (1994).

Utilising all the spacings obtained from digitisation and the spacings obtained by spectral analysis on each of the four bands given by the 7 transects defined for the area, a frequency graph was plotted as in figure 5.8. The results for digitisation show the dominance of lineament spacing of 3, 4, 8, 10 and 13 pixels. Spectral analysis showed a dominance of lineament spacing of 5, 9, 13, 17, 20 and 25 pixels

The dominant spacing from spectral analysis are the 5, 9 and 20 compared to 3, 4 and 8 obtained from the digitisation method. The slight difference of spacings from both methods is probably due to the problems associated with digitisation techniques such as operator biases, and the fact that the techniques are not directly comparable as they sample the data differently. Nevertheless, it can be concluded that spectral analysis produces comparable results with much greater ease, and is more objective as it does not involve interpretation skills when mapping the lineaments.

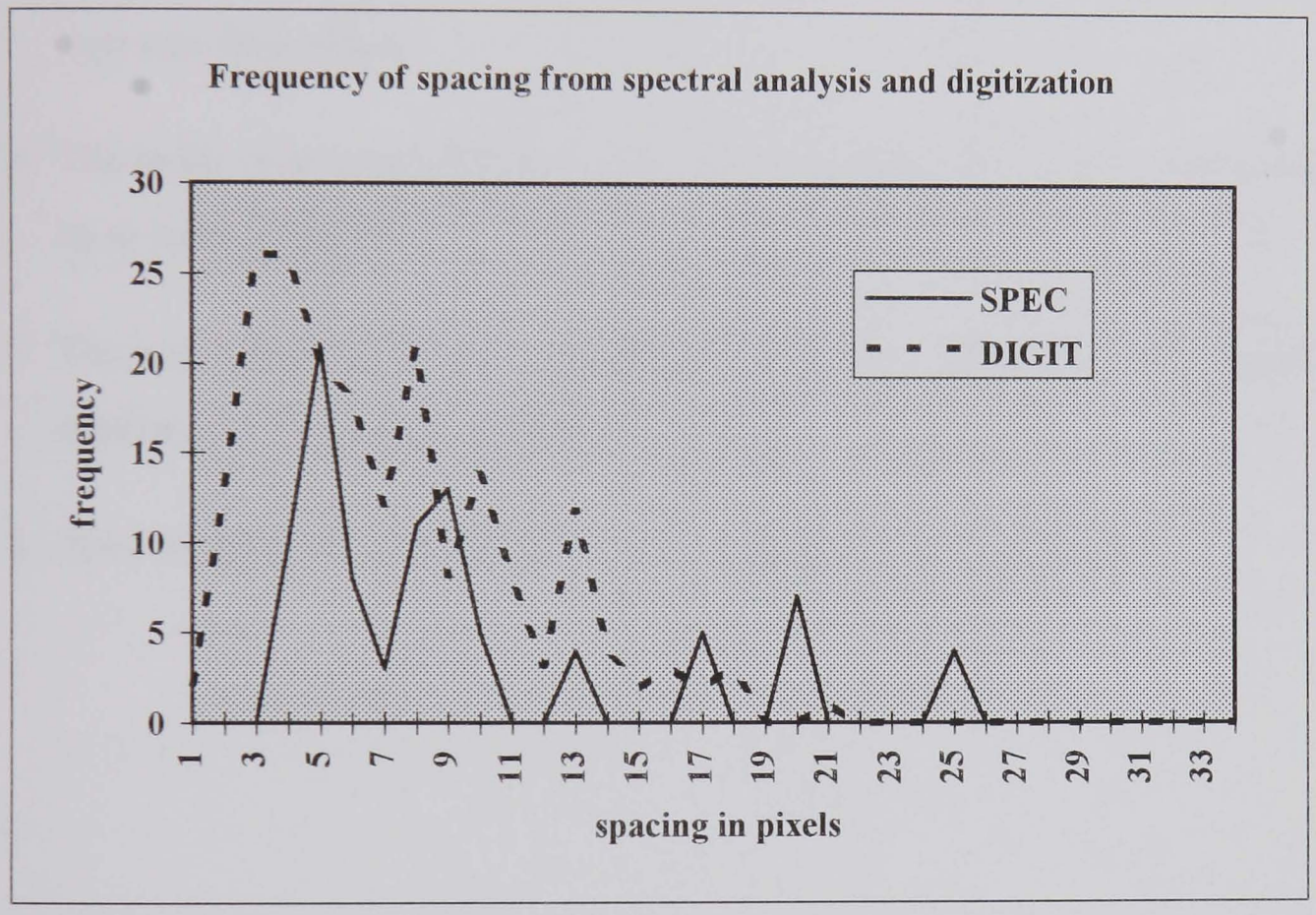

Figure 5.8 Result of analysis using digitization method and spectral analysis

5.7 Conclusion

It can be concluded that:

1. The result of spectral analysis of multispectral images is independent of the band used. Therefore which ever band is most convenient can be used.

2. Peaks on the transect record lineament position and spacing obtained by cursor measurements of lineaments agrees with the result from spectral analysis.

3. Image processing experiments reveal that there is no benefit in using processed over raw data values.

4. The result of spectral analysis is affected when the transect is off perpendicular by at least 10 degrees .

5. There is a slight duffrence in spacing obtained from spectral analysis and those obtained by digitisation for the same image.

6. Spectral analysis indeed measures the spacing between lineaments.

Chapter Six

Application Case Studies.

6.0 Introduction

The preceding chapters introduced lineaments from satellite images and the technique of spectral analysis. It was established that the spacing between lineaments can be obtained using spectral analysis on a transect taken perpendicularly to the orientation of lineaments.

The aim of this chapter is to use the newly established method of spectral analysis to perform morphometric analysis on images depicting linear sand dunes and images depicting glacial lineaments. It is anticipated that the result will support or disprove past contentions made about these lineaments, or at the very least, it will provide the first quantitative measure of these widespread lineament patterns and, thus may help in finding answers to some key geomorphological questions.

To achieve the above objectives, this chapter makes use of satellite images of the Kalahari desert depicting aeolian lineaments, and images of Canada depicting glacial features produced by the Laurentide Ice Sheet of the Pleistocene Epoch.

The lineaments for this study area are of the parallel type i.e. groups of lineaments that all align in the same direction within an area. This is typical of the aeolian and glacial lineament type described in chapter 3. It is expected that any systematic change of the processes responsible for the formation of lineaments will manifest itself in the morphometry of the lineaments.

The morphometric parameter of interest for these lineaments is the spacing between them which can also be thought of as density. Spacings obtained from

spectral analysis for a set of lineaments will be compared with spacings obtained from different areas of the same image or from different areas of different images and explanations sought for the variations if there are any. To do this a number of hypotheses have been made.

The first step in analysing the lineaments is to devise a sampling procedure. This involved identifying and defining lineaments based on their orientation and extent. This was achieved by making interpretative sketches of lineament orientation using tracing overlays upon mosaics (using inkjet prints.) This gave a general overview of the orientation of the lineaments so as to aid the positioning of the transects. It is important to note that this output was only schematic in that individual lineaments were not mapped, for this would have been time consuming and defeat the purpose of spectral analysis as a faster and more objective method of establishing the spacing between lineaments.

After establishing the general orientation of the lineaments on the entire image, the different sets (lineaments of sub-parallel arrangement) were defined and transects located at appropriate positions making sure that they were perpendicular to the orientation, and also that the transects were long enough to account for the spacing of the lineaments. The transects were all greater than 100 data points in length as advised by Chatfield (1989).

Many transects were used in this research, thus warranting a systematic method of labelling so as to avoid confusion. For example, for an image called Dunes, a transect file of this image was labelled TDUA41 where the first letter stands for transect, the second and third letters are the first two letters of the name of the image, the fourth letter is the area where the transect was taken on the image, the fifth character is the image band, and the last character is the transect number. TDUA41 is therefore transect number one of area A of the Dune image utilising band 4.

The overall structure of this chapter is shown in the flow diagram of figure 6.1

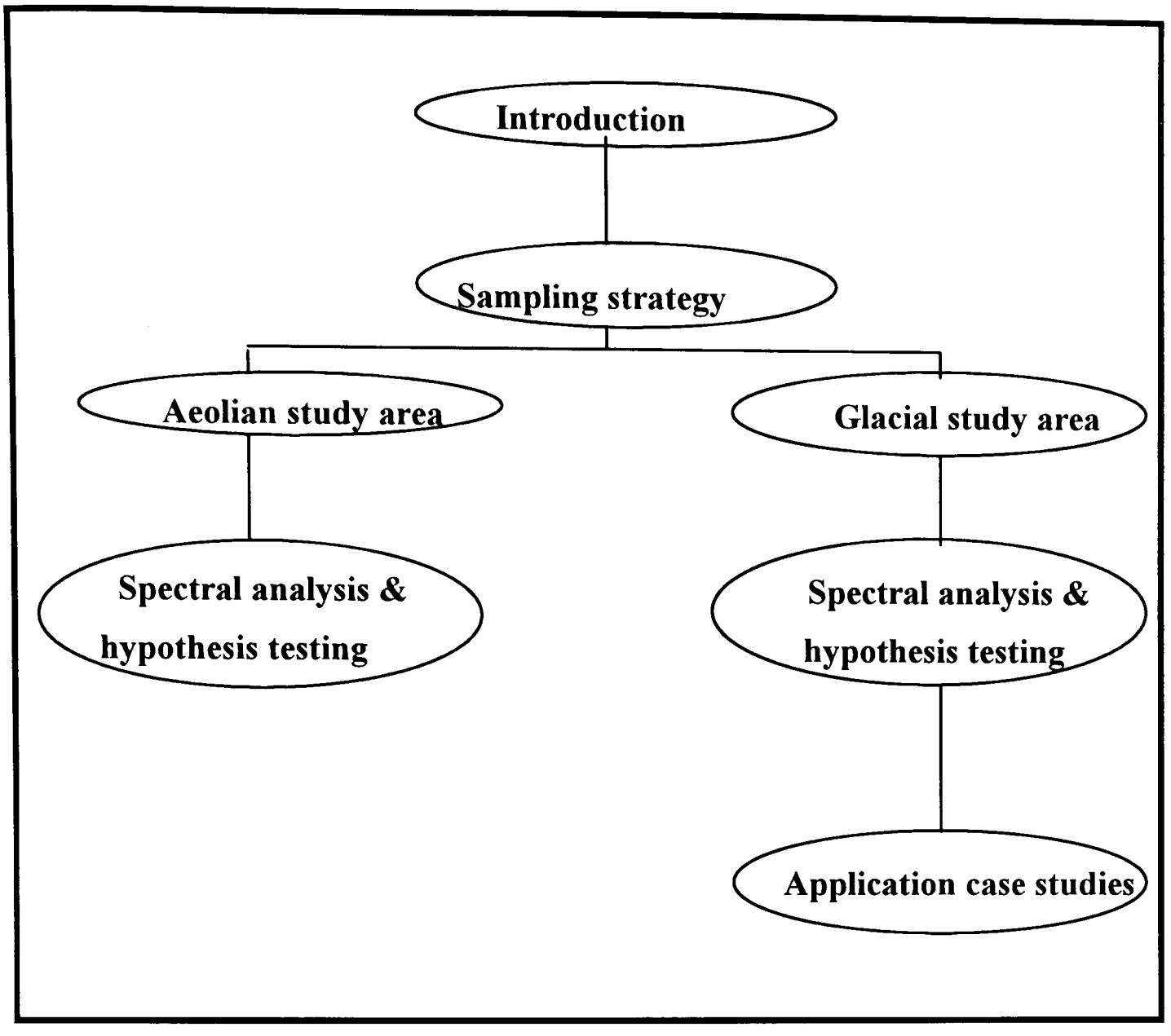

Figure 6.1
Flow diagram of structure of chapter six

CASE STUDY ONE

AEOLIAN DUNES

6.1 The Kalahari Study Area

This study area is within the Kalahari dune desert described by Thomas (1984) as the Mega Kalahari and situated between latitude *23°00'* and *28°30'* south, and longitude *18°00'* and *22°30''* east. It covers parts of Angola, Namibia, Botswana, Zimbabwe and South Africa.

The actual area for the research lies between latitude *25°50'* to *26°10'* south and longitude *19°47'* to *20°07'* east and covers an area of about 950 square kilometres (Figure 6.2).

Figure 6.2 is a Landsat TM image of the study area depicting aeolian lineaments. In this image, two lineament sets have been identified as area A and area B. The orientation of the two sets are similar. The only difference is in the nature of the lineaments, those in area A appear to be larger in width and can be considered as simple in nature and those in area B appear smaller and slightly tortuous but still fairly simple in nature. This is in accordance to Lancaster's (1986) observation of lineaments of this area as simple. Although other studies by Goudie (1969; 1970), Thomas (1986), Thomas and Martin (1987) observed considerable local variation of these lineaments, the whole area however does appear simple and linear in accordance with McKee's (1979) terminology.

This dune field has been described by Lewis (1936), Grove (1969), Goudie (1969; 1970), Lancaster (1979; 1980; 1981; 1984), Malick *et. al.* (1981), Thomas (1984; 1988), and aspects of the morphometry of this dune field have been studied by many authors, for example Lancaster (1986; 1988) studied grain size characteristics, spacing, height and width of these lineaments while Thomas (1988), and Thomas and Martin (1987) studied the relationships between the dune height and spacing, dune spacing and grain size, and the variation of the dune spacing within the sand sea.

The aim of characterising these lineaments is to establish whether:

figure 6.2

1. the Lineaments are regularly spaced.
2. there is a systematic change of the spacing across the dunefield.
3. and thirdly to quantify the actual lineament spacing in metres.

These three questions form the basis of the hypotheses for analysing the linear sand dunes. The spacing of these dunes may be related to whether an equilibrium form has been reached. The quantified lineament spacing will be compared with results obtained by other workers who have used different methods.

6.1.1 Spectral Analysis of the Kalahari Sand Dunes

Spectral analysis was performed on transects defined in each of the study areas A and B of Figure 6.3. Lineament orientation in the image is NW-SE trending and so the transects were therefore defined in the NE-SW direction in order to make them perpendicular (Figure 6.3). This is necessary as the perpendicular distance gives the shortest distance between parallel lineaments which is the spacing of the lineaments.

In area A, 23 transects were located with lengths ranging from 418 data points to 456 data points while in area B, 11 transects were made with lengths ranging from 180 to 362 data points. The lengths of the transect are long enough to account for all the frequencies that could be present in the area. The transects were extracted from band 4 of the image which falls in the reflective infra-red (0.76-0.90 micro-metres) part of the spectrum. This band is especially responsive to the amount of vegetation present in a scene. The dunes are visible on the image because of a combination of vegetation cover and varying reflectivity due to slope changes.

The reason for choosing band four was mainly because it gave a good contrast to the lineaments. However, any other band except band 6 (thermal and low spatial resolution) would have given the same results as was demonstrated in chapter five.

The results of the analysis are presented in table 6.1 and figure 6.4.

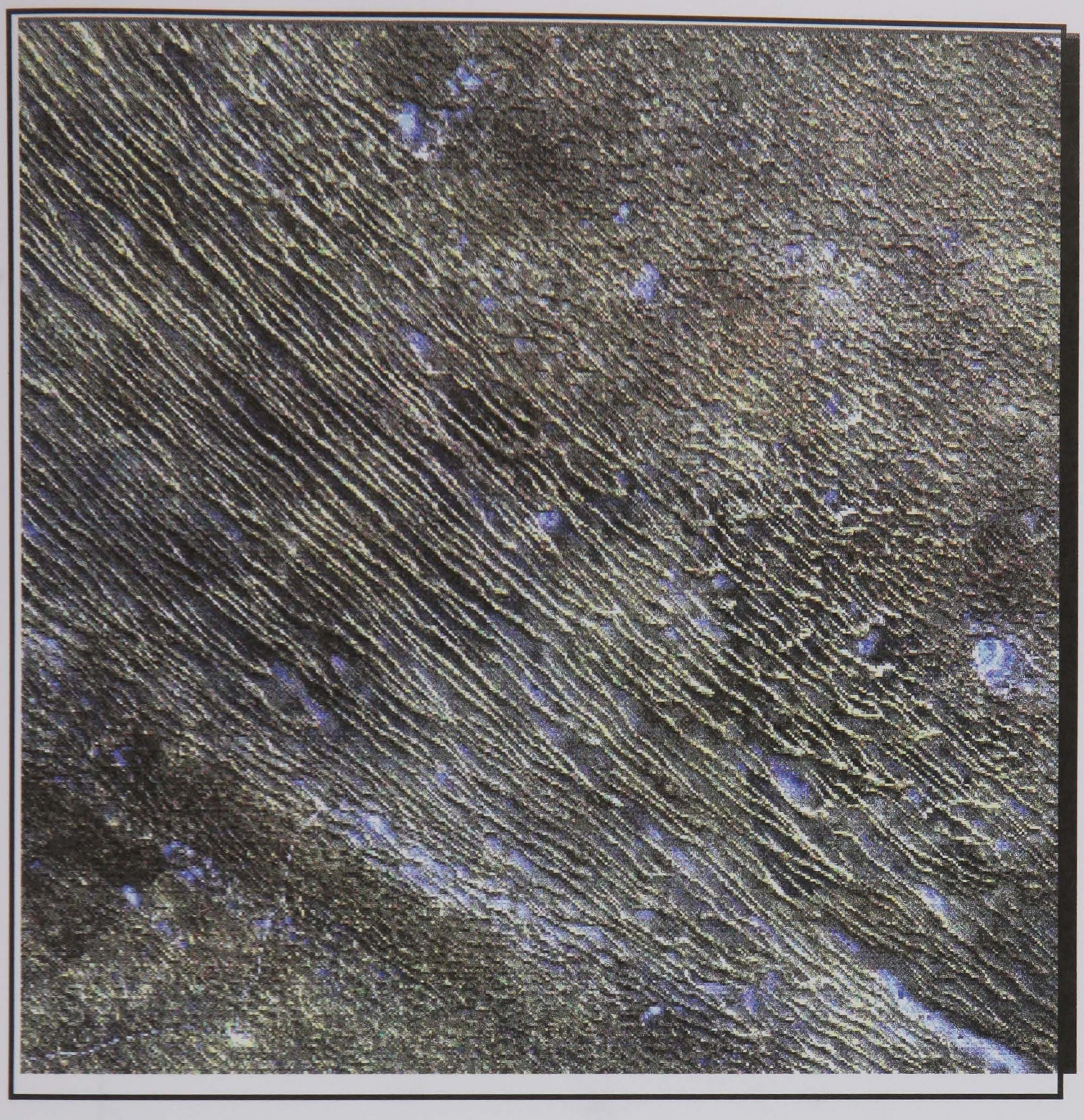

Figure 6.2 Landsat TM image of the Kalahari study area depicting linear sand dunes as lineaments.

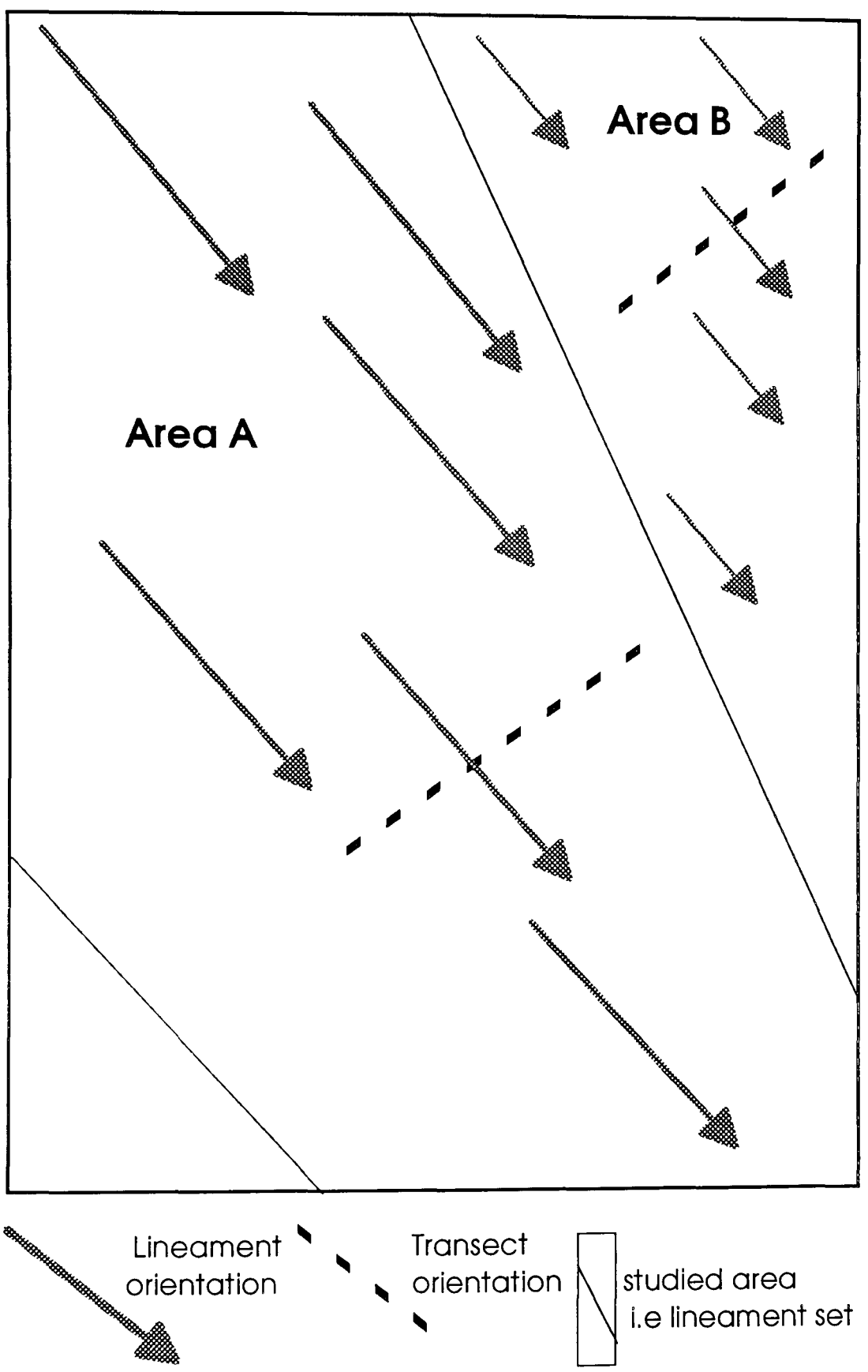

Figure 6.3
Sketch diagram of the studied area in Dunes image showing orientation of lineaments and transects.

Table 6.1a

Result of spectral analysis for the linear Dune image area A

TRANSECT	SPACINGS IN PIXELS				
TDUA41			10		
2			10	8	
3		14	10		
4				8	
5			11	8	
6				9	7
7				9	
8				8	
9			12	8	
10			11	8	
11			12	8	
12		12	10		
13			10		
14			12	9	
15			11	8	
16		14		8	
17			10		7
18			10		
19			11		
20			10		
21			11		
22			11		
23			10		7

Table 6.1b

Result of spectral analysis for the linear Dune image area B

TRANSECT	SPACINGS IN PIXELS			
TDUB41	12	8		
2	11		7	
3	11	8		
4		8	6	
5	12	8		
6		8	6	
7	12			
8		9	6	
9	10			
10	12	8		
11	12			

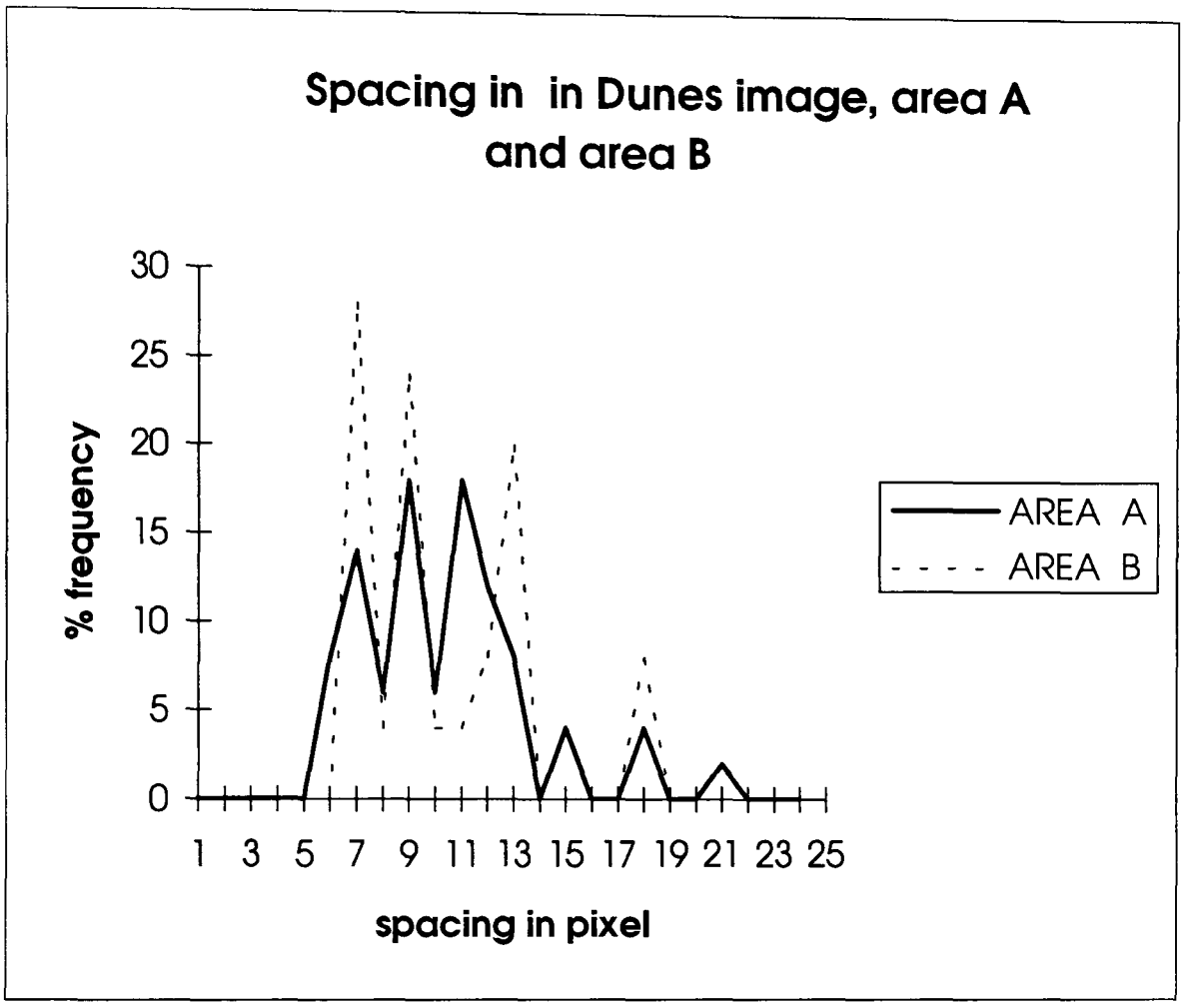

Figure 6.4
Percentage frequency of spacing from area A and area B of Dunes Image

6.1.2 Hypothesis Testing

The result of spectral analysis of linear sand dunes should be interpreted in relation to the questions posed by the following hypotheses:

1. **Hypothesis One:** ***Lineament spacing is regular across the dunefield.***

The results tabulated in table 6.1 show that spectral analysis has established the presence of regularity i.e. dominant periodicities in all the transects for areas A and B. The values for each transect in the table are for wavelengths i.e. spacing in pixels. The analysis shows that there are multiple spacings present within transects and in the area as whole. The spacings are therefore multimodally distributed. For the transect TDUA45, for example, the spacings are 8 and 11 pixels corresponding to 240 and 330 metres respectively.

The regularity of spacing in the area must have been influenced by systematic processes of creation. The presence of multiple spacing in the areas questions whether more than one process was operating in this dunefield, or whether the dunes record a number of dune-building phases.

2. **Hypothesis Two:** There is no systematic change in the spacing in each of the study areas

This is of interest to examine if there is a systematic change in spacing in the up or down wind direction. Any such variation may be related to, inter alia, sand supply from a point source, down wind sand sorting or diminishing competence of the aeolian process and instability of dunes. To test this hypothesis, trend analysis was performed to the transects which were plotted such that the transects plotted on the x axis from transect 1 through to 23 and 1 to 13 representing the down wind direction while the spacing in pixels were plotted on the y axis. There is likely to be more than one value on the graph for each transect as a result of the presence of multiple spacings. The results of these analyses are discussed in chapter seven.

CASE STUDY TWO

GLACIAL LINEAMENTS

6.3 Glacial Lineaments in Canada.

Subglacial processes have been responsible for the formation of streamlined lineaments at a variety of scales and aligned parallel to the direction of former ice flow over a sediment substrate.

A knowledge of the formation of these features can only be sought from geomorphogical evidence exposed after ice retreat since they were formed beneath the ice which makes it difficult or impossible to observe the processes in operation.

A review of the multitude of process hypotheses that have been proposed for the formation of these lineaments is beyond the scope of this thesis. Published papers that have arisen from the Drumlin Symposia series demonstrate the wide ranging controversy that exists. There are three mains school of thoughts, lodgement-based deposition processes, subglacial deformation, and catastrophic subglacial floods (Smalley and Unwin, 1968; Smalley and Piotrowski, 1987; Menzies, 1979, 1984; Menzies and Rose, 1987, 1989;; Dardis and McCabe, 1983); An attempt here is made to characterise the spacing of glacial lineaments and to examine the variation of spacings within lineament fields and between fields.

This section is concerned with lineaments in Canada comprising the ice flow landform assemblage of mega-scale glacial lineaments, drumlins, megaflutes, and fragmentary drift elements (Boulton and Clark, 1990a; 1990b; Clark, 1990; 1993; 1994).

Utilising images from Canada, spectral analysis was used to establish the presence or absence of regularity in the spacing of lineaments and the variation of these lineaments within areas and between areas.

6.4 Specific objectives for the application of spectral analysis

There are three main reasons for wishing to gain quantitative measures for the spatial frequency of ice flow lineaments:

1. To test a number of hypotheses that seek to relate lineament morphometry to ice velocity and glaciodynamic setting.

2. To acquire quantitative measures that characterise glacial lineaments and to use these to test propositions about the fundamental scale continuity of the ice flow landform assemblage.

3. To provide quantitative support for the task of identifying discrete ice flow events from complex lineament patterns.

6.5 Lineament spacing, glaciodynamic setting, and ice velocity

Many authors have proposed the relationship of lineament formation with ice pressure and velocity. For example Reynolds (1885), Mead (1929), Von Englen (1938), Demorest (1939), Terzapghi (1943) Alden (1918), Fairchild (1929), Flint (1947), Smalley (1966), Hill (1968), Smalley and Unwin (1968), Dyson (1952), Hoppe and Schytt (1953), Stalker (1960), Nye (1965; 1969; 1975), Venon (1966), Cowan (1968), Peterson (1969), Folk (1971), Rothlisberger (1972), Shaw and Freschauf (1973), Menzies (1979), have all suggested pressure and velocity to be a causal effect in their different theories for the formation of drumlins.

In attempting to explain the genesis of mega scale lineaments, Clark (1993; 1994) suggested that fast ice velocity is the most important factor and proposed that the

maximum length of lineament should be a function of ice velocity and flow duration. With many studies proposing a relationship between lineament formation and ice velocity, it seems logical to formulate hypotheses about lineament spacing which should take into consideration variation in ice flow velocity.

There is also some debate as to the zone of the ice sheet (glaciodynamic setting) under which glacial lineaments are thought to form. For example, drumlins are assumed to have been formed in close proximity to ice margins by Alden (1911), Taylor (1931), Gravenor (1953), Charlesworth (1957), Flint (1957), Wright (1957), Thwaites (1963), Thornbury (1969), Smalley and Unwin (1968), Piotrowski (1987). Contrary to this belief of ice margin environment as an area of drumlin formation is another school of thought. Rose (1987; 1989) found drumlins to be close to the source of the ice sheet rather than at the margin, and Clark (1994) hypothesises that drumlins may simultaneously form along flowlines extending for many hundreds of kilometres.

Taking the supposed velocity -morphometry relationship and the uncertainty about glaciodynamic setting together, it is possible to consider a number of tests. Whilst it is impossible to establish the actual velocity of former ice flow, it is possible to make inferences about relative velocities based on glaciodynamic setting.

The basal ice velocity distribution from an ice sheet centre to the margin is illustrated in figure 6.5. Given a large lineament field which extends for hundreds of kilometres beneath the non-marginal part of a former ice sheet, we can infer that there was a systematic increase in velocity down-ice.

In addition to up and down ice changes in velocity, the actual pattern of flow can also allow inferences about relative velocity to be made.

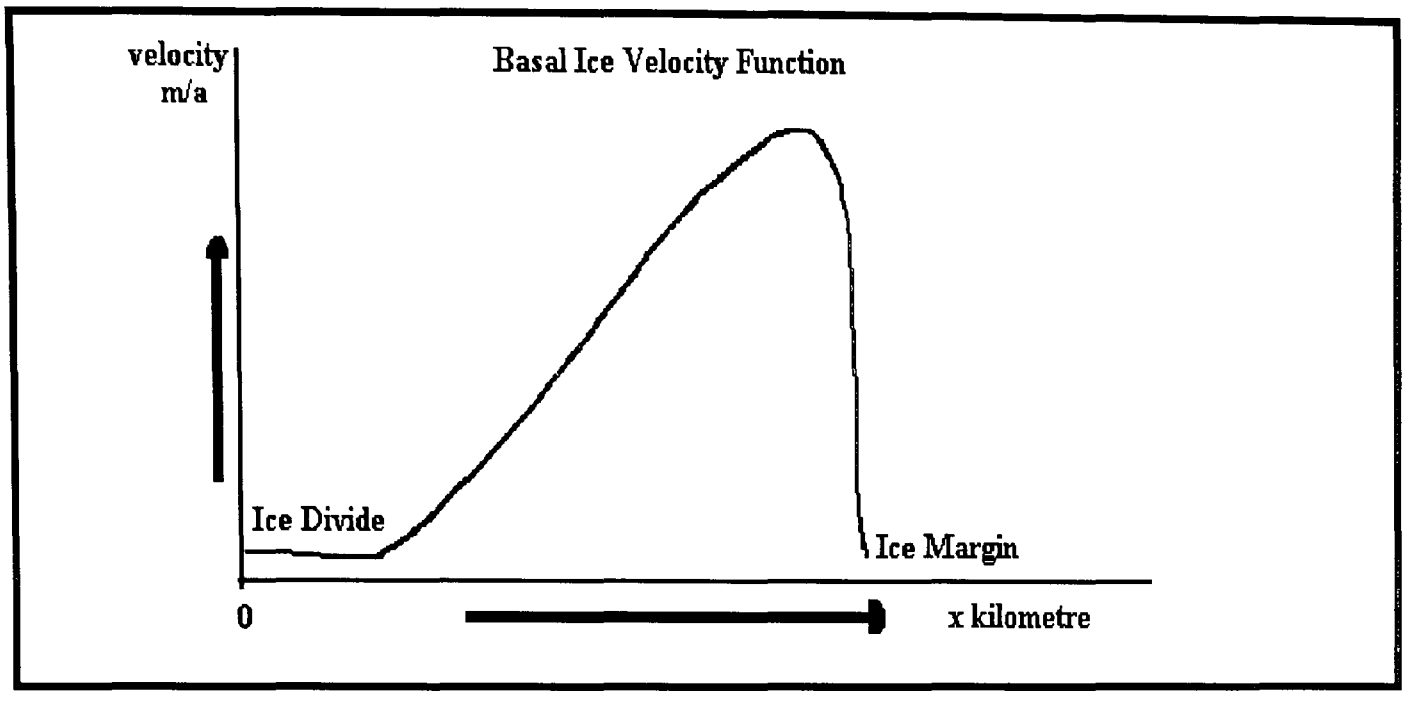

Figure 6.5 Basal Ice Velocity distribution from an ice sheet centre

(after Boulton *et.al.* 1985)

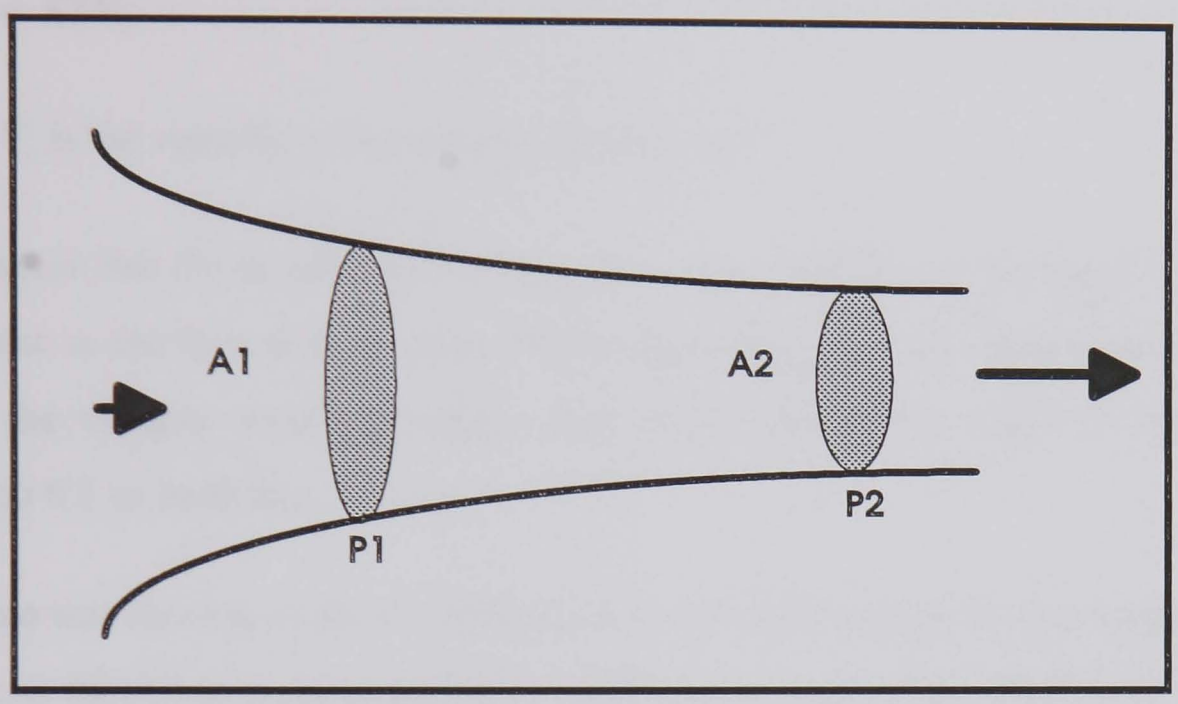

Figure 6.6
Streamlined flow of ice through a tube of varying surface area.
Velocity through smaller area, A2 is greater than
through larger area, A1

As a non turbulent flow, if ice is assumed to move from point P1 to point P2 in a tube as shown in figure 6.6 where the cross-sectional area of point P1 is A1 and that of point P2 is A2, then the same volume of ice it would leave each region towards the right as it would enter from the left during the same time interval (Jones and Childers, 1992).

This relationship is represented by the equation of continuity given by

$$\mathbf{A1V_1 = A2V_2} \qquad \mathbf{6.1}$$

where V_i is the velocity of ice at point i in the tube

This means that the product of the area of a cross-section and the speed of ice at any point in the flow is a constant everywhere along the tube. Where the tube is small, the velocity would be higher that where the tube is large in order for equation 6.1 to hold true.

If the ice was moving as shown in figure 6.6, and if lineaments formed beneath the ice, those formed at point 2 may have a different morphometry than those formed at point 1, if there is a relationship between lineament morphometry and velocity.

Ice flow patterns observed from the arrangement of lineaments may take some of the following topologies (figure 6.7) which permit inferences to be made about relative velocities:

1. **Parallel Flow:** A parallel flow pattern of lineaments is presumed to have formed under a regime of velocity with little spatial variation.

2. **Convergent and Divergent Flow:** Under conditions of convergent flow the velocity must necessarily be greater at the zone of convergence, and the converse for divergent flow patterns.

3. **Venturi Flow:** Flow patterns of this type are occasionally found, and for these cases the velocity must be much greater at the narrow part of the pattern.

a

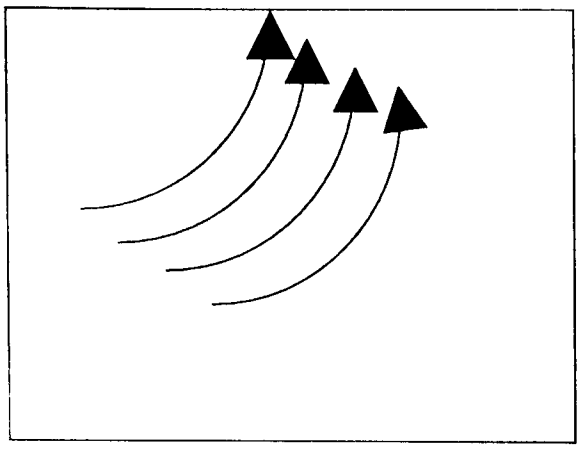

b

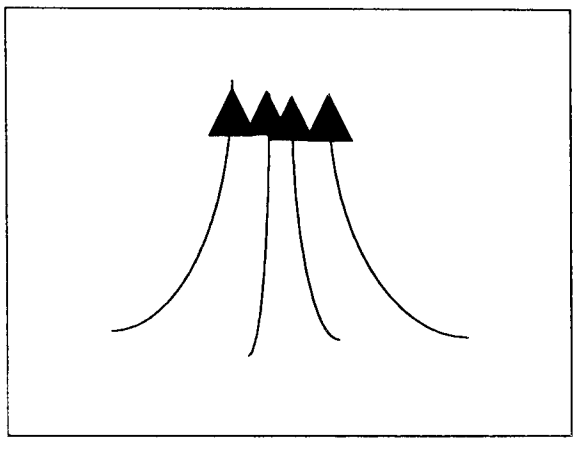

c

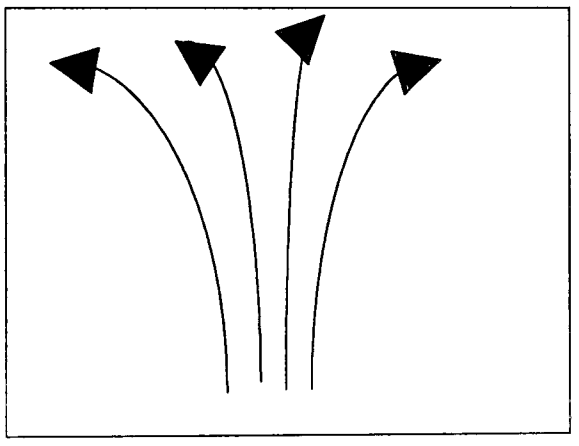

d

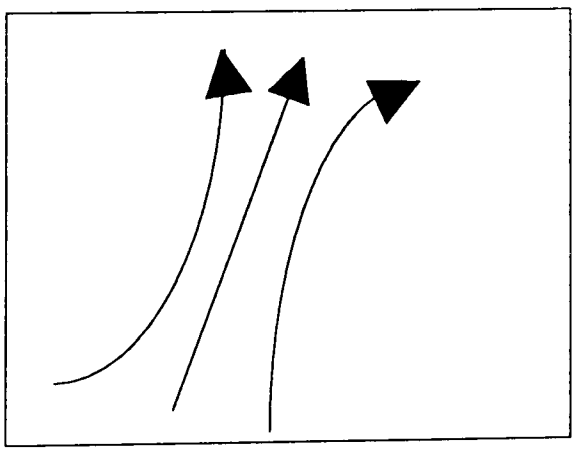

Figure 6.7
Topology of ice flow patterns (a) parallel flow (b) convergent flow (c) divergent flow (d) venturi flow

From the above discussion it is possible to derive two hypotheses for testing:

1. **Hypothesis One:** Over large distances down-ice, the change in velocity will be reflected in lineament spatial frequency.

2. **Hypothesis Two:** Within parallel, convergent, divergent and venturi flow topologies, there will be systematic variations in lineament spatial frequency in accordance with the inferred velocity variations.

Thus far it has been assumed that the different ice flow topologies were formed almost simultaneously in a single event, i.e. a period of steady ice flow that produced the lineament pattern in isochronous manner. As mentioned earlier, whilst isochronous formation of lineaments has its proponents (e.g. Prest, 1984; Rose, 1987; Clark, 1994) others believe that lineaments are only formed close to ice margins and that the overall lineament pattern is formed time transgressively as the ice margin retreats such that lineaments are younger inwards figure 6.8.

It may be possible to use morphometry to test whether a given lineament field was formed isochronously or time-transgressively as in the latter case, it would be expected that there would be many discordances in morphometry resulting from ice dynamic adjustments during margin retreat. For the isochronous case it would be expected that the morphometry variation would be much more gradual and systematic

A third hypothesis is therefore introduced:

3. **Hypothesis Three:** Spatial Frequency of lineaments can be used to test for isochronous versus time transgressive formation of lineaments.

Attempts will be made to test these hypotheses using spectral analysis in section 6.8

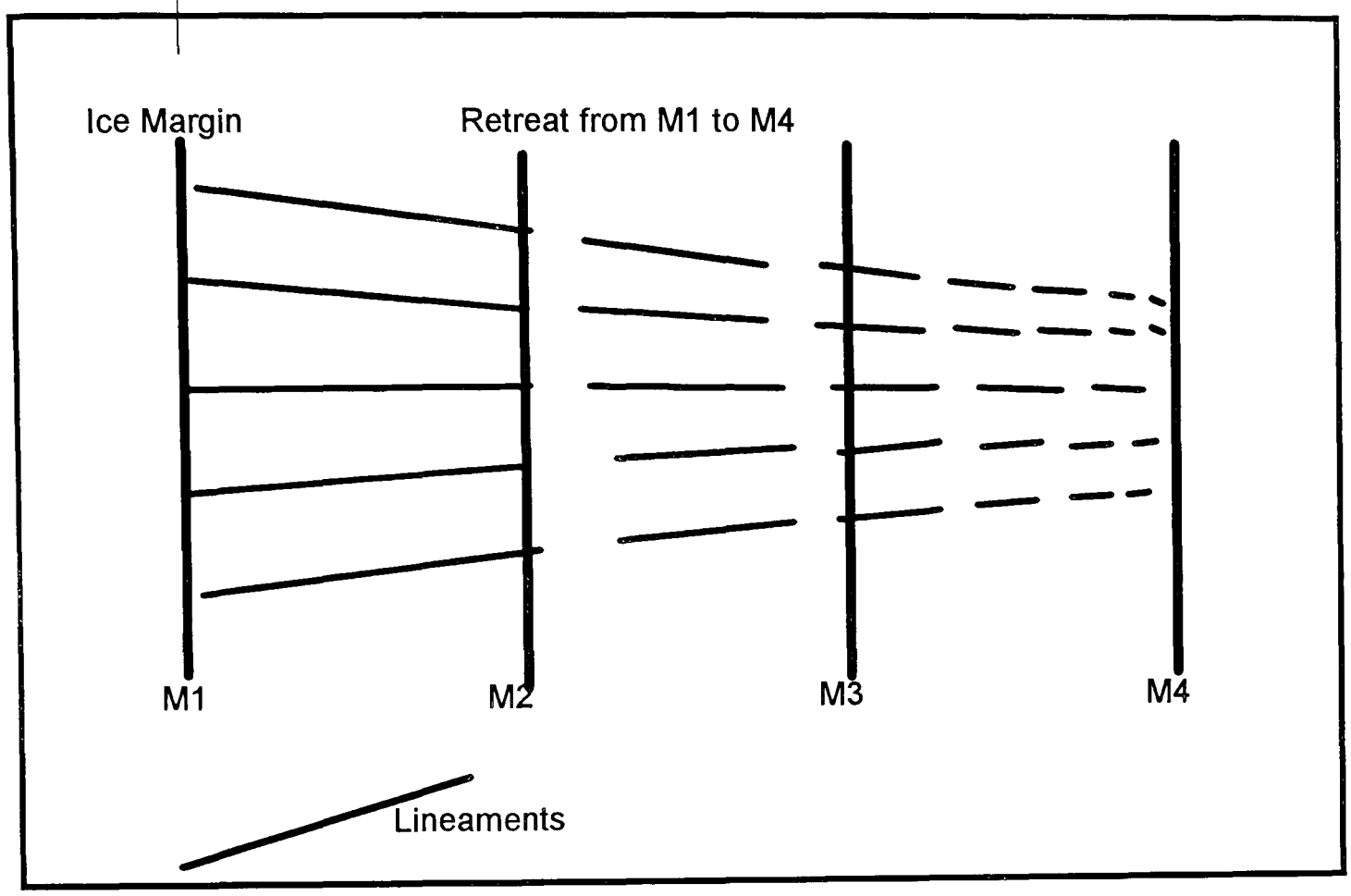

Figure 6.8
Time trangressive theory of lineament formation, lineaments are younger inwards.

6.6 Spatial frequency of the ice flow landform assemblage.

Geomorphologists have provided labels for components of the ice flow landform assemblage such as flutes, megaflutes, drumlins and mega-drumlins. These are presumed to be distinctive landform types that exist at certain loosely defined scales, such as flutes 10-100 metres in length, megaflutes 1000 metres in length (Clark, 1990). It is unclear as to whether these landforms do occupy specific scale ranges (length, height, spacing etc.) or whether there is a scale continuum from flutes through to mega-lineaments and that the labels are largely illusory. This is important as if there was a single scale continuum for ice flow landforms then a single process may be responsible for their formation, whereas if the scale distribution is multimodal then a different mechanism may be required to account for the formation of different scales of features. Figure 6.9 illustrates the multimodal case.

Using spacing as a measure of spatial frequency it should be possible to use spectral analysis to determine the scale distribution of landforms within the assemblage. A fourth hypothesis is therefore defined.

4 **Hypothesis Four:** The spatial frequency of lineaments tends towards a distribution that approximates to a scale continuous distribution.

6.7 Spatial frequency characterisation of ice flow sets

Given a complex pattern of lineaments such as in figure 6.10, the researcher aiming to make an ice flow reconstruction needs to group them into discrete flow sets. This interpretative process is based mainly on finding parallel features and

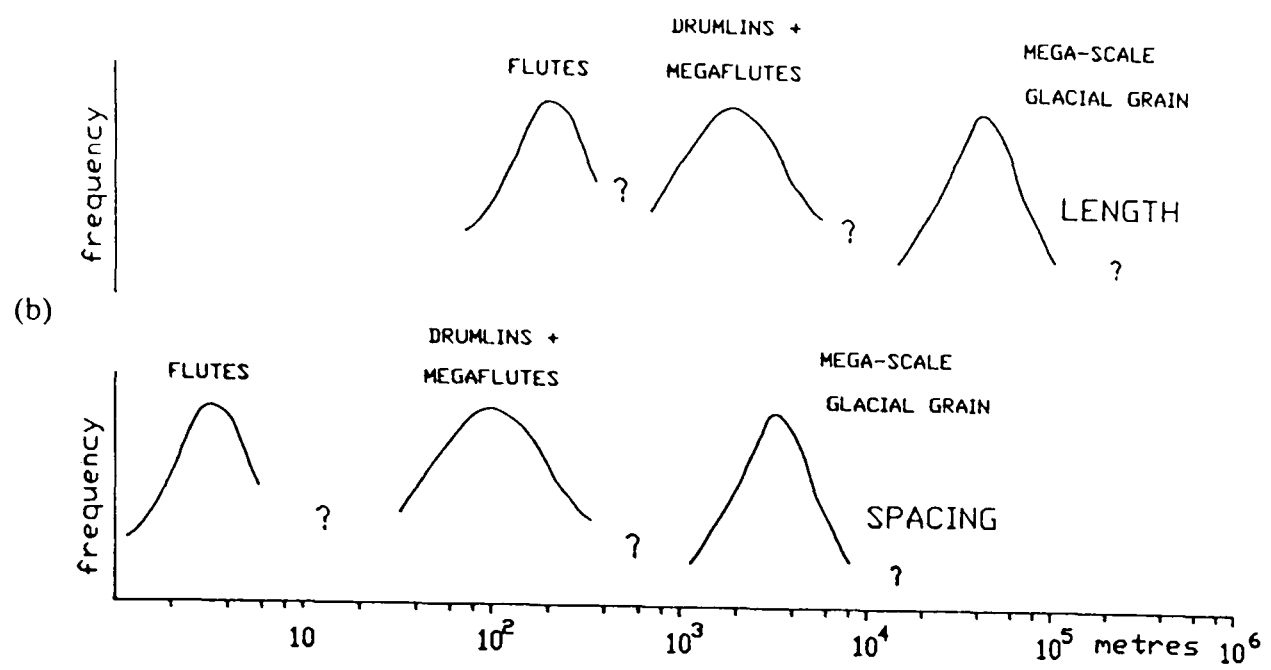

Figure 6.9 Schematic representation of principal spatial frequencies of the assemblage of ice-moulded landforms (Clark, 1993) showing concentration of spatial frequencies at specific frequencies.

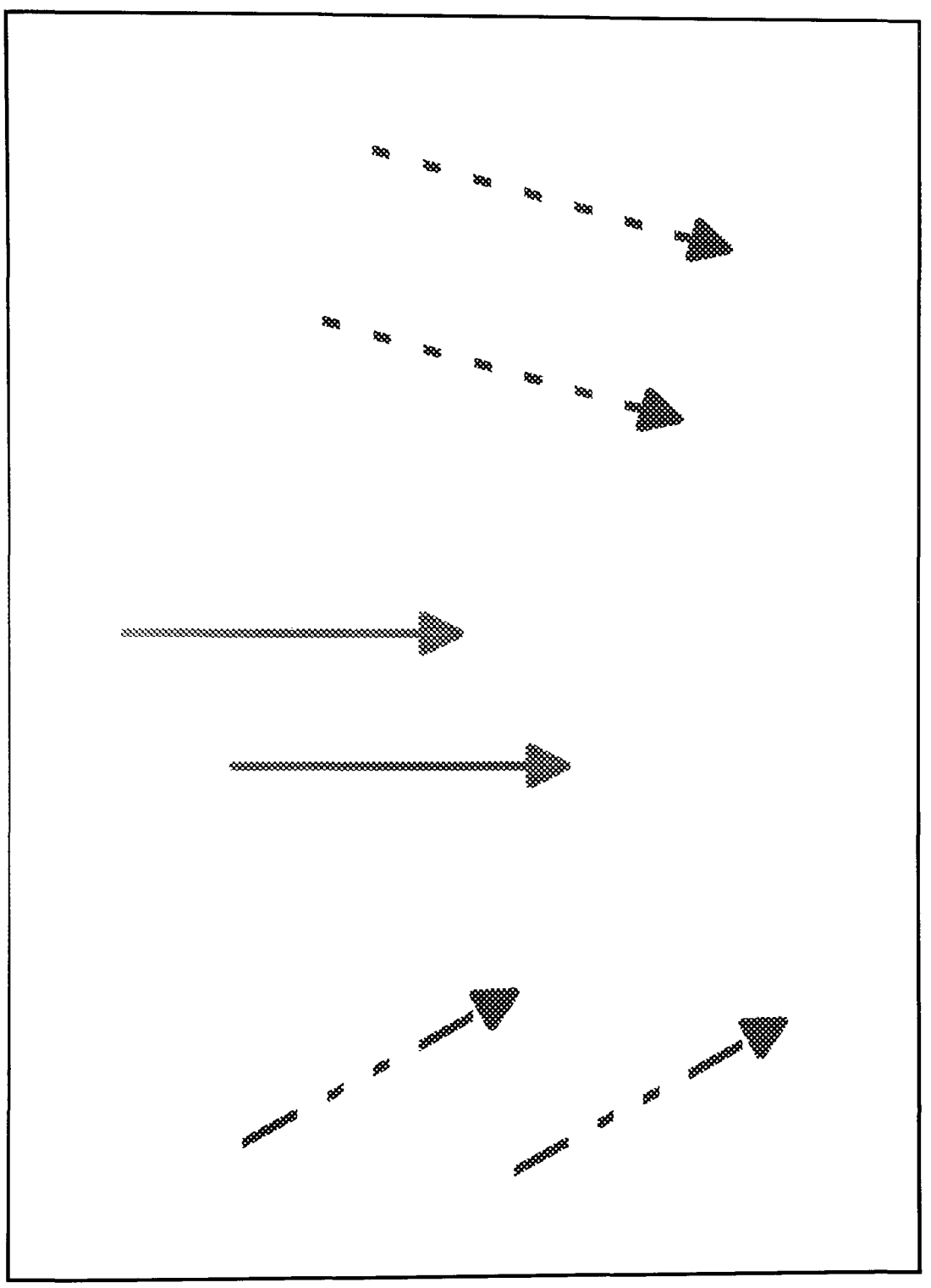

Figure 6.10
Complex pattern of lineament which can render confusion whether Flow is convergent or made of different flow sets

grouping them, which is fine for most cases. However as shown in the hypothetical example of figure 6.10, there could be two possible interpretations of ice flow configuration; a single convergent pattern or three separate flow sets. It may be possible to use spatial frequency information to determine the appropriate flow pattern if the different flow sets have unique spatial frequencies.

6.8 Case Studies

This section describes the application of spectral analysis to images depicting lineaments in Canada, in order to test the outlined hypotheses and to examine if spatial frequency is a useful measure for characterising ice flow sets.

6.8.1 Methodology

To test the set hypotheses vis a vis glacial lineaments, a number of satellite images of Canada (Figure 6.11) were utilised, ranging from scanned hard copy images to digital Landsat TM and MSS images.

In each of the satellite images, a hard copy of the entire area was produced and was used to trace some of the lineaments on the image in order to ascertain the general trend of the lineaments and also to establish distinctive flow sets. This was to guide the positioning and orientation of the transects, and also in interpreting the results of the spectral analysis.

Analysis was performed utilising band 1 for the Landsat MSS images. This is the green band with wavelength in the range of $0.50-0.60\mu m$. This band is useful for discriminating water bodies being one of the features that enhances lineaments. Band 4 was utilised for the Landsat TM image. This is the reflective infra-red band with wavelength in the range of $0.76-0.90\mu m$. The choice of band is not

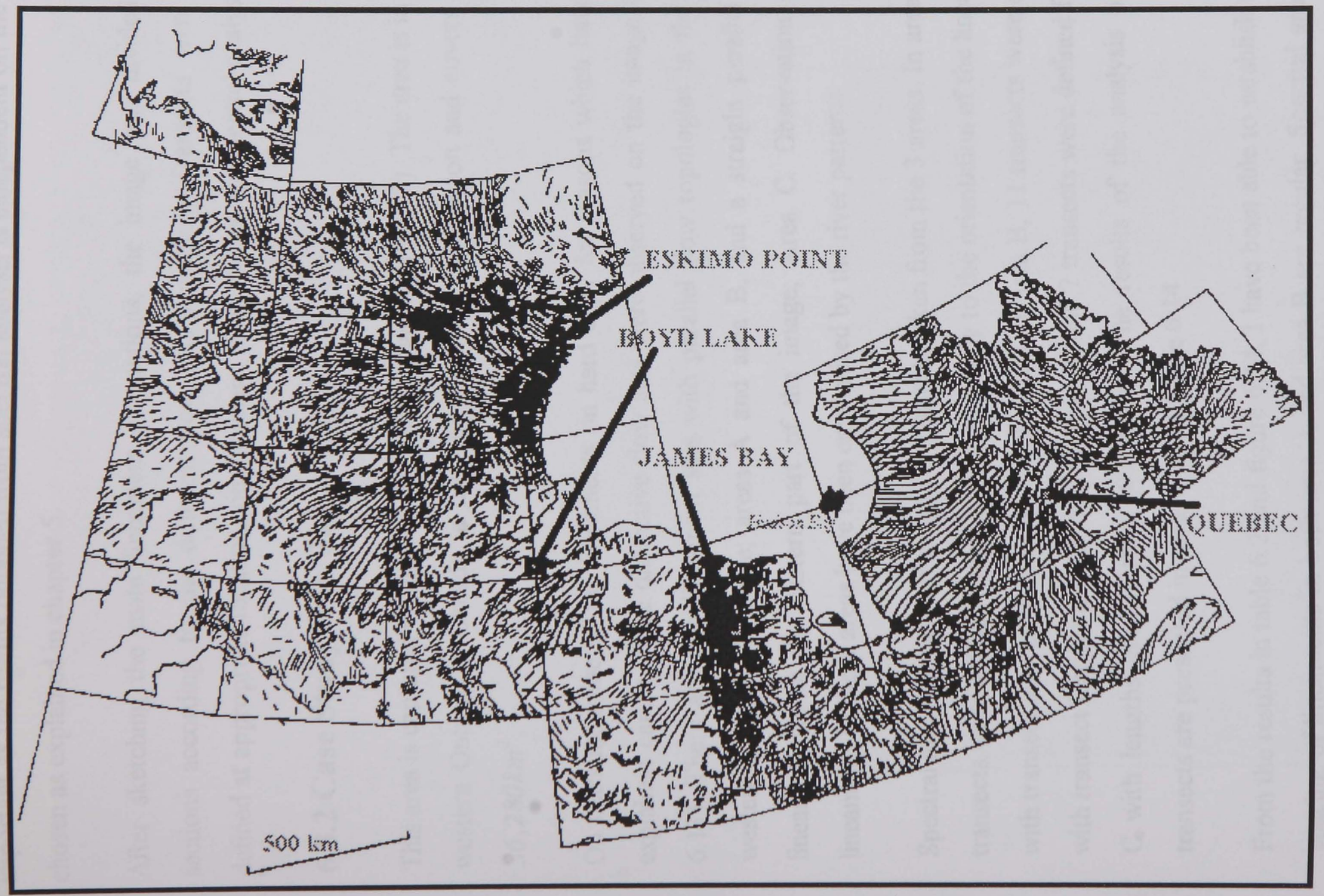

Figure 6.11 Summarised ice-flow lines in Canada, interpreted from mapping of glacial lineaments using Landsat images { Clark,1990). The map shows the areas where images: James Bay, Quebec, Boyd Lake and Eskimo Point were selected for the case studies.

important as the results obtained from spectral analysis is independent on the band chosen as explained in chapter 5.

After sketching the main lineament orientations, the image was divided into sections according to the different flow sets identified. Transects were then defined at appropriate locations on the image to be utilised for spectral analysis.

6.8.2 Case Study One, James Bay

This area is captured by the Landsat MSS image (figure 6.12). The area is in north western Ontario in Canada in the Alta Wapiskat river region and covers about $36,280km^2$.

On marking some of the lineaments on hard copy for reasons which have been explained earlier, three distinctive flow sets were observed on the image (figure 6.13). There are two lineament sets with parallel flow topologies in the south western part of the image; areas A and area B, and a straight parallel mega lineament set in the eastern part of the image; Area C. Observation of the lineaments in these areas have been emphasised by the river patterns.

Spectral analysis was performed on transects taken from the 3 areas. In area A, 19 transects were defined running perpendicularly to the orientation of the lineaments with transect lengths greater than 600 pixels. In area B, 11 transects were defined with transect lengths greater than 500 pixels, and 7 transects were defined for area C with lengths greater than 500 metres. The results of the analysis of these transects are presented in table 6.2 and figure 6.14

From the results in table 6.2 and figure 6.14, I have been able to establish that the spacing of lineaments in both area A and area B are regular. Spectral analysis of lineaments in area C did not show any dominant wavelength hence no values is presented for this area.

A

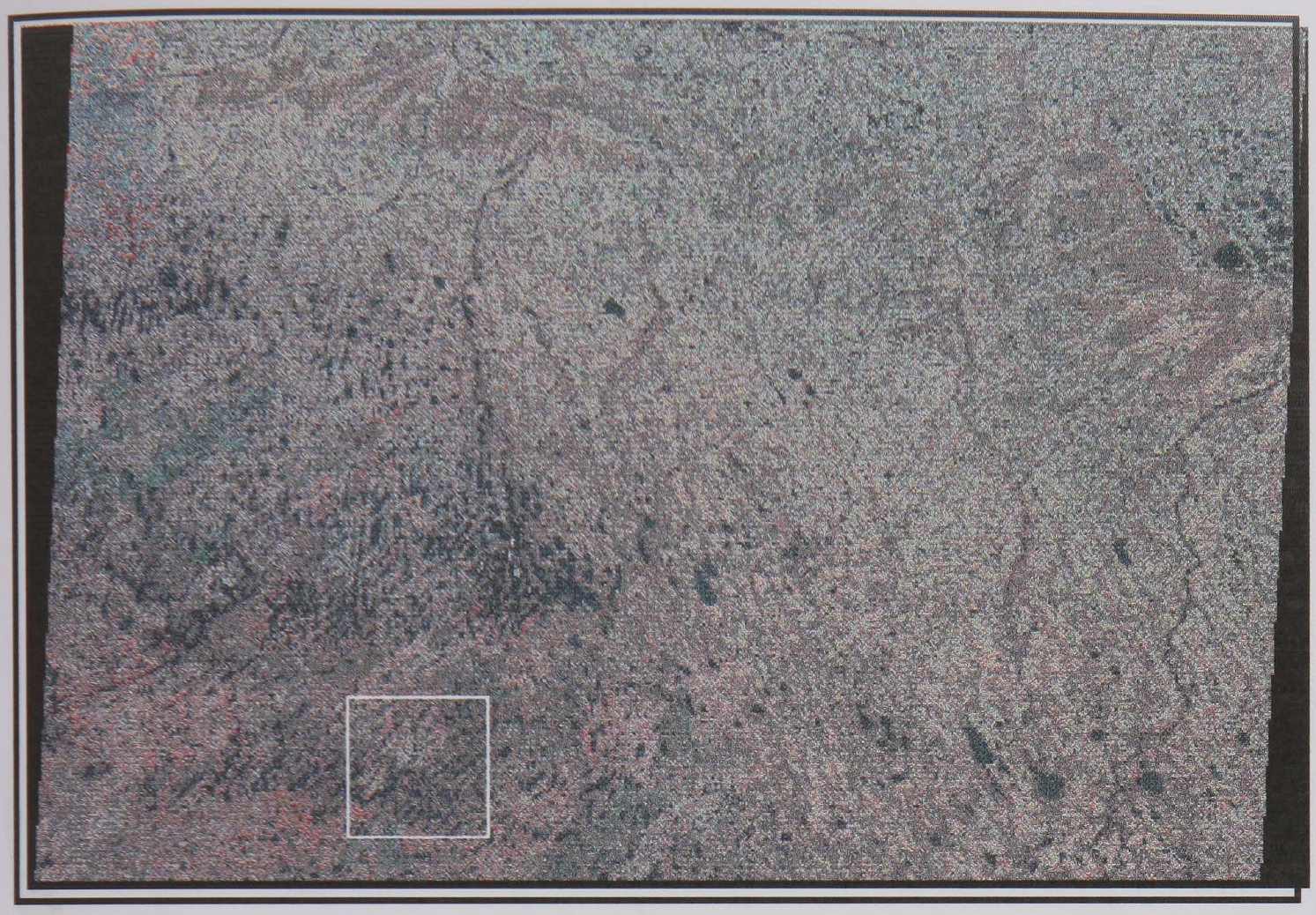

B

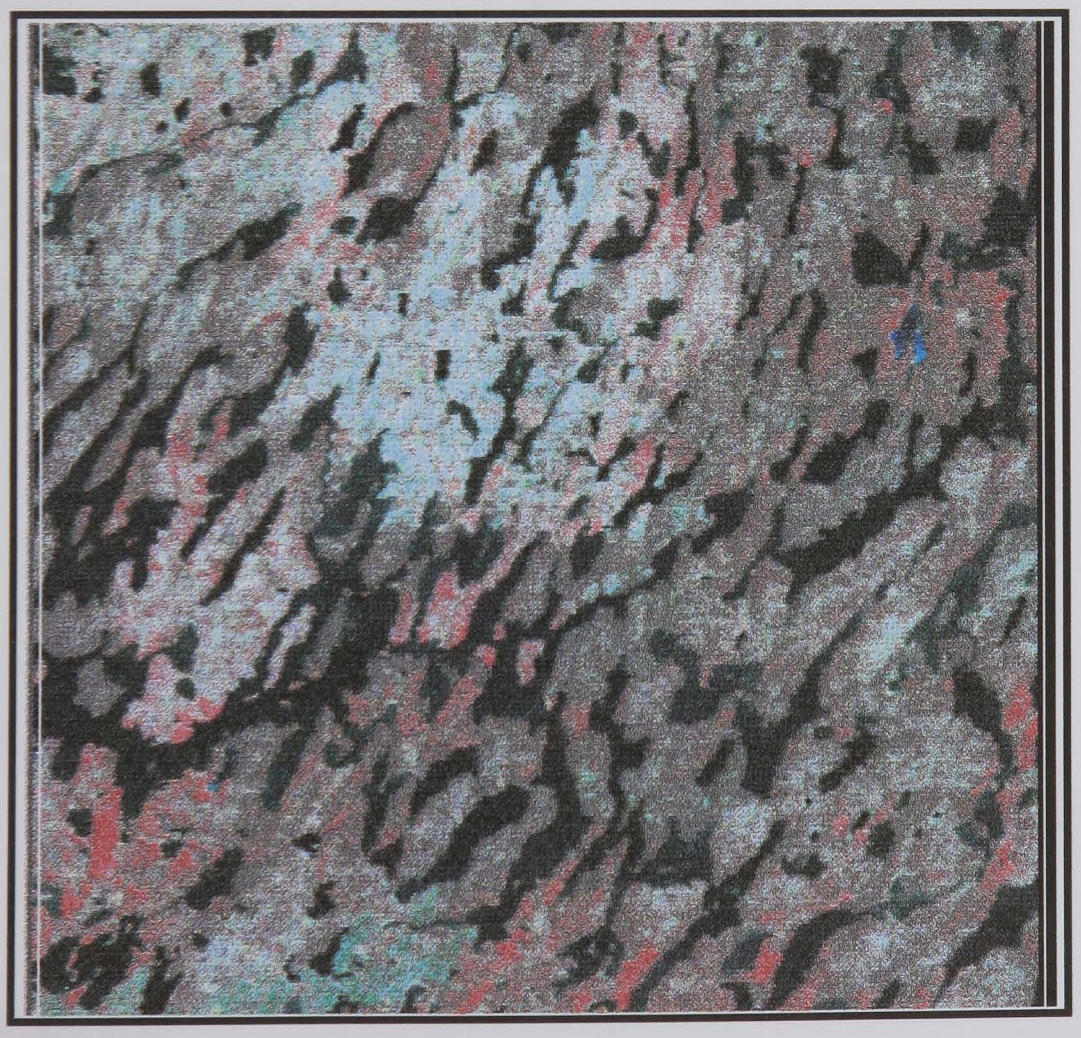

Figure 6.12 (A) Landsat MSS image of James Bay study area. (B) Enlargement of the boxed area in (A) showing the mega-scale glacial lineaments

Table 6.2a

Result of spectral analysis of lineaments in the James Bay image area A

TRANSECT	SPACINGS IN PIXELS				
TJAA11		20			
2		20			
3				14	
4			16		
5		20			
6			16		
7				14	
8				14	
9			16		
10			16		
11		20			
12				14	
13					
14					6
15					
16					7
17				13	
18					
19			16		

Table 6.2b

Result of spectral analysis of lineaments in the James Bay image area B

TRANSECT	SPACINGS IN PIXELS						
TJAB11			16				
2				13			
3					11		
4				13			
5							
6		20					
7					10		
8						7,	5
9		20			10		
10					9		6
11							7

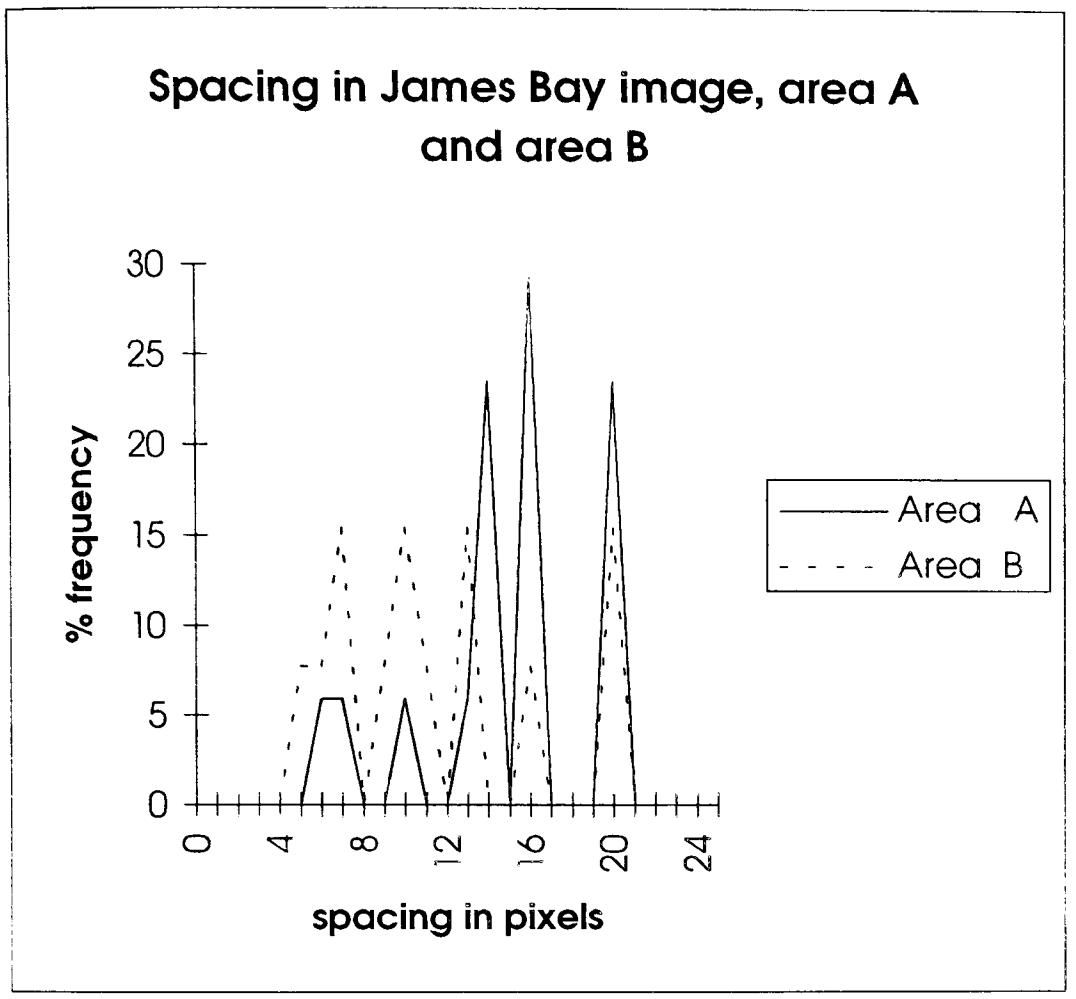

Figure 6.14
Percentage frequency of spacing from area A and area B of James Bay image (1 pixel = 79m)

The variation of lineament spacings for both areas ranges from 6 pixels (474 metres) to 20 pixels (1580 metres) and the graph of the frequency of all spacing for each of the study areas shows that the dominant spacings for area A are 7, 10, 14, 16 and 20 pixels and 7, 10, 13, 16 and 20 pixels for area B. Lineaments from area A and B can therefore be considered as identical in character. The spacing of lineaments in area C did not prove regular and hence no result for this area is presented.

The lack of cyclicity in the spacing of lineaments in area C suggests that the mega scale lineaments in this area could have been formed by a different process from that which formed lineaments in area A and B. This is in accordance with Prest's (1983) assertion that the mega scale lineaments in area C were formed by the late and final advance of glacier out of Hudson Bay, possibly a surge, while lineaments in area A and B were formed by active ice as the glacial margin receded toward Hudson Bay and James Bay. This suggests a difference in morphometry between lineaments formed under steady state and surging conditions, and is thus an important finding.

The geomorphological significance of the results from this case study are discussed in chapter seven.

6.8.3 Case Study Two, Quebec Image

This area is captured by the Landsat MSS image (figure 6.15) and falls within latitude 53.15 degrees north and longitude 71.45 degrees east. It covers an area of about $36,196km^2$ square.

The image (figure 6.15), represented by the sketch in figure 6.16 shows mega-scale lineaments and smaller ones trending from the North East to South West direction, that are believed to have been formed by the Labrador-Quebec ice dome. Observation of the image also revealed a broader set of lineaments which

A

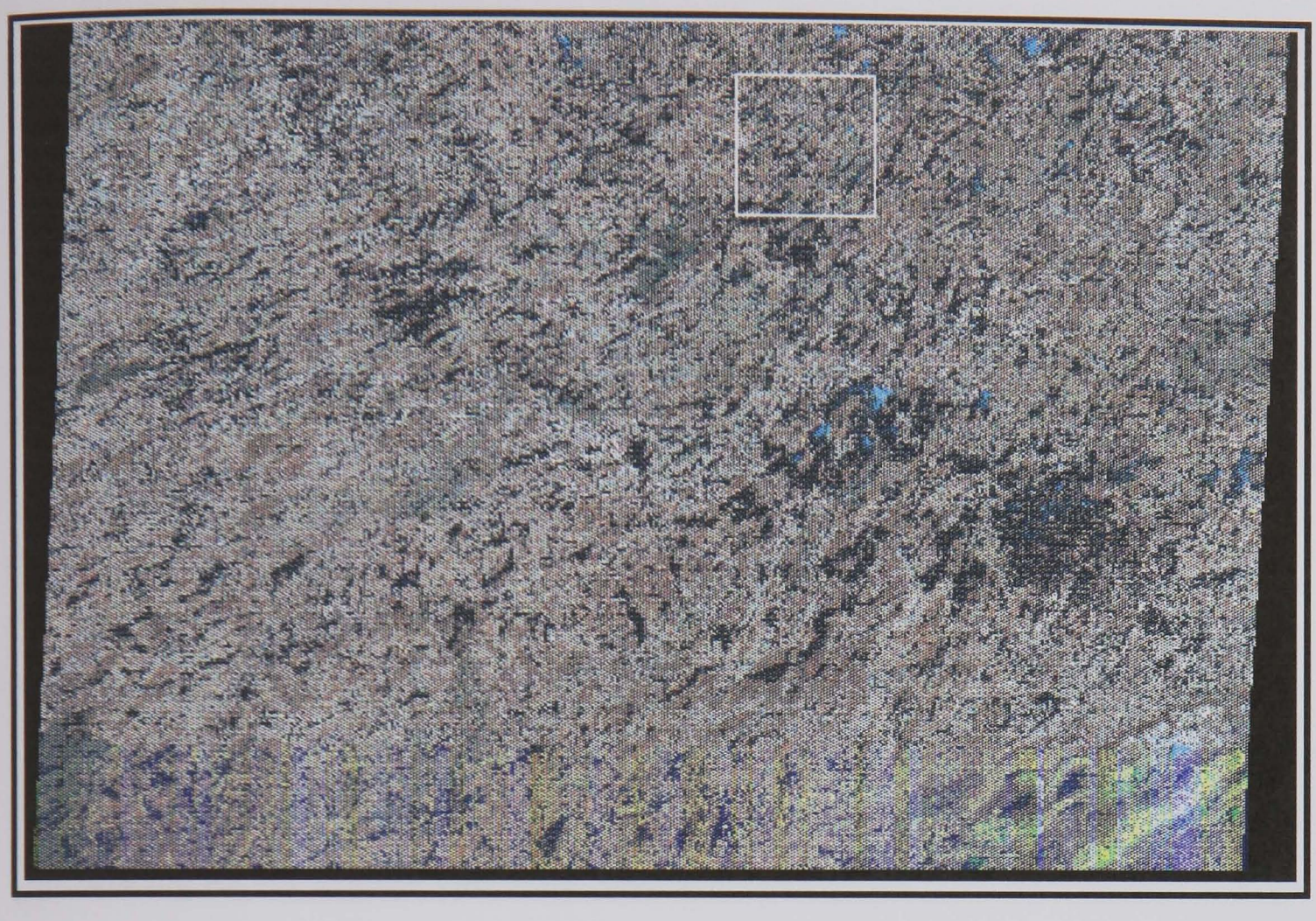

B

Figure 6.15 (A) Landsat MSS image of Quebec study area. (B) Enlargement of the boxed area in (A) showing the mega-scale glacial lineaments

trend in the NE-SW direction. In area A of the image can also be found cross cutting lineaments trending in the NNE-SSW direction. Observation of lineaments is aided by sediments and boundaries of linear water bodies such as lakes. The flow topology of lineaments in this area can be described as parallel.

In quantifying the spacing between lineaments in this image, two areas were selected, areas A and B. To check for the broad mega lineaments in the image, a third set of longer transects were defined across the image passing through both areas A and B. In area A, 15 transects were defined with lengths greater than 400 and 15 transects were also defined for area B with lengths over 700. For the set of transects across the image, 13 were defined with longer lengths ranging from 800 to 2000. Results of analysis of transects are presented in figure 6.17 and table 6.3.

The results shows that the spacing of lineaments in the Quebec image are regular. From the frequency graph of the spacings, it can be observed that lineament spacing for each of the two areas falls between 5 pixels (395 metres) and 33 pixel (2607 metres) with a mode for both areas at 9 pixels (711 metres). Area B shows a predominant spacing of 9 pixels while area A also confirms this spacing with additional spacings of 7 and 16 pixels. This is probably due to the cross cutting in the area. Spectral analysis for longer transects taken across the image gave identical results. The aim of using longer transect for the entire image was to see if the broader mega lineaments observed on the image were regular. No new information was achieved by doing this. The results were identical to those obtained from analysing transects in area A and area B. The mega lineaments could therefore be considered to have an irregular spatial arrangement, a finding which fits in with the mega lineaments of the James Bay image.

Inorder to check for the variation of lineament spacing over a significant distance down ice, 3 Landsat MSS images were commissioned for the Quebec area. The

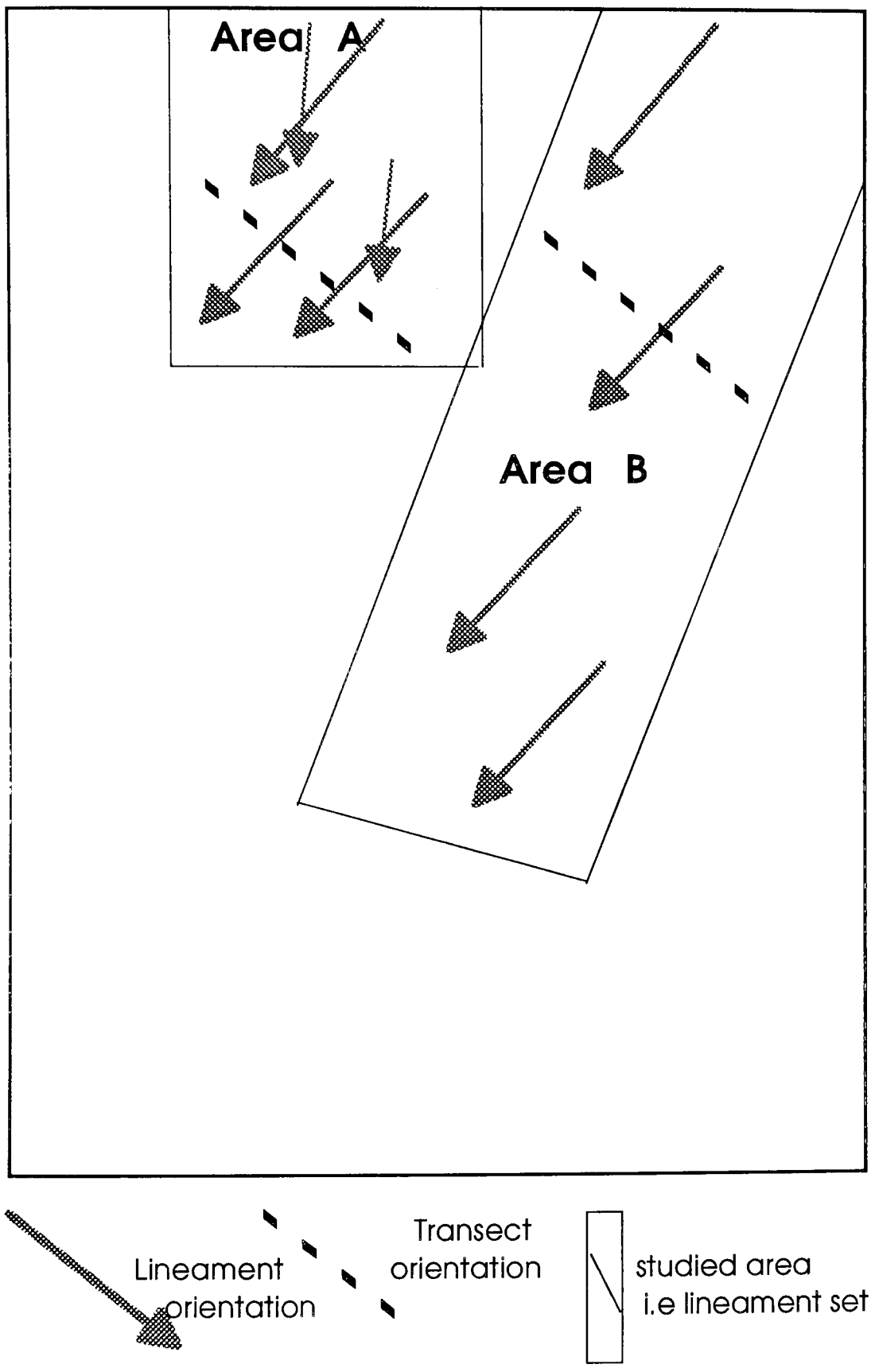

Figure 6.16
Sketch diagram of the studied area in Quebec image showing orientation of lineaments and transects

Table 6.3a

Result of spectral analysis for the Quebec image area A

TRANSECT	SPACINGS IN PIXELS					
TQUA11			16			
2			16	9		
3			16			7
4			14	8		
5			16	9		
6		33		9		6
7			13			7
8				9		
9		33			7,	5
10			13	9		
11		20		9		6
12						
13						
14				11		7
15		20		9		6

Table 6.3b

Result of spectral analysis for the Quebec image area B

TRANSECT	SPACINGS IN PIXELS					
TQUB11				10		
2				9		
3				8		
4				9		
5				9		
6				10		
7						
8				9		
9				9		6
10						
11				10		
12			13			
13						
14					7,	5
15				9		

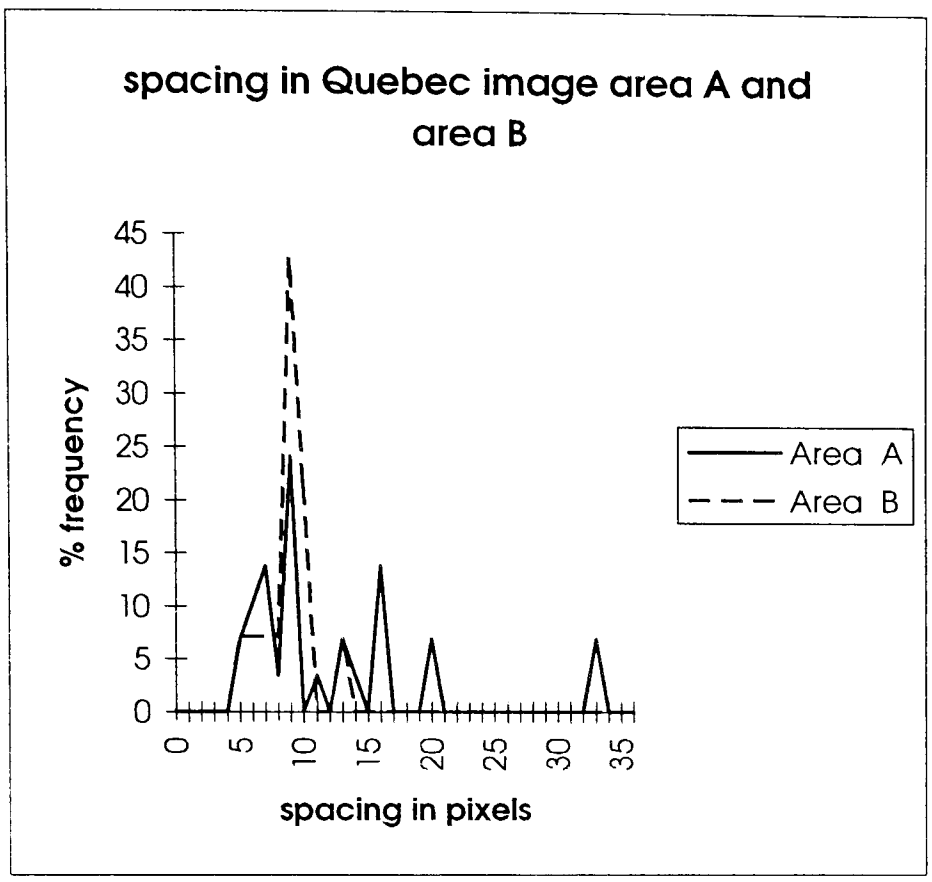

Figure 6.17
Percentage frequency of spacing from area A and area B of Quebec Image (1 pixel = 79m)

scenes were chosen such that they were adjacent to each other and covered a maximum distance of about 700 km down ice. Unfortunately two of these images did not reveal good lineaments field and were thus discarded for this investigation.

The geomorphological significance of the results from this case study are discussed in chapter seven.

6.8.4 Case Study Three, Boyd Image.

This area was captured by Landsat TM imagery (figure 6.18). The area is located within latitude 56.25 degrees north and longitude 96.25 degrees east around Boyd Lake in the North Western Territories. It covers an area of about $36,198km^2$

The image shows a dominant NE-SW trend of mega-scale glacial lineaments. Another lineament set can be seen trending and cross-cutting the strong NE-SW lineaments and aligned ENE-WSW. Clark (1993) identified this pattern and showed that the ENE-WSW lineaments are drumlins which are visibly superimposed upon the mega-scale glacial lineaments. The flow topology of each of the set of lineaments can be described as parallel.

In studying the lineament spacing in this image, two study areas were defined, area A and B (figure 6.19). Area A was further divided in to two section areas Ai and Aii. 19 transects were selected for both areas with area Ai having 8 transects and area Aii, 11 transects with lengths greater than 500. 15 transects were defined for area B with lengths greater than 600. The orientation of the transects were made perpendicular to the orientation of the mega-scale lineaments.

Results of the analysis are presented in figure 6.20 and table 6.4. The results proved that the spatial arrangement of lineaments in these areas are regular and that the spacings of lineaments in these areas fall between 3 pixels (90 metres) and 17 pixels (510 metres) with area A having a dominant spacing of 4 and 7 pixels and area B having a dominant spacing of 4,7, 9, and 13 pixels. The multiple

A

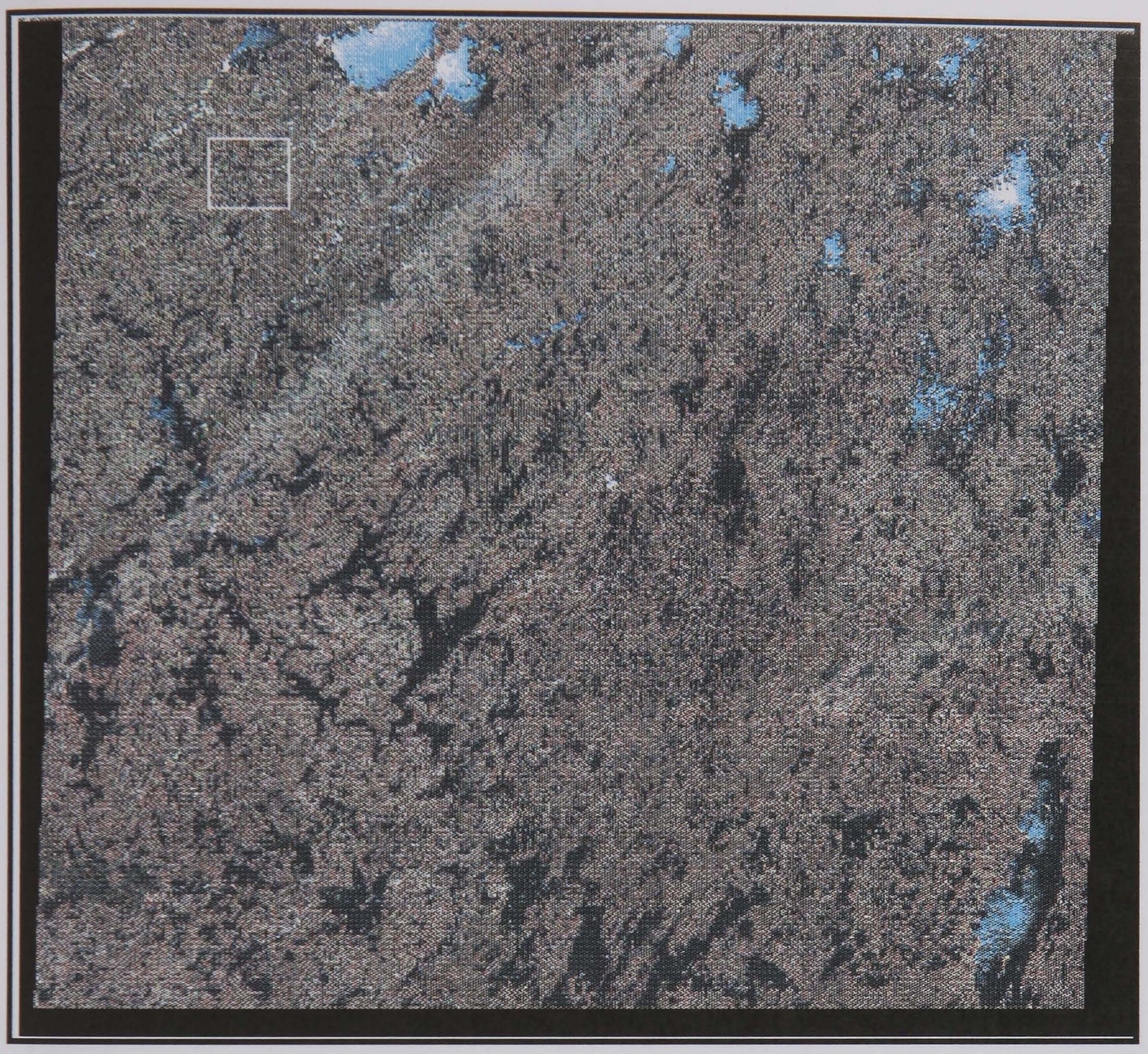

Figure 6.18 (A) Landsat TM image of Boyd Lake study area

B

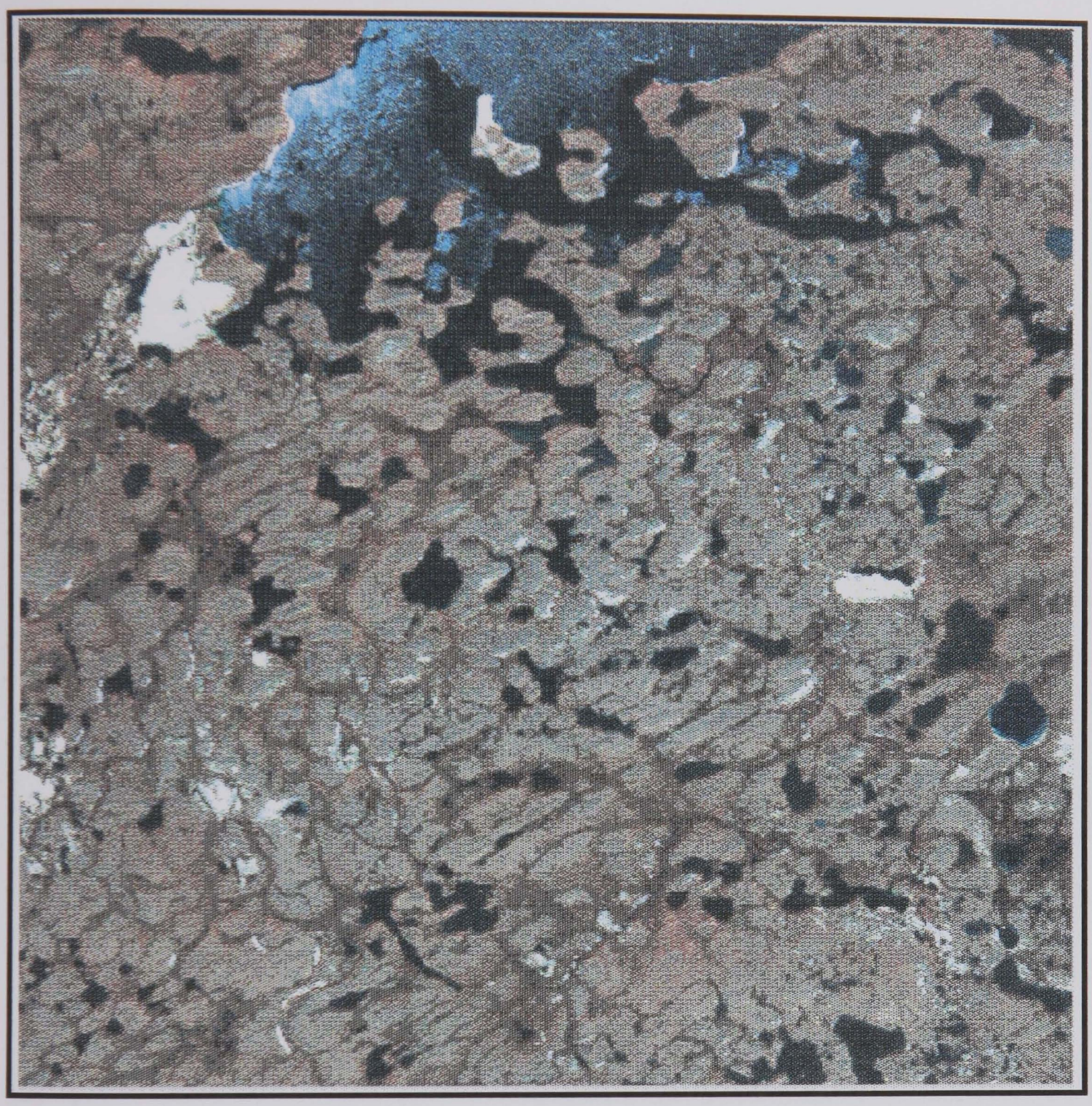

Figure 6.18 (B) Enlargement of the boxed area in (A) showing glacial lineaments

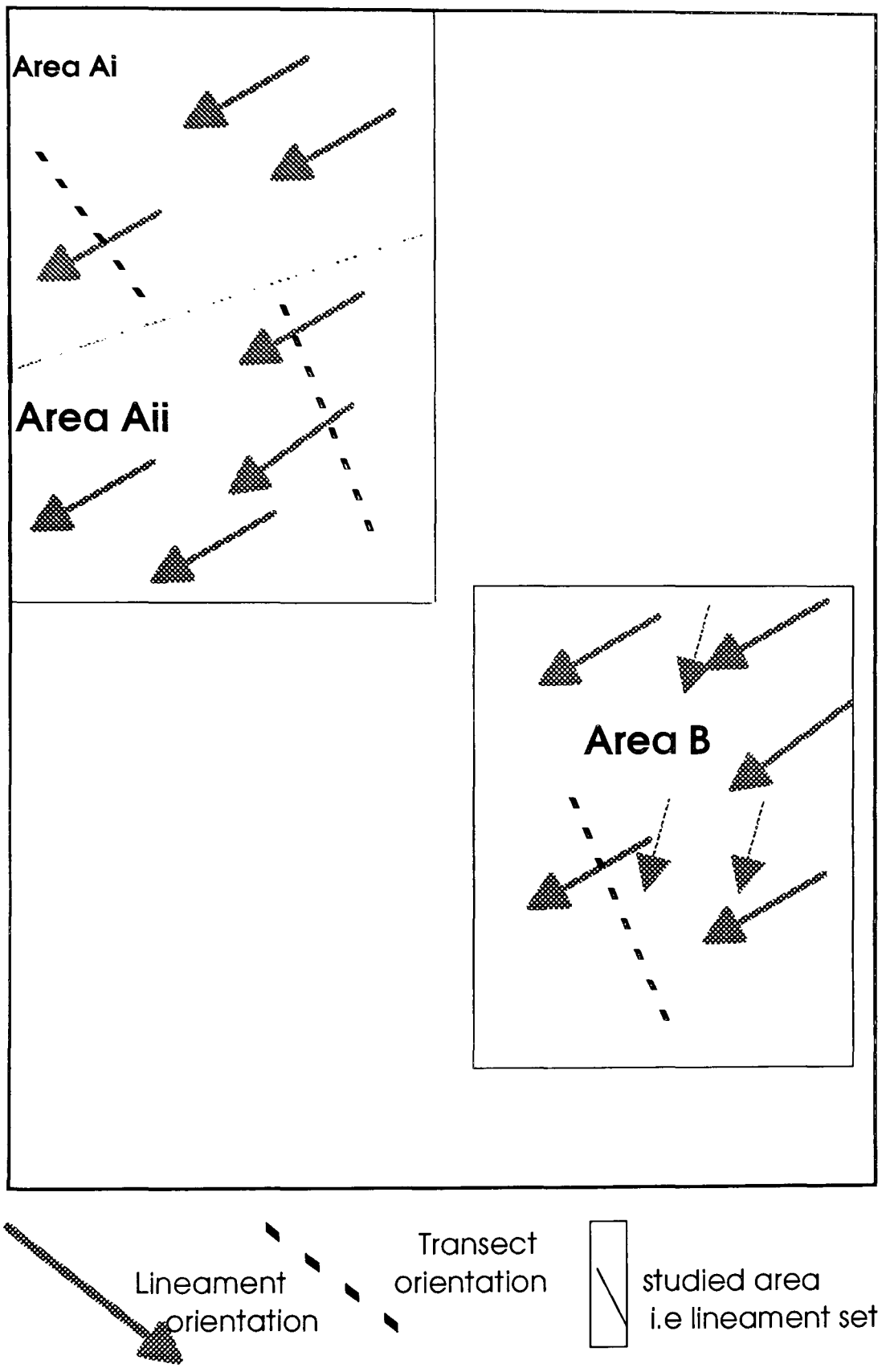

Figure 6.19
Sketch diagram of the studied area in Boyd image showing orientation of lineaments and transects

Table 6.4a

Result of spectral analysis for the Boyd image area A

TRANSECT	SPACINGS IN PIXELS							
TBOB11							4,	3
2					7		5	
3					8		5	4, 3
4					8		5	4
5					8		5	
6					7		5	4, 3
7				9	7		5	4, 3
8			11		7		6	4
9				10	7	6,	5	4
10			11		7		6	4
11			13		7		6	4, 3
12				10			6	4
13							6	4, 3
14				10			6	4
15			13				6	4
16			14		7		5	3
17					7		5	4, 3
18							6	3, 2
19			11		7			4

Table 6.4b

Result of spectral analysis for the Boyd image area B

TRANSECT	SPACINGS IN PIXELS					
TBOB11		11		8		
2		13	9		6	
3		13		7		4
4		13		7	6	
5		17	10			
6			9	7	5	4
7		13	9		6	4
8		13	9			4
9		13		7		
10						4
11			9		6	3
12		13		7	5	
13		13		7		4
14		13		7	5	
15			10	7		4

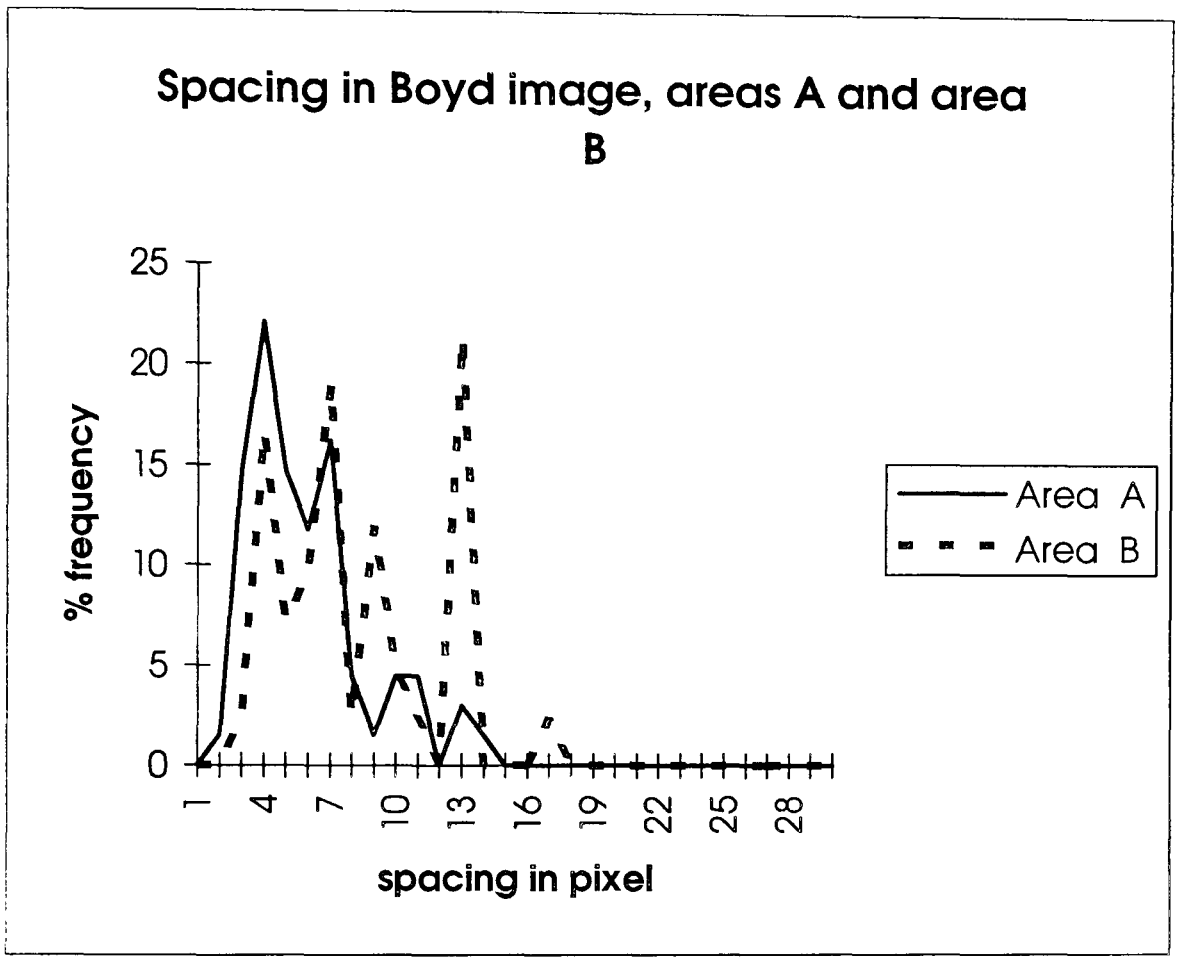

Figure 6.20
Percentage frequency of spacing from areas A and area B of Boyd image

spacing in area B is due to the cross-cutting since it is in this area that cross-cutting of the ENE-WSW lineaments are most apparent.

The geomorphological significance of the results from this case study are discussed in chapter seven.

6.8.5 Case Study Four, Eskimo Point Image

This area was captured by a Landsat MSS image (figure 6.21). The area is located in the North Western Territory of Canada around Eskimo point. The lineaments in this image can be observed as continuous linear forms of spindle-shaped sediment ridges whose linear pattern is made apparent by their lateral edges or boundaries with linear water bodies. The image captures an area of about $36,247km^2$. The topology of these flow sets can either be described as a single convergent flow or two parallel flows crossing one another towards the Hudson Bay.

The flow pattern trending WNW-ESE in the north east of the image, forms the lineaments of area A, at the centre of the image can be observed lineaments trending in the W-E, this is area B, and Area C is located in the south of the image with WSW-ENE trending lineaments (Figure 6.22).

Spectral analysis was performed on transects defined in each of the study areas. The transects were positioned such that their orientation was perpendicular to the orientation of the lineaments. 16 transects were defined for area A with lengths greater than 600 and 19 transects were defined for area B while 21 transects were defined for area C with lengths greater than 300. The results of spectral analysis on this image are presented in figure 6.23 and table 6.5. The results confirm that the spatial arrangement of lineaments in this image are regular. The spacing of lineaments for the whole image falls between 3 pixels (237 metres) and 33 pixels (2607 metres) with the majority of lineament spacings of 5 and 6 pixels. From the frequency graph of the results, it can be observed that the dominant spacing for area A is 6 pixel and that for area C is 5 pixels while area B exhibits dominant

A

B

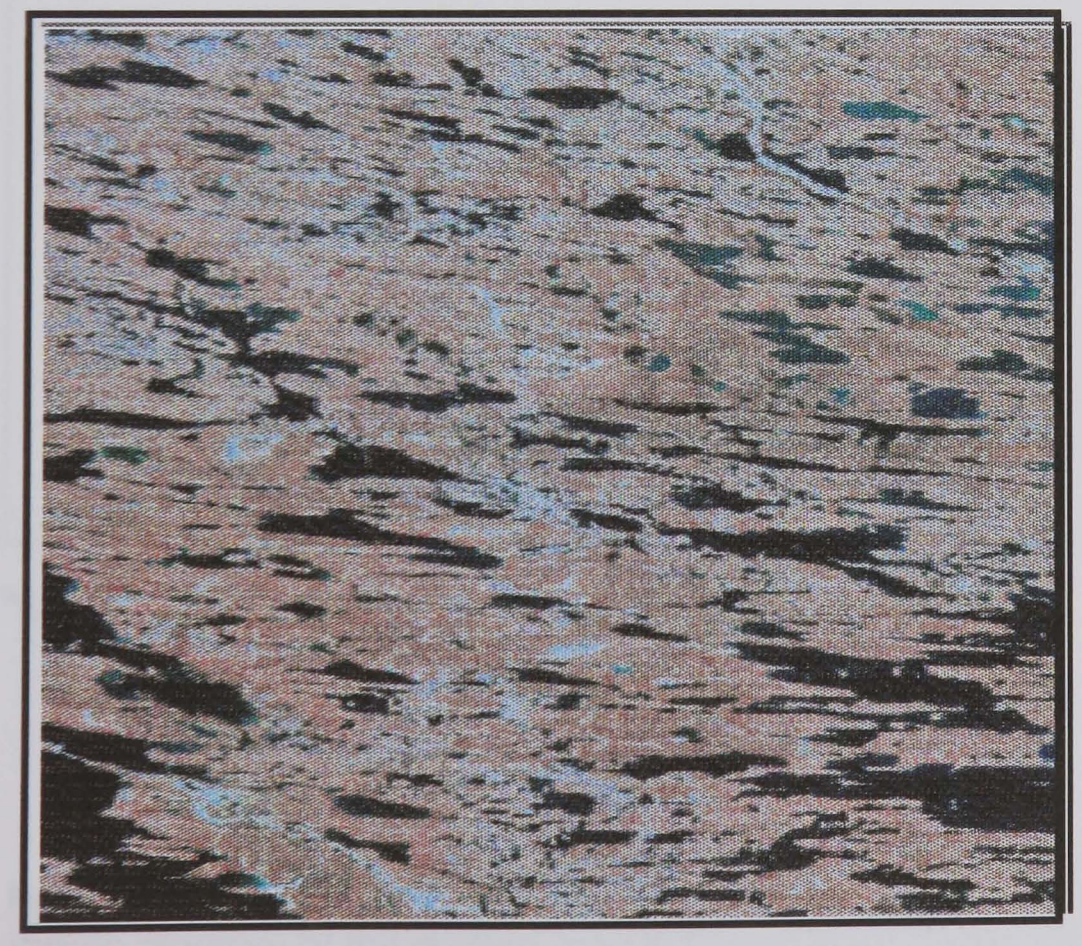

Figure 6.21 (A) Landsat MSS image of Eskimo Point study area. (B) Enlargement of the boxed area in (A) showing the mega-scale glacial lineaments

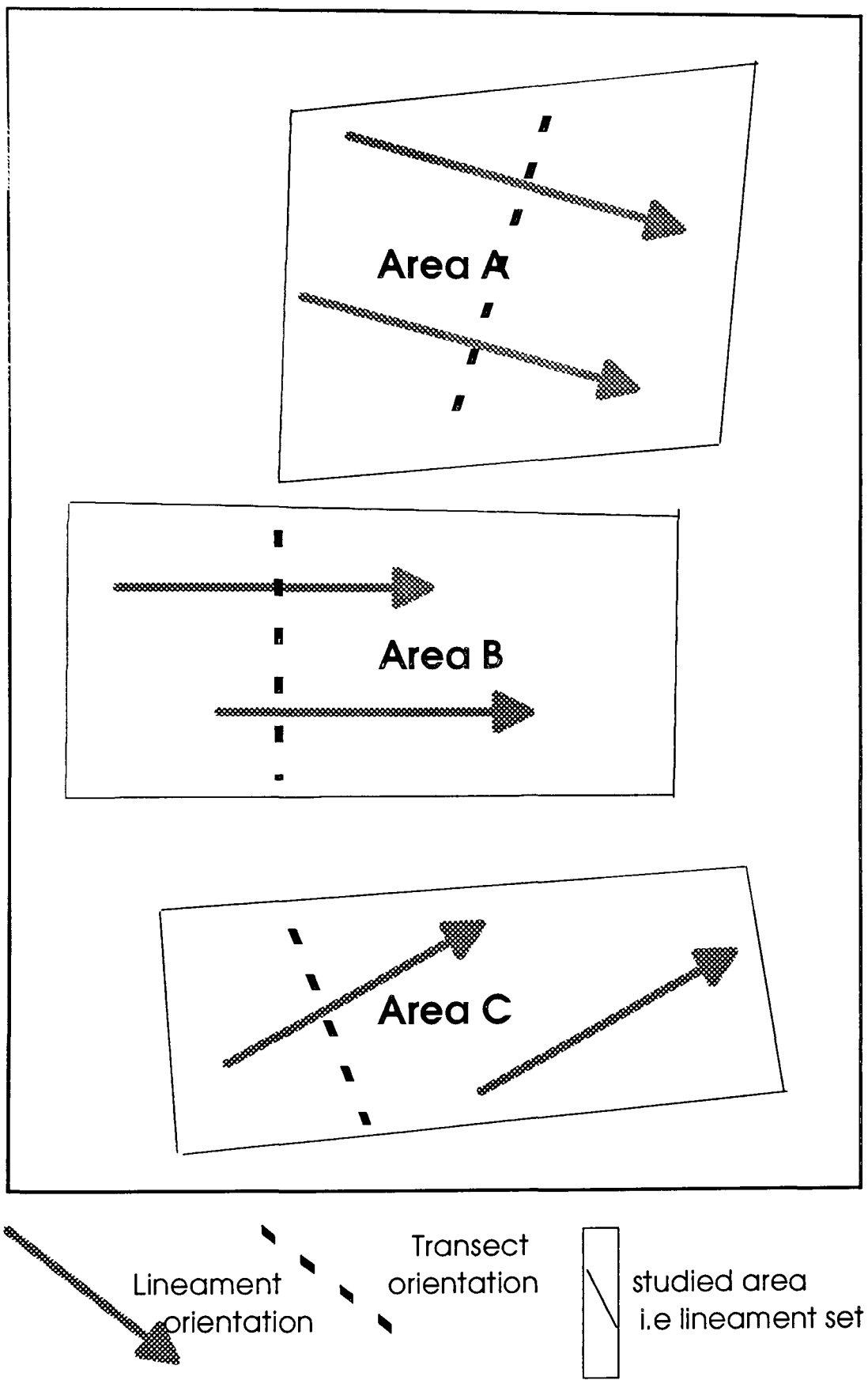

Figure 6.22
Sketch diagram of the studied area in Eskimo Point image showing orientation of lineaments and transects.

Table 6.5a

Result of spectral analysis for the Eskimo Point image area A

TRANSECT	SPACINGS IN PIXELS						
TEPB11				7			
2			9				4
3		11				6	3
4							
5							
6						6	
7		13				5	
8		11			5,	6	4
9					5,	6	
10						6	4
11						5	
12						6	4
13		14		7		5	
14				7		5	
15						6	
16						6	4

Table 6.5b

Result of spectral analysis for the Eskimo Point image area B

TRANSECT	SPACINGS IN PIXELS						
TEPB11		25		9	7		5	
2		20			8		6	
3		33		10	7		5	
4		33		10		5,	6	4
5		25	12		7		5	
6				10			5	4
7		17			8		6	4
8		17		10	7			4
9		25		9			6	
10		25		10			6	4
11			14	10	7		5	
12			12		8		5	
13			12				6	
14		20			8		6	
15		17				5,	6	
16		33	11			5,	6	
17			14	9				
18		33		9			6	
19		25			8		5	

Table 6.5c

Result of spectral analysis for the Eskimo Point image area C

TRANSECT	SPACINGS IN PIXELS								
TEPC11		17				7		5	4
2		20		10				5	
3		20		10				5	
4		33	12					5	4
5		33		9				5	4
6			12					6	
7		33		10			5,	6	4
8		25		10		7		5	
9		17				8			4
10		20					5,	6	3
11			12			7			
12		20	11			7			
13		17			7,	8			4
14			12			7			
15		25				7		5	3
16		25	14			8		5	4
17						8			
18			12			7			
19				10				5	
20		33					5,	6	4
21			12					5	

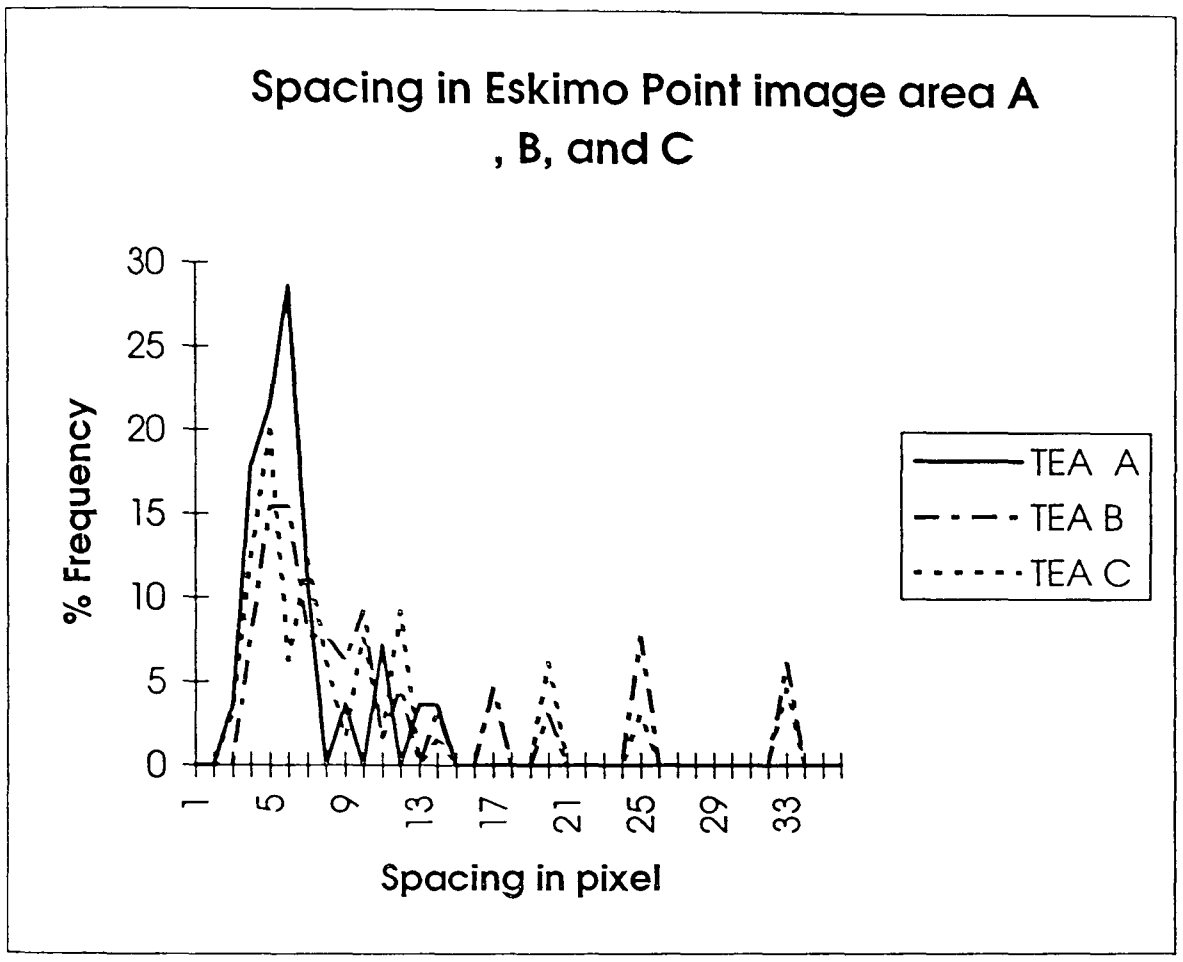

Figure 6.23
Percentage frequency of spacing from area A, B and area C of Eskimo Point image

spacings of 5 and 6 pixels. This suggests that lineaments in area B are a mixture of those in area A and C and that the flow pattern is not convergent but of two parallel sets. Spectral analysis has thus been applied in this circumstance to determine the appropriate flow pattern for this lineament field. This is in contradiction to the flow pattern indicated on the Glacial Map of Canada (Prest, 1968).

The geomorphological significance of the results from this case study are discussed in chapter seven.

6.8.6 Case Study Five, Victoria island Image

The image for this area was scanned and stored in a format that can be read by ERDAS, the image processing software used in this research. The scanned image had 1000 rows and 850 columns. Using the scale on the hard copy, the pixel size was calculated to be 125 metres. The image therefore covered an area of about $13,281km^2$ of the Victoria island in the North Western Territory and shows streamlined lineaments trending to the south western part of the image figures 6.24 and 6.25.

To analyse this image, five transects were chosen for the area with lengths greater than 200. Spectral analysis of these transects gave the results presented in table 6.6. From the table, it can be observed that regularity of the spacing of lineament in this image has been established. The five transects gave lineaments spacing of 3 pixel (375 metres) to 17 pixels (2125 metres) with the majority of spacing of 9 pixels(1125 metres) and 6 pixels (750 metres). The main conclusion from using the scanned image is that regularity of the lineament spacing was established for this lineament set. Due to the limited number of transects used, inferences about the set hypotheses established earlier will not be considered.

Table 6.6

Result of spectral analysis for the Victoria scanned Image.

TRANSECT	SPACINGS IN PIXELS					
TVI11		17	9		5	
2			9	6		
3		17	9	6	5	
4			9	6		3
5			10	7	5	

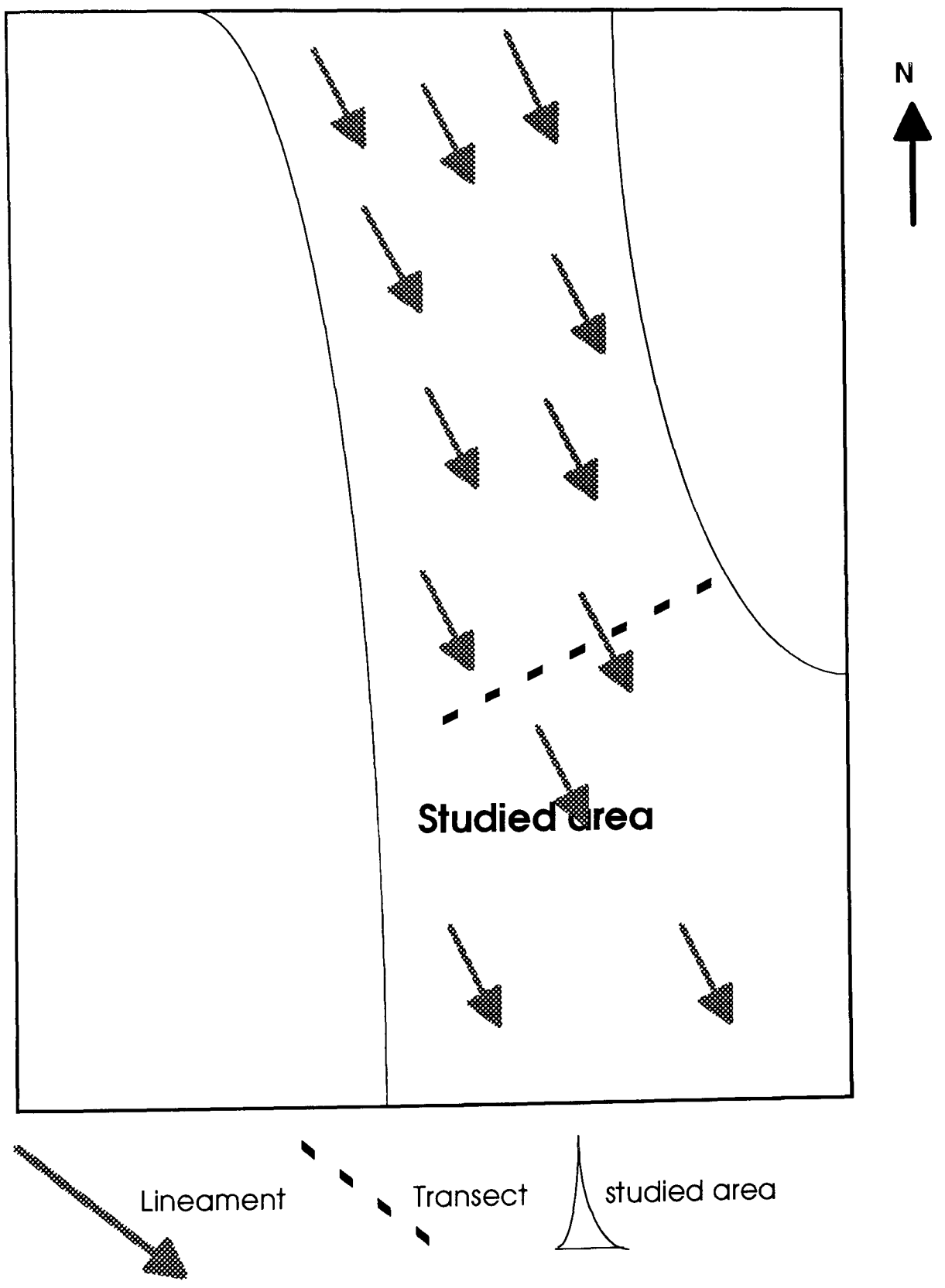

Figure 6.24

Sketch diagram of the studied area in Victoria image showing

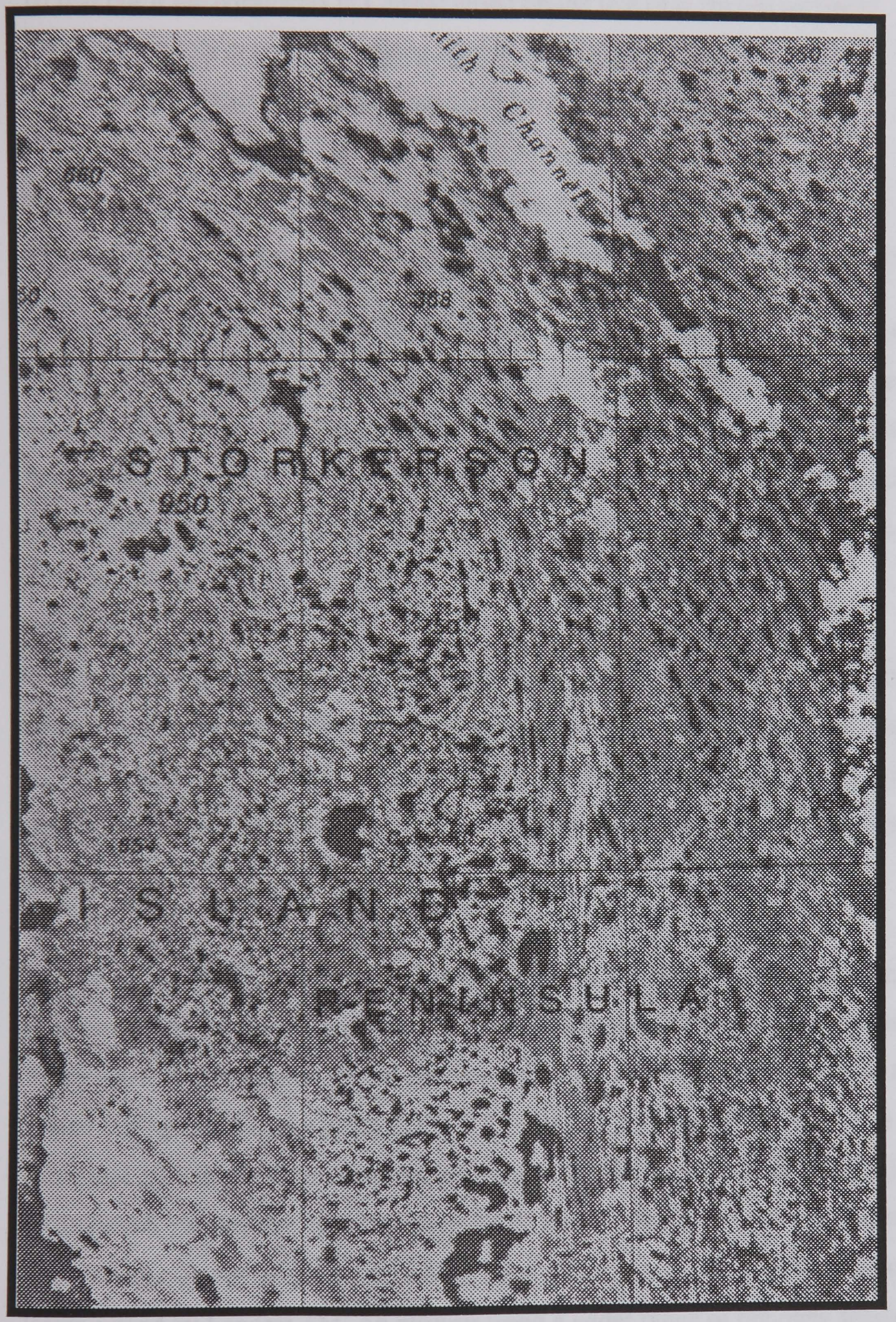

Figure 6.25 Scanned image of victoria study area

6.8.7 Joint spatial frequency of lineaments.

To find out if the lineaments in Canada based on the five case studies represent distinctive land form types occupying specific scale ranges, the results of the spatial frequency from each study area were combined as in figure 6.26.

The aim of doing this was to test hypothesis four; whether the distribution of spatial morphometry approximates to a scale continuous distribution. In order to

achieve this, the spacing obtained for each of the study areas were standardised by converting the pixel values to metres. Histogram analysis of the result produced the graph of figure 6.26. The graph shows that there is a concentration of spatial frequencies between 150 and 750 metres. The hypothesis that these glacial features represented by these lineaments have a scale continuous distribution is therefore accepted.

It is important to note here that these analysis involved all the 155 transects that were used for this study. The test transects used in chapter five contain an average of 79 lineaments per transect. This means that more than 12 000 lineaments were considered for this analysis which is more than the sample size that has been used by others.

The above finding is not surprising and it is probably due to the limited scale range (Landsat MSS) of images used for each of the study area. This therefore is bound to introduce a bias against lineaments spacing which are lower or higher than the spatial resolution of Landsat MSS. Clark (1990) and Shuman (1989) were able to show that each scale of remotely sensed imagery would reveal varying distribution of lineament parameters. It is therefore likely that the spatial frequencies for this study relates mostly to those that have been picked by Landsat MSS and to a lesser extend by Landsat TM. An analysis using a wider range of remotely sensed

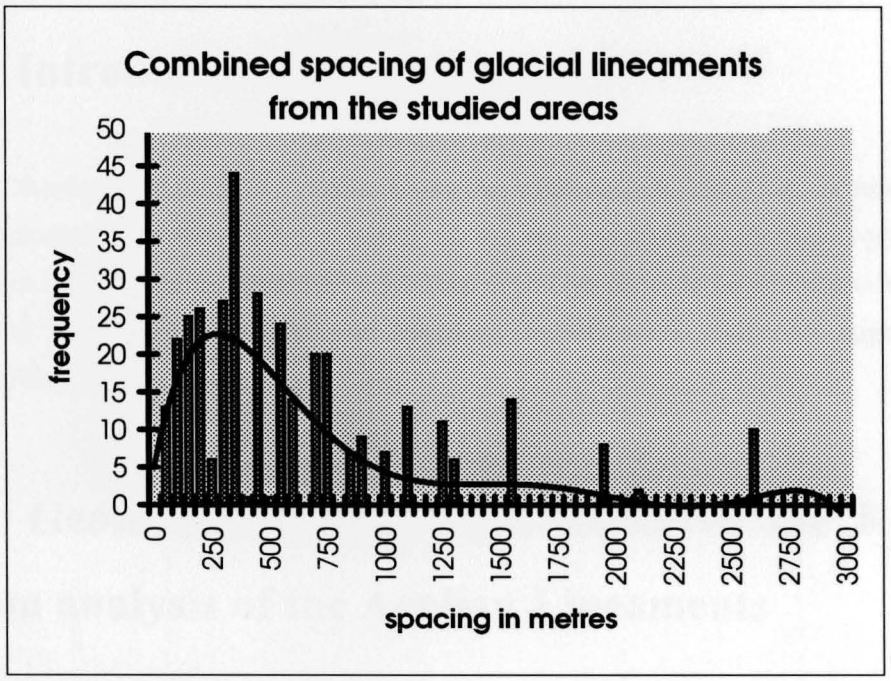

Figure 6.26
Joint spatial frequencies of lineaments in the studied areas
(Solid line is trend line formed by fitting a polynomial curve on the results)

scale images from sub-metre resolution to kilometres could tell a different story about the distribution of glacial lineaments.

Chapter 7

Discussion and Conclusion

7.0 Introduction

This chapter discusses the results from the case studies and gives a summary of the research. The discussion is based on the set hypotheses relating to glacial and aeolian lineaments established in chapter six. The chapter also gives conclusions arrived at from the results and suggests future work that can augment the research.

7.1 Geomorphological Significance of the Results from analysis of the Aeolian Lineaments

The origin and development of linear sand dunes are problematic and while it is beyond the scope of this thesis to answer questions about the origin and development of linear sand dunes, an attempt is here made to explain the significance of dune spatial frequency with respect to the set hypotheses about these landforms.

The establishment of regularity within the dune system in the studied image shows that some systematic process has acted upon the sediments in this area to effect this. The frequency histogram (Figure 6.4) for the lineament spacings from this dune field show the presence of multiple spacings and therefore questions more than one process to have acted in the formation of the linear sand dunes, or that the landscape is the result of a number phases of dune development.

a

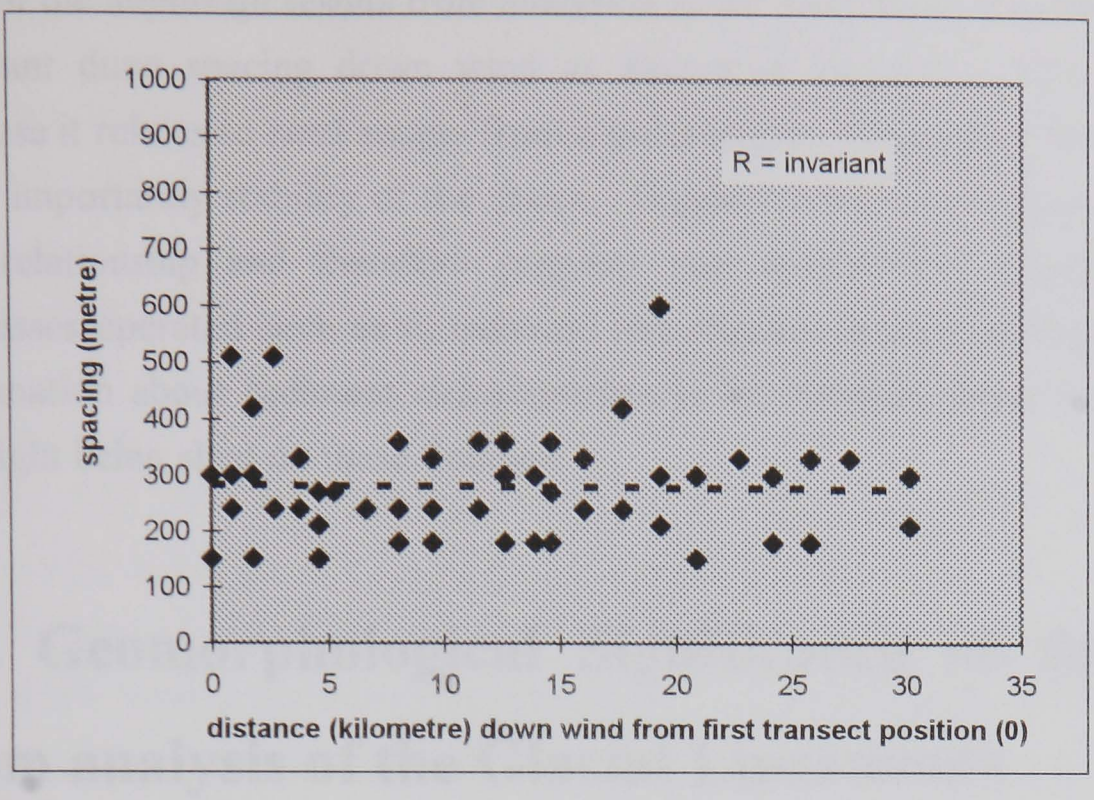

b

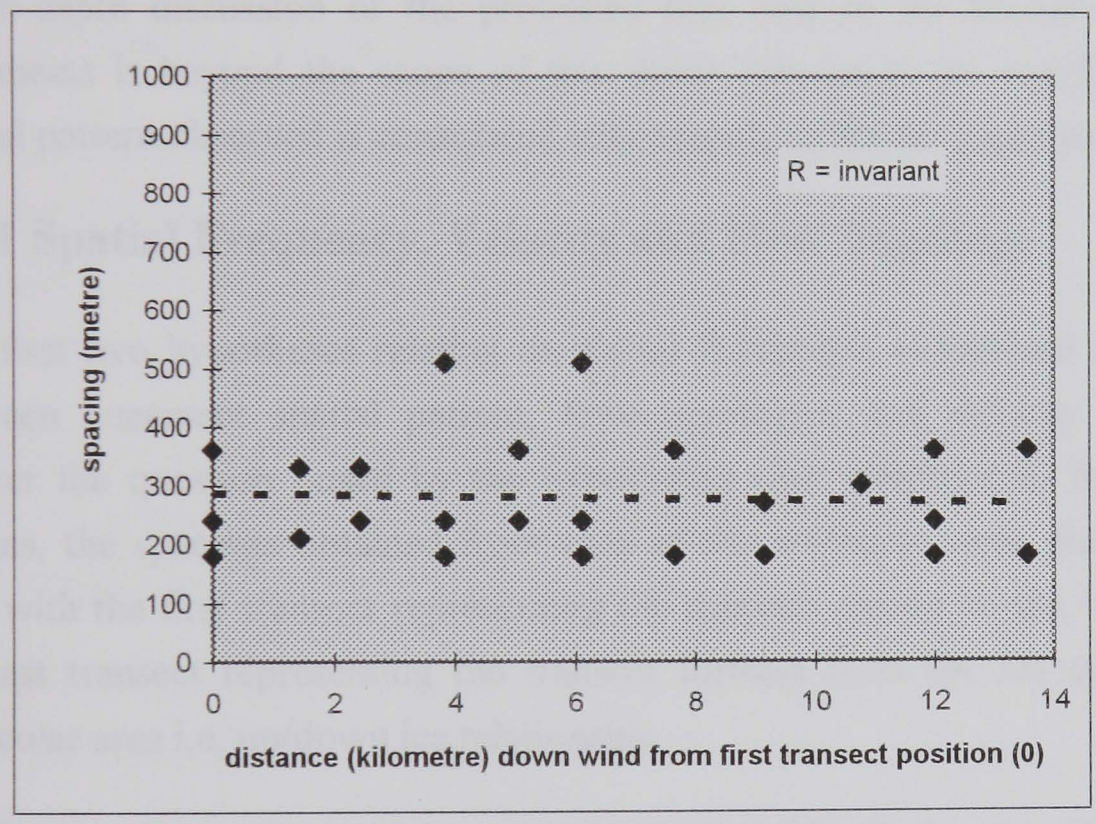

Figure 7.1

Variation of spacing within (a) area A, and (b) Area B, Dunes Image Graph of two areas show stability and no major systematic variation within the areas.

One of the important results from analysing linear sand dunes was the discovery of constant dune spacing down wind as shown in figure 7.1. This is important because it relates to sand supply from a point source, down wind sand sorting and most importantly stability of the dunes. Figure 7.1 however shows invariancy in this relationship and therefore suggests that mechanisms relating to aeolian processes operated such as to maintain this stability in dune spacing. The lack of information about sediment characteristics in the Kalahari Dune Desert prevents any light being shed on these findings.

7.2 Geomorphological Significance of the Result from analysis of the Glacial Lineaments

An in-depth discussion of the processes that lead to the formation of glacial lineaments is beyond the scope of this thesis. However the significance of the spatial pattern observed is considered with respect to the set hypotheses.

7.2 1 Spatial Frequency, Velocity and Flow Topology

The first two hypotheses relating to glacial lineaments considered a relationship between lineament spatial pattern, flow topologies and velocity. In order to answer the question posed by the hypotheses with reference to the case study images, the spacings obtained from each of the transects were plotted for each area with the first transect representing the transect closest to the ice centre and the last transect representing the transect furthest from the ice centre for that particular area i.e. up/down ice relationship.

This form of regression considers all the periodicities from each of the transects and as such whole scale regression might be inappropriate as the different periodicities might behave out of synchrony in the down ice direction. For this reason, each test area was divided into its component periodicities and regression applied accordingly. It must be noted that there is a degree of subjectivity in the grouping of data into its periodic components. The most appropriate method for doing this was to use the peaks from the graph of frequency against spacing (Figures 6.14, 6.17, 6.20, 6.24). Exploration of regression per periodic component for each of the case studies is reported below

1. James Bay Image

Analysis of the James Bay image revealed parallel flow lineaments which were categorised into three classes based on their spacings. These were the 6 to 10 pixel spacings, 13 to 16 pixel spacings and spacings over 19 pixels forming the third classes. When all the spacings for each area were considered together with respect to the position of the transects down ice, a declining trend down ice was observed with regression coefficient of -0.538 and -0.446 for areas A and B respectively (Figure 7.2). When the spacings were isolated into the three classes described above with respect to the position of their transects down ice, a different story was revealed (Figure 7.3). An invariant relationship was observed for the 20 and over pixel spacing for both areas A and B. The same relationship was observed with the 13 to 16 pixels spacing for area A. The 6 to 11 pixels grouping for both areas A and B, and the 13 to 15 pixels group for area B however showed a downward trend (Figure 7.3) with a high regression coefficient of -0.87, 0.756 and -0.535 respectively.

Regression analysis of the different groupings has shown that the spacings for the different groupings behave differently down ice and the conclusion is that some lineament spacings for this image show a highly significant decrease down ice while some are invariant down ice.

The groupings representing downward trends signify decreasing lineament spacing down ice suggesting the possibility of a relationship between ice velocity and morphometry in accordance with hypothesis 1.

This is significant as a relationship has often been sought, the most common of which has been lineament length or elongation factor with velocity. Here we have quantitative proof that a spacing-velocity relationship exists. It is possible that the decrease in spacing (i.e. higher density) with higher velocities reflects greater elongation factors of lineaments and tighter packing, but this requires further analysis.

The lack of regularity, as measured by spectral analysis, in area C is of interest as it suggests that surge conditions produce a different morphometry of bedforms.

a

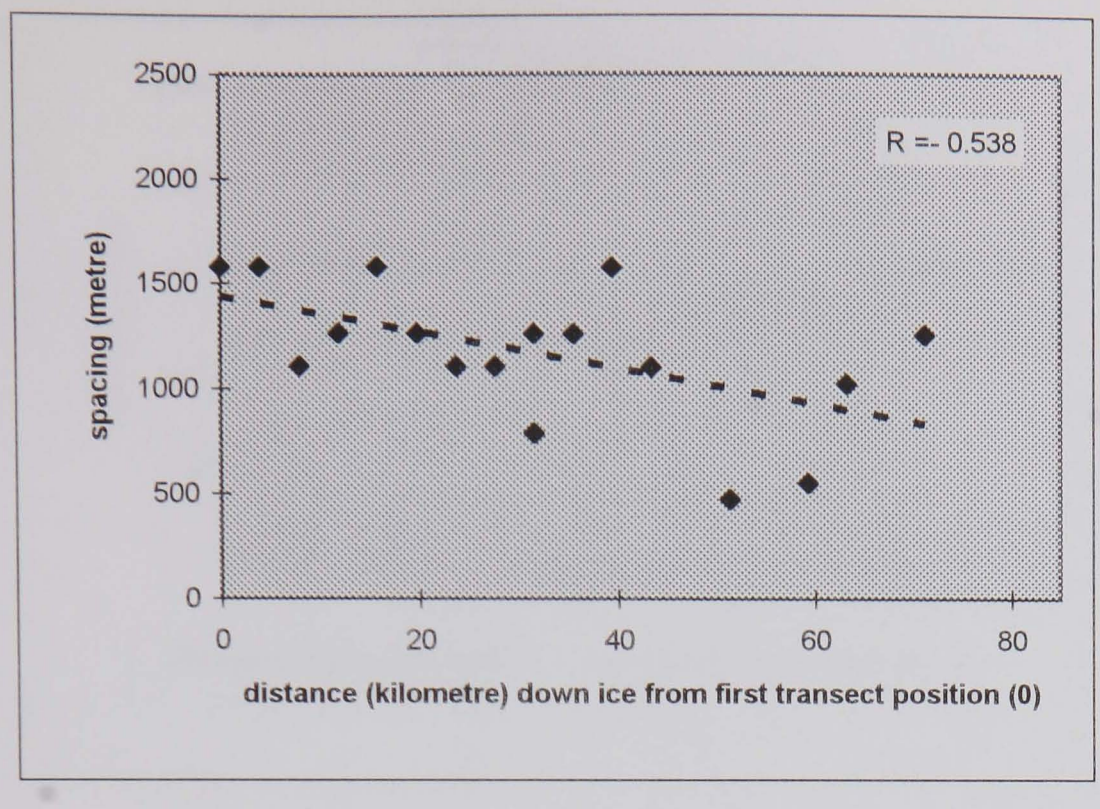

b

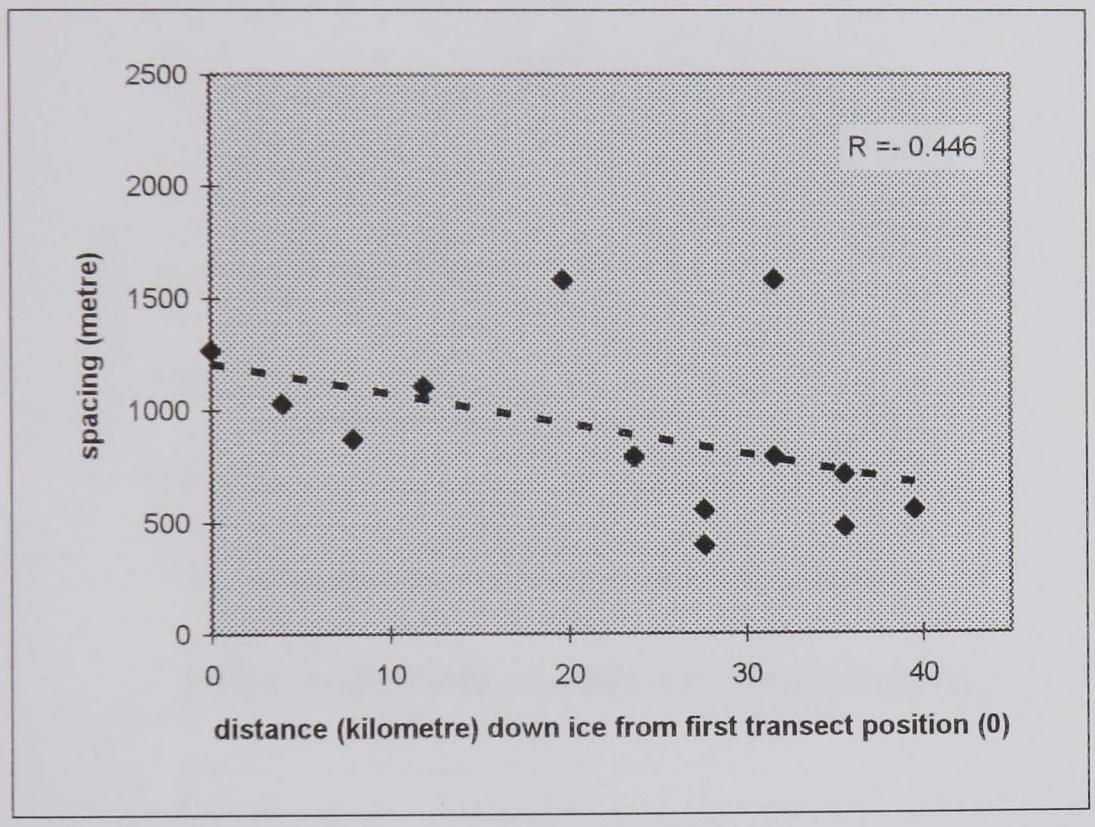

Figure 7.2
Down Ice variation of spacing between transects (a) area A, and (b) Area B, James Bay image. Graph of two areas show a slight downward trend.

A

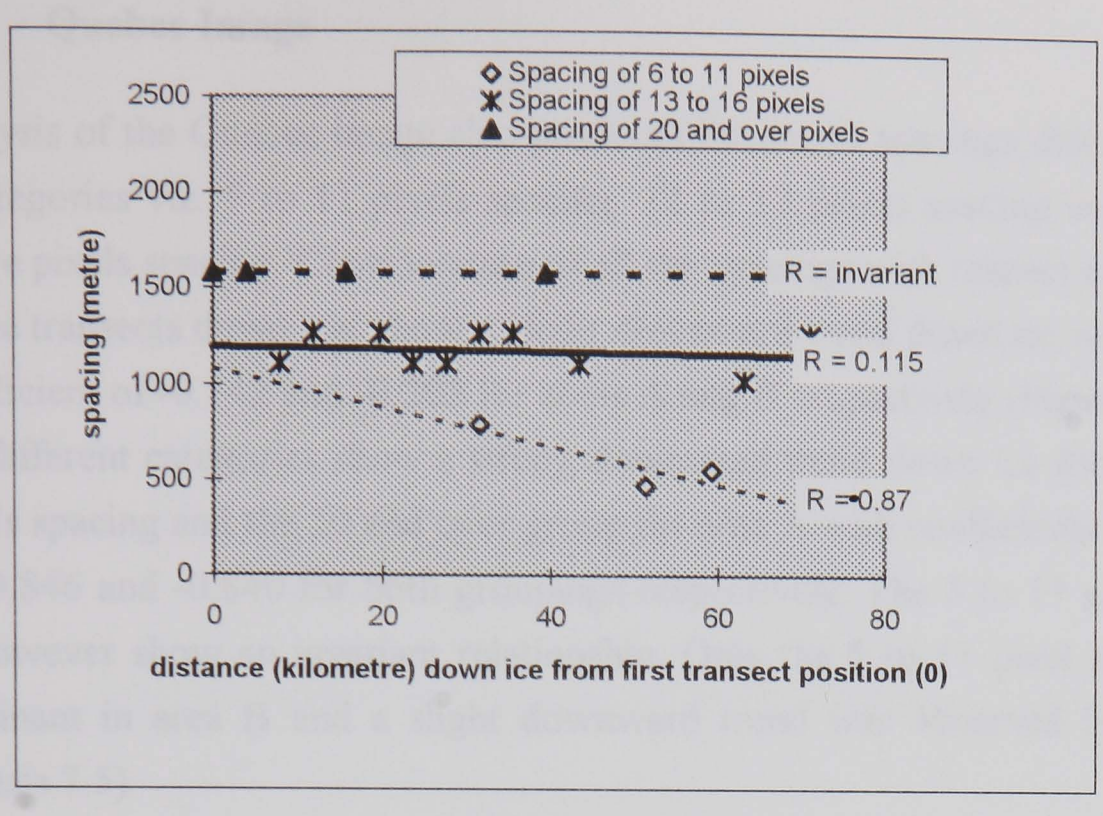

B

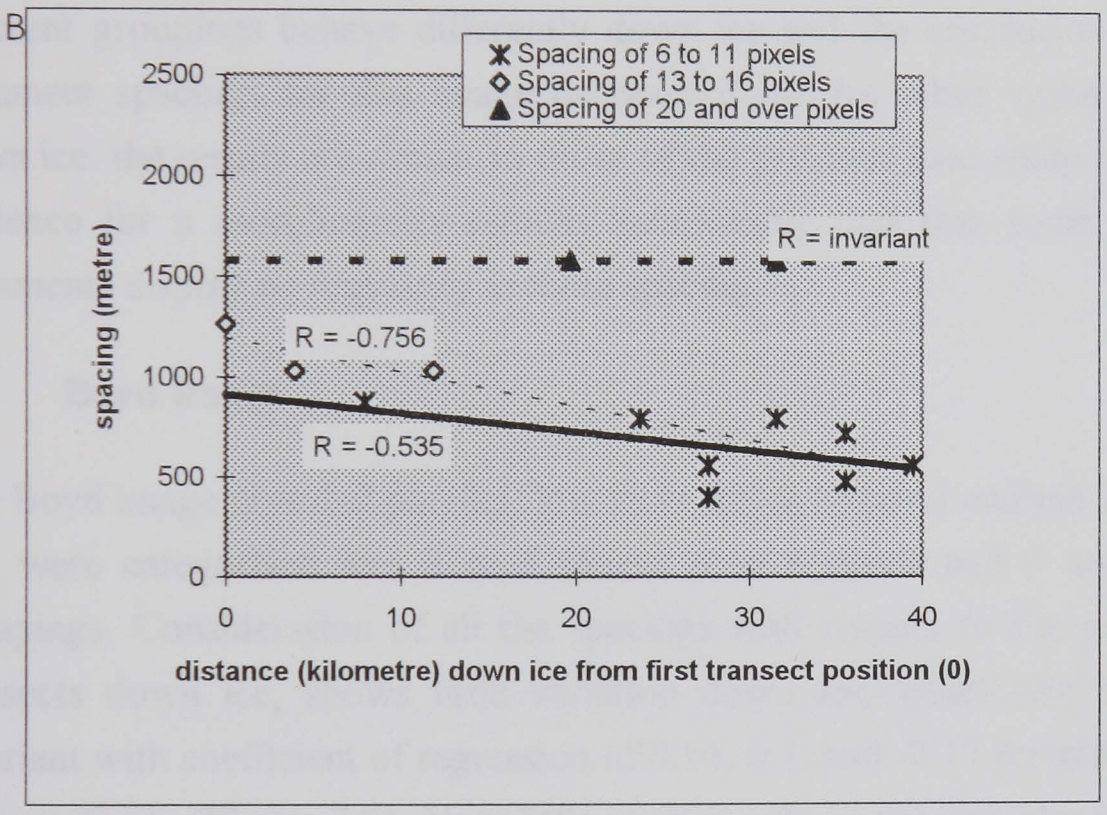

Figure 7.3
Down Ice variation of different set of spacing between transects (a) area A, and (b) Area B, James Bay image. Graph of two areas show a downward trend for spacings of 6 to 11 pixels and those of 13 to 16 pixels.

2. Quebec Image

Analysis of the Quebec image also produces lineament spacings distinguished into 3 categories viz. 5 to 11 pixels spacing, 12 to 17 pixels spacing and the 20 and above pixels spacing. Consideration of all the spacings with respect to the position of the transects down ice, show a slight downward trend down ice with regression coefficient of -0.142 and -0.202 for areas A and B respectively (Figure 7.4). While the different categories show a strong downward trend down ice for the 12 to 17 pixels spacing and the 20 and over group for area A with coefficients of regression of -0.846 and -0.840 for both groupings respectively. The 5 to 11 group for area A however show an invariant relationship. Only the 5 to 11 pixel spacings were dominant in area B and a slight downward trend was observed for this group (Figure 7.5)

Regression analysis of the different groupings has shown that the spacings for the different groupings behave differently down ice and the conclusion is that some lineament spacings for this image decrease down ice while some are invariant down ice. the results are similar to those of the previous case study in that there is evidence for a morphometry-velocity relationship and that some of the mega lineaments display no regularity in these spacing.

3. Boyd Image

The Boyd image revealed parallel flow from which spectral analysis gave spacings that were categorised into 3 to 5 pixels, 6 to 8 pixels and 9 and over pixels groupings. Consideration of all the spacings with respect to the position of the transects down ice, shows little variation down ice, which can be considered invariant with coefficient of regression of 0.14, 0.1, and -0.17 for areas Ai, Aii and B respectively (Figure 7.6). Very little variation down ice was observed when the spacings were separated into the above groupings except for area Aii where lineament spacing representing the 9 and over pixels groups showed a slight upward trend (Figure 7.7). The overall trend for lineaments in this image is therefore one of invariancy down ice suggesting that there is no relationship between inferred velocity and morphometry.

A

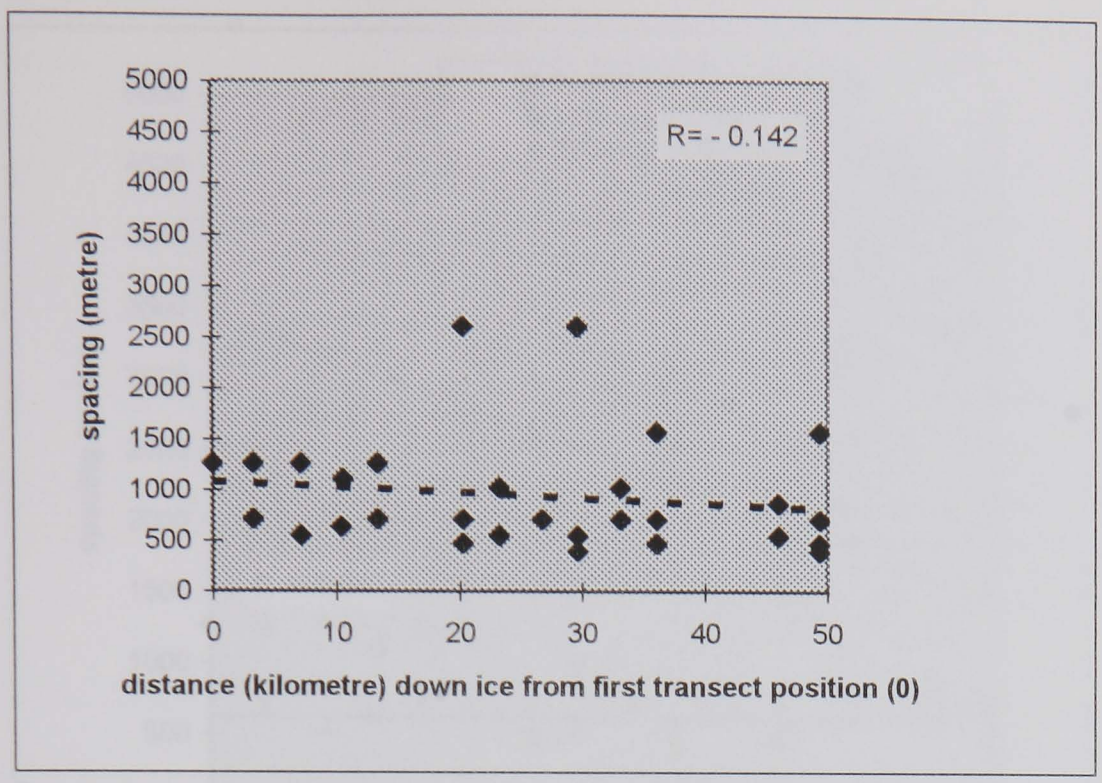

B

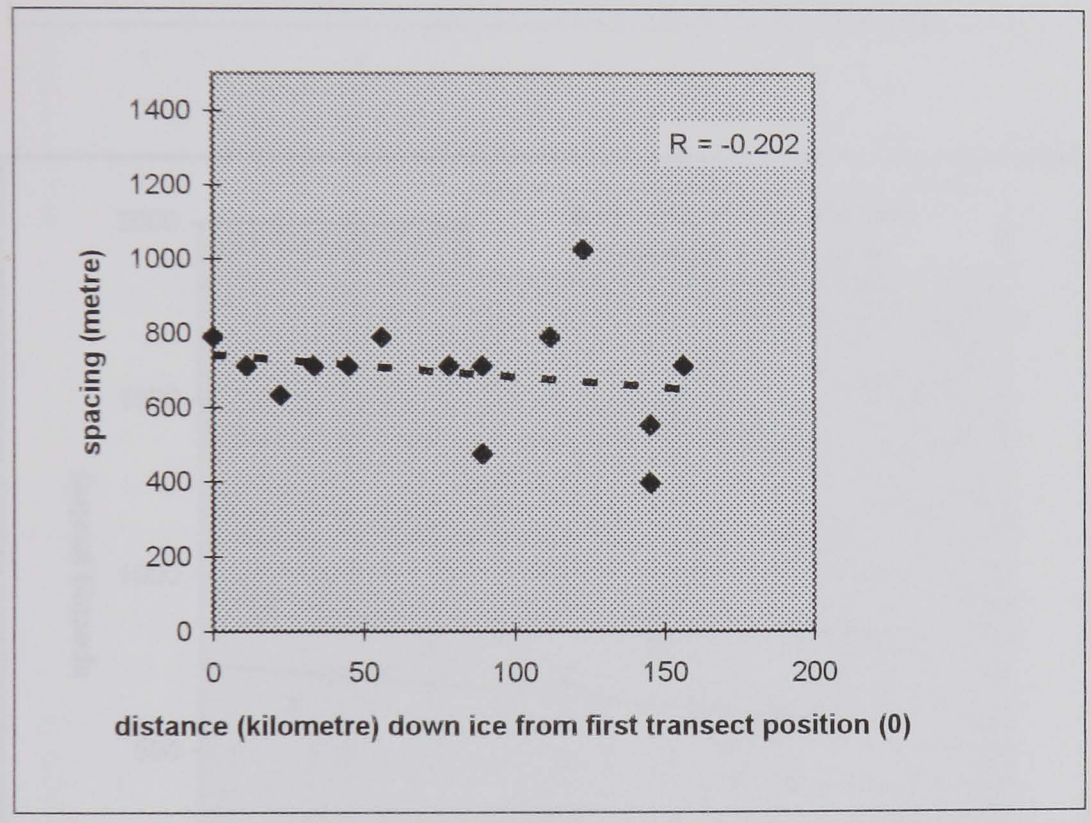

Figure 7.4
Down Ice variation of spacing between transects (a) area A, and (b) Area B, Quebec image. Graph of two areas show a slight downward trend.

A

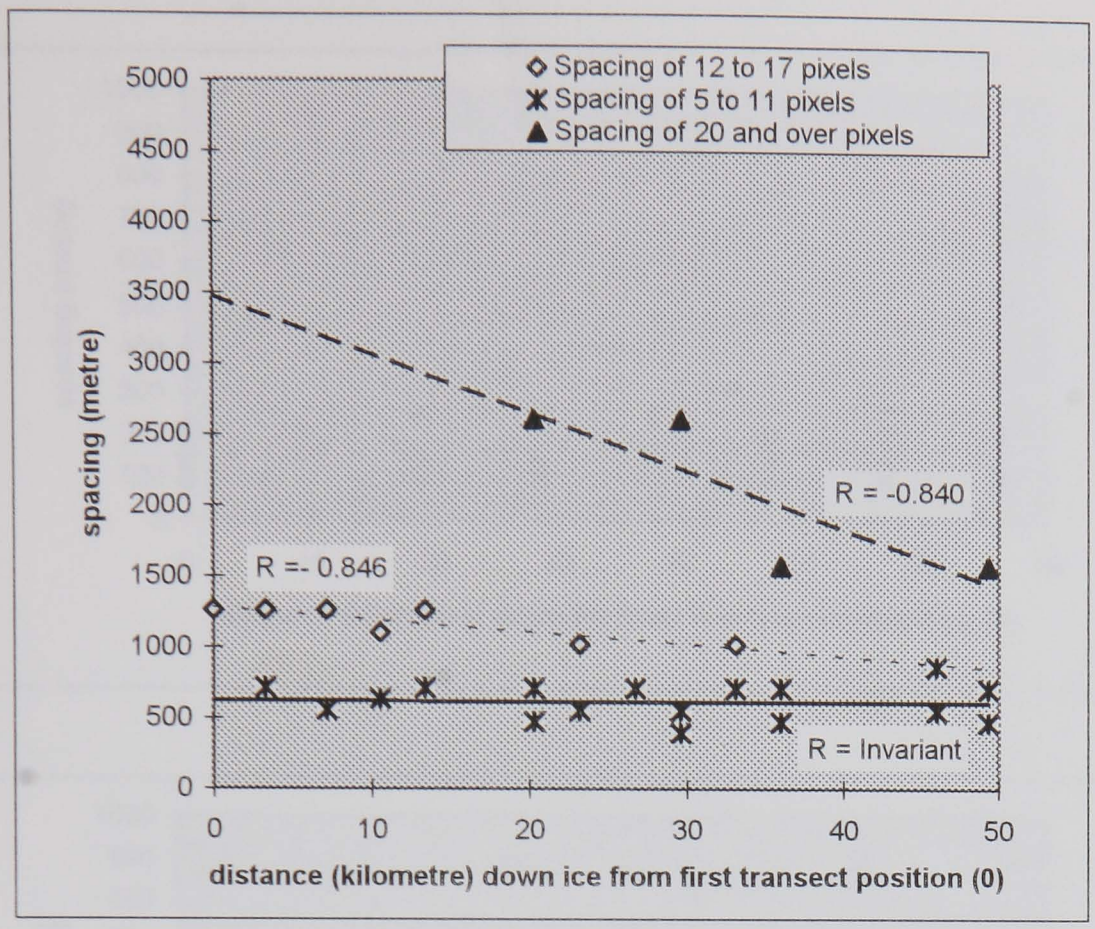

B

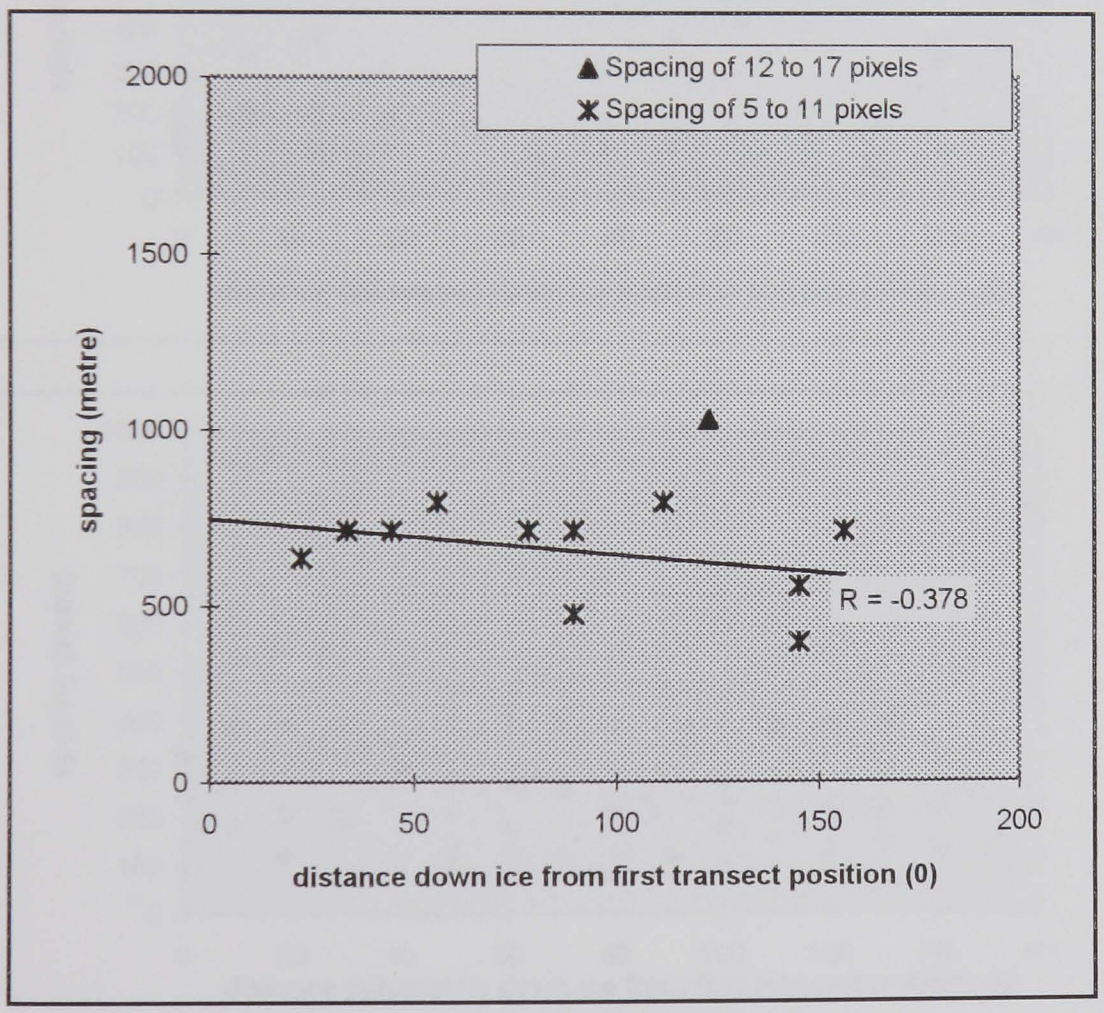

Figure 7.5
Down Ice variation of spacing between transects (a) area A, and (b) Area B, Quebec image. Graph of two areas show a downward trend for spacing of 5 to 11 pixels for both areas A and B and a downward trend for spacings of 12 to 17 pixels for area A

A i

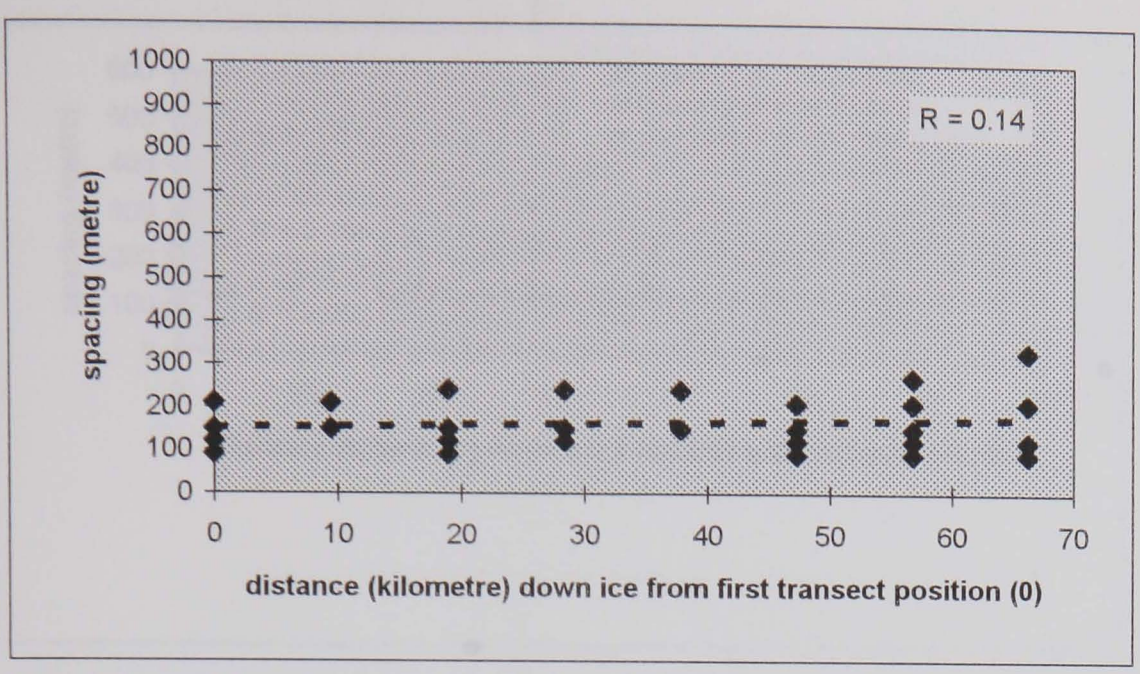

A ii

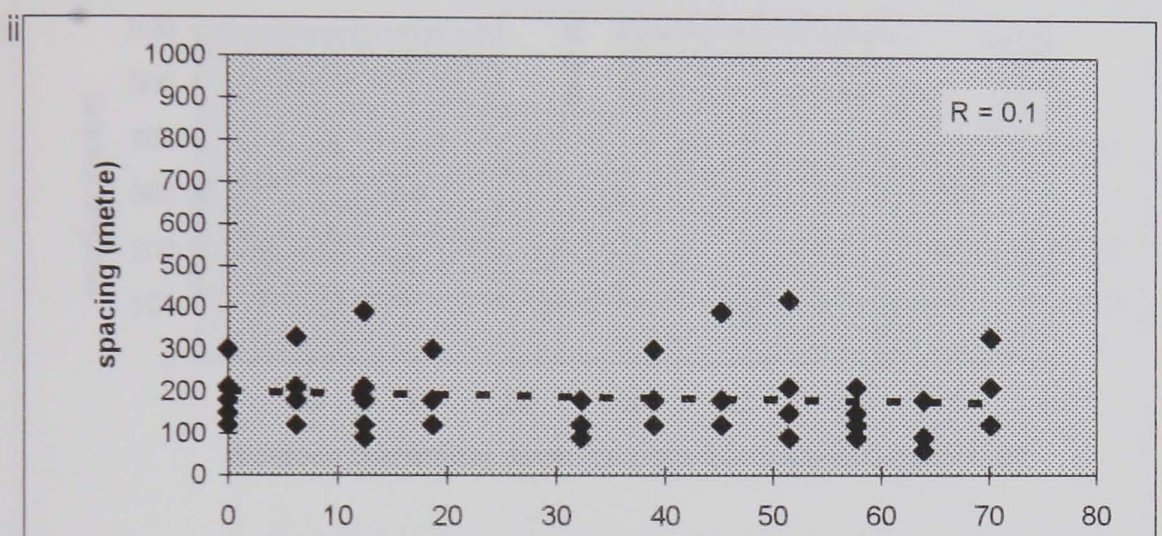

B

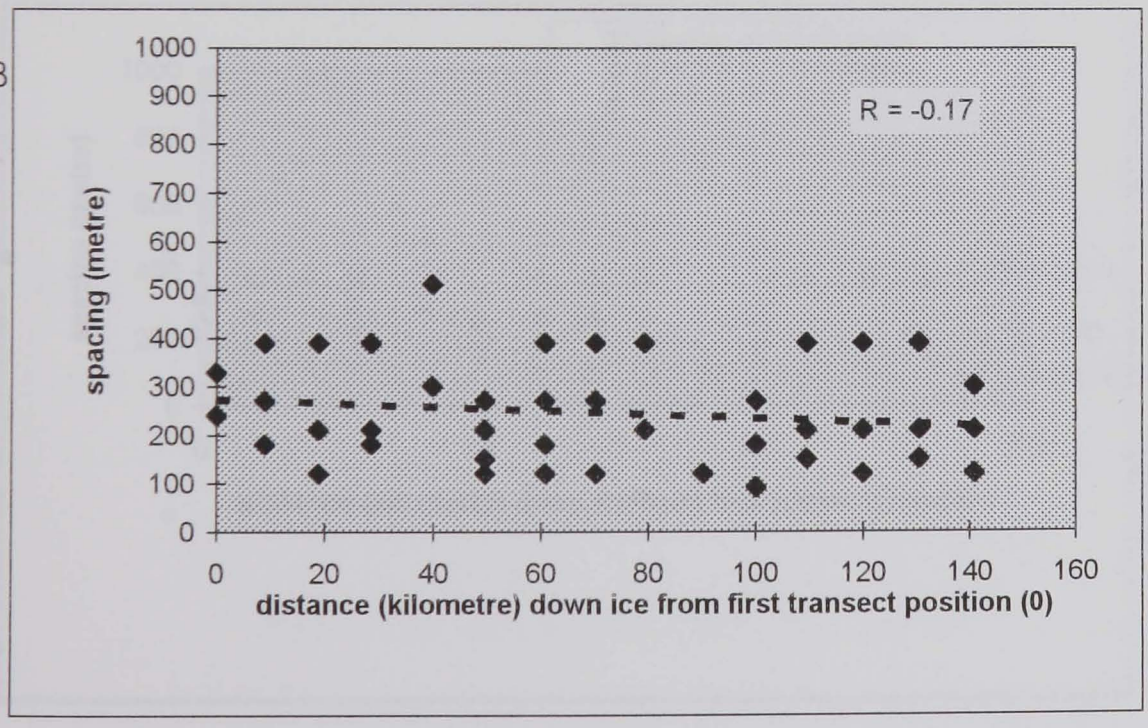

Figure 7.6
Variation of spacing within (a) areas A, and (b) Area B, Boyd image.

A i

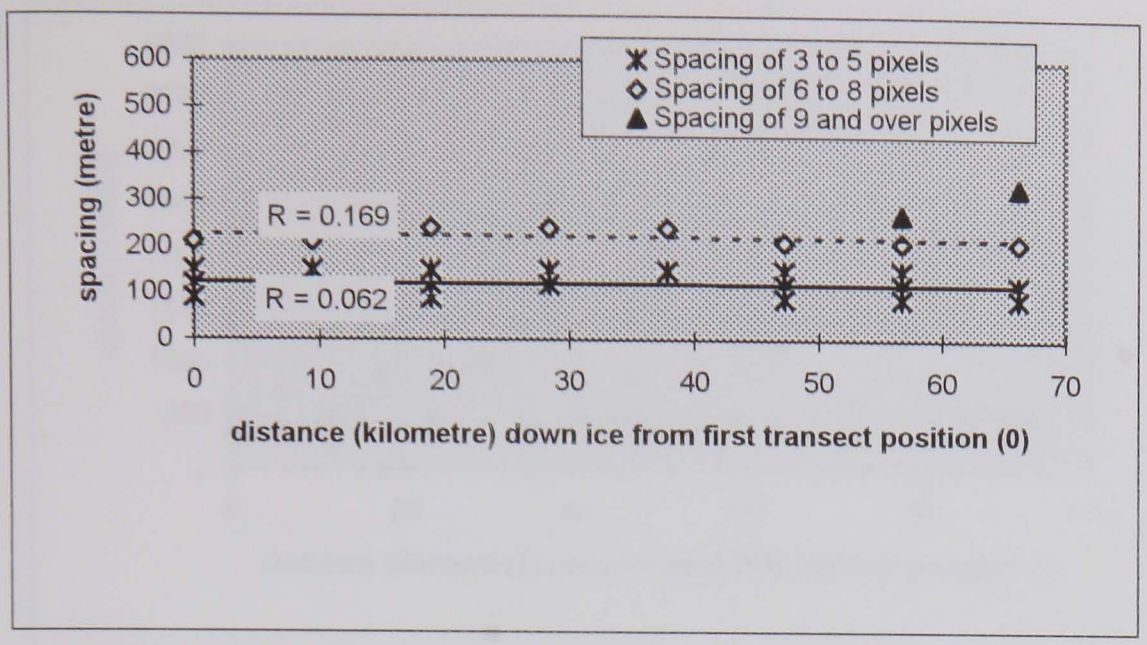

A ii

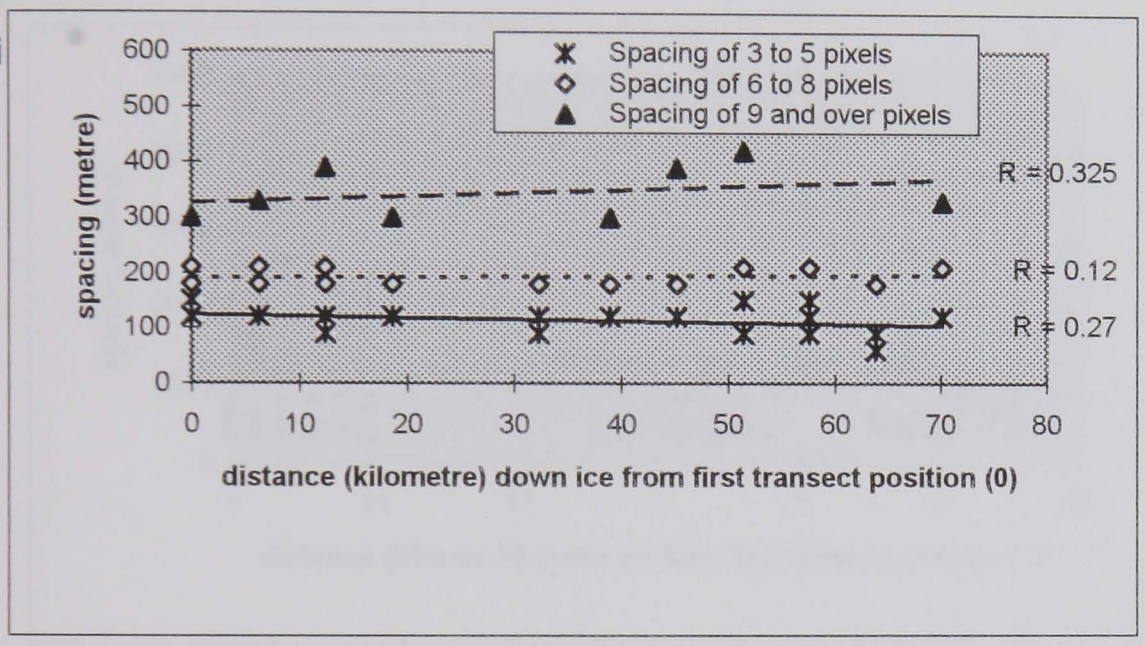

B

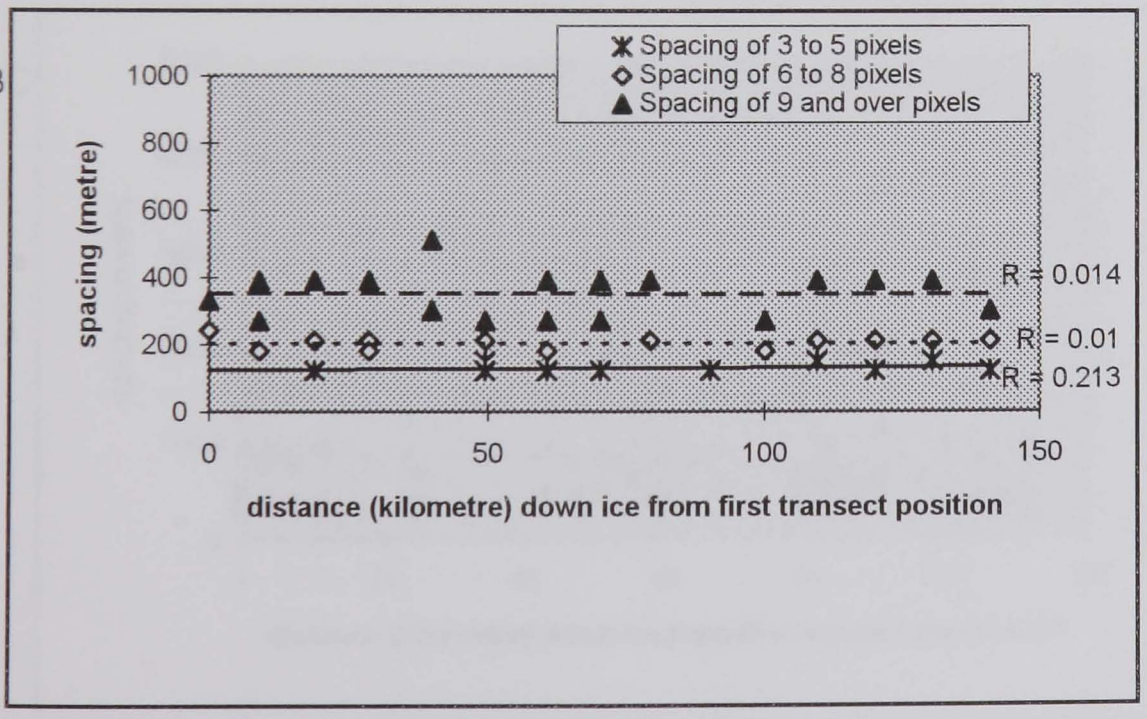

Figure 7.7
Variation of spacing within (a) areas A, and (b) Area B, Boyd image Graph shows no systematic change in spacing down ice

A

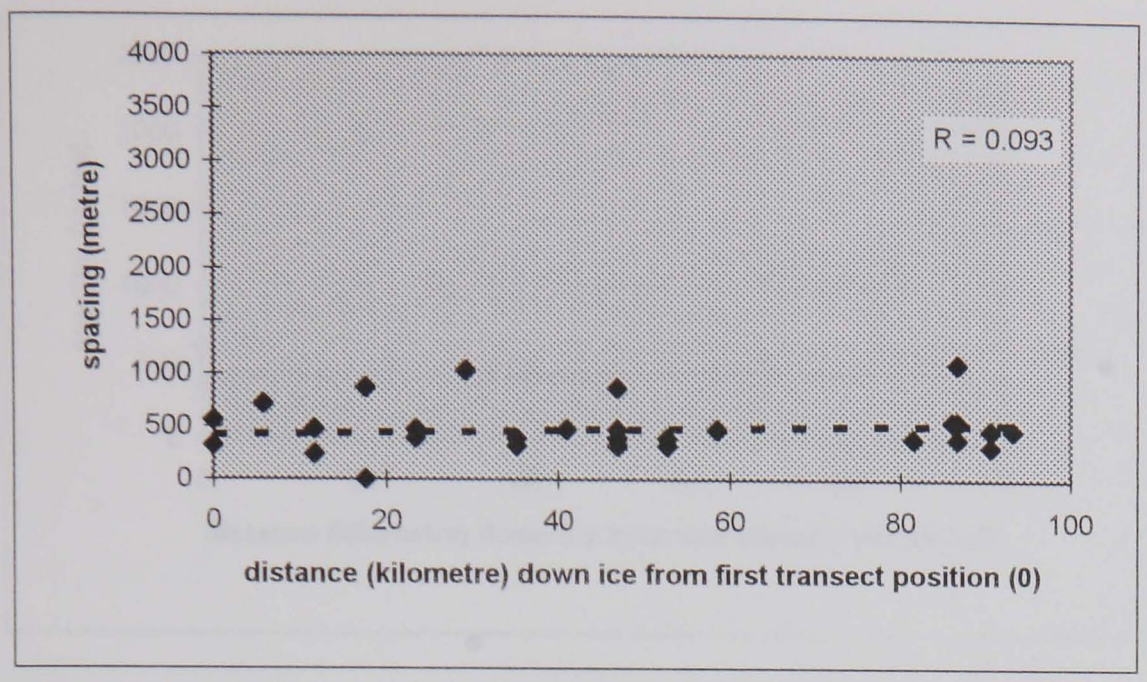

B

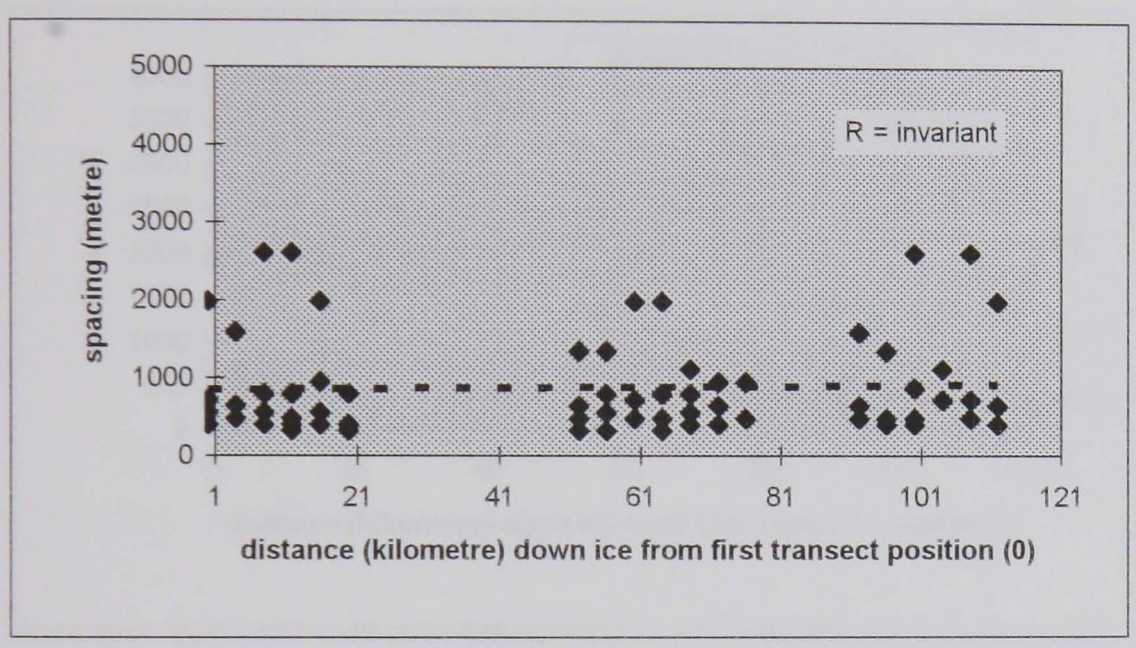

C

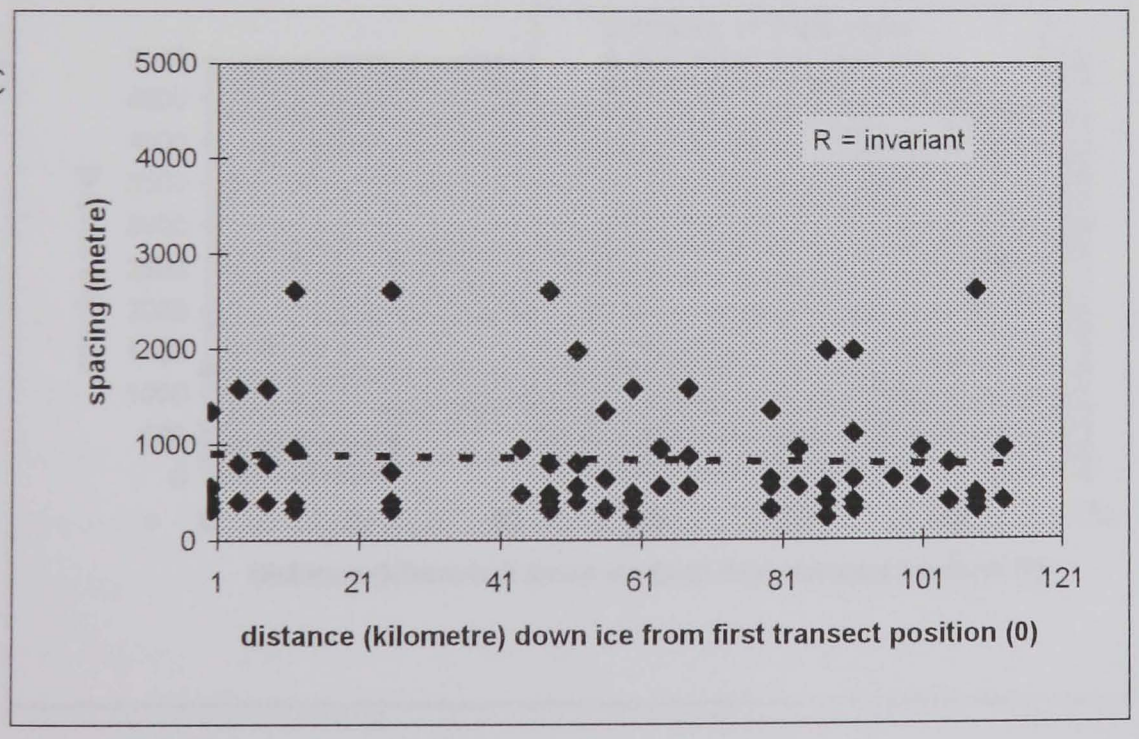

Figure 7.8
Variation of spacing within (a) areas A, (b) Area B, and (c) Area C, Eskimo Point image.

A

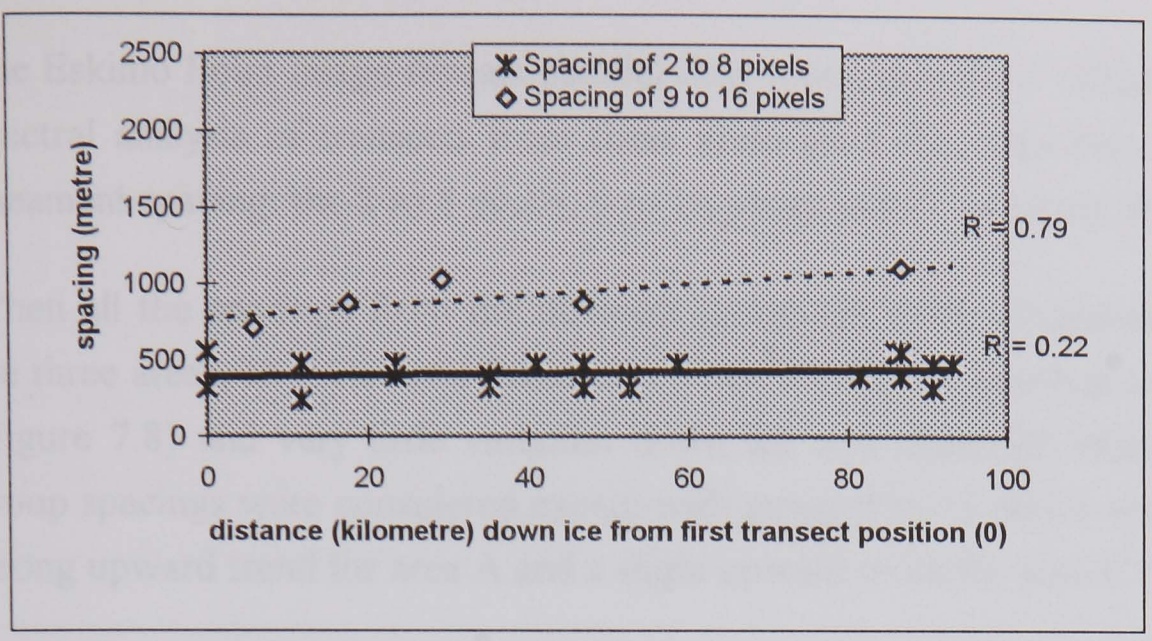

B

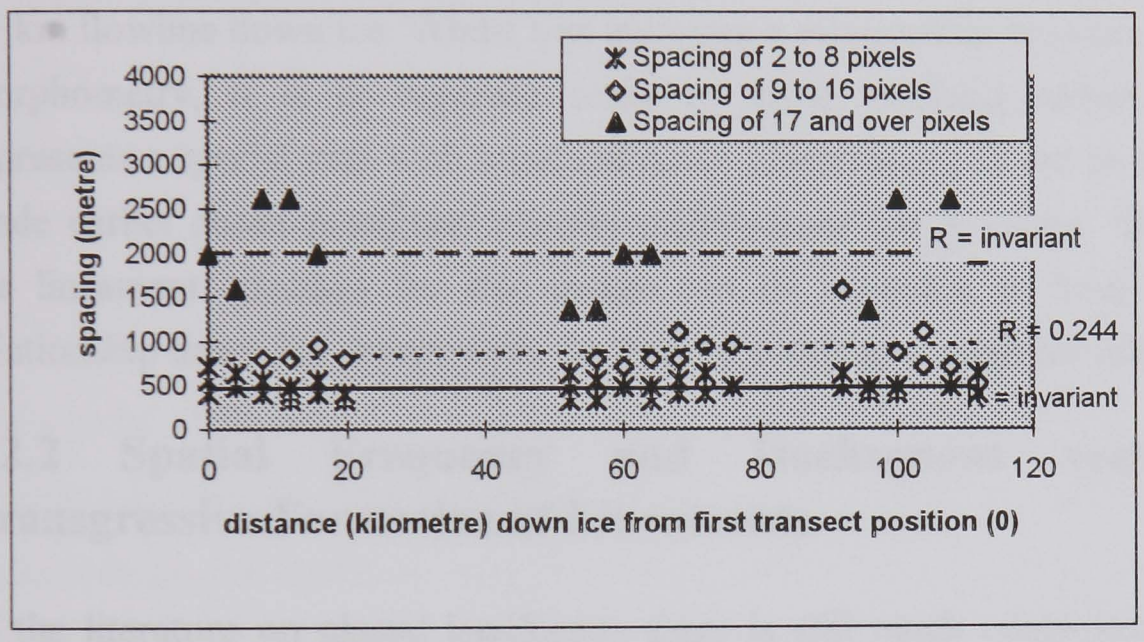

C

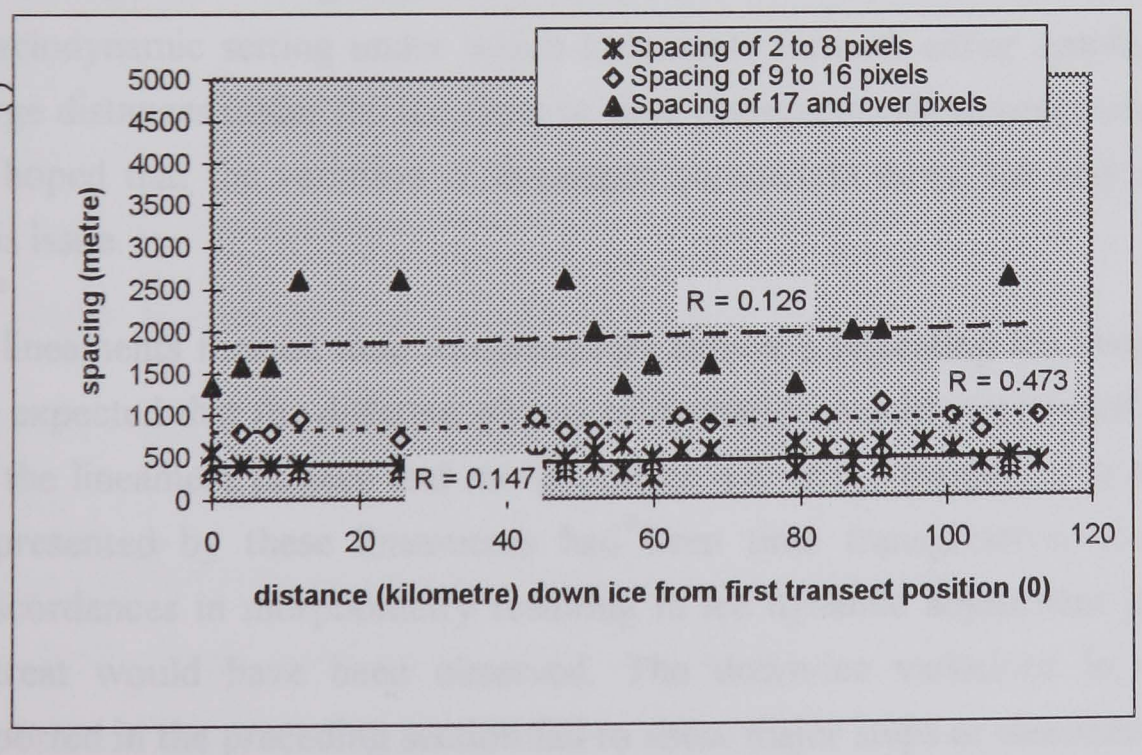

Figure 7.9
Variation of spacing within (a) areas A, (b) Area B, and (c) Area C, Eskimo Point image.

4. Eskimo Point Image

The Eskimo Point image reveals parallel flow topologies for 3 different areas and spectral analysis of transects from these areas gave the following categories of lineament spacing: the 2 to 8 pixels, 9 to 16 pixels and 17 and over pixels spacing.

When all the spacings from the different groupings were considered for each of the three areas, an invariant relationship down ice for the spacings were observed (Figure 7.8) and very little variation down ice was observed when each of the group spacings were considered except with group 9 to 16 pixels which showed a strong upward trend for area A and a slight upward trend for area C (Figures 7.9).

This is interesting as it shows an increase in spacing from 650m to 1100m over an 85 km flowline down ice. Whilst this indicates a relationship between velocity and morphometry, it is in opposite sense to those outlined earlier. Either this represents a special case with some unknown complicating factor or the inferences made earlier about presumed velocity distributions are incorrect. On the whole, the lineament spacings for this image can be regarded to have an invariant relationship down ice except with for 9 to 16 pixels groupings for area A and C.

7.2.2 Spatial Frequency and Isochronous versus Time Transgressive Formation of Lineaments.

In the literature on glacial landforms, there is still much controversy about the glaciodynamic setting under which lineaments formed: either synchronously over large distances under the ice sheet or time transgressively during margin retreat. It is hoped that the variation of lineament parameters down ice may shed light on this issue.

If lineaments formed time trangressively behind a retreating ice margin, it should be expected that the different phases of formation would yield major discordances in the lineament pattern and morphometry. i.e. If the formation of the landforms represented by these lineaments had been time transgressive, then significant discordances in morphometry resulting in ice dynamic adjustment during margin retreat would have been observed. The down-ice variations in morphometry reported in the preceding section fail to show major steps or discordances.

It is usual in ice sheet reconstruction to simply assume isochronous and time transgressive formation. A technique for establishing which case is true is demonstrated here.

7.2.3 Spatial Frequency and Scale Continuity

In attempting to explain the processes that generated lineaments, some authors have argued the case of multiple processes responsible for the formation of the different scaled glacial features that are thought to exist. If this multi process and multi-spatial frequency notion is to be considered then one would expect the joint frequency distribution of the spacing of lineaments for the entire study area to have a multi-modal distribution showing different spatial frequencies. This however was not the case as the results expressed in figure 6.22 show instead a concentration of spatial frequencies in the range 150 to 2600 metres as a Chi square distribution with a mode of 350 metres.

In spite of an estimated sample size of 12000 lineaments, there is no evidence for a multimodal distribution in the sample range of 60-3000 metres. There is no evidence for abrupt steps in the distribution whose presence might indicate scale limitations to the operation of a process. It is therefore concluded that for glacial lineaments from drumlins through to mega-lineaments, there is a scale continuum which implies that a single process is responsible for their formation, i.e. that the same mechanism, but with a different boundary parameters e.g. sediment rheology, is responsible for the formation of drumlins, megaflutes, mega-drumlins and mega lineaments.

The distribution is positively skewed which shows that whilst there is a favoured spatial frequency of 350 metres, that a high number of much larger forms in the range of 750-2600 metres spacing also occur. Proposed theories for lineament generation must therefore be capable of producing forms across the scale range and with a single mechanism. This is important as the results therefore favour the deformational theories of lineament generation against the subglacial melt-water school of thought which invokes different scale dependent processes.

7.3 Summary of the Thesis

The objective of this research was to develop a method of quantifying the parameter of spacing/density of parallel lineaments on images and to apply this method in geomorphometrical analysis of glacial and aeolian landforms represented as lineaments on images.

In order to have a full understanding of the term lineament, chapter two was devoted to explaining the term, their parameters and the reasons for wanting to study them.

As the source of data for analysis in this research was remotely sensed images, the factors that affect lineament expression on these images were discussed in chapter three.

Chapter four explained the method of spectral analysis used for analysing the spacings between parallel lineaments on satellite images. Spectral analysis was used on radiometric transects taken across lineament fields. This was done with a FORTRAN 77 programme written and some adopted from NAG libraries.

Having established a method of analysing spacings between lineaments, it was necessary to test the validity and sensitivity of the method and this was done in chapter five where sensitivity of the method to different image processing routines and the different spectral bands for Landsat MSS and TM images were tested. The chapter also tested for the effect of transect misalignment off perpendicularity and the result of spectral analysis was compared to manual measurement and digitisation techniques of measuring spacing between lineaments.

The established method of analysing the spacing between lineaments was used in chapter six to quantify glacial lineaments from images of Canada and aeolian lineaments from the Kalahari desert, and also to seek the geomorphological significance from the results. The conclusion of the research was discussed in chapter seven.

7.4 Conclusion

This section outlines the conclusions arrived at from this research. As this research was to develop a methodology for analysing parallel lineaments and then to apply this method to analysing some of the lineaments, the conclusion will be separated into a methodological conclusion and an application conclusion.

7.4.1 Methodological conclusion

A method of quantifying the spacing of parallel lineaments on remotely sensed images has been developed based on spectral analysis. As mentioned earlier, the two main sources of inaccuracies are likely to arise from the non-detection of sub-pixel lineaments and errors resulting from transect misalignment to the perpendicular. The subpixel problem and the nyquist frequency limit the scale to which interpretation can be made from the results. On the other hand, transect misalignment was demonstrated to have limited effect on the results.

The following methodological conclusion can therefore be drawn:

1. The presence of any regularity in a radiometric transect representing lineaments could be detected and isolated by spectral analysis provided that the lineament spacings are not smaller than the Nyquist wavelength (minimum wavelength = twice spatial resolution of the image).

2. The result of spectral analysis of multispectral images is independent of the band used. Therefore which ever band is most convenient can be used.

3. Image processing experiments reveal that there is no benefit in using processed over raw data values for spectral analysis.

4. The result of spectral analysis is affected when the transect is off perpendicular by at least 10 degrees. This means that transect alignment by eye is perfectly adequate.

5. There is a slight difference in spacing obtained from spectral analysis and those obtained by digitisation for the same image.
6. Besides isolating the spacing between lineaments, spectral analysis can also be used for frequency domain filtering and characterising terrain type.

7.4.2 Application Conclusion

A. AEOLIAN APPLICATION

From the case study with aeolian sand dunes from the Kalahari Dune Desert, it can be concluded that :

1. Spectral analysis of radiometric transects from remotely sensed imagery can be used to characterise an aspect(spacing) of sand dune morphometry.

2. There is no significant trend in spacing up or downwind, and the spacing remains similar even for dunes of different widths in this study area indicating equilibrium in spacing irrespective of dune width or position in the overall dune field.

3. The summary statistics for the study area are:

Table 7.1 Summary statistics of aeolian study area.

Mean spacing	Min. spacing	Max. spacing	standard error
261 metres	150 metres	600 metres	0.260

Table 7.2 Results of analysis of the linear sand dunes by other workers

Statistics	Thomas (1986)	Lancaster (1988)	Fowajuh (1995)
Mean	270m		261m
Minimum	20m	200m	150m
Maximum	590m	450m	600m
Standard Deviation	0.104		
Standard Error			0.260

B. GLACIAL APPLICATION

The following conclusion can be drawn from the morphometrical analysis of approximately 12, 000 glacial lineaments:

1. It is possible to make quantitative measurement of the spacing between parallel glacial landforms that appear as lineaments on satellite images using spectral analysis.

2. A significant relationship has been discovered between lineament morphometry and inferred ice velocity. Closer spacing (higher density) seems to correspond with higher ice velocities. This requires further investigation, with a view to using the inverse solution which enables information about former ice dynamics to be inferred from lineament pattern.

3. The measured morphometry of lineaments down ice is systematic i.e. invariant, or linear up/down ice. The lack of significant discordances in the in the down ice direction shows that the lineaments must have been formed in an Isochronous manner. It therefore proves that these landforms are not restricted to formation in a marginal position as is commonly thought. It is argued that spectral analysis can be used to determine the synchroneity of formation of lineaments, which is crucial in ice sheet reconstructions (Clark, 1994; Kleman and Borgström in press).

4. The joint distribution of spatial frequency for all the case studies shows a Chi square distribution with a concentration of power (spatial frequency of lineaments) at a particular range of frequencies (150 to 750 metres). This is in contrast to the multimodal distribution hypothesised by Clark (1993) and therefore proves that the distribution of these landforms is scale continuous. This implies that a single mechanism of formation produced all lineaments in the scale range that can be observed on satellite images.

5. Spectral analysis of spatial frequency has been used to characterise and thus demarcate different ice flow sets. There seems to be a difference in morphometry between lineaments formed under steady state and surging conditions.

6. The joint summary statistics for the study areas are:

Table 7.3 Summary statistics of glacial study area.

Mean spacing	Min. spacing	Max. spacing	standard error
652.6 metres	**60 metres**	**2607 metres**	**29.36**

7.5 Further Research

The following new lines of research can be pursued from the result of this research:

1. Time and data constraints have restricted the application of this method to the case studies of chapter 6. It would be highly desirable to extend this analysis to much wider areas, so that down-ice measurements could be made over many hundreds of kilometres which would help in drawing more certain conclusions. In the case of glacial lineaments, an ice sheet wide synthesis of spatial frequency would be desirable, and for linear dunes, the whole dune field rather than just a single Landsat image. Hypothesis 2 for example remained unanswered due to a lack of data and time available.

2. To aid the morphometry work, it is also necessary to collect information at a smaller scale than that available from satellite imagery. This may need to be achieved by manual interpretation and digitising and the analysis approach utilised in Clark and Wilson (1994). Such research is already underway.

3. Other morphometric parameters, in the case of glacial lineaments their length is of critical importance, probably more so than the spatial frequency dealt with here. The results from this thesis could be usefully compared with length data from the same areas, but there is a problem in that this will need to be achieved by manual interpretation. Current automatic lineament detection algorithm are not advanced enough for this type of feature. Using the morphometry established from this analysis, they should be input into a GIS where they can be correlated with other parameters. For the case of glacial lineaments, there is a need to understand how these spatial frequencies relate to sediment rheology and thickness, ice centres, and topography. While for aeolian lineaments there is a need to understand how these frequencies relate to the different wind regimes, grain size distributions, nature of the underlying substrate and vegetation cover and growth characteristics.

4. There is a need to carry out 2-D spectral analysis on orthogonal transects and fourier analysis on the image. In the former case, this will not only be able to detect all possible scales of pattern which might be present in the transect but it is also sensitive to directional components. 2-D Fourier analysis on the image may be useful in texture analysis for detecting drift cover.

5. Using the spatial frequency obtained from spectral analysis and other parameters about these lineaments, it would be useful to develop a model for aeolian and glacial morphometry in order to understand their behaviour and also to compare it with other areas.

Bibliography

Alden, W. C., 1905, The Drumlins of South-Eastern Wisconsin, *U. S Geological Survey Bulletin,* 273, p9-46.

Alden, W. C., 1911, Radiation of Glacial Flow as a Factor in Drumlin Formation, *Geological Society 0f America Bulletin,* 22, p733-744.

Alden, W. C., 1918, The Quaternary Geology of S. E. Wisconsin, *U. S. Geological Survey Professional Paper 106.*

Anderson, R. Y. and Koopman, L. H., 1963, Harmonic Analysis of varve Time Series, *Journal of Geophysical Research,* 68, p877-893.

Andre, M., 1991, *An Introduction to Image Processing*, London: Chapman and Hill, p281-305.

Balek, J. and Andel, J., 1971, Analysis of Periodicity in Hydrology Sequences, *Journal of Hydrology*, 14, p66-82.

Bauer, A., Fontanel, A., and Grau, G., 1967, The Application of Optical Filtering in Coherent Light to the Study of Aerial Photographs of Greenland Glaciers, *Journal of Glaciology,* 6, p781-793.

Berger, Z., 1982, The use of Landsat data for detection of Buried and Obscured Geologic Structures in the East Texas Basin, U. S. A: *Procceeding of the International Symposium on Remote Sensing of the Environment, Second Thematic Conference , Remote Sensing for Exoloration Geology, Fort Worth, Texas* p579-589Geology,Cora.

Blackman, R. B. and Tukey, J. W, 1959, *The Measurement of Power Spectra, from the Point of View of Communications Engineering*, Dover, New York.

Blom, R. G., 1988, Effects of Variation in Look Angle and Wavelenth in Radar Images of Volcanic and Aeolian Terrains, or Now you see it, now you don't, *International Journal of Remote Sensing,* 9, p945-965.

Blom, R. G., and Daily, M., 1982, Radar Image Processing for Rock-type Discrimination, *IEEE Transactions on Geoscience Electronics*, GE-20, p343-351.

Bloomfield, P., 1976, *Fourier Analysis of Time Series: An Introduction*, Wiley, New York.

Borengasser, M. X., and Taranik, J. V., 1988, Structural Geology and Regional Tectonics of the Mineral County Area, Nevada, using Shuttle Imaging Radar-B and Digital Aeromagnetic Data, *International Journal of Remote Sensing*, 9, p967-980.

Boulton, G. S., 1982, Subglacial Processes and the Development of Glacial Bedforms, In: R. Davidson-Arnott; W. Nickling, and B. D. Fahey (eds.), *Research in Glacial, Glacio-Fluvial and Glaciolacustrine Systems, Geo Books, Norwich*, p1-31.

Boulton, G. S., 1987, A Theory of Drumlin Formation by Subglacial Sediment Deformation, In: J. Menzies, and J. Rose (eds.), *Drumlin Symposium*, A. A. Balkema, Rotterdam, p25-80.

Boulton, G. S., and Clark, C. D., 1990a, A highly Mobile Laurentide Ice Sheet Revealed by Satellite Images of Glacial Lineations, *Nature,* 346, p813-817.

Boulton, G. S., and Clark, C. D., 1990b, The Laurentide Ice Sheet Through the last Glacial Cycle: Drift Lineations as a key to Dynamic Behaviour of Former Ice Sheets. *Trans. R. Soc. Edinburgh, Earth Science.,* 81, p327-347

Breed, C. S. and Grow, T., 1979, Morphology and Distribution of Dunes in Sand Seas Observed by Remote Sensing, In: E. D., Mckee (ed.), *A Study of Global Sand Seas. U.S. Geological Survey Professional Paper*, 1052, p253-302.

Buckley, R. C., 1981, Parallel Dunefield Ecosystems: Southern Kalahari and Central Australia, *Journal of of Arid Environment*, 4, p287-298.

Carson, J. E., 1963, Analysis of Air and Soil Temperature by Fourier Techniques, *Journal of Geophysical Research*, 68, p2217-2232.

Charlesworth, J. K., 1939, Some Observations on the Glaciation of North-East Ireland, *Proceedings of the Royal Irish Academy*, 45, p255-295.

Charlesworth, J. k., 1957, *The Quaternary Era. Ont.,* Edward Arnold, London, 2 Volumes.

Chatfield, C., 1984, *The Analysis of Time Series: An Introduction*, 3rd edition, Chapman and Hall, London.

Chatfield, C. and Pepper, M. P. G., 1971, Time-series Analysis an Example from Geophysical Data, *Applied Statistics*, 20, p217-238.

Chorley, R. J., 1959, The shape drumlins, *Journal of Glaciology*, 3, p339-344.

Clark, C. D., 1990, Remote Sensing Scales Related to the Frequency of Natural Variation; an Example from Paleo-Iceflow in Canada, *IEE Transactions of Geoscience and Remote Sensing* , 28, p503-508.

Clark, C.D., 1993, Mega-scale glacial lineations and cross-cutting ice flowlandforms, *Earth Surface Processes and Landforms*, 18, p1-29.

Clark, C. D., 1994, Large-scale Ice-moulding: A Discussion of Genesis and Glaciological Significance, *Sedimentary Geology*, 91, p253-268.

Clark, C. D., and Wilson, C., 1994, Spatial Analysis of Lineaments, *Computers and Geosciences,* 20, p1237-1258.

Clark, C. D. and Fowajuh, C. G., 1993, Remote Sensing as a Quantitative Tool for Examining Glacially streamlined Bedforms, *Proceedings of the third International Geomorphology Conference held in McMaster University,* Canada, 23-28th August, 1993, p122.

Clark, M.M., 1971, Comparism of SLAR Images and Small-Scale Low Sun Aerial Photographs, *Bull. Geol. Soc. Am.*, 82, p1735-1742.

Colvocoresses, A.P., 1979, Proposed Parameters for Mapsat, *Photogrammetric Engineering and Remote Sensing,* 45, p501-506.

Cooley, J. W. and Tukey, J. W., 1965, An Algorithm for the Machine Computation of Complex Fourier Series, *Mathematical Computation*, 19, p297-301.

Cowan, W. R., 1968, Ribbed Morraine: Till Fabric Analysis and Origin, *Canadian Journal of Earth Science*, 5, p1145-1159

Crandall, C.J., 1969, Radar Mapping in Panama, *Photogrammetric Engineering*, 35 .

Curran, P.J, 1985, *Principles of Remote Sensing*, Longman, London.

Curran, P.J., 1980, Multispectral Remote Sensing of Vegetation Amount, *Progress in Physical Geography,* 4, p315-341.

Curran, P.J., and Milton, E.J., 1983, The Relationship between the Chlorophyll Concerntration, LAI and Reflectance of a Simple Vegetation Conopy, *International Journal of Remote Sensing,* 4, p247-256.

Daniell, P. J., 1946, Discussion on the Symposium on Autocorrelation in Time Series, *Journal of the Royal Statistical Society* (suppl.), 8, p88-90.

Daoust, J., Gwyn, Q. H. J., and Christian, R., 1989, Methode Assistee par Ordinateur d'Identification et d' Analyse des Lineaments geologiques a l'aide d'une Image Ros (Resultats Preliminaires), *International Geoscience and Remote Sensing Symposium, 12th Canadian Symposium on Remote Sensing, Vancouver, Canada*, Volume 1, p101-104.

Dardis, G. F. and McCabe, A. M., 1983, Facies of Subglacial Channel Sedimentation in Late Pleistocene Drumlins, Northern Ireland, *Boreas*, 12, p263-278.

Davis, J. C., 1973, *Statistics and Data Analyis in Geology*, New York: Wiley.

De Loor, G.p., 1983, Introduction and some General Aspects of Image Formation in Radar, In: De Loor (ed) *Radar Remote Sensing*, Harwood Academic Publishers, Amsterdam.

Demorest, M., 1939, Glacial Movement and Erosion, a Criticism, *American Journal of Science,* 237, p594-905.

Deroin, J. P. and Tamain. A. L. G., 1990, Spot Data and the Montpellier Igneous Rocks as Keys to a New large-Scale Technonic Interpretation of the Bas Languedoc (Southern France), *ISPRS Journal of Photogrammetry and Remote Sensing*, 45, p404-418.

Doornkamp, J.C. and King, C.A.M., 1971, *Numerical Analysis in Geomorphology*, Arnold, London.

Drury, S.A., 1987, *Image Interpretation in Geology*, Allen and Unwin, London.

Dyson, J. L., 1952, Ice-Ridged Moraines and their Relationship to Glaciers, *American Journal of Science,* 250, p204-211 .

Embabi, N. S., 1991, Dune Types and Patterns in the United Arab Emirates using Landsat TM data, *24th International Symposium on Remote Sensing of Environment*, Rio de Janeiro, Brazil.

Fairchield, H. L., 1929, New York Drumlins, *Proceedings of Roch. Academic Science*, 7, p1-37.

Fairchild, H. L., 1907, Drumlins of Central Western New York, *New York State Museum Bulletin*, III, p391-443.

Ferguson, R. I., 1975, Meander Irregularity and Wavelength Estimation, *Journal of Hydrology,* 26, p315-333.

Fisher, R. A., 1929, Test of Significance in Harmonic Analysis, *Proceedings of the Royal Society,* Series A, 125, p54-59 .

Flint, R. F., 1947, *Glacial Geology and the Pleistocene Epoch*, Wiley, New York.

Flint, R. F., 1957, *Glacial and Pleistocene Geology*, Wiley, New York.

Folk, R. L., 1971, Genesis of Longitudinal and Oghurd Dunes Elucidated by Rolling Upon Grease, *Bull. Geol. Soc. Am.,* 82, p3461-3468.

Fowajuh, G.C. and Clark, C.D., 1992, Characterisation of parallel lineaments on remotely sensed imagery, *Proceedingsof the 18th Annual Conference of the Remote Sensing Society, Dundee,* 553-559.

Gentleman, W. M. and Sande, G., 1966, Fast Fourier Transforms-For Fun and Profit, *Proceedings of the AFIPS Conference*, 29, p563-578 .

Gibert, J.P., and Paul, S., 1976, Directions Tectoniques Teledetectees par Radar Lateral Aeroporte dans la Region de Chaudes -Aigues (Cantal, France), *Photogrammetria,* 32, p15-24.

Gillerman, E., 1970, Roselle Lineaments of Southeast Missouri, *Geol. Soc. Am. Bull., 81, p975-982.*

Gillespie, A. R., 1980, Digital Techniques of Image Enhancement, In: B. S., Siegel, and E. H., Gillespie (eds.), *Remote Sensing in Geology*, Wiley, New York .

Goetz, A. F. H. and Rowan, L. C., 1981, Geologic Remote Sensing, *Science,* 211, p781-791.

Gonzalez, C. R. and Wintz, P., 1987, *Digital Image Processing*, 2nd edition, Addison-Wesley, Massachusetts.

Goudie, A. S., 1969, Statistical laws and Dune Ridges in Southern Africa, *Geographical Journal,* 135, p404-406.

Goudie, A. S., 1970, Notes on some major dune types in sourthern Africa, *South African Geographical Journal,* 52, p93-101.

Granger, C. W. J., 1966, The Typical Shape of an Economic Variable, *Econometrica*, 34, pp150-161.

Granger, C. W. J. and Hughes, A. O., 1968, Spectral Analysis of Short Series- a Simulation Study, *Journal of the Royal Statistical Society,* Series A, 131, p83-99.

Gravelle, S. and Akhavi, M. S., 1989, Apllication of GIS and Remote Sensing for Lineament Mapping of Sttructural Features in the Rouyn-Beauchastel property, Quebec, *International Geoscience and Remote Sensing Symposium, 12th Canadian Symposium on Remote Sensing, Vancouver, Canada,* 1, p116-118.

Gravenor, C. P., 1953, The Origin of Drumlins, American *Journal of Science,* 251, p674-681.

Gravenor, C. P., 1974, The Yarmouth Drumlin Field, Nova Scotia, Canada, *Journal of Glaciology,* 13, p45-54.

Grenander, U. and Rosenblatt, M., 1957, *Statistical Analysis of Stationary Time Series,* Wiley, New York.

Grove, A. T., 1969, Landforms and Climatic Change in the kalahari and Ngamiland, *Geographical Journal, 139, 191-212.*

Grover, K. and Quegan, S., 1993, Radiometric Quality of SAREX-92 Data Set over Tapajos, *Proceedings of the 19th Annual Conference of the Remote Sensing Society, Towards Operational Applications, held on the 16th-17th September, Chester.*

Hardisty, J., 1993, Time Series Analysis using Spectral Techniques: Oscillatory Currents, *Earth Surface Processes and Landforms, 18, p855-862.*

Heindenrich, C., 1964, Some Observations on the Shape of Drumlins, *Canadian Geographer*, 8, p101-107.

Henninger, B. R., 1984, Landsat Application to Development of a Tectonic Model for Hydrocarbon Exploration of Devonian Shales in West Central Virginia, *Procceeding of the International Symposium on Remote Sensing of the Environment, Third Thematic Conference , Remote Sensing for Exoloration Geology, Colorado, p65-75.*

Hill, A. R., 1968, *An Analysis of the Spatial Distribution and Origin of Drumlins in North Down and South Antrim, Northern Ireland*, Unpublish thesis, Queen's University, Belfast.

Hill, A. R., 1973, The Distribution of Drumlins in County Down, Ireland, *Annals of the Association of American Geographers, 63, p226-240.*

Hobbs, W.H., 1904, Lineaments of the Atlantic border region, *Geological Society of America Bulletin, 15, p483-506.*

Hollinworth, S. E., 1931, The Glaciation of Western Edenside and adjoining areas, and the Drumlins of Edenside and the Solway Basin, *Quaterly Journal of the Geological Society of London, 87, p281-359.*

Hoppe, G. and Schytt, V., 1953, Some Observations Fluted Moraine Surfaces , *Geographical Annals, 35, p105-515.*

Jenkins, G. M. and Watts, D. G., 1968, *Spectral Analysis and its Applications*, Holden-Day, San Francisco.

Jensen, J.R., 1986, *Introductory Digital Image Processing, A Remote Sensing Perspective,* Prentice-Hall, Englewood Cliffs, New Jersey.

Jones, E. R., and Childers, R. L., 1992, *Contemporary College Physics,* Addison-Wesley, Reading.

Joshi, A. K., 1989, Automatic Detection of Lineament from Landsat Data, *International Geoscience and Remote Sensing Symposium, 12th Canadian Symposium on Remote Sensing, Vancouver, Canada, Volume 1, p85-88.*

Karczewski, A., 1976, Morphometric Features of Drumlins in Western Pomerania, *Quaestiones Geograhicae, 3, p35-42.*

Kendal, M. and Ord J. K., 1990, *Time Series*, 3rd edition, Edward Arnold,London.

Kirk, J.N., 1970, *A regional study of radar lineament patterns in the Quachita Mountains*, CRES Tech. Rep. 177-4, University of Kansas, p61.

Kleeman, T. and Woodruff Jr., C. M., 1989, lineament iddentification and the Edwards Aquifer of central Texas, *International Geoscience and Remote Sensing Symposium, 12th Canadian Symposium on Remote Sensing, Vancouver, Canada, Volume 1, p105-107.*

Knight, J. K., and Clark, C. D., 1993, Reconstruction of Former Ice Sheet Dynamics Utilising a Geographical Information System (G.I.S) Approach, *Proceedings of the third International Geomorphology Conference held in McMaster University, Canada, 23-28th August, 1993, p171.*

Knighton, A. D., 1982, Asymmetry of River Channel Cross-Sections: Part II. Mode of Development and Local Variation, *Earth Surface Processes and Landforms, 7, p117-131.*

Koopmans, B.N., 1983, *Side-Looking Radar, a tool for Geological Surveys*, In: De Loor (ed) Radar Remote Sensing, Harwood Academic Publishers, Amsterdam.

Koopmans, B. N., 1988, A Comparative Analysis of Dyke Lineaments Mapped from Shuttle Imaging Radar and Large Format Camera Photography in Hyperarid Areas of the eastern Desert, Egypt, and Red Sea Hills, Sudan, *International Journal of Remote Sensing, 9, p981-995.*

Krul, L., 1983, *Introduction to the use of Radar in Remote Sensing*, In: De Loor (ed) Radar Remote Sensing, Harwood Academic Publishers, Amsterdam.

Lake, S. D. and Munday, T. J. and Dewey, J. F., 1984, Lineament Mapping and Analysis in the Wessex Basin of Southern England: A Comparison between MSS and TM Data, *Proceedings of the Tenth Anniversary International Conference: Satellite Remote Sensing -Reviews and Preview, Reading, p361-372.*

Lancaster, N., 1979, *Quaternary Environments in the Arid Zone of Sourthern Africa,* Department of Geography and Environmen, University of the Witwatersrand, Occasional Paper 22: 73p .

Lancaster, N., 1980, Dune systems and palaeoenvironments in southern Africa, *Palaeontologia Africana,* 23, p185-189.

Lancaster, N., 1981, Grain size characteristics of Namib Desert linear sand dunes, *Sedimentology,* 28, p115-122.

Lancaster, N., 1982, Dunes on the Skeleton Coast , Namibia (South West Africa): Geomorphology and Grain Size Relationships, *Earth Surface Processes and Landforms,* 7, p575-587.

Lancaster, N., 1986, Grain-size characteriostics of linear dunes in the southwestern Kalahari, *Journal of Sedimentary Petrology,* 56, p395-400.

Lancaster, N., 1988, Development Of Linear Dunes in the South Western Kalahari, Souther Africa, *Journal of Arid Environments,* 14, p233-244.

Lancaster, N., Greeley, R., and Christensen, P. R., 1987, Dunes of the gran Desierto Sand-sea, Sonora, mexico, *Earth Surface Processes and Landforms,* 12, p277-288.

Lattman, L. H. and Parizek. R. R, 1964, Relationship between Fracture Traces and the Occurrence of Ground-water in Carbonate rocks, *Journal of Hydrology,* 2, p73-91.

Leachtenauer, J. C., 1977, Optical Power Spectrum Analysis: Scale and Resolution Effects, *Photogrammetric Engineering and Remote Sensing,* 43, p1117-1125.

Lee, W. H. K. and Kaula. W. M., 1967, A Spherical Harmonic Analysis of the Earth's Topography, 1967, *Journal of Geophysical Research,* 72, p 753-758.

Lewis, A. D.,1936, Sand Dunes of the Kalahari within the Union, *South African Geographical Journal,* 12, p23-32.

Livingston, I., 1986, *Geomorphological Significance of Wind Flow Patterns over a Namib Linear Dune,* In Nickling, W. G. (Ed.), Aeolian Geomorphology, Boston, Allen and Unwin, p97-112.

Lyon, R.J.P., and Lee, K., 1970, Remote Sensing in exploration for mineral deposits, *Economic Geology,* 65, p785-800.

MacDonald, H. C., 1980, *Techniques and Apllication of Imaging Radars*, in Siegal, B. S. and Gillespie, A. R., eds., Remote Sensing in Geology: John Wiley & Sons, New York, p297-336.

Mallick, D. I. J., Habgood, F., and Skinner, A. C., 1981, A Geological Interpretation of Landsat Imagery and Air Photography of Botswana, *Overseas Geology and Mineral Resources,* 56, p1-35.

Marion, A., 1991, *An Introduction to Image Processing* , Chapman and Hall, London.

Mather, P.M., 1987, *Computer Processing of Remotely Sensed Images- An Introduction*, John Wiley & Sons, Surrey.

Mathews, M. D., Jones, V. T., and Richers, D. M., 1984, Remote Sensing and Surface Hydrocarbon Leakage, *Procceeding of the International Symposium on Remote Sensing of the Environment, Third Thematic Conference , Remote Sensing for Exoloration Geology, Colorado*, p663-670670.

McCauley, J. F., Grolier, M. J., and Breed, C. S., 1977 , Yardangs, In: D. O. Doehring (ed.) *Geomorphology in Arid Regions*, State University of New York, Binghampto, p233-269.

Mckee, E. D., 1979, Introduction to a study of Global Sand Seas, In: E. D. Mckee (ed.), *A Study of Global Sand Seas*, U. S. Geological Professional Paper, 1052, p1-19.

Mead, W. J., 1925, The Geologic role of Dilatancy, *Journal of Geology*, 7, p685-698.

Menzies, J., 1979, A Review of the Literature on the Formation and Location of Drumlins, *Earth Science Review*, 14, p315-359.

Menzies, J., 1984, *Drumlins*: A Bibliography, Geo Books, Norwich, 127p.

Menzies, J. and Rose, J. (eds.), 1987, *Drumlin Symposium*, A. A. Balkema, Rotterdam, 360p.

Menzies, J. and Rose, J. (Editors), 1989, Subglacial Bedforms-Drumlins, Rogen Moraine and Associated Subglacial Bedforms, *Sedimentary Geology*, 62, p117-430.

Miller, J. W., 1972, Variations in New York Drumlins, *Annals of the American Association of Geography*, 62, p418-423 .

Moik, J., 1980, *Digital Processing of Remotely-Sensed Images*, NASA Special Publication 431, Washington DC.

Muller, E. H., 1963, Geology of Chautauqua County, New York, part 11, Pleistocene Geology, *New York State Meseum Bulletin*, no. 392.

Nowroozi, A. A., 1967, Table for Fisher's Test of Significance in Harmonic Analysis, *Geophysical Journal of Royal Astrological Society*, 12, p517-520.

Nye, J. F., 1965a, Stability of a Circular Cylindrical Hole in a Glacier, *Journal of Glaciology*, 5, p505-507.

Nye, J. F., 1965b, The Flow of a Glacier in a Channel of Rectangular, Elliptic or Parabolic Cross-Section, *Journal of Glaciology*, 5, p661-690.

Nye, J. F., 1969, The Effect of Longitudinal Stress on the Shear Stress at the Base of an Ice Sheet, *Journal of Glaciology*, 8. p207-213.

Nye, J. F., 1973, Water at the Bed of a Glacier. Symposium on the Hydrology of Glaciers, *Int, Assoc. Sci. Hydrology*, 95, p189-194.

O'Leary, D.W., Friedman, J.D., and Pohn, H.A, 1976, Lineament, Linear, Lineation: Some proposed new standards for old terms, *Geological Society of America Bulletin*, 87, p1463-1469.

Parizek. R. R, 1967, Application of Fracture Traces and Lineaments to Ground-water Prospecting, In: D. P. Gold, and R. R. Parizek (eds.), *Field Guide to Lineaments and Fractures in Central Pennslyvania, Second International Conference on the New Basement Tectonics, Department of Geosciences, The Pennsylvania State University*, p38-59

Park, C.F., and MacDiarmid, R.A., 1970, *Ore Deposits*, 2nd ed., Freeman, San Francisco.

Parzen, E., 1961, Mathematical Considerations in the Estimation Spectra, *Technometrics*, 3, p167-190.

Peterson, W. S. B., 1969, The Physics of Glaciers, Pergamon, Oxford.

Pinder, D. A. and Witherick, M. E., 1972, The Principles, Practice and Pitfalls of Nearest-Neighbour Analysis, *Geography*, 57, p277-288.

Piotrowski, J. A., 1987, Genesis of the Woodstock Drumlin Field, Southern Ontario, Canada, *Boreas*, 16, p249-265.

Podywysocki, M. H., Moik, J. G. and Shoup, W. C., 1975, Quantification of Geologic Lineaments by Manual and Machine Processing Techniques, *NASA Earth Resource Survey Symposium, Hauston, Texas*, TM-X-58168, p885-905.

Prest, V. K., 1983, *Canada's Heritage of Glacial Features*, Geological Survey of Canada, Miscellaneous Report 28, 119p .

Prest, V. K., 1984, The Late Wisconsin Glacier Complex, In: R. J. Fulton,(ed.), *Quaternary Stratigraphy of Canada: A Canadian Contribution to IGCP Project 24, Geological Survey of Canada*, Paper 84-10, p21-36.

Punkari, M., 1982, The Ice Lobes of the Scandinavian Ice Sheet during the Deglaciation in Finland, *Boreas*, 9, p307-310.

Pye, K., 1993, Late Quaternary Development of Coastal Parabolic Megadune Complexes in North Eastern Australia, In: K. Pye and N. Lancaster (eds.) *Special Publication Number 16 of the International Association of Sedimentologists, Blackwell Scientific Publications, Oxford*, p23-44.

Pye, K., and Lancaster, N. (eds.), 1993, *Aeolian Sediments, Ancient and Modern*, Special Publication Number 16 of the International Association of Sedimentologists, Blackwell Scientific Publications, Oxford.

Raj, K. G., 1989, Origin and Significance of Hemavathi-Tirthahalli Mega-Lineament- A Concept, *International Geoscience and Remote Sensing Symposium, 12th Canadian Symposium on Remote Sensing, Vancouver, Canada*, Volume 1, p116-118.

Rayner, J. N., 1967, A Statistical Model for the Explanatory Description of Large Scale Time and Spatial Climate, *Canadian Geographer*, 11, p68-86.

Rayner, J. N., 1971, *An Introduction to Spectral Analysis*, London: Pion Press.

Reed, B., Galvin, C. J. Jr., Miller, J. P., 1962, Some Aspects of Drumlin Geometry, *American Journal of Science*.

Reynolds, O., 1885, On the Dilatancy of Media Composed of Rigid Particles in Contact, *Philosophical Magazine*, Fifth Series, 127, p469-481.

Rose, J., 1987, Drumlins as Part of a Glacier Bedform Continuum., In J. Menzies, and J. Rose (eds.), *Drumlin Symposium*. A. A. Balkema, Rotterdam, p103-116.

Rose, J., 1989, Glacier Stress Patterns and Sediment Transfer Associated with the Formation of superimposed Flutes, In J. Menzies, and J. Rose (eds.) *Subglacial Bedforms-Drumlins, Rogen Moraine and Associated Subglacial Bedforms*, Sedimentary Geology, 62, p151-176.

Rose, J. and Letzer, J. M., 1975, Drumlin Measurements: a Test of the Reliability of Data Derived from 1:25000 Scale Topographic maps, *Geological Magazin*, 112, p361-371.

Rothlisberger, H., 1972, Water Pressure in Intra and Subglacial Channels, *Journal of Glaciology*, 11, p177-203.

Rowan, L.C., and Lathram, E.H., 1980, Mineral Exploration, In: B. S. Siegal, and A. R. Gillespie (eds.), *Remote Sensing in Geology*, Wiley, New York.

Sabins, F. F., 1978, *Remote Sensing, Principles and Interprestation*, W. H. Freeman and Co., San Francisco.

Sabins, F.F., Blom, R., and Elachi, C., 1980, Seasat radar image of San Andreas Fault, California, *American Association of Petroleum Geology*, 65, p619-629.

Saunders, D. F. and Thomas, G. E., 1973, Evaluation of Comercial Utility of ERTS-1 Imagery in Structural Reconnaissance for Mineral and Petroleum, *Procceedings Symposium of Significant Results obtained from ERTS-1, Goddard Space Flight Center*, p523-530.

Sharpe, D. R., 1985, The Stratified nature of Deposits in Streamlined Glacial Landforms on Southern Victoria Island, District of Franklin, *Current Research Part A, Geologiocal Survey, Canada, Paper*, 85-1A, p365-371.

Shaw, J., 1980, Drumlins and Large Scale Fluting Related to Glacier Folds, *Arctic. Alpine Research*, 12, p287-298.

Shaw, J., 1983, Drumlin Formation Related to Inverted Melt-water Erosional Marks, *Journal of Glaciology*,29, p461-479.

Shaw, J., 1994, Hairpin Erosional Marks, Horseshoe Vortices and Subglacial Erosion, *Sedimentary Geology*, 91, p269-283.

Shaw, J. and Freschauf, R. C., 1973, A Kinematic Discussion of the Formation of Glacial Flutings, *Canadian Geographer*, 17, p19-35.

Shimshoni, M., 1971, On Fisher's Test of Significance in Harmonic Analysis , Geophysical *Journal of the Royal Astronomical Society*, 23, p373-377.

Short, N.M., 1982, *The Landsat Tutorial Workbook- Basics of Satellite Remote Sensing*, Nasa, Washington, DC.

Shuman, C.A, 1989, Remote sensing of fracture indicators near the Moodus, Connecticut, seismic area, *Proceedings of the International Geoscience and Remote Sensing Symposium 12th Canadian Symposium on Remote Sensing, vol. 1, Vancouver, Canada*, p208-111.

Shuman, C.A, 1991, Joints, Facture Traces, and Lineaments: A multiple Scale Analysis of Fracture Features Across the Appalachian plateau in New York, *Procceedings of the 8th Thematic Conference on Geologic Remote Sensing*.

Simonett, D. S., 1983, The Development and Principles of Remote Sensing, In: Colwell, R. N (Editor), *Manual of Remote Sensing*, American Society of Photogrammetry, Falls Church, Virginia .

Slater, P.N., 1980, *Remote Sensing Optics and Optical Systems*, Addison-Wesley, Reading, Massachusetts.

Smalley, I. J., 1966, Drumlin Formation: A Rheological Model, *Science*, 151, p1379-1380.

Smalley, I. J. and Piotrowski, J. A., 1987, Critical Strength/ Stress ratios at the \ Ice-Bed Interface in the Drumlin Formating Process: From 'Dilantancy' to ' Cross-Over', In: J. Menzies, and J. Rose (eds.), *Drumlin Symposium*, A. A., Balkema, Rotterdam, p81-86.

Smalley, I. J. and Unwin, D. J., 1968, The Formation and Shape of Drumlins and their distribution and Orientation in Drumlin Fields, *Journal of Glaciology*, 7, p377-390.

Speight, J. G., 1965, Meander Spectra of the Angabunga River, *Journal of Hydrology*, 3, p1-15.

Stalker, A., 1960, Ice-Pressed Drift Forms and Associated Deposits in Alberta, *Geological Survey of Canada, Bulletin*, 57, p1-38.

Staskowski, R. J., 1985, The Leelanau, Benzie and Grand Traverse, Michigan Anomalies-Structural and Geobotanical Indicators of Hydrocarbon Microseepage, *Procceeding of the International Symposium on Remote Sensing of the Environment, Third Thematic Conference , Remote Sensing for Exploration Geology, Colorado*, p53-63.

Stefouli, M. and Osmaston. H. A., 1984, The Remote Sensing of Geological Linear Features Using Landssat: Matching Analytical Approaches to Practical Applications, *Proceedings of the Tenth Anniversary International Conference: Satellite Remote Sensing -Reviews and Preview, Reading*, p227-236.

Stone, R. and Dugundi, J., 1965, A Study of Microrelief in a Mapping Classification, and Quantification by Means of a Fourier Analysis, *Engineering Geology*, 1, p91-187.

Stromberg, W. D. and Farr, T. G., 1986, A fourier Based Textural Feature Extraction Procedure., *IEE Transactions on Geoescience and Remote Sensing*.

Taylor, F. B., 1931, Distribution of Drumlin and its Bearing on their Origin,, *Bull. Geol. Soc. Am.*, 42, p201.

Terzaghi, K., 1943, *Theoretical Soil Mechanics*, Wiley, New York.

Thomas, D. S. G., 1984, Ancient Ergs of the former Arid Zones of Zimbabwe, Zambia and Angola, *Transactions, Institute of British Geographers, New* Series, 9, p75-88.

Thomas, D. S. G., 1986, Dune pattern statistics applied to the Kalahari Dune Desert, Southern Africa, *Zeitschrift fur Geomorphologie NF*, 30, p231-242.

Thomas, D. S. G., 1988, Analysis of linear dune sediment-form relationships in the Kalahari Dune Desert, *Earth Surface Processes and Landforms*, 13, p545-553.

Thomas, D. S. G. and Martin , H. E., 1987, Grain-size characteristics of linear dunes in the southwestern Kalahari- discussion, *Journal of Sedimentary Petrology*, 57, p572-573.

Thornbury, W. D., 1969, *Principles of Geomorphology*, Wiley, New York.

Thumult, J., 1984, Tectonic Pattern Analysis in Covered Terrains of the Athabasca Basin, *Procceedings of the International Symposium of Remote Sensing of the Environment, 3rd Thematic Conference , Remote Sensing for Exploration Geology, Colorado Springs, Colorado*, p593-602.

Thwaites, F. T., 1963, *Outline of Glacial Geology*, Edwards Brothers, Ann Arbor, Michigan.

Townshend, J. R. G. and Justice, C. O., 1990, The Spatial Variation of Vegetation Changes at very Coarse Scales, *International Journal of Remote Sensing*, 11, p149-157.

Townshend, J.R.G., 1981, The Spatial Resolving of Earth Resources Satellites, *Progress in Physical Geography*, 5, p32-55 .

Trenhaile, A. S., 1971, Drumlins: their Distribution, Orientation, and Morphology, *Canada Geographers*, 15, p113-126.

Trenhaile, A. S., 1975, The Morphology of a Drumlin Field, *Annals Association of American Geographers,* 66, p517-529.

Tsoar, H., 1978, *The Dynamics of Longitudinal Dunes*, Final Technical Report, U.S. Army European Research Office, p171.

Tsoar, H., 1983, The Dynamics of Longitudinal (Seif) Dunes, *Sedimentology*, 30, p567-578.

Tsoar, H., 1989, Linear Dunes- Forms and Formation, *Progress in Physical Geography,* 13, p507-528.

Tsombos, P. I. and Kalogeropoulos. S. I., 1990, Remote Sensing as Apllied to Mineral Exploration in the Chalkididki Peninsula, Northern Greece, *SPRS Journal of Photogrammetry and Remote Sensing*, 45, p344-354.

Tucker, C.J., 1979, Red and Photographic Infrared Linear Combinations for Monitoring Vegetation, *Remote Sensing of Environment*, 10, p127-150.

Unwin, D. J. and Hepple, L. W., 1974, The Statistical Analysis of Spatial Series, *Statistician*, 23, p211-227.

Vernon, P., 1966, Drumlins and Pleistocene Ice Flow over the Ards Peninsula/Strangford Lough area, County Down, Ireland, *Journal of Glaciology*, 6, p401-409.

Vincent, R. K. and Coupland, D. H., 1979, Petroleum Exploration with Landsat in Bay County, Michigan -an Interim Case Study, *Procceeding of the International Symposium on Remote Sensing of the Environment, Ann Arbor, Michigan*, p379-387.

Von Engeln, O. D., 1938, Glacial Geomorphology and Glacier Motion, *American Journal of Science,* 235, p426-440.

Wang, J., and Howarth, P. J., 1989, Edge Following as Graph Searching and Hough Transform Algorithms for Lineament Detection, *International Geoscience and Remote Sensing Symposium, 12th Canadian Symposium on Remote Sensing, Vancouver, Canada,* Volume 1, p101-104.

Ward, F. and Shapiro, R., 1961, Meteorological Periodicities, *Journal of Meteorology,* 18, p635-656.

Wasson, R. J. and Hyde, R., 1983, Factors Determining Desert Dune Type, *Nature*, 30, p337-339.

Webster, R., 1977, Spectral Analysis of Gilgai Soil, Australian *Journal of Soil Research,* 15, p191-204.

Weilchowsky, C. C. and Davidson, D. M., 1983, Petroleum Exploration in the Kingston Salient, Ouachita Orogen, Oklahoma-Texas, using Landsat Imagery, *Procceeding of the International Symposium on Remote Sensing of the Environment, Third Thematic Conference , Remote Sensing for Exoloration Geology, Colorado Springs, Colorado*, p37-51 Springs, Cololorado.

Wilson, I. G., 1972a, Aeolian Bedforms-their Development and Origins, *Sedimentology*, 19, p173-210.

Wilson, I. G., 1972b, Universal Discontinuities in Bedforms Produced by the Wind, *Journal of Sedimentary Petrology*, 42, p667-669.

Wise, D. U., 1982, Linesmanship and the Practice of Linear Geo-art, Geological Society of America Bulletin, 93, p886-888.

Wright, H. E., 1957, Stone Orientation in Wadena Drumlin Field, Minnesota, *Geographical Annal*, 39, p19-31.

Yesou, H. and Rolet. J., 1990, Regional Mapping of the South Armorican Shear Zone (Britatany, France) using Remotely Sensed Spot Imagery, *SPRS Journal of Photogrammetry and Remote Sensing,* 45, p419-427.

APPENDIX A

Computer Program for carrying out Spectral Analysis

SPECTAN.F

SPECTAN.F is a FORTRAN 77 program adopted from the NAG and Ghost-88 libraries for performing spectral analysis on radiometric transects.

PROGRAM LISTING

```
C     PROGRAM for carrying out spectral analysis on radiometric transect. Transect output
C     is in the format given in Table 4.3 where the first ten lines are the header information
C     containing the image size, transect co-ordinates, size of transect and the spectral band
C     chosen for the transect. This program reads a transect of length NC. It selects the
C     mean correction option, a tapering proportion of 0.1, the Tukey window and a cut-off
C     point for the window at lag 100. It chooses to have NC auto-covariances calculated
C     and unlogged spectral estimates at a frequency division of 2π/200. It then calls
C     G13CAF to calculate the univariate spectrum. The test statistics is also calculated and
C     the result is a print out of the autocovariances, the power spectrum and the test
C     statistics, and also a graph of the transect and the power spectrum. Graphs were
C     plotted with routine from GHOST-88 program.


C     PARAMETERS...
      INTEGER          NXG, NCMAX
      PARAMETERS       (NXG=1000, NCMAX=500)
      INTEGER          NIN,NOUT
      PARAMETER        (NIN=7, NOUT=6)
C     LOCAL SCALARS
      REAL  *8         PX, SUMXG, XXG, VAR, AMEAN
      INTEGER          I, IC, IFAIL, IW, KC, L, LG, MTX, MW, NC, NG, NX
      CHARACTER*200    HEADER, FNAME(13)
C     LOCAL ARRAYS
      REAL *8          G(50), C(NCMAX), STATS(4), XG(NXG), CO(NXG),
                       RO(NXG), XGG(50), XGG1(50)
      REAL             XGG1(50), XGS(NGX), R(NXG)
      DIMENSION        YMIN(2), YMAX(2)
      DATA             YMIN/0.65,0.20/,YMAX/0.95,0.50/
```

```
C       EXTERNAL SUBROUTINE
C       EXTERNAL G13CAF
C       EXECUTABLE STATMENTS
        WRITE (NOUT,*)  ' RESULTS OF ANALYSIS OF TRANSECT ' TITTLE
        PRINT*,'INPUT TRANSECT LENGTH AND NUMBER OF COVARINCES'
        READ(5,*) NX, NC

C       READING THE TRANSECT FILE
        DO 1 JJ=1,2
        PRINT*,'INPUT FILE = '
        READ (NIN,*) FNAME
        IF (FNAME(1:1).EQ.'Q'.OR.FNAME(1:1).EQ.'Q') GOTO 1000
        OPEN(NIN, FILE=FNAME)

C       SKIP HEADING IN THE TRANSECT FILE
        READ(NIN,*) (HEADER (I),I=1,10)

C       READING THE DN VALUES IN THE TRANSECT FILE
        IF (NX.GT.0 .AND. NX .LE.NXG .AND. NC.GT.0 .AND. NC.LE.NCMAX) THEN
        READ(NIN,*,END=20) (RO(I), CO(I), XG(I),I=1,NX)
19      NX=I-1

C       CALCULATING VARIANCE FOR USE IN TESTING SPECTRAL
        ESTIMATES
        SUMXG=0.0
        VAR=0.0
        DO 2 I=1,NX
        SUMXG=SUMXG + XG(I)
2        CONTINUE
        AMEAN =SUMXG/NX
        DO 3 I=1,NX
        VAR=VAR+(XG(I)-AMEAN)**2
3       CONTINUE
        VAR=2*VAR/NX
```

```
C     DETREENDING THE TRANSECT ( FIRST ORDER DIFFERENCE)
      DO 4 I=1, NX
 4    XG(I)=XG(I+1)-XG(I)

C     PLOTTING THE TRANSECT
      CALL PAPER(1)
      DO 5 J=1,NX
      XGS(J)=XG(J)
 5    R(J)=J
      CALL MAP (1.0,300.0,-10.0,70.0)
      CALL PSPACE(0.3,0.6,ymin(jj),ymax(jj))
      CALL AXORIG(1.0,-10.0)
      CALL AXES
      CALL CURVEM(2)
      CALL CURVEO(R,XGS,1,NX)
      CALL PCSCEN(150.0,-19.0,'DN Spatial Position in Pixels ')
      CALL PLOTCS(140.0,60.0, FNAME)
      CALL CTRORI(90.0)
      CALL PCSCEN(-40.0, 30.0,'DN Values')

C     CALCULATING THE SPECTRAL ESTIMATE
      MTX=2
      PX=0.1e0
      IW=3
      MW=72
      IC=0
      KC=800
      L=144
      LG=0
      IFAIL=1
      CALL G13CAF (NX, MTX, PX, IW, MW, IC, NC, C, KC, L, LG, NXG, XG, NG,
                                        STATS, IFAIL)
      IF(IFAIL.NE.0) THEN
      WRITE(NOUT,100)'G13CAF FAILS. IFAIL=',IFAIL
      END IF
```

```
      IF (IFAIL.EQ.0 .OR. IFAIL .GE.4) THEN
      WRITE (NOUT,*) 'COVARIANCES'
      WRITE(NOUT,110) (I, C(I), I=1,NC)
      WRITE(NOUT,*)
      WRITE (NOUT,*) 'SPECTRAL ESTIMATES'
      WRITE(NOUT,110) (I-1, XG(I), I=1,NG)
      WRITE(NOUT,*)

C     CALCULATING THE FISHER TEST RATIOS
      WRITE (NOUT,*) 'TEST USING CALC. VARIANCE'
      XXG=0.0
      DO 6 I=1,MW+1
      XXG=XXG + XG(I)
      XGG(I)=XG(I)/XXG
      XGG1(I)=XG(I)/VAR
6     CONTINUE
      WRITE(NOUT, 110) (I-1, XGG1(I), I=1, MW)

C     PLOTTING THE POWER SPECTRAL DENSITY FUNCTION
      CALL PSPACE(0.85,1.15,YMIN(JJ),YMAX(JJ))
      CALL MAP(1.0,41.0,0.0,20.0)
      CALL AXORIG(1.0,0.0)
      CALL AXES
      DO 7 J=1,NX
      XGS(J)=XG(J)
7     R(J)=J
      CALL CURVEM(2)
      CALL CURVEO(R,XGS,1,NX)
      CALL CTRORI(0.0)
      CALL PCSCEN(20.0,-2.0,'Cycles per 80 Pixels')
      CALL PLOTCS(9.0,18.0, ptitle)
      CALL  CTRORI(90.0)
      CALL PCSCEN(-4.0,10.0,'Power')
      CALL CTRORI(0.0)
```

```
      CLOSE(NIN)
1     CONTINUE
1000  CALL GREND
      END IF
      END IF
      STOP
100   FORMAT (1X,A,I3)
110   FORMAT (1X,I4,F10.4,I5,F10.4,I5,F10.4,I5,F10.4)
      END
```

The Parameters

1 NX INTEGER

on entry: the length of the time series, n.

Constrain: NX≥1

2 MTX INTEGER

MTX specifies whether the data are to be initially mean

MTX = 0 for no mean correction

MTX = 1 for mean correction

constraint: $0 \leq MTX \leq 1$

3 PX REAL

PX specifies the proportion of the data to be tapered by the split cosine bell tapered

constraint: $0.0 \leq PX \leq 1.0$

4 IW INTEGER

Choice of the lag window. IW =1 for rectangular, 2 for Barlett, 3 for Tukey or 4 for Parzen.

constraint: $1 \leq IW \leq 4$

5 MW INTEGER

'Cut-off' point, M, of the lag window.

constraint: $1 \leq MW \leq NX$

6 IC INTEGER

Indicates whether covariances are to be calculated in the routine or supplied in the call to the routine: IC = 0 if covariances are to be calculated and IC ≠ 0 if covariances are to be supplied.

7 NC INTEGER

The number of covariances to be to be calculated in the routine

constraint: MW ≤ NC ≤NX

8 C(NC) REAL ARRAY

This contains the NC calculated covariances

9 KC INTEGER

KC specifies the order of the Fast Fourier Transform (FFT)used to calculate the covariances.

constraint: KC ≥ NX + NC

10 L INTEGER

This is the frequency division, of the spectral estimates

constraint: L ≥ 2 x MW - 1

11 LG INTEGER

Indicates whether unlogged or logged spectral estimates are required: LG=0 for unlogged, LG ≠ 0 for logged

12 NXG INTEGER

The length of the array XG, as declared in the program from which G13CAF is called.

constraint: NXG ≥ Max. (KC, L) if covariances are calculated rather than supplied

13 XG(NXG) REAL ARRAY

On entry, this is the NX data points if the covariances are to be calculated and on exit it is the NG spectral estimates

14 NG INTEGER

This is the number of spectral estimate on exit

15 IFAIL INTEGER

IFAIL = 0 unless the routines detect an error.

16 AMEAN INTEGER

This is the mean of the transect.

17 VAR INTEGER

This is the variance of the transect

Adopted from:

NAG Fortran library Mark15, The Numerical Algorithm Group Limited.

GHOST Graphical Output System, 1991 Version 8 by W. A. J Prior, AEA Technology, Culham Laboratory, Abingdon.